Stoichiometric and catalytic reactions of ruthenium multi N-heterocyclic carbene complexes

Cybulski, Mateusz

Award date:
2018

Awarding institution:
University of Bath

STOICHIOMETRIC AND CATALYTIC REACTIONS OF RUTHENIUM MULTI N-HETEROCYCLIC CARBENE COMPLEXES

Mateusz Krzysztof Cybulski

A thesis submitted in partial fulfilment of the requirements for the degree of

Doctor of Philosophy

University of Bath

Department of Chemistry

September 2017

Signed……. Date…….

CONTENTS

Chapter 4: C-O Bond Activation of DPEphos *via* Attack of Nucleophilic Ru-H in RuL_4H_2

Chapter 5: Reactivity of ruthenium dihydride complexes with $P(C_6F_5)_3$

Chapter 6: Experimental procedures and characterising data

ACKNOWLEDGEMENTS

First and foremost, I would like to thank my boss, *capo di tutti capi* Professor Mike Whitlesey for giving me the opportunity to work in his lab as a final year MChem and then a PhD student. I have been very fortunate to have you as my supervisor and I will always be grateful for your support and kindeness.

Many thanks go my lab mates, both past and present, who have created a great atmosphere to work in and made my time in Bath most enjoyable and unforgettable. In particular, I would like to thank Dr Ian Riddlestone for his invaluable help and advice, Dr Lee Collins for teaching me to be thorough and 'doing things properly' and Dr Rebecca Poulten for sharing all the goss and animal facts! Without you, BOTTY time would have been just a boring coffee break! I would also like to acknowledge Dr Sara Sabater for constantly pushing me to come up with fresh stuff to annoy her with and a steady supply of Hobonobonobos, and Dr Maialen Espinal-Viguri for her hospitality.

I would like to express my gratitude to Dr Mary Mahon and Dr John Lowe for their help with X-ray crystallography and NMR spectroscopy. Their knowledge, expertise and patience have been of great value. I would like to show my greatest appreciation to Prof. Stuart Macgregor, Dr David McKay and Nick Beattie for their work on DFT calculations. It has been a real pleasure collaborating with you!

Finally, I would like to thank my parents and my brother Paweł, without whom I would have never decided to come to the UK and embark on this fascinating journey with chemistry. Your continuous love, support and encouragement mean a lot to me and will never be forgotten!

ABSTRACT

This thesis describes the stoichiometric and catalytic C-F bond activation of fluoroarenes using a series of N-heterocyclic carbene (NHC) containing *trans*-dihydride complexes of ruthenium; the tetrakis-carbene complexes $[Ru(NHC)_4H_2]$ (NHC = IMe_4, IMe_2) and the mixed carbene-phosphine species $[Ru(NHC)_2(PPh_3)_2H_2]$ and $[Ru(NHC)_2(P\text{-}P)H_2]$ (NHC = IMe_4, IEt_2Me_2; P-P = dppe, dppp, dppm). On the basis of a combination of experimental and computational evidence that these complexes react *via* attack of their nucleophilic hydride ligands, related and altogether serendipitous discoveries involving bond cleavage of DPEphos and tris(pentafluorophenyl)phosphine are also described.

The tetrakis-NHC complex, $[Ru(IMe_4)_4H_2]$ (**1**), proved to be a remarkably efficient and regioselective catalyst for the hydrodefluorination (HDF) of C_6F_6 to the 1,4-substituted isomer of $C_6F_2H_4$ at room temperature. Experimental studies showed that **1** reacted without any creation of a vacant coordination site at the metal involving loss of an NHC. DFT calculations provided complete support for this and showed that reactivity involved nucleophilic attack of the Ru-H in a concerted manner to account for the observed selectivities.

$[Ru(NHC)_2(PPh_3)_2H_2]$ (NHC = IEt_2Me_2 (**8**), IMe_4 (**9**)) were capable of bringing about up to 5 HDF steps on C_6F_6 to afford C_6FH_5, but only at elevated temperature. The activity was compromised by poor regioselectivity, which was attributed to the reaction occurring through both five- and six-coordinate Ru species, as well as competitive C-H activation and $PPh_3/HSiR_3$ substitution processes. This was circumvented by use of bidentate phosphines, which allowed for almost

quantitative HDF of C_6F_6 to C_6FH_5 using [Ru(IMe_4)$_2$(P-P)HF] (P-P = dppe (**22**), dppp (**23**)).

C-O bond cleavage of DPEphos was observed upon thermolysis with **9** to afford the phosphinophenolate product, [Ru(IMe_4)$_2$(PPh_3)($Ph_2PC_6H_4O$)H] (**29**). In the case of the N-ethyl substituted precursor **8**, C-O activation was accompanied by C-N cleavage of the carbene to give the phosphinocarbene phosphinophenolate complex, [Ru(IEt_2Me_2)($IEtMe_2(C_6H_4)PPh_2$)($Ph_2PC_6H_4O$)H] (**31**). Whereas the reactivity of both **8** and **9** (suggested computationally) is believed to arise as a result of the nucleophilic *trans*-H-Ru-H geometry, DPEphos activation was also found to occur with the *cis*-dihydride [Ru(DPEphos)$_2H_2$] (**33**) to give [Ru(DPEphos)($Ph_2PC_6H_4O$)H] (**34**).

$P(C_6F_5)_3$ underwent facile C-F activation with both **9** and [Ru(PPh_3)$_4H_2$] (**32**) to give [Ru(IMe_4)$_2$($PF_2(C_6F_5)$)(C_6F_5)H] (**36**) and [Ru(PPh_3)$_3$HF] (**37**) respectively. The latter reacted with tertiary silanes and HBpin to afford the silyl trihydride complexes [Ru(PPh_3)$_3$(SiR_3)H_3] (R= Et (**38**), Ph (**39**)) and σ-borane dihydride species ([Ru(PPh_3)$_3$(HBpin)H_2]) respectively.

ABBREVIATIONS

Analytical

br	broad
ca.	circa
COSY	correlation spectroscopy
d	doublet
DFT	density functional theory
equiv	equivalent(s)
EXSY	exchange spectroscopy
HMBC	heteronuclear multiple bond correlation
HMQC	heteronuclear multiple quantum coherence
HSQC	heteronuclear single quantum coherence
i	*ipso*
IRC	intrinsic reaction coordinate
$^{n}J_{xy}$	coupling constant of X to Y across n bonds
m	*meta*
m	multiplet
MW	molecular weight
m/z	mass to charge ratio
NMR	nuclear magnetic resonance
o	*ortho*
p	*para*
q	quartet
rt	room temperature
s	singlet
t	triplet
T	temperature
TOF	turnover frequency (TON h^{-1})
TON	turnover number = (moles of fluoroaromatic product(s) x number of HDF steps)/ moles of catalyst
w_h	peak width at half height
VT	variable temperature
‘vt’	virtual triplet
XRD	X-ray diffraction

δ	NMR chemical shift

Units

°	degrees
°C	degrees Celsius
Å	Ångström
atm	atmosphere
g	gram
h	hour(s)
Hz	hertz
K	Kelvin
MHz	megahertz
mg	milligram
min	minute(s)
µL	microlitre(s)
mL	millilitre(s)
µmol	micromole(s)
mmol	millimole(s)
mol	mole(s)
ppm	parts per million

Chemical

Acac	acetylacetonate
Ar	generic aryl group
Ar^F	fluoroaryl group
BAr^F_4	tetrakis(3,5-bis(trifluoromethyl)phenyl)borate
BDP	bis(diphenylphosphino)benzene
bpy	2,2’-bipyridine
COD	1,5-cyclooctadiene
Cp	cyclopentadienyl
Cp*	pentamethylcyclopentadienyl
Cy	cyclohexyl
Dipp	2,6-diisopropylphenyl
Dippp	1,3-bis(diisopropylphosphino)propane
DMAP	*p*-*N*,*N*-dimethylaminopyridine
DMF	dimethylformamide

DMSO	dimethylsulfoxide
Dppm	1,1-bis(diphenylphosphino)methane
Dppe	1,2-bis(diphenylphosphino)ethane
Dppp	1,3-bis(diphenylphosphino)propane
DCEphos	bis[2-(dicyclohexylphosphino)phenyl]ether
DPEphos	bis[(2-diphenylphosphino)phenyl]ether
Et	ethyl
HDF	hydrodefluorination
ICy	1,3-dicyclohexylimidazol-2-ylidene
IEt_2Me_2	1,3-diethyl-4,5-dimethylimidazol-2-ylidene
IMe_2	1,3-di(methyl)imidazol-2-ylidene
IMe_4	1,3,4,5-tetramethylimidazol-2-ylidene
IMes	1,3-di(2,4,6-trimethylphenyl)imidazol-2-ylidene
^{i}Pr	isopropyl
IPr	1,3-di(2,6-diisopropylphenyl)imidazol-2-ylidene
$I^{i}Pr_2$	1,3-di(isopropyl)imidazol-2-ylidene
L	generic ligand
M	generic metal
Me	methyl
$NaBAr^{F}_4$	tetrakis[3,5-bis(trifluoromethyl)phenyl]borate
NHC	N-heterocyclic carbene
PCF	tris(pentafluorophenyl)phosphine
PFNB	pentafluoronitrobenzene
Ph	phenyl
Phen	phenanthroline
Pin	pinacolato group
R	alkyl or aryl
^{t}Bu	*tert*-butyl
TEMPO	(2,2,6,6-Tetramethylpiperidin-1-yl)oxyl
THF	tetrahydrofuran
TMS	trimethylsilyl
X^-	generic anion
Xantphos	4,5-Bis(diphenylphosphino)-9,9-dimethylxanthene

CHAPTER ONE

Introduction

1.1. C-F bonds and applications of organofluorine compounds

The C-F bond is the strongest single carbon-element bond (105.4 kcal mol^{-1} in CH_3F) in organic chemistry.[1,2] The strength of the C-F bond arises from the high electronegativity of fluorine (Pauling electronegativity, $\chi = 3.98$), which imparts a significant ionic bond character and consequently a relatively large dipole. The small size of the fluorine atom (Table 1.1; occupying a smaller volume than methyl, amino or hydroxyl groups, but larger than a hydrogen atom)[3] means that its introduction into an organic molecule does not increase significantly the overall molecular size. However, fluorine incorporation carries important implications for the electronic and hence physicochemical properties (e.g. acidity/basicity, dipole moment or lipophilicity) of the target organic compound. The high polarity of the C-F bond leads to a low energy σ* antibonding orbital, which can accept electron density from the adjacent electron donating groups and ultimately reduce the net basicity. A decrease in the pK_a can quite often result in an improved membrane permeation and thus enhanced bioavailability of drug molecules.[4,5] Moreover, the replacement of an oxidisable C-H group by an inert C-F unit increases the metabolic stability of medicinal compounds, whereas the electrostatic interactions associated with the C-F bond (e.g. dipole-dipole, charge-dipole, hyperconjugation, hydrogen bonding) influence the conformations of organofluorine compounds and their binding affinity to enzymes/proteins. Recent surveys report that approximately 20% of all pharmaceuticals contain fluorine,[6–10] including "blockbuster" drugs such as Lipitor or Risperdal (Figure 1.1). Fluorine containing compounds have been also extensively

employed in the synthesis of agrochemicals[11,12] (ca. 25% of all marketed herbicides)[13] and in the development of novel functional materials,[14] such as liquid crystals, plastics, dyes, membranes and polymers.

Table 1.1: The Van der Waals radii and average C-X bond lengths of selected elements.

X =	H	C	N	O	F
Van der Waals radii [Å]	1.20	1.70	1.55	1.52	1.47
C-X bond lengths [Å]	1.09	1.54	1.47	1.43	1.35

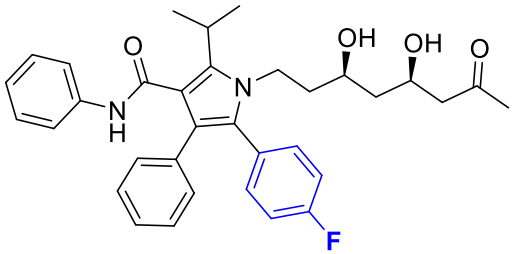

Lipitor
lipid lowering agent

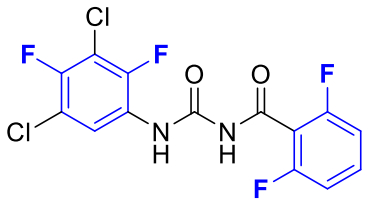

teflubenzuron
insecticide

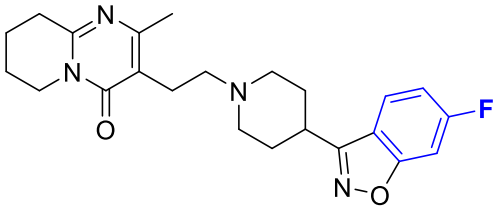

Risperdal
antipsychotic

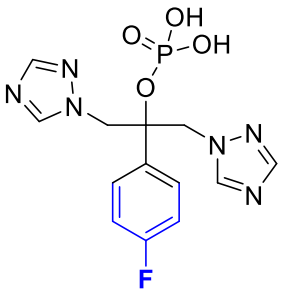

Fosfluoconazole
antifugal

Figure 1.1: Examples of important partially fluorinated aromatics.

1.2. Fluorine incorporation

Despite the integral and pivotal role of fluorine and carbon-fluorine bonds in all aspects of the modern chemical industry, introduction of fluorine into organic

molecules remains challenging. Industrially, selective monofluorination of aromatic compounds is achieved in the Balz-Schiemann reaction (Scheme 1.1), developed as early as 1927.[15] Despite large scale applications, the process suffers from considerable drawbacks such as harsh conditions involving high temperatures or the presence of toxic, corrosive and potentially explosive arenediazonium salts.

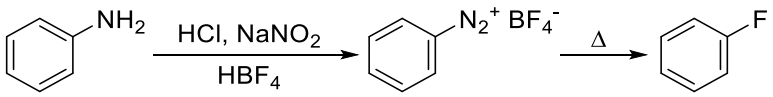

Scheme 1.1: The Balz-Schiemann reaction for the monofluorination of aromatic compounds.

Although recent years have witnessed a dramatic development in methods for the installation of fluorine, practical and broadly useful late-stage fluorination reactions, i.e. such that would allow chemo- and stereoselective fluorination of molecules with high structural and functional complexity, remain underdeveloped.[16] An example of recently developed methodology for the fluorination of pharmaceutically active molecules is shown in Scheme 1.2. The combination of Ag_2O and the electrophilic fluorinating agent, F-TEDA-PF_6, exhibited remarkable functional group tolerance and facilitated sp^2 C-F bond formation under mild reaction conditions. However, the strategy suffered from the need for the preparation of toxic organotin compounds as starting materials.[17] Contemporary carbon-fluorine bond forming reactions have been extensively covered in several reviews by Ritter and will not be discussed in this section.[18–22]

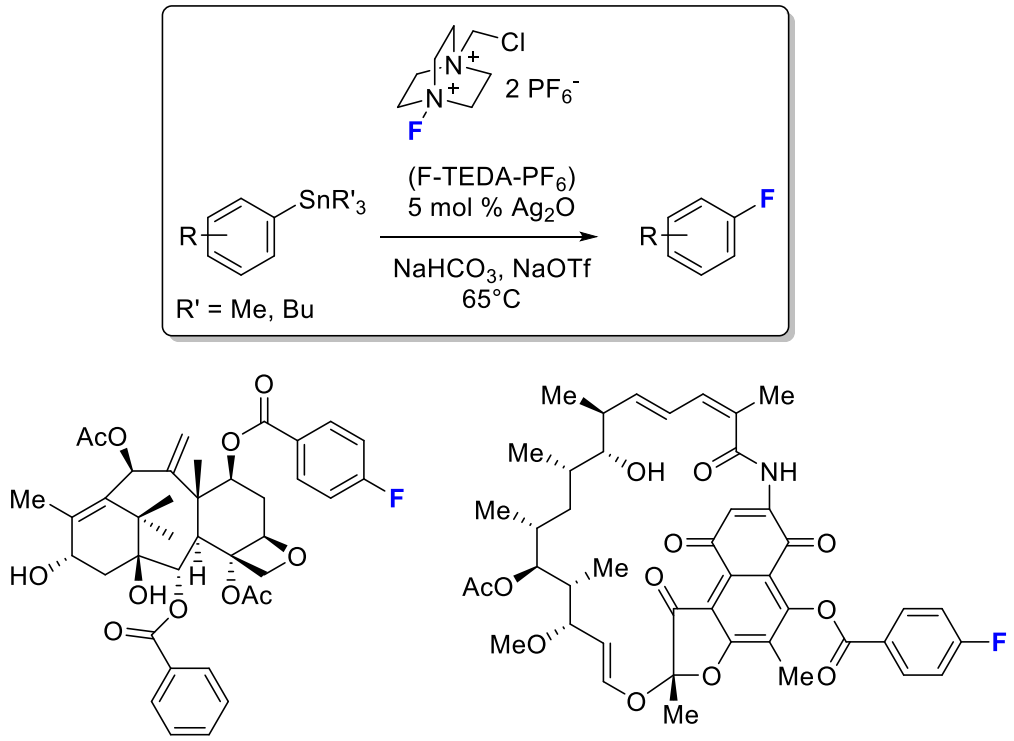

Scheme 1.2: Silver-catalysed late-stage fluorination of complex aryl stannanes using Ag_2O and F-TEDA-PF_6 (top) to obtain fluorinated derivatives of taxol (anticancer; left) and rifamycin (antibiotic; right).

Another way to envisage incorporation of fluorine is the reverse process in which fluorine is selectively removed from a more fluorinated substrate to afford a product with a defined partial substitution pattern. The simplest derivatisation of a C-F bond is the replacement of fluorine with hydrogen, a reaction referred to as hydrodefluorination (HDF).[23–28] This approach benefits from the abundance of perfluorinated compounds and represents a promising alternative to the fluorination reactions, which commonly suffer from functional-group interference. For example, current method for the synthesis of the key intermediate 2,4,5-trifluorobenzeneacetic acid en route to the antidiabetic drug Sitagliptin requires seven steps (Scheme 1.3).[29] Conceivably, a more sustainable and atom-efficient HDF approach could considerably shorten the synthetic sequence to just a single step.

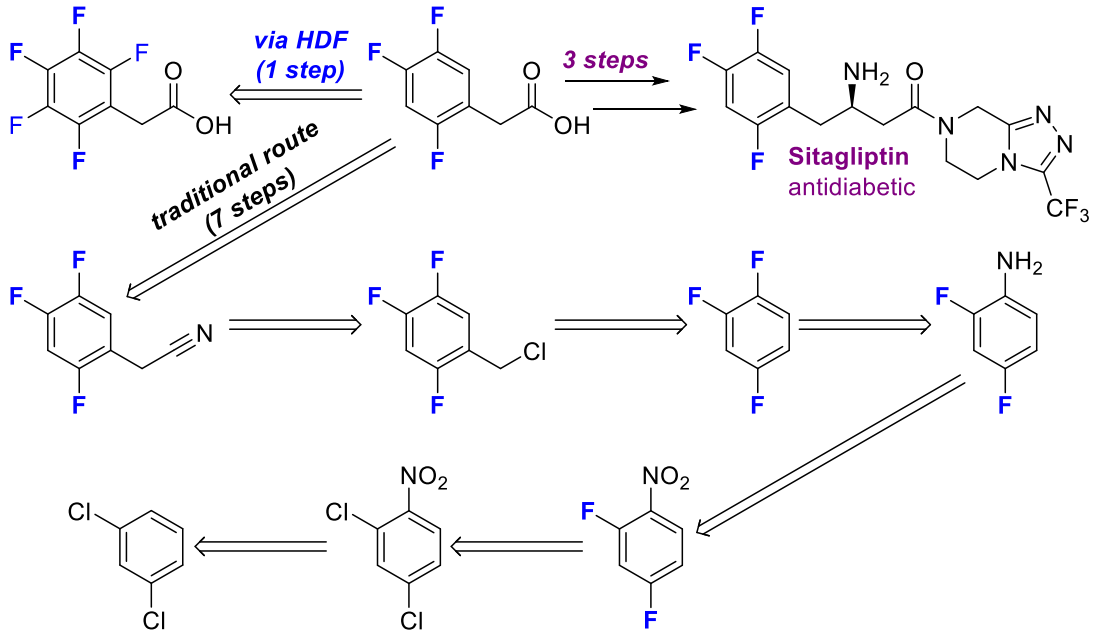

Scheme 1.3: Potential expedient synthesis of key Sitagliptin intermediate *via* HDF.

The HDF methodology could also be potentially implemented in the conversion of chlorofluorocarbons (CFCs) to their hydrogenated derivatives (HCFCs). CFCs have been associated with ozone layer depletion and global warming as they are highly resistant to oxidative degradation and hence have an extremely long half-life.[30] However, the HDF process is fundamentally difficult on both thermodynamic and kinetic grounds. Firstly, the energetic penalty associated with the C-F bond cleavage has to be compensated for by the formation of a stronger X-F bond (X= Si, B, Sn, Al or transition metal). Formation of a C-H bond (CH_3-H = 105 kcal mol^{-1}; C_6H_5-H = 113 kcal mol^{-1}) is not exothermic enough to provide the necessary driving force for the reaction. Secondly, fluorine substituents are weak Lewis bases and fluoride is a poor leaving group, which renders the C-F bond kinetically inert. This issue can be overcome by the employment of organometallic complexes, which facilitate C-F bond activation by lowering activation barriers and consequently M-F and/or M-C bond formation.

In order to develop a truly applicable, and hence catalytic, HDF system and turn it into a viable synthetic tool for the preparation of complex fluorinated molecules, fundamental studies on small and simple perfluorinated model substrates are required to understand the underpinning aspects of the process, such as regio- and chemoselectivity, as well as catalyst activity. Control of regiochemistry is crucial for the synthesis of compounds with a well-defined pattern of fluorine substituents. As will become apparent, in the majority of reported metal catalysed HDF reactions that employ a common model substrate such as pentafluorobenzene (C_6F_5H), it is the C-F bond *para* to the hydrogen that undergoes functionalisation to afford 1,2,4,5-$C_6F_4H_2$. Such reactivity is not unexpected as the same isomer of tetrafluorobenzene is also generated in a traditional stoichiometric nucleophilic aromatic substitution reaction, where $LiAlH_4$ is used as a hydride source (Scheme 1.4).[31] Similarly, chemoselective activation of C-F bonds in the presence of C-H bonds is another potential obstacle that needs to be overcome to realise an efficient HDF system.[32] Although the former is more thermodynamically favourable to cleave, the latter is often kinetically accessible and many second and third row late transition metal complexes display lower activation barriers for C-H bond activation.[33–37]

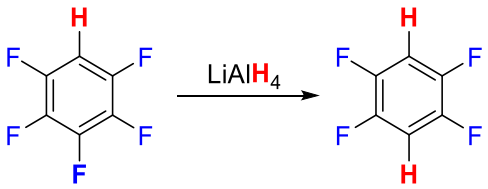

Scheme 1.4: Example of non-catalytic HDF in which a nucleophilic aromatic substitution reaction of C_6F_5H and $LiAlH_4$ leads to the formation of the *para*-substituted isomer of tetrafluorobenzene.

The following sections provide an overview of late transition metal mediated HDF processes, with particular focus on the most recent advances in fluoroaromatic HDF strategies, mechanistic considerations, substrate scope and catalytic performance.

1.3. Catalytic HDF by late transition metal complexes

1.3.1. Group 8: Iron and ruthenium

The only example of iron catalysed HDF was reported by Holland and co-workers, who showed that three- and four-coordinate iron(II) fluorides with bulky β-diketiminate (nacnac) ligands (**Fe1** and **Fe2** respectively) were capable of bringing about catalytic HDF of simple perfluoroarenes in the presence of tertiary silanes (Scheme 1.5).[38] Thus, hexafluorobenzene (C_6F_6), pentafluoropyridine (C_5F_5N) and octafluorotoluene ($C_6F_5CF_3$) each underwent a single HDF step to afford C_6F_5H, 2,3,5,6-C_5F_4HN and 2,3,5,6-$C_6F_4HCF_3$ respectively, consistent with high selectivity for the C-F bond *para* to the most electron-withdrawing group (N or CF_3). Despite high catalyst loading (20 mol %), the reactions did not exceed five turnovers due to catalyst decomposition. Moreover, HDF was found to be greatly influenced by solvent polarity and the silane employed. The highest conversions were achieved with Et_3SiH in THF at just 45°C, while use of $PhSiH_3$ in the same solvent led to complete catalyst deactivation at room temperature. Although catalyst instability hindered detailed mechanistic investigation, it was proposed that the rate-limiting step for the HDF of perfluoroarenes was the generation of an undetected active iron hydride intermediate formed from the iron fluoride and the silane. As no C-F activation was found in the absence of R_3SiH and there was no evidence of reaction between isolated hydride complexes, [{(nacnac)FeH}$_2$] (**Fe3**) and fluoroarenes, the

unseen species was proposed to be the silane adduct of the hydride i.e. [(nacnac)Fe(η^2-R_3SiH)H)] or, alternatively, the silyl complex [(nacnac)FeSiR_3], which would activate aromatic C-F bonds by a nucleophilic attack mechanism. HDF of $C_6F_5CF_3$ with and without dihydroanthracene (DHA) as a radical trap gave an almost identical extent of conversion to 2,3,5,6-$C_6F_4HCF_3$, indicating that outer-sphere electron transfer was unlikely to be in operation. An oxidative addition pathway was also ruled out, as insertion of either of the iron(II) complexes into a C-F bond would result in a formation of uncommon, high-valent (nacnac)Fe(IV) species. There was no catalysis when H_2 was used as the terminal reductant.

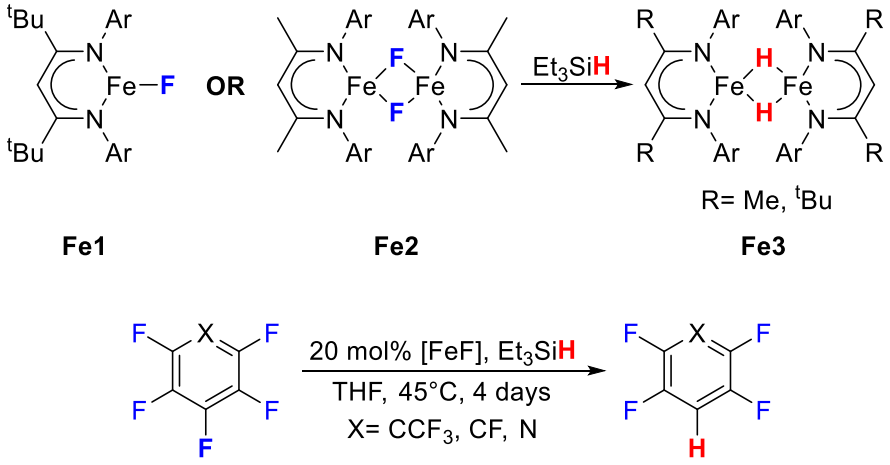

Scheme 1.5: Iron (II) fluoride catalysed HDF of fluoroarenes.

More recent studies on iron promoted C-F activation focused on the stoichiometric reactivity of the electron-rich Fe(0) complex [$Fe(PMe_3)_4$] with fluorinated substrates bearing imine[39] or ketone[40] directing groups, as well as with more common perfluorinated reagents such as octafluorotoluene, hexafluorobenzene and pentafluoropyridine.[41]

For the purpose of this thesis, all work on ruthenium catalysed HDF reported by our group is reviewed in detail in Section 1.4. To date, the only other

example of Ru mediated catalytic HDF is a recent study by Nikonov and Mai who showed that [Cp'Ru(NHC)H_3] (Cp' = Cp, Cp*; NHC = IMes, IPr) complexes can act as efficient precursors for the catalytic HDF of a range of fluoroaromatics using ^{i}PrOH as the reducing agent.[42] Catalytic performance was found to be influenced by the steric bulk of the NHC and Cp' ligands, with the highest activity observed for [Cp*Ru(IPr)H_3]. Importantly, C_6F_5H could be converted to a mixture of 1,2,4,5-$C_6F_4H_2$, 1,2,4-$C_6F_3H_3$ and 1,4-$C_6F_2H_4$ (60, 21 and 7% respectively) in 4 h at 70°C with a catalyst loading of 0.5 mol% in the presence of Na_2CO_3 (1.2 equiv). Kinetic studies were consistent with a mechanism based on NHC dissociation to generate the electron-deficient [Cp*RuH_3] fragment (**Ru1**) which reversibly coordinated fluoroarene (to give **Ru2**; Scheme 1.6). The HDF step was postulated to proceed *via* a nucleophilic attack of a Ru-bound hydride on the fluoroaromatic substrate. Of note was the proposed transition state (**TS(Ru1-Ru2)**) featuring a σ-C-F rather than η^2-(C=C) bond coordination of the fluorinated aromatic ring to the metal centre. Subsequent displacement of the ruthenium bound fluoride ligand in **Ru3** by ^{i}PrOH gave the alkoxide intermediate (**Ru4**), which upon β-H elimination regenerated the catalytically active trihydride species (*via* **Ru5**). Accumulation of HF inhibited the catalysis, although in the presence of stoichiometric amounts of Na_2CO_3, this could be trapped to facilitate the catalytic process.

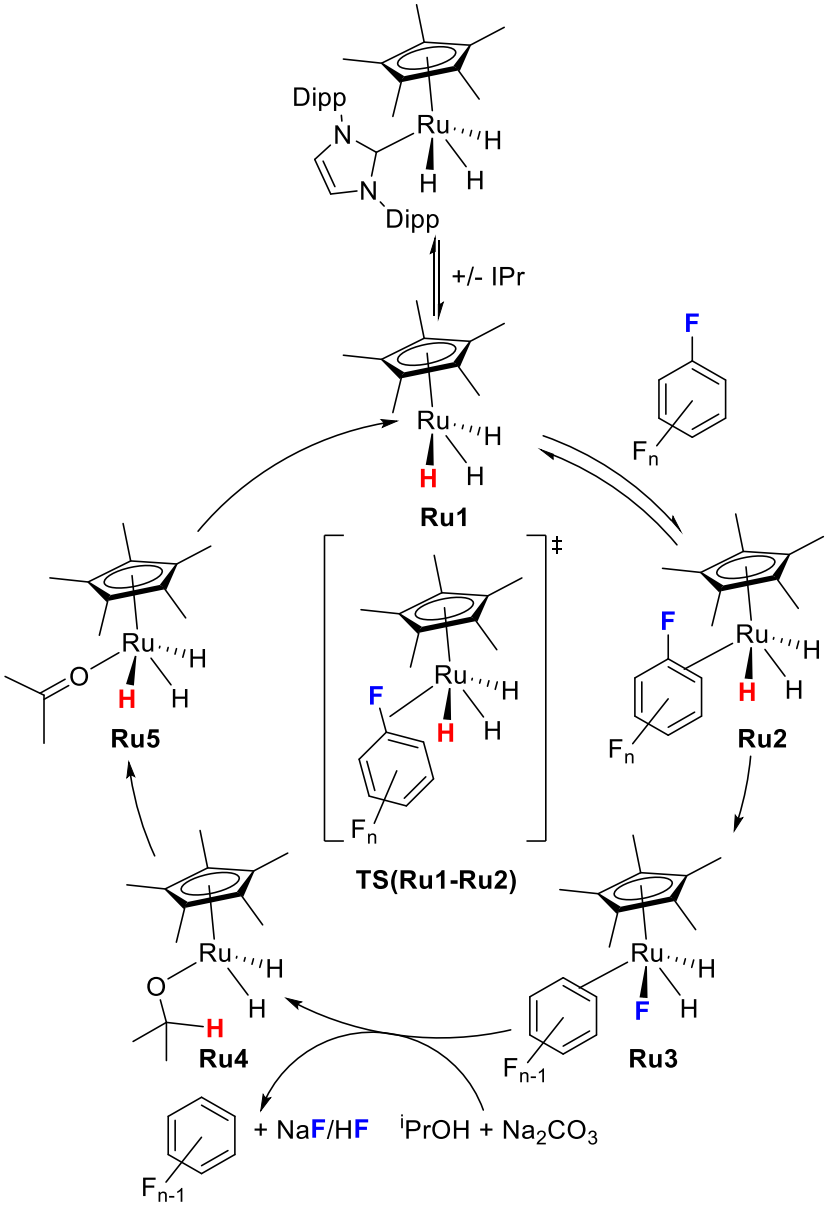

Scheme 1.6: Proposed catalytic cycle for the HDF of fluoroaromatics by [Cp*Ru(IPr)H_3] using ^{i}PrOH.

1.3.2. Group 9: Cobalt, rhodium and iridium

In 2013, Li and coworkers reported the monohydrodefluorination of perfluoroarenes catalysed by [Co(PMe_3)$_4$] using sodium formate as the hydrogen source.[43] Selective *para*-C-F bond activation was observed for octafluorotoluene, pentafluoropyridine and pentafluorobenzene to afford 2,3,5,6-$C_6F_4HCF_3$, 2,3,5,6-

C_5F_4HN and 1,2,4,5-$C_6F_4H_2$ respectively. The reactions proceeded with high conversions (73-100%) under relatively mild conditions (80°C) using 10 mol% of cobalt precursor. The reaction mechanism was studied by NMR and *in situ* IR spectroscopy, which allowed the identification of key intermediates shown in Scheme 1.7. The first step of the proposed catalytic cycle involved oxidative addition of the C-F bond of the perfluoroarene substrate at the Co(0) centre to afford the Co(II) aryl fluoride complex (**Co1**). This was followed by F^-/$HCOO^-$ ligand exchange (to generate **Co2**) and subsequent decarboxylation of the carboxyl group to give the Co(II) aryl hydride species (**Co3**). Subsequent reductive elimination of the HDF product completed the cycle.

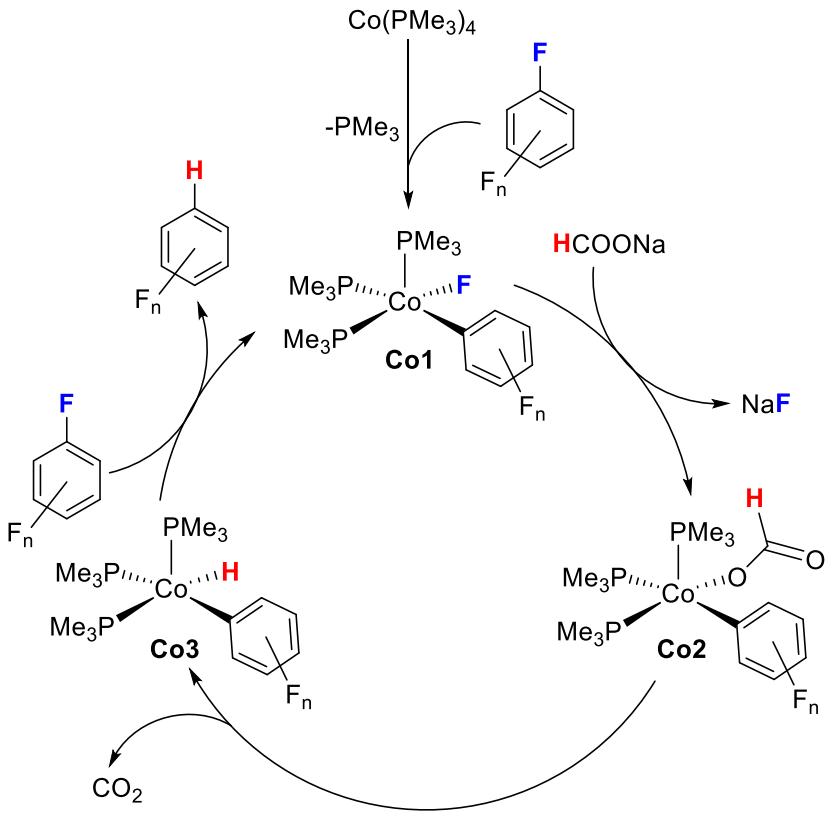

Scheme 1.7: Catalytic cycle for the HDF of perfluoroarenes by [$Co(PMe_3)_4$].

Rhodium complexes have proved to be among the most efficient and most prevalent compounds for C-F activation. Indeed, the Rh(I) silyl complex,

[$Rh(PMe_3)_3(SiMe_2Ph)$], was the first homogeneous catalyst for the HDF of C_6F_6 and C_6F_5H (Scheme 1.8).[44] The initial C-F bond activation step to bring about metathesis of the silyl complex (**Rh1**) to the fluoroaryl species (**Rh2**) was postulated to involve either electron transfer from the metal centre to the substrate with generation of a perfluorobenzyl radical followed by F^- attack on silicon, or a redox process featuring insertion of rhodium into a C-F bond followed by elimination of Si-F. Regeneration of **Rh1** was achieved by oxidative addition of R_3Si-H to give a six-coordinate Rh(III) species (**Rh3**) followed by C-H reductive elimination. Turnover numbers of up to 38 and 33 were achieved for C_6F_6 and C_6F_5H respectively. High chemo- and (*para*-) regioselectivity was evidenced by a selective conversion of C_6F_5H to 1,2,4,5-$C_6F_4H_2$. Hydrogenolysis of C-F bonds was also achieved using H_2 as a hydrogen source.[45] However, in this case base was required for the C-F activation step to take place. The exact mechanism for this central step of the catalytic cycle was postulated to involve electron transfer from the rhodium hydride complex (E= H; **Rh4**) to the fluoroaromatic substrate and concomitant release of the F^- anion.

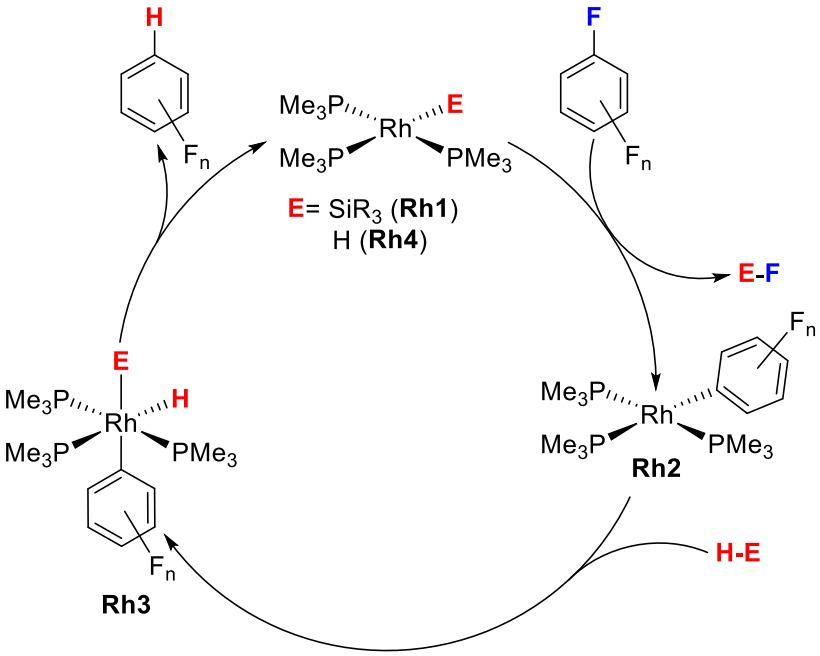

Scheme 1.8: Catalytic cycle for the HDF of fluoroarenes by $[Rh(PMe_3)_3E]$ (E= SiR_3, H).

Grushin employed $[Rh(PCy_3)_2(H)Cl_2]$ (5 mol%) for the catalytic hydrogenolysis of the C-F bond in the nonactivated substrate 1-fluoronaphthalene substrate, which was converted to naphthalene in >90% selectivity at 45% conversion under 5.5 atm H_2 and highly basic conditions (40% NaOH).[46] Due to the generation of a mixture of electron-rich Rh hydride complexes, the exact nature of the catalytically active species was unclear, making mechanistic considerations impossible. Interestingly, residual air rendered the reaction heterogeneous and allowed for the reduction of highly unreactive fluorobenzene to benzene with 55% conversion and a TON value of 88. Formation of toluene, anisole or aniline was also achieved from the HDF of the corresponding monofluoroarenes with 35, 29 and 95% conversion respectively.

Braun's laboratory described catalytic HDF of pentafluoropyridine to 2,3,5,6-tetrafluoropyridine using $[Rh(PEt_3)_3(4\text{-}C_5NF_4)]$ as the catalyst and H_2 (1 atm)

as the reductant, with turnover numbers of up to 12 after 2 days at room temperature.[47] The same research group later reported HDF of a range of fluorinated aromatics (hexa- and pentafluorobenzene, pentafluoropyridine and 2,3,5,6-tetrafluoropyridine) catalysed by the dimetallic rhodium hydride complex, [{Rh(dippp)(μ-H)}$_2$] (**Rh5**) in the presence of Et_3SiH.[48] With a modest catalyst loading of 5 mol %, turnover numbers of up to 19 were achieved after 48 h at 50°C. Under stoichiometric conditions, **Rh5** reacted with 2,3,5,6-C_5F_4HN and C_6F_5H to give the corresponding $(\mu\text{-F})_2$ bridged dimer [{Rh(dippp)(μ-F)}$_2$] (**Rh6**) and the 1,2-hydrodefluorinated products, 2,3,6-$C_5F_3H_2N$ and 1,2,3,4-$C_6F_4H_2$ respectively. This *ortho*-regioselectivity contrasted to the *para*-regioselectivity observed under catalytic conditions. The difference was suggested to be a consequence of two competing catalytic cycles (Scheme 1.9). **Rh6** was found to react with Et_3SiH to give Et_3SiF and either **Rh5** to close the cyclic process, or alternatively form the η^2-silane hydride intermediate (**Rh7**), which rapidly releases Et_3SiH to generate the highly reactive mononuclear rhodium hydride species, [Rh(dippp)H] (**Rh8**). This could undergo dimerisation to regenerate **Rh5** or react with fluoroarene with *para*-regioselectivity to complete the second catalytic cycle.

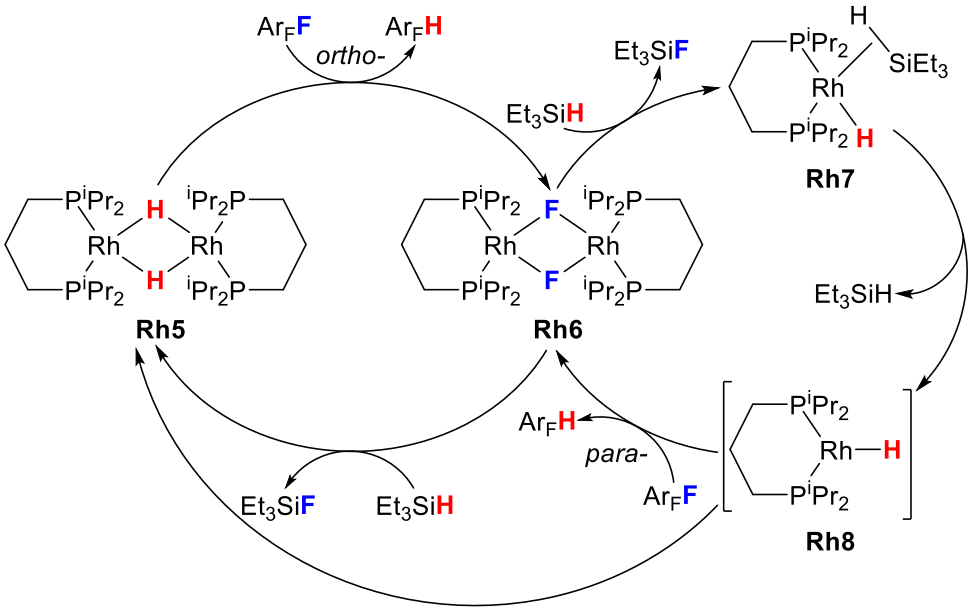

Scheme 1.9: Catalytic cycle for the HDF of fluoroarenes by [{Rh(dippp)(μ-H)}$_2$].

Ogo and co-workers developed a new Rh(I) catalyst, [Cp*Rh(bpy)] (**Rh9**) for the efficient HDF of $C_6F_5CF_3$, $C_6F_5CH_3$, C_6F_6 and C_6F_5H.[49] The highest turnover number of 380 was achieved after 48 h at room temperature for hexafluorobenzene using 0.1 mol % catalyst loading and ~8 atm H_2. HDF of octafluorotoluene, 2,3,4,5,6-pentafluorotoluene and pentafluorobenzene proceeded with high *para*-regioselectivity to afford 2,3,5,6-$C_6F_4HCF_3$, 2,3,5,6-$C_6F_4HCH_3$ and 1,2,4,5-$C_6F_4H_2$ respectively. C-F bond activation was shown to occur *via* a nucleophilic aromatic substitution pathway to afford the isolable cationic Rh(III) fluoroaryl complex (**Rh10**; Scheme 1.10), which reacted with H_2 to release the HDF product and generate the undetectable Rh(III) hydride species **Rh11**. Base (Et_2NH) assisted Rh-H cleavage, releasing H and reforming **Rh9**.

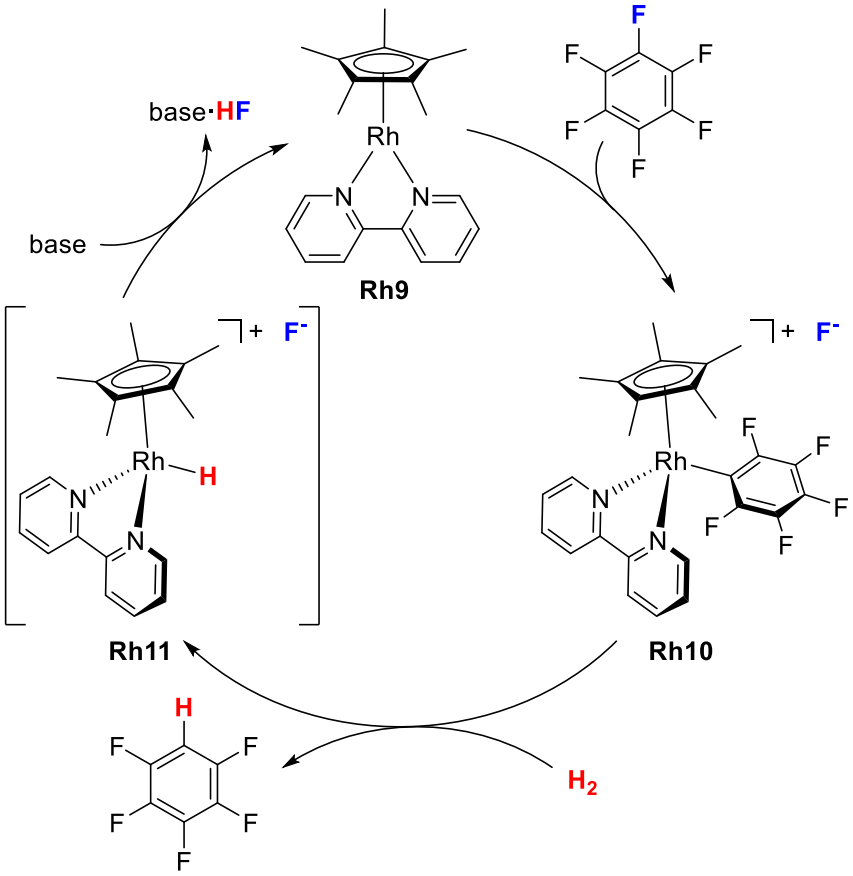

Scheme 1.10: Catalytic cycle for the HDF of C_6F_6 by [Cp*Rh(bpy)].

Around the same time, Crimmin's group reported the use of [Cp*Rh(μ-Cl)Cl]$_2$ as a highly efficient and selective precatalyst for the HDF of a series of partially fluorinated arenes using a β-diketiminate aluminium dihydride ((nacnac)AlH$_2$) as the terminal reductant.[50] Of note was the highly regioselective activation of a C-F bond *ortho* to an existing C-H bond (Scheme 1.11; Section 1.4), such that for example pentafluorobenzene was converted to a mixture of 1,2,3,4-$C_6F_4H_2$, 1,2,3-$C_6F_3H_3$ and 1,2-$C_6F_2H_4$. The optimal reaction conditions employed a temperature of 100°C and 2 mol% catalyst loading in the presence of 1 equiv of (nacnac)AlH$_2$. This particular reductant proved to be crucial for the overall HDF process, as no HDF took place with Et_3SiH or $PhSiH_3$. Moreover, a stoichiometric reaction between (nacnac)AlH$_2$

and the rhodium chloride precatalyst afforded a new, catalytically competent heterobimetallic complex featuring an uncommon Rh-H-Al interaction.

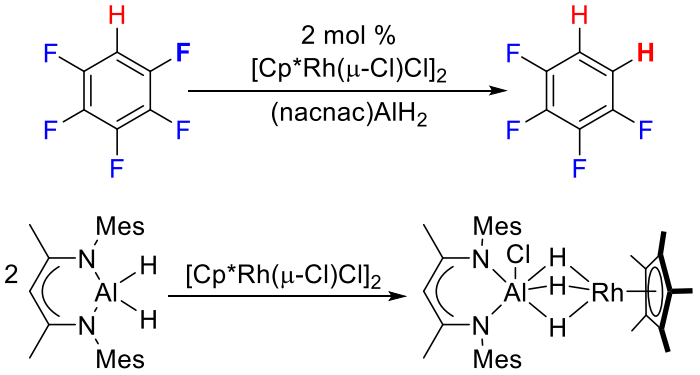

Scheme 1.11: Catalytic HDF of C_6F_5H using [Cp*RhCl(μ-Cl)Cl]$_2$ and (nacnac)AlH_2 (top), and synthesis of the Rh/Al heterobimetallic species (bottom).

Schwartsburd et al. carried out mechanistic studies on the catalytic HDF of polyfluorotoluenes ($C_6F_5CF_3$ and 2-$C_6F_4HCF_3$) in the presence of Et_3SiH using 6-membered ring NHC rhodium hydride complexes, [Rh(6-NHC)$(PPh_3)_2$H] (NHC = 6^{i}Pr (**Rh12**), 6-Et, 6-Me; Scheme 1.12).[51] These were shown to facilitate up to three HDF steps on octafluorotoluene to afford 2,5-$C_6F_2H_3CF_3$ and a corresponding Rh-F complex (e.g. [Rh(6-^{i}Pr)$(PPh_3)_2$F] (**Rh13**)). However, their effectiveness was suppressed by the competing C-H activation of lower fluorine containing aromatics (e.g. 2,3,5,6-$C_6F_4HCF_3$) and irreversible formation of Rh-fluoroaryl complexes, such as [Rh(6-^{i}Pr)$(PPh_3)_2(C_6F_4CF_3)$] (**Rh14**).

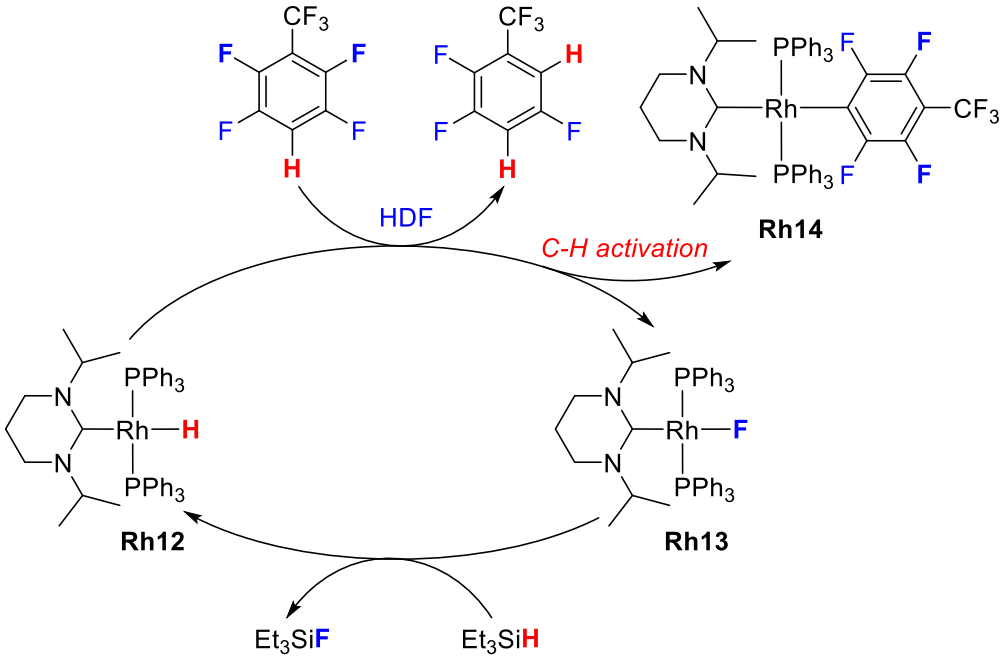

Scheme 1.12: Competing C-F (HDF) and C-H activation pathways of [Rh(6-^{i}Pr)(PPh_3)$_2$H] with 2,3,5,6-$C_6F_4HCF_3$.

Weaver exploited the tris[2-phenylpyridinato-C,N]iridium(III) ([Ir(ppy)$_3$]) complex for the first photocatalytic HDF of a series of fluorinated aromatics *via* an outer-sphere electron transfer mechanism using Et^{i}Pr$_2$N as the hydrogen source.[52] The choice of the catalyst was based on its coordinative saturation and hence inability to form a M-F bond, which in turn avoided the need for fluorophilic terminal reductants. The proposed mechanism for the reaction is shown in Scheme 1.13. The initially generated $C_6F_6^{\bullet-}$ species was postulated to fragment into a fluoride anion and a $C_6F_5^{\bullet}$ radical, which would abstract a proton from the amine radical cation to ultimately afford C_6F_5H and an iminium cation. A number of perfluoroarenes containing a variety of functional groups such as trifluoromethyl, ketone, ester, nitrile, oxazole or aliphatic amine, could be quantitatively monohydrodefluorinated. The effectiveness of the catalyst was evaluated by

determining the TON in the presence of C_5F_5N. The outstanding value of 22,550 was achieved after 96 h at 45°C.

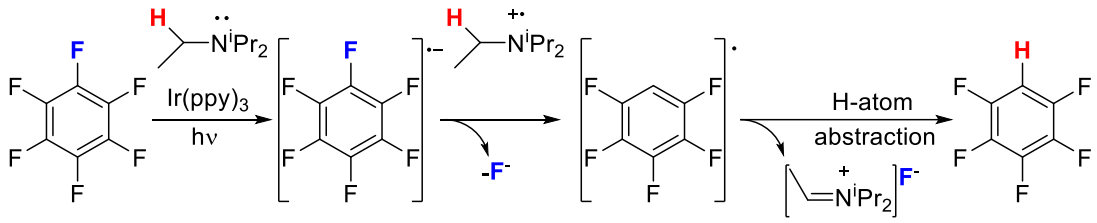

Scheme 1.13: Potential mechanism for the photocatalytic HDF of hexafluorobenzene by [Ir(ppy)$_3$] in the presence of Et^{i}Pr$_2$N.

More recently, the efficient HDF of fluorinated aromatics was achieved with transfer hydrogenation catalysts possessing a bifunctional Ir/NH moiety.[53] Half sandwich complexes bearing a C-N chelating ligand derived from benzylic amines (**Ir1** and **Ir2**) promoted HDF of a variety of electron-deficient perfluoroarenes (C_6F_5CN, $C_6F_5NO_2$, $C_6F_5SO_2NMe_2$, $C_6F_5CF_3$, $C_6F_5COCH_3$, $C_6F_5COOCH_3$) in the presence of ^{i}PrOH or K_2CO_2H (Scheme 1.14). The remarkable activity of the system was demonstrated in the conversion of pentafluoropyridine to 2,3,4,6-C_5F_4HN after 1 h at room temperature. The TON for this reaction exceeded 250 at a catalyst loading of 0.2 mol%. Preliminary mechanistic studies involving treatment of a model for the catalytic intermediate (**Ir3**) with stoichiometric amounts of C_5F_5N indicated that the reaction involved nucleophilic attack of the Ir-H on the fluoroarene substrate.

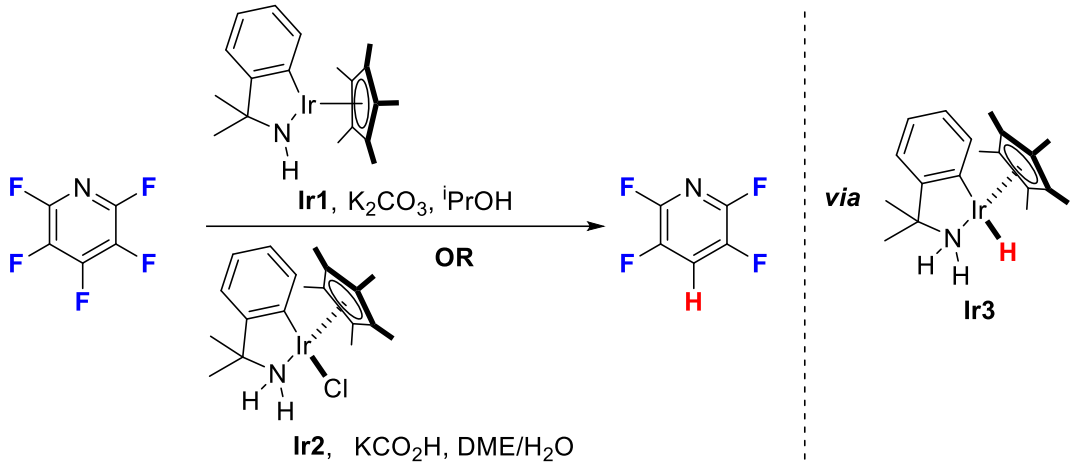

Scheme 1.14: Catalytic HDF of pentafluoropyridine by iridium amine and amido complexes.

1.3.3. Group 10: Nickel, palladium and platinum

HDF of fluoronaphthalene, fluorotoluene, fluoroanisole and fluoropyridine by a postulated monocoordinate Ni(0) IMes complex **Ni1** (generated *in situ* from $Ni(acac)_2$, Et_2CHONa and NaH) was the first example of homogeneous catalytic C-F bond reduction using nickel and the first example of an HDF process in which a transfer hydrogenation approach strategy was adopted (Scheme 1.15).[54] After 3 h at 100°C, substrates such as 2-fluoroanisole and 2-fluoronaphthalene were converted to the corresponding HDF products in quantitative yield. The catalysis was thought to be initiated by the insertion of **Ni1** into the C-F bond of a substrate to afford a Ni(II) fluoroaryl fluoride complex (**Ni2**), which underwent F^-/Et_2CHO^- exchange to give the alkoxide species **Ni3**. Loss of ketone gave a Ni(II) fluoroaryl hydride intermediate (**Ni4**), which then reductively eliminated Ar^F-H to complete the cycle.

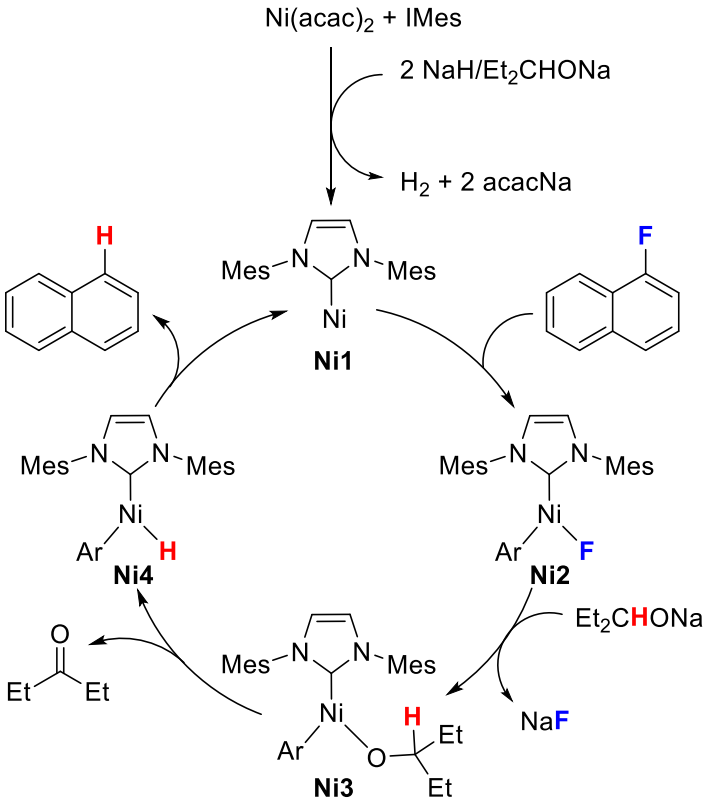

Scheme 1.15: Proposed catalytic cycle for the HDF of fluoroarenes by an *in-situ* generated "[Ni(NHC)]" fragment.

Cao and co-workers employed $LiBEt_3H$ and $LiAl(O^tBu)_3H$ as the reductants for the HDF of a variety of fluoroarenes and trifluorotoluenes with $NiCl_2$ and $[Ni(PCy_3)_2Cl_2]$ as precatalysts. The combination of $NiCl_2/LiBEt_3H$ reduced both sp^2 and sp^3 hybridised C-F bonds, albeit at a high catalyst loading (40 mol %), whilst the bisphosphine complex was selective for aromatic C-F bonds at a significantly lower concentration (5 mol%).[55] An improved catalytic protocol utilised both nickel precursors as cocatalysts at 2 mol % loading,[56] while the replacement of $LiBEt_3H$ by the cheaper and safer $LiAl(O^tBu)_3H$ allowed for the use of just $[Ni(PCy_3)_2Cl_2]$.[57] This system was capable of multiple HDF steps, converting both $C_6F_5CF_3$ and $C_6H_5CF_3$ to toluene, and hexafluorobenzene to benzene, in yields of 73, 80 and 53% respectively. The reaction was postulated to involve a PCy_3 supported Ni(0)/Ni(II)

redox couple (Scheme 1.16), akin to that in the aforementioned Ni-NHC system. Thus, the dichloride precatalyst was reduced with $LiAl(O^tBu)_3H$ to the two-coordinate Ni(0) complex, $[Ni(PCy_3)_2]$ (**Ni5**) which oxidatively added the C-F bond of the aryl fluoride to give the new Ni(II) fluoroaryl fluoride species **Ni6**. Fluoride abstraction (to generate **Ni7**) and reductive elimination from the nickel aryl hydride complex (**Ni8**) furnished the HDF product regenerating the active Ni(0) species **Ni5**.

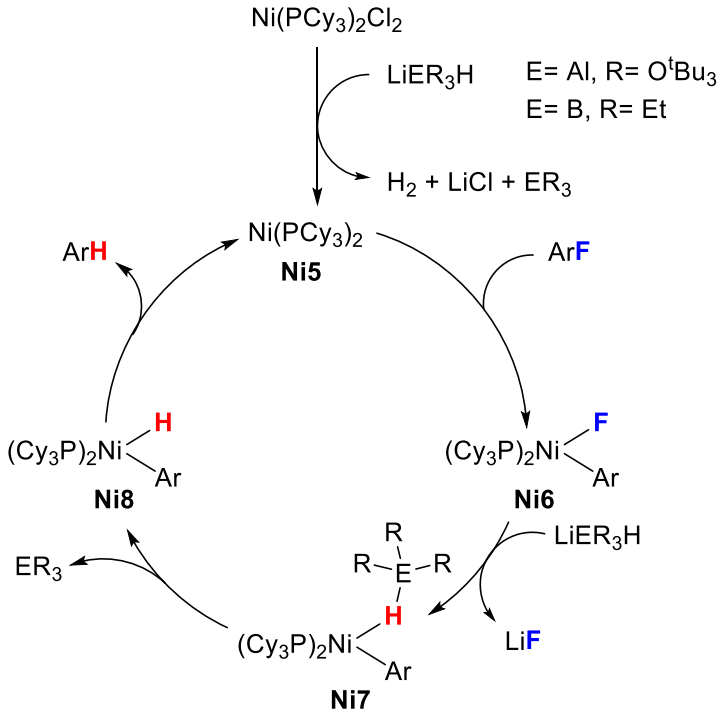

Scheme 1.16: Catalytic cycle for the HDF of fluoroarenes by $[Ni(PCy_3)_2Cl_2]$.

Radius developed a dimeric Ni-NHC complex, $[Ni_2(I^iPr_2)_4(COD)]$ for the *para*-regioselective HDF of hexafluorobenzene and octafluorotoluene in the presence of silanes.[58] Thus, with C_6F_6, 1,2,4,5-$C_6F_4H_2$ was formed after 2 days at 60°C with 5 mol % of the Ni(0) catalyst. Experimental findings pointed to a mechanism (Scheme 1.17) involving fluoroarene coordination to the mononuclear fragment $[Ni(I^iPr_2)_2]$ (**Ni9**), C-F oxidative addition (at **Ni10**) to give a Ni(II) fluoroaryl fluoride species (**Ni11**), H/F exchange with the silane reductant and lastly

reductive elimination of the HDF product from the Ni(II) fluoroaryl hydride complex **Ni12**, *via* **Ni13**.

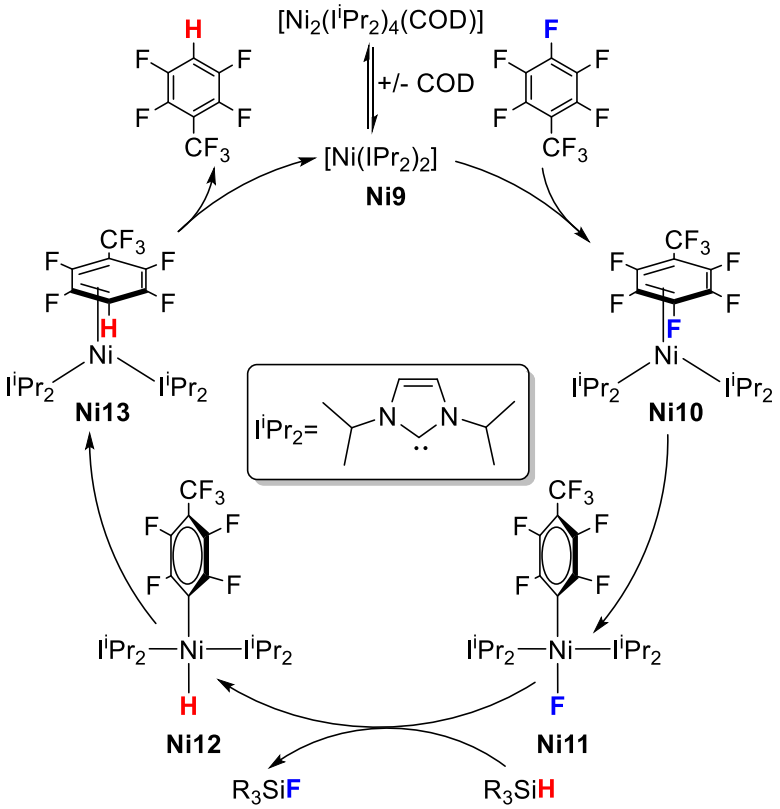

Scheme 1.17: Catalytic cycle for the HDF of octafluorotoluene by [Ni(I^iPr_2)$_2$].

The η^2-coordination of perfluoroarene could be directly observed in the reaction of C_6F_6 with a different dinuclear nickel complex, [Ni(dippe)(μ-H)]$_2$.[59] The hexafluorobenzene ring was found to insert between the two [Ni(dippe)] fragments prior to oxidative addition of the C-F bond to afford [Ni(dippe)(C_6F_5)H]. At 5 mol % catalyst loading, the hydride bridged dimer promoted HDF of a series of perfluoroarenes (C_6F_6, C_6F_5H, 1,2,3,4-$C_6F_4H_2$ and C_5F_5N) in the presence of excess PEt_3 and Et_3SiH to yield *para*-substituted products (1,2,4,5-$C_6F_4H_2$, 1,2,4-$C_6F_3H_3$ and 2,3,5,6-C_5F_4HN respectively) in high yields (94-100%) with turnover numbers of ca. 40 after 3 days at 120°C. In the absence of added phosphine, lower yields, poorer selectivities and catalyst degradation were observed. Further investigation

revealed that PEt_3 was capable of mediating HDF of fluoroarenes by itself, rendering the process metal- and silane-free with quantitative yields under the exact conditions used previously in the presence of Ni. The proposed mechanism for the uncatalysed formation of the HDF products involved nucleophilic attack by the very basic PEt_3 followed by F-migration to phosphorus, β-hydride elimination to release ethene, nucleophilic hydride addition and finally elimination of the fluorophosphine Et_2FP (Scheme 1.18).

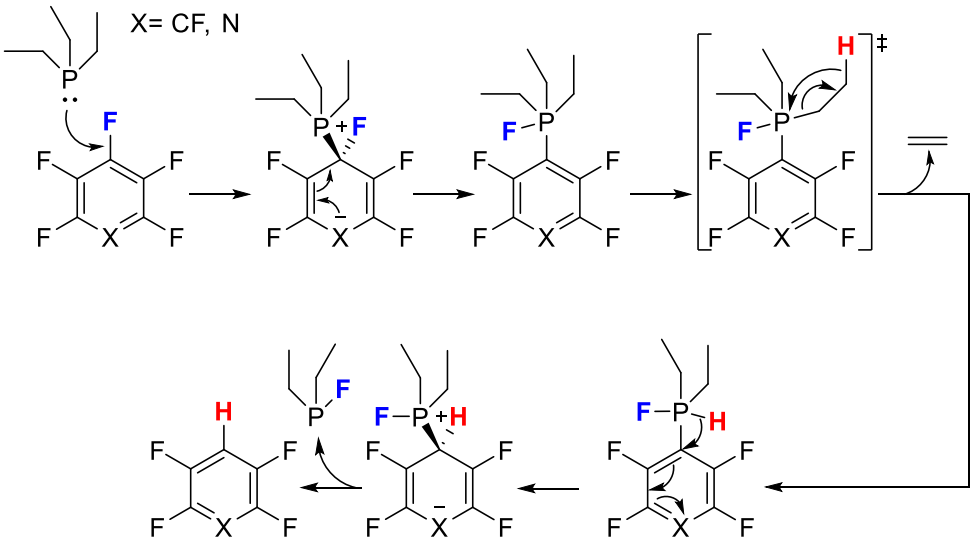

Scheme 1.18: Proposed mechanism for the phosphine mediated HDF of perfluoroarenes.

Zhang's group developed an efficient method for the preparation of partially fluorinated aromatics in nickel and palladium catalysed, chelation-assisted HDF of N-heterocycle-substituted polyfluoroarenes (e.g. 2-(pentafluorophenyl)-pyridine) with Et_3SiH (Scheme 1.19). Simple and readily available Ni[60] and Pd[61] complexes ($NiCl_2 \cdot 6H_2O$ and $[Pd(C_3H_5)Cl]_2$) in the presence of ancillary ligands (phen or dppe) afforded *ortho*-hydrodefluorinated products in moderate to high yields.

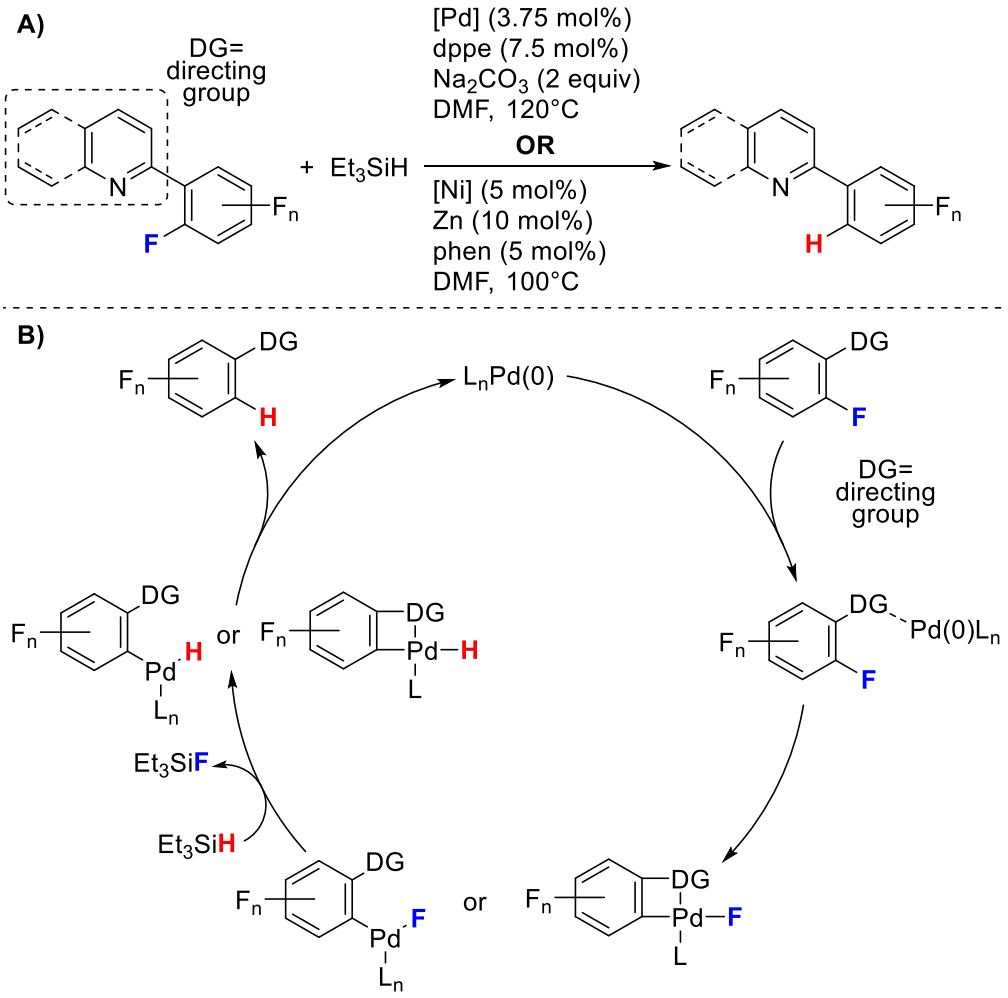

Scheme 1.19: A) Palladium- and nickel-catalysed *ortho*-selective HDF of N-containing-heterocycle polyfluoroarenes, B) Proposed mechanism for the Pd mediated, chelation-assisted HDF process.

The bisphosphine palladium (0) complexes, $[Pd(PR_3)_2]$ (R = ^{i}Pr, Cy) were shown to catalyse HDF of pentafluoropyridine using HBPin as the hydrogen source.[62] After 3 days at 60°C, 2,3,5,6-tetrafluoropyridine was selectively obtained in yields of 44 and 30% with 10 mol% $[Pd(P^{i}Pr_3)_2]$ and $[Pd(PCy_3)_2]$ respectively. Employment of $[Pd(P^{i}Pr_2(CH_2CH_2OCH_3))_2]$ led to superior catalytic performance and led to higher conversions (80%) at lower catalyst loading (5 mol %) over shorter reaction time (2 days).[63] The catalytic cycle resembled those for previously described nickel systems and involved a Pd(0)/Pd(II) redox couple (Scheme 1.20).

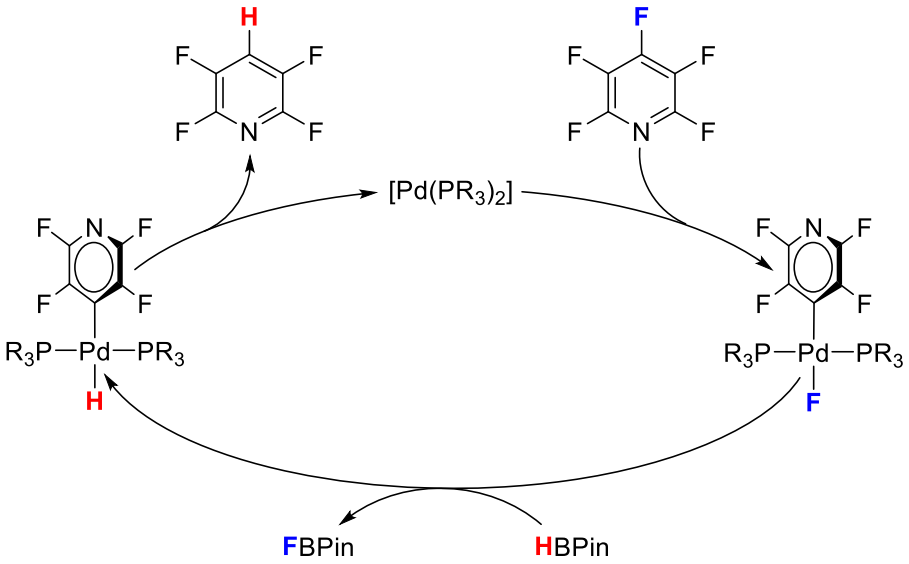

Scheme 1.20: Catalytic cycle for the HDF of pentafluoropyridine by $[Pd(PR_3)_2]$ complexes.

1.3.4. Group 11: Copper and gold

In the presence of $PhMe_2SiH$, the combination of CuCl, KO^tBu and bis(diphenylphosphino)benzene (BDP) exhibited high HDF reactivity towards a broad scope of polyfluoroarenes with preferred *para*-regioselectivity.[64] For example, after 12 h, 3 mol% CuCl/KO^tBu together with 1 mol% BDP gave conversions of 60 and 95% of pentafluorobenzene and pentafluoropyridine to 1,2,4,5-$C_6F_4H_2$ and 2,3,5,6-C_5F_4HN respectively. NMR studies suggested a copper hydride complex, [(BDP)CuH] to be the catalytically active species, which interconverted to the copper fluoride intermediate, [(BDP)CuF] in the HDF step (Scheme 1.21). DFT calculations supported a mechanism involving a concerted nucleophilic attack of Cu-H on the C-F bond.

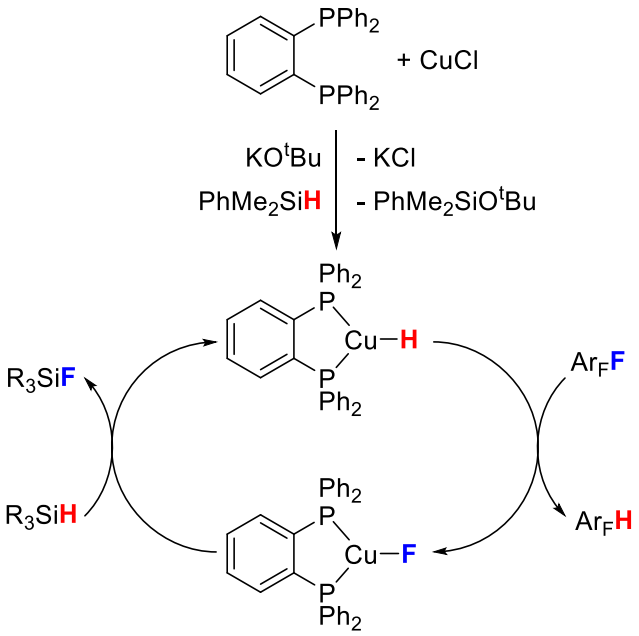

Scheme 1.21: Catalytic cycle for the HDF of fluoroarenes by BDP stabilised copper hydride species.

Tricoordinate gold(I) complexes supported by xantphos-type ligands proved to be remarkably active catalysts for the HDF of a series of perfloroarenes.[65] For example, up to 1000 turnovers could be achieved for pentafluoronitrobenzene with 1 mol% of [(^{t}BuXantphos)Au][$AuCl_2$] and diphenylsilane after 24 h at 80°C. The system tolerated a broad range of functional groups, allowing selective HDF to be performed in the presence of ketone, ester, carboxylate, alkenyl, alkynyl and amide groups. DFT studies on a model pentafluoropyridine substrate indicated that the key step in the catalytic cycle (Scheme 1.22) was the direct oxidative addition of a C-F bond to the two-coordinate cationic Au(I) centre **Au1** to give the tetrafluoropyridyl fluoride intermediate **Au2**. Release of the HDF product from **Au2** and regeneration of **Au1** occurred *via* an unusual 5-membered ring transition state in which the silane was bound to both the Au-F and the *ipso*-carbon of the coordinated fluoroaryl ligand (**Au3**).

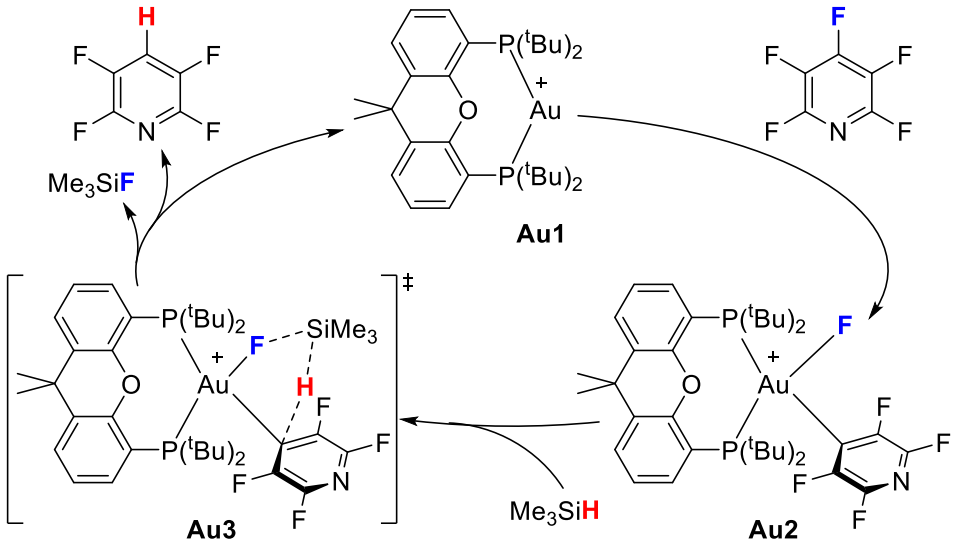

Scheme 1.22: Catalytic cycle for the HDF of pentafluoropyridine by a ^{t}BuXantphos supported Au(I) complex.

An unusual HDF mechanism rationalised the reactivity of the NHC supported gold(I) hydride complexes shown in Scheme 1.23.[66] Although [(IMes)AuH] (**Au4**) failed to activate C-F bonds of $C_6F_5NO_2$, a π-π interaction between the two reagents could be detected by NMR and UV-vis spectroscopy. In the presence of silane, poor conversions to tetrafluoronitrobenzene were achieved (18%) due to the high calculated activation barrier of 40.8 kcal mol^{-1}. However, upon addition of strongly electron-donating *p-N,N*-dimethylaminopyridine (DMAP), the reaction became catalytic, affording the *para*-substituted HDF product 2,3,5,6-$HC_6F_4NO_2$ in a high yield (90%). The formation of a π-π interaction between DMAP and $C_6F_5NO_2$ facilitated hydrogen transfer from **Au4** to the pyridyl N atom of DMAP and lowered the C-F bond activation barrier from an unrealistic 40.8 kcal mol^{-1} to 31.6 kcal mol^{-1}. Two possible mechanisms for the catalytic HDF cycle were proposed on the basis of combined experimental and theoretical studies. In the absence of DMAP, the π-π complex formed between **Au4** and $C_6F_5NO_2$ promotes oxidative addition of the C-F bond to afford the gold (III) species,

[(IMes)Au($C_6F_4NO_2$)HF] (**Au5**), which subsequently converts to gold (I) fluoride, [(IMes)AuF] (**Au6**) upon reductive elimination of 2,3,5,6-$HC_6F_4NO_2$. In the presence of DMAP, **Au4** interacts with the π-π stacked DMAP/$C_6F_5NO_2$ intermediate leading to protonation of the pyridyl nitrogen prior to HDF of $C_6F_5NO_2$, release of 2,3,5,6-$HC_6F_4NO_2$, and formation of **Au6**.

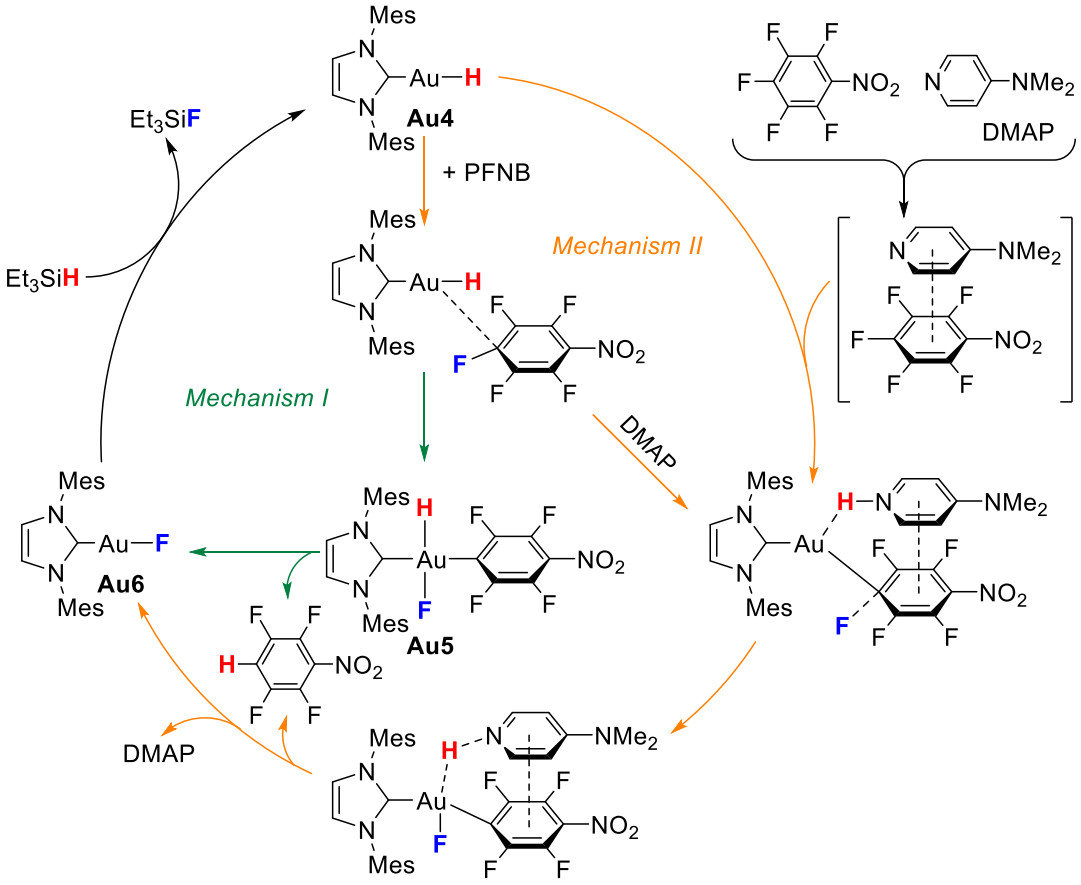

Scheme 1.23: Computed catalytic cycle for the HDF of $C_6F_5NO_2$ by [(IMes)AuH] in the absence (Mechanism I) and presence (Mechanism II) of DMAP.

1.3.5. Heterodimetallic systems

Mata et al. designed a heterodimetallic triazolyl-di-ylidene bridged ruthenium-palladium complex (**RuPd**), which proved to be a very efficient catalyst for the HDF of aromatic and aliphatic C-F bonds of low fluorine content arenes (e.g.

1,4-$C_6F_2H_4$, 1,2-$C_6F_2H_4$ and C_6FH_5) and trifluoromethyltoluenes respectively (Scheme 1.24).[67] Quantitative yields could be achieved for most substrates in short reaction times and under mild reaction conditions (0.5-5 mol % catalyst loading, 80°C, 1-2 h), with TON values as high as 660. However, the catalyst showed poor C-F bond chemoselectivity, as the reduction of C-Br, C-Cl and C=O bonds was also observed. A 1:1 mixture of the two respective homobimetallic complexes (Pd/Pd and Ru/Ru) led to poorer product yields (e.g. 49 % of C_6H_6 in the reaction with C_6FH_5), while the two individual species were totally inactive. This indicated the synergistic action of the two metals within the single-frame ligand. It was proposed that the Pd centre mediated C-F activation and that the Ru centre brought about reduction of the substrate *via* transfer hydrogenation from ^{i}PrOH/NaO^{t}Bu. The same research group later co-immobilised related pyrene-tagged palladium and ruthenium monomeric complexes onto a reduced graphene oxide surface to obtain a heterogeneous system that was a highly effective catalyst for the HDF of a range of fluoroarenes.[68]

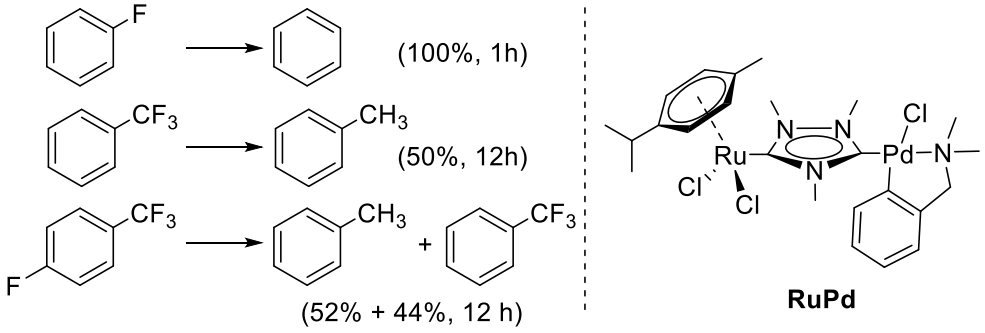

Scheme 1.24: Catalytic HDF of aromatic and aliphatic C-F bonds by the heterodimetallic Ru/Pd complex (**RuPd**). Numbers in parentheses are the reported yields and reaction times respectively.

1.4. Ruthenium N-heterocyclic carbene dihydride complexes

In 2009, our group developed a series of ruthenium NHC dihydride complexes, $[Ru(NHC)(PPh_3)_2(CO)H_2]$ (NHC= IPr (**I**), IMes (**II**)) for the catalytic HDF of C_6F_6, C_6F_5H and C_5F_5N with alkylsilanes (Scheme 1.25A).[69] Most remarkable was the very high (98%) and unusual *ortho*-regioselectivity (Section 1.3) exhibited by **I** (10 mol%), which converted pentafluorobenzene to the 1,2,3,4-isomer of $C_6F_4H_2$ in 20 h at 70°C in THF with Et_3SiH (TON= 7.0, TOF= 0.36 h^{-1}). Kinetic studies indicated that the process was initiated by the loss of PPh_3 to give the 16 electron species, $[Ru(NHC)(PPh_3)(CO)H_2]$ which carried out stoichiometric C-F activation of C_6F_5H to afford isolable, coordinatively unsaturated hydride fluoride complexes, $[Ru(NHC)(PPh_3)(CO)HF]$. The catalytic cycle was closed by the silane acting as a terminal reductant and providing hydrogen to regenerate the catalytically active dihydride. A driving force for the reaction was the formation of the strong Si-F bond in the fluorosilane byproduct. The unusual selectivity of the reaction was investigated with the aid of DFT calculations on the IMes system (**II**), which revealed two possible pathways for the HDF process (Scheme 1.25B).[70,71] The stepwise pathway begins with the coordination of C_6F_5H to the five-coordinate monophosphine dihydride species **A** (E = + 5.5 kcal mol^{-1}) to give the η^2-fluoroarene adduct **B** (E = +8.6 kcal mol^{-1}), followed by the intramolecular nucleophilic attack of the ruthenium hydride ligand at the *ortho*-position on the bound C_6F_5H ring. The resultant Meisenheimer type intermediate **C** (E = +15.9 kcal mol^{-1}) is stabilised by the interaction between the metal centre and the aromatic carbon *ortho* to the C-H bond. The rate determining C-F bond cleavage step leads to the elimination of HF and simultaneous formation of the Ru-σ-flouroaryl complex **D** (E = -8.4 kcal mol^{-1}). Finally, protonolysis of the Ru-C bond by a weakly associated HF molecule,

accompanied by the transfer of F to Ru, affords the hydride fluoride complex **E** (*E* = -36.3 kcal mol^{-1}) and the HDF product, 1,2,3,4-$C_6F_4H_2$. In the concerted pathway, direct Ru-H/C-F exchange takes place in an intramolecular fashion to afford the *para*-substituted isomer of tetrafluorobenzene, 1,2,4,5-$C_6F_4H_2$ in a single step. The stepwise mechanism was found to be more kinetically accessible with an overall computed energy barrier 4.7 kcal mol^{-1} below that for the concerted mechanism, consistent with the *ortho*-selectivity observed experimentally. Moreover, the nature of the NHC ligands was shown to play a crucial role in both promoting the HDF process and dictating the regioselectivity. The full experimental system (**II**) facilitated the PPh_3/C_6F_5H substitution and stabilised the key C-F bond breaking transition state through F···HC interactions, which also accounted for a modest computed activation barrier (20.0 kcal mol^{-1}) for the generation of 1,2,3,4-$C_6F_4H_2$, significantly lower than for the other tetrafluorobenzene isomers, 1,2,3,5- and 1,2,4,5-$C_6F_4H_2$ (22.9 and 22.8 kcal mol^{-1} respectively). In comparison, a less sterically encumbered model system for calculations, $[Ru(IMe_2)(PH_3)_2(CO)H_2]$ yielded higher barriers for both steps. Although C-H activation of C_6F_5H was predicted to be kinetically accessible, its reversibility implied that activation of C-F bonds could be targeted in the presence of C-H bonds. Theoretical studies were extended to define the scope and regioselectivity of HDF in other $C_6F_{6-n}H_n$ species (Figure 1.2). The results showed that the C-F bond dissociation energies not only increased with larger n, but were also determined by the number of *ortho*-F and, to a lesser extent, *meta*-F substituents present. For the concerted pathway, HDF occurred preferentially at sites with two *ortho*-fluorines (e.g. 2-position in 1,2,3,4-$C_6F_4H_2$ and 1,2,3-$C_6F_3H_3$), as these have the most activated and hence weakest C-F bonds (energy barriers were calculated at 23.7 and 25.7 kcal mol^{-1} for 1,2,3,4-$C_6F_4H_2$ and

1,2,3-$C_6F_3H_3$ respectively). In contrast, for the stepwise pathway, HDF was directed to sites with only one *ortho*-fluorine (e.g. 1-position in 1,2,3,4-$C_6F_4H_2$ (22.6 kcal mol^{-1}) and 1,2,3-$C_6F_3H_3$ (23.2 kcal mol^{-1})) as the presence of a second *ortho*-F substituent resulted in an increased strain and thus higher energy of the C-F bond breaking transition state. In the case of 1,2,4-$C_6F_3H_3$ where two distinct C-F bonds are *ortho* to each other, HDF was governed by the number of *meta*-fluorines. Thus, the C-F bond at the 2-position was calculated to be weaker than that at the 1-position, due to the presence of one *ortho*- and one *meta*-F substituent (c.f. one *ortho* but no *meta*-fluorines for the C-F bond at 1-position). Although the two mechanisms had complementary regioselectivities, the stepwise pathway was predicted to have the lowest energy profile for the HDF reaction.

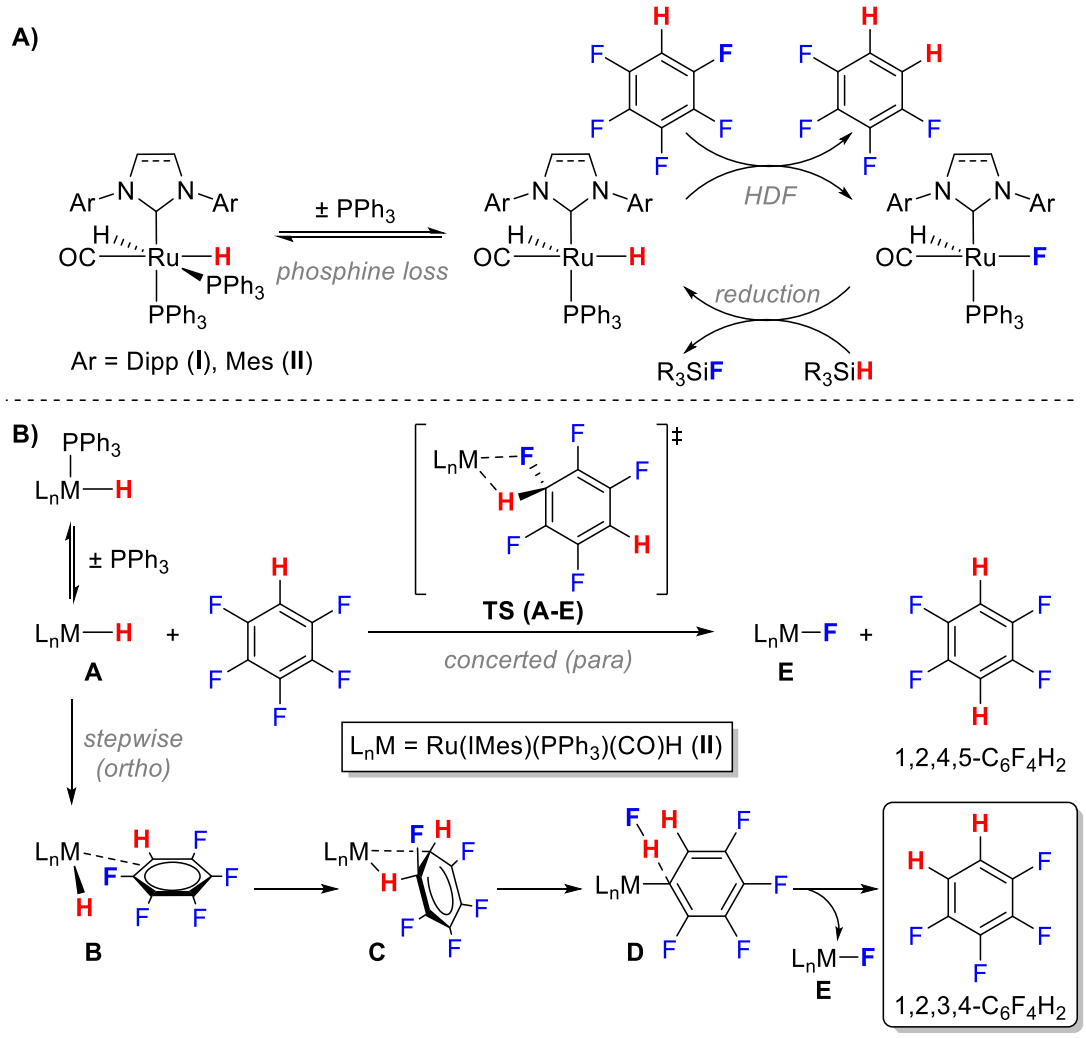

Scheme 1.25: A) Catalytic cycle for the HDF of C_6F_5H to 1,2,3,4-$C_6F_4H_2$ by [Ru(NHC)(PPh_3)$_2$(CO)H_2], B) Mechanisms of nucleophilic attack by the Ru-H ligand in [Ru(IMes)(PPh_3)$_2$(CO)H_2] (**II**) at C_6F_5H established by DFT calculations.

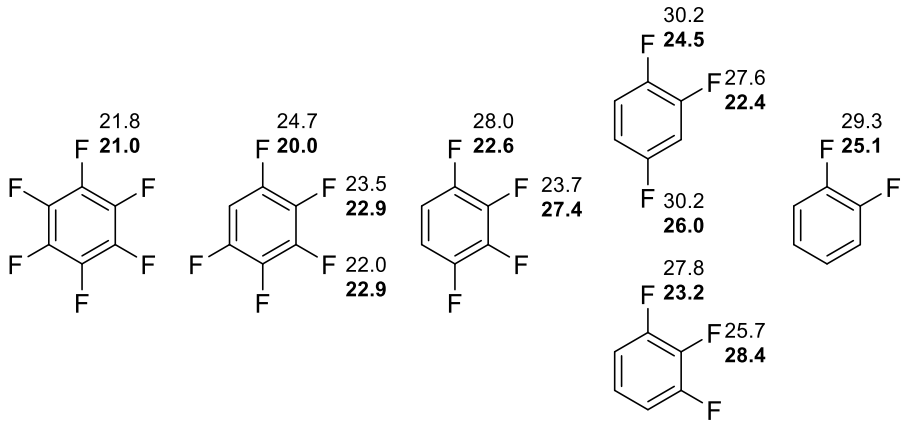

Figure 1.2: Calculated activation barriers (kcal mol^{-1}) for HDF of $C_6F_{6-n}H_n$ species at $[Ru(IMes)(PPh_3)_2(CO)H_2]$ (**II**). Values in bold are for the stepwise pathway and those in plain text are for the concerted pathway.[71]

Further experimental and computational studies focused on the HDF of C_5F_5N at $[Ru(NHC)(PPh_3)_2(CO)H_2]$ (**I** and **II**).[72] Again, this proved to be highly dependent on the NHC ligand (Scheme 1.26). With IPr catalyst (**I**), reaction took place preferentially at the *ortho*-position to give as the major product 2,3,4,5-C_5F_4HN; this could undergo further HDF to afford a mixture of 2,3,5-$C_5F_3H_2N$ (32 %) and $C_5F_2H_3N$ isomers (3,5- (27%) and 2,5- (41%)). The pattern of reactivity was attributed to operation of the stepwise mechanism, in which a N→Ru σ-interaction stabilised the C-F bond activation transition state. In contrast, the IMes counterpart (**II**) was predicted to react along a concerted pathway and favoured *para*-HDF, also seen experimentally. However, competing C-H activation of 2,3,5,6-C_5F_4HN ultimately led to the formation of the catalytically inactive Ru-fluoropyridyl complex, $[Ru(IMes)(PPh_3)(CO)(4\text{-}C_5F_4N)H]$.

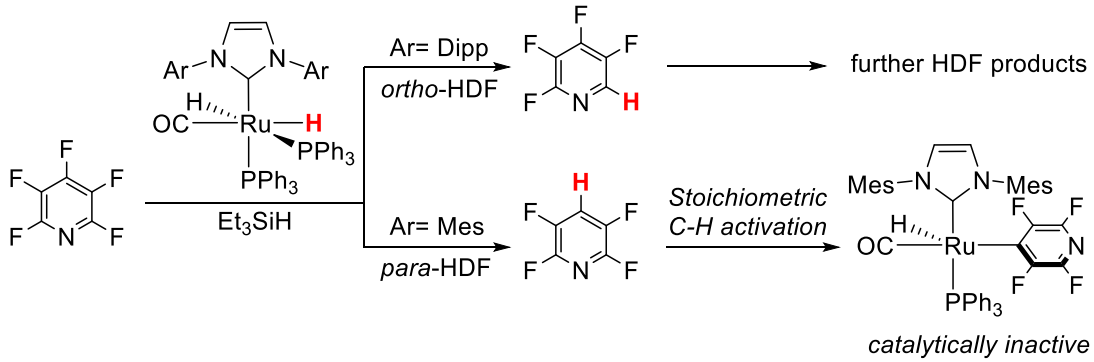

Scheme 1.26: Catalytic HDF of C_5F_5N at $[Ru(NHC)(PPh_3)_2(CO)H_2]$ (**I** and **II**).

1.5. Thesis synopsis

This thesis is primarily focused on the catalytic HDF of hexafluorobenzene using ruthenium hydride complexes bearing NHC ligands. **Chapter 2** describes the synthesis of $[Ru(NHC)_4H_2]$ compounds and their application in both stoichiometric and catalytic C-F bond activation reactions. Details on joint experimental and computational studies are provided. HDF chemistry is explored further in **Chapter 3**, which compares the catalytic performance of the species in **Chapter 2** to those of a series of mixed carbene/phosphine complexes. Competitive C-H activation and $PPh_3/HSiR_3$ substitution pathways are discussed. **Chapter 4** illustrates the ability of Ru(NHC) and $Ru(PR_3)$ precursors to bring about the unprecedented C-O activation of a DPEphos ligand. Mechanistic insights gained through DFT calculations are outlined. **Chapter 5** describes the synthesis and characterisation of $[Ru(PPh_3)_3HF]$ and outlines studies of its reactivity towards fluorophilic substrates.

1.6. References for Chapter 1

(1) O'Hagan, D. *Chem. Soc. Rev.* **2008**, *37*, 308.

(2) Hunter, L. *Beilstein J. Org. Chem.* **2010**, *6*, 38.

(3) Bondi, A. *J. Phys. Chem.* **1964**, *68*, 441.

(4) Purser, S.; Moore, P. R.; Swallow, S.; Gouverneur, V. *Chem. Soc. Rev.* **2008**, *37*, 320.

(5) Böhm, H.-J.; Banner, D.; Bendels, S.; Kansy, M.; Kuhn, B.; Müller, K.; Obst-Sander, U.; Stahl, M. *ChemBioChem* **2004**, *5*, 637.

(6) O'Hagan, D. *J. Fluorine Chem.* **2010**, *131*, 1071.

(7) Kirk, K. L. *J. Fluorine Chem.* **2006**, *127*, 1013.

(8) Bégué, J.-P.; Bonnet-Delpon, D. *J. Fluorine Chem.* **2006**, *127*, 992.

(9) Wang, J.; Sánchez-Roselló, M.; Aceña, J. L.; del Pozo, C.; Sorochinsky, A. E.; Fustero, S.; Soloshonok, V. A.; Liu, H. *Chem. Rev.* **2014**, *114*, 2432.

(10) Zhou, Y.; Wang, J.; Gu, Z.; Wang, S.; Zhu, W.; Aceña, J. L.; Soloshonok, V. A.; Izawa, K.; Liu, H. *Chem. Rev.* **2016**, *116*, 422.

(11) Jeschke, P. *Pest Manag. Sci.* **2010**, *66*, 10.

(12) Theodoridis, G. In *Advances in Fluorine Science*; Elsevier, 2006; Vol. 2, pp 121–175.

(13) Fujiwara, T.; O'Hagan, D. *J. Fluorine Chem.* **2014**, *167*, 16.

(14) Berger, R.; Resnati, G.; Metrangolo, P.; Weber, E.; Hulliger, J. *Chem. Soc. Rev.* **2011**, *40*, 3496.

(15) Balz, G.; Schiemann, G. *Berichte Dtsch. Chem. Ges. B Ser.* **1927**, *60*, 1186.

(16) Kirk, K. L. *Org. Process Res. Dev.* **2008**, *12*, 305.

(17) Tang, P.; Furuya, T.; Ritter, T. *J. Am. Chem. Soc.* **2010**, *132*, 12150.

(18) Campbell, M. G.; Ritter, T. *Chem. Rev.* **2015**, *115*, 612.

(19) Furuya, T.; Kamlet, A. S.; Ritter, T. *Nature* **2011**, *473*, 470.

(20) Liang, T.; Neumann, C. N.; Ritter, T. *Angew. Chem. Int. Ed.* **2013**, *52*, 8214.

(21) Neumann, C. N.; Ritter, T. *Angew. Chem. Int. Ed.* **2015**, *54*, 3216.

(22) Furuya, T.; Klein, J. E. M. N.; Ritter, T. *Synthesis* **2010**, *2010*, 1804.

(23) Nova, A.; Mas-Ballesté, R.; Lledós, A. *Organometallics* **2012**, *31*, 1245.

(24) Whittlesey, M. K.; Peris, E. *ACS Catal.* **2014**, *4*, 3152.

(25) Hu, J.-Y.; Zhang, J.-L. In *Organometallic Fluorine Chemistry*; Braun, T., Hughes, R. P., Eds.; Topics in Organometallic Chemistry; Springer International Publishing, 2015; pp 143–196.

(26) Pike, S. D.; Crimmin, M. R.; Chaplin, A. B., *Chem. Commun.* **2017**, *53*, 3615.

(27) Kuehnel, M. F.; Lentz, D.; Braun, T. *Angew. Chem. Int. Ed.* **2013**, *52*, 3328.

(28) Chen, W.; Bakewell, C.; Crimmin, M. R. *Synthesis* **2017**, *49*, 810.

(29) Weaver, J. D. *Synlett* **2014**, *25*, 1946.

(30) Shine, K. P.; Sturges, W. T. *Science* **2007**, *315*, 1804.

(31) Brooke, G. M. *J. Fluorine Chem.* **1997**, *86*, 1.

(32) Johnson, S. A.; Huff, C. W.; Mustafa, F.; Saliba, M. *J. Am. Chem. Soc.* **2008**, *130*, 17278.

(33) Liu, W.; Welch, K.; Trindle, C. O.; Sabat, M.; Myers, W. H.; Harman, W. D. *Organometallics* **2007**, *26*, 2589.

(34) Clot, E.; Besora, M.; Maseras, F.; Mégret, C.; Eisenstein, O.; Oelckers, B.; Perutz, R. N. *Chem. Commun.* **2003**, *4*, 490.

(35) Clot, E.; Oelckers, B.; Klahn, A. H.; Eisenstein, O.; Perutz, R. N. *Dalton Trans.* **2003**, 4065.

(36) Reinhold, M.; McGrady, J. E.; Perutz, R. N. *J. Am. Chem. Soc.* **2004**, *126*, 5268.

(37) Clot, E.; Eisenstein, O.; Jasim, N.; Macgregor, S. A.; McGrady, J. E.; Perutz, R. N. *Acc. Chem. Res.* **2011**, *44*, 333.

(38) Vela, J.; Smith, J. M.; Yu, Y.; Ketterer, N. A.; Flaschenriem, C. J.; Lachicotte, R. J.; Holland, P. L. *J. Am. Chem. Soc.* **2005**, *127*, 7857.

(39) Xu, X.; Sun, H.; Shi, Y.; Jia, J.; Li, X. *Dalton Trans.* **2011**, *40*, 7866.

(40) Xu, X.; Jia, J.; Sun, H.; Liu, Y.; Xu, W.; Shi, Y.; Zhang, D.; Li, X. *Dalton Trans* **2013**, *42*, 3417.

(41) Zheng, T.; Li, J.; Zhang, S.; Xue, B.; Sun, H.; Li, X.; Fuhr, O.; Fenske, D. *Organometallics* **2016**, *35*, 3538.

(42) Mai, V. H.; Nikonov, G. I. *ACS Catal.* **2016**, *6*, 7956.

(43) Li, J.; Zheng, T.; Sun, H.; Xu, W.; Li, X. *Dalton Trans.* **2013**, *42*, 5740.

(44) Aizenberg, M.; Milstein, D. *Science* **1994**, *265*, 359.

(45) Aizenberg, M.; Milstein, D. *J. Am. Chem. Soc.* **1995**, *117*, 8674.

(46) Young, R. J.; Grushin, V. V. *Organometallics* **1999**, *18*, 294.

(47) Braun, T.; Noveski, D.; Ahijado, M.; Wehmeier, F. *Dalton Trans.* **2007**, 3820.

(48) Zámostná, L.; Ahrens, M.; Braun, T. *J. Fluorine Chem.* **2013**, *155*, 132.

(49) Nakai, H.; Jeong, K.; Matsumoto, T.; Ogo, S. *Organometallics* **2014**, *33*, 4349.

(50) Ekkert, O.; Strudley, S. D. A.; Rozenfeld, A.; White, A. J. P.; Crimmin, M. R. *Organometallics* **2014**, *33*, 7027.

(51) Schwartsburd, L.; Mahon, M. F.; Poulten, R. C.; Warren, M. R.; Whittlesey, M. K. *Organometallics* **2014**, *33*, 6165.

(52) Senaweera, S. M.; Singh, A.; Weaver, J. D. *J. Am. Chem. Soc.* **2014**, *136*, 3002.

(53) Matsunami, A.; Kuwata, S.; Kayaki, Y. *ACS Catal.* **2016**, *6*, 5181.

(54) Kuhl, S.; Schneider, R.; Fort, Y. *Adv. Synth. Catal.* **2003**, *345*, 341.

(55) Wu, J.; Cao, S. *ChemCatChem* **2011**, *3*, 1582.

(56) Zhao, W.; Wu, J.; Cao, S. *Adv. Synth. Catal.* **2012**, *354*, 574.

(57) Xiao, J.; Wu, J.; Zhao, W.; Cao, S. *J. Fluorine Chem.* **2013**, *146*, 76.

(58) Fischer, P.; Götz, K.; Eichhorn, A.; Radius, U. *Organometallics* **2012**, *31*, 1374.

(59) Arévalo, A.; Tlahuext-Aca, A.; Flores-Alamo, M.; García, J. J. *J. Am. Chem. Soc.* **2014**, *136*, 4634.

(60) He, Y.; Chen, Z.; He, C.-Y.; Zhang, X. *Chin. J. Chem.* **2013**, *31*, 873.

(61) Chen, Z.; He, C.-Y.; Yin, Z.; Chen, L.; He, Y.; Zhang, X. *Angew. Chem. Int. Ed.* **2013**, *52*, 5813.

(62) Breyer, D.; Braun, T.; Penner, A. *Dalton Trans.* **2010**, *39*, 7513.

(63) Breyer, D.; Braun, T.; Kläring, P. *Organometallics* **2012**, *31*, 1417.

(64) Lv, H.; Cai, Y.-B.; Zhang, J.-L. *Angew. Chem. Int. Ed.* **2013**, *52*, 3203.

(65) Zhan, J.-H.; Lv, H.; Yu, Y.; Zhang, J.-L. *Adv. Synth. Catal.* **2012**, *354*, 1529.

(66) Lu, J.; Khetrapal, N. S.; Johnson, J. A.; Zeng, X. C.; Zhang, J. *J. Am. Chem. Soc.* **2016**, *138*, 15805.

(67) Sabater, S.; Mata, J. A.; Peris, E. *Nat. Commun.* **2013**, *4*, 2553.

(68) Sabater, S.; Mata, J. A.; Peris, E. *Organometallics* **2015**, *34*, 1186.

(69) Reade, S. P.; Mahon, M. F.; Whittlesey, M. K. *J. Am. Chem. Soc.* **2009**, *131*, 1847.

(70) Panetier, J. A.; Macgregor, S. A.; Whittlesey, M. K. *Angew. Chem. Int. Ed.* **2011**, *50*, 2783.

(71) Macgregor, S. A.; McKay, D.; Panetier, J. A.; Whittlesey, M. K. *Dalton Trans.* **2013**, *42* , 7386.

(72) McKay, D.; Riddlestone, I. M.; Macgregor, S. A.; Mahon, M. F.; Whittlesey, M. K. *ACS Catal.* **2015**, *5*, 776.

CHAPTER TWO

C-F bond activation using *trans*-[Ru(NHC)$_4$H$_2$] complexes

2.1. Synthesis of *trans*-[Ru(NHC)$_4$H$_2$] complexes

Building on the previous work on catalytic HDF using ruthenium NHC hydride complexes (Section 1.4) which highlighted the importance of hydride nucleophilicity, the development of new systems which would display improved activity and regioselectivity was targeted. It was reasoned that the presence of four highly electron donating NHC ligands and the unusual *trans*-disposition of strong *trans*-influence hydride ligands in *trans*-[Ru(IMe$_4$)$_4$H$_2$] (**1**), would not only render the complex coordinatively saturated throughout any catalytic cycle (c.f. PPh_3 loss from **I** and **II**), but also impart strong nucleophilic character to Ru-H. Previously reported by Wolf et al.,[1] **1** could only be isolated as an impure solid in low yield from the reduction of *trans*-[Ru(IMe$_4$)$_4$Cl$_2$] with $LiAlH_4$ in THF. A new synthetic protocol involving KC_8/H_2 in THF as the reductant allowed the isolation of **1** as an analytically pure, yellow, microcrystalline solid in high (80%) yield (Scheme 2.1). The complex proved to be extremely moisture sensitive and decomposed rapidly upon exposure to air or even adventitious water as demonstrated by an apparent change in colour to pink during cannula filtration using standard Schlenk line techniques. This necessitated the full work-up to be carried out in a glovebox. Additional steps were also required to ensure complete exclusion of H_2O, including prolonged drying of glass microfiber filter papers (days at 140°C and vacuum overnight), followed by treatment (rinsing) with dry Et_2O prior to their use for removal of graphite from the reaction mixture.

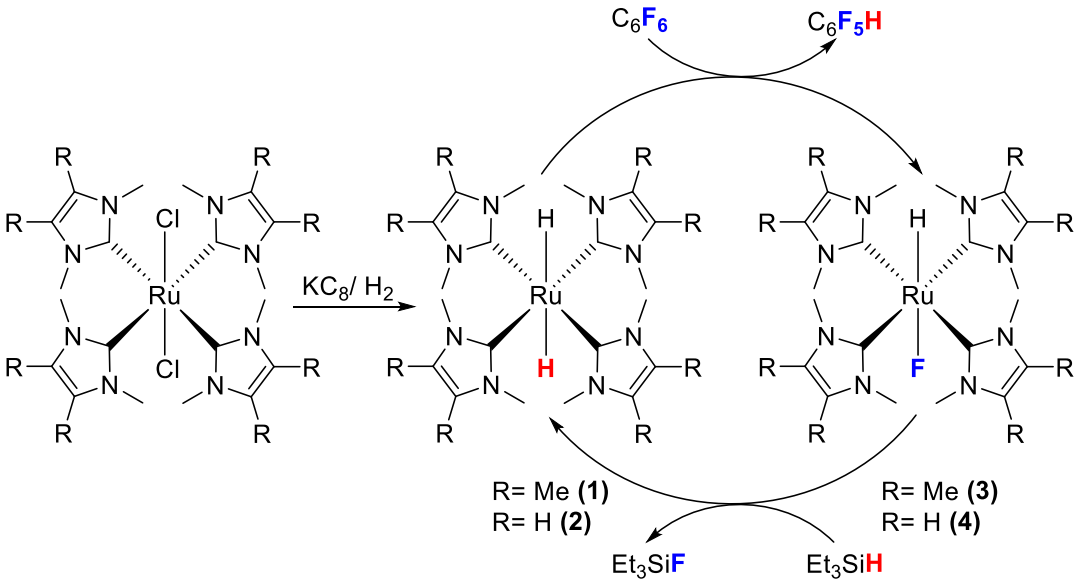

Scheme 2.1: Formation of *trans*-[Ru(NHC)$_4$H$_2$] complexes (**1** and **2**) from [Ru(NHC)$_4$Cl$_2$] and KC$_8$/H$_2$ and subsequent HDF of C$_6$F$_6$ to generate the corresponding *trans*-[Ru(NHC)$_4$HF] complexes (**3** and **4**) and C$_6$F$_5$H.

The highly symmetric nature of **1** was reflected by a very simple ^{1}H NMR spectrum in THF-d_8 consisting of just three singlet resonances at δ 3.37, 1.97 and -8.14 in a 24:24:2 ratio. **1** underwent facile H/D exchange in C$_6$D$_6$ within the time of dissolution as indicated by the appearance of two signals at δ -7.45 and δ -7.29, assigned as RuH$_2$ and RuHD isotopologues respectively (Figure 2.1). Moreover, these were accompanied by splitting of the resonance at δ 3.80, most likely arising from H/D exchange into the N-Me groups. Adopting the same synthetic procedure, an IMe$_2$ analogue, *trans*-[Ru(IMe$_2$)$_4$H$_2$] (**2**) could be prepared from the parent dichloride, *trans*-[Ru(IMe$_2$)$_4$Cl$_2$] in 78% yield. The complex exhibited increased air and moisture stability compared to **1**, as well as reduced propensity for H/D scrambling in C$_6$D$_6$.[i] The

[i] Formation of the RuHD isotopologue of **2** was observed only after prolonged heating at high temperatures (90°C).

^{1}H NMR spectrum of **2** displayed a similar pattern of singlet resonances at δ 6.43, 3.49 and -7.45 integrating in an 8:24:2 ratio, while the carbenic carbon (Ru-C_{NHC}) gave rise to a sharp singlet at δ 212.6 in the $^{13}C\{^{1}H\}$ NMR spectrum (c.f. δ 212.0 for **1**). The molecular structure of **2** is shown in Figure 2.2 and features a square bipyramidal arrangement of four carbenes and a *trans*-H-Ru-H geometry, akin to the structure of **1**. The asymmetric unit comprised of 1/8 of a molecule with identical Ru-C bond distances (2.056(2) Å, c.f. 2.058(2)-2.064(2) Å for **1**) and (*cis*-) C-Ru-C bond angles (90.00°). Similarly to **1**, the carbene ligands were tilted with respect to the H-Ru-H axis (H1-Ru1-C1-N1 40.4°, c.f. 42.3° and 44.0° in **1**).

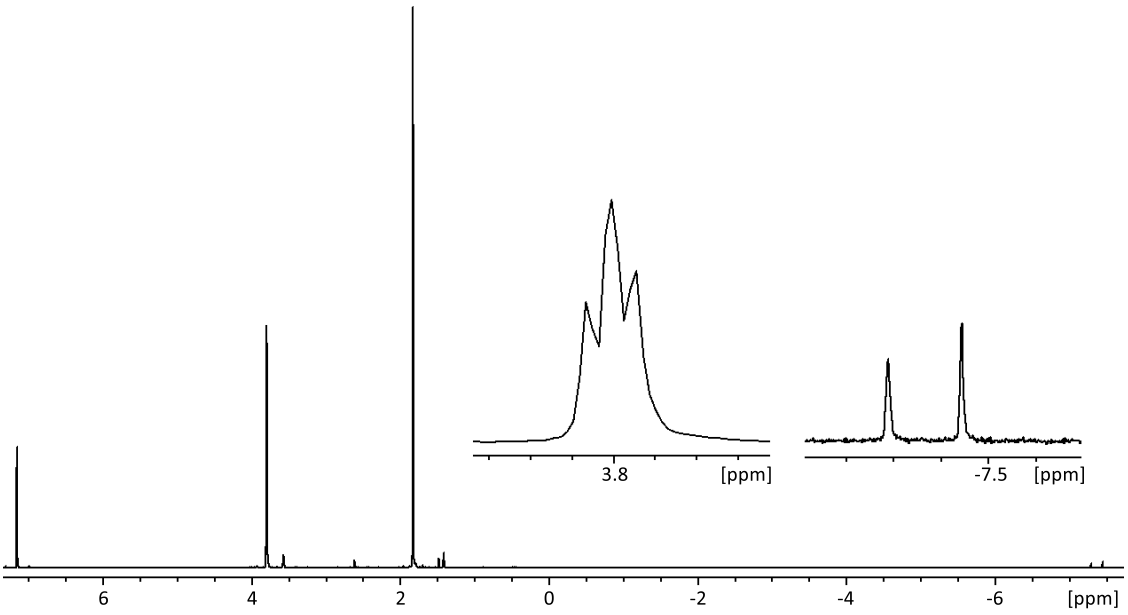

Figure 2.1: ^{1}H NMR spectrum (C_6D_6, 500 MHz, 25°C) of [Ru(IMe_4)$_4H_2$] (**1**). Insets show H/D exchange into N-Me groups and RuH_2.

Attempts to synthesise *trans*-[Ru(IEt_2Me_2)$_4H_2$] met with limited success as the species could only be generated *in-situ* in a reaction between *trans*-[Ru(IEt_2Me_2)$_4Cl_2$] with KC_8/H_2 in THF-d_8 at 70°C for 2 h. Analysis of the pale yellow reaction mixture by

^{1}H NMR spectroscopy revealed a characteristic RuH singlet at δ -8.05 (2H), a triplet methyl (NCH_2CH_3) signal at δ 0.43 ($^{3}J_{HH}$ = 6.9 Hz, 24H), a singlet backbone methyl resonance at δ 2.00 (24H) and two sets of multiplets at δ 3.67 (8H) and 6.08 (8H) arising from diastereotopic methylene (NCH_2CH_3) protons. No solid could be isolated following the same work-up procedure used for **1**, possibly due to the even greater sensitivity of the N-Et analogue.

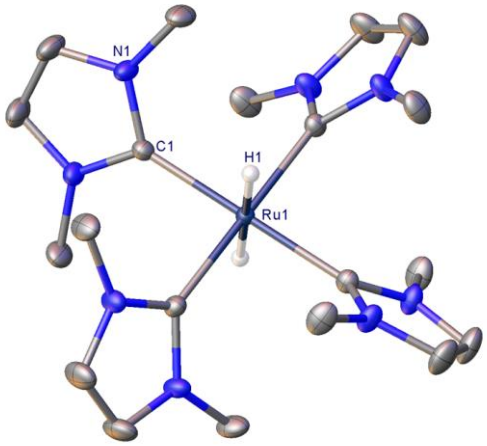

Figure 2.2: Molecular structure of *trans*-[Ru(IMe$_2$)$_4$H$_2$] (**2**). Thermal ellipsoids are represented at 30% probability. Hydrogen atoms, with the exception of hydride ligands, have been omitted for clarity.

2.2. Stoichiometric C-F activation of fluoroarenes and synthesis of *trans*-[Ru(NHC)$_4$HF] complexes

Addition of 1 equiv of C_6F_6 to benzene solutions of **1** and **2** brought about rapid formation of *trans*-[Ru(IMe$_4$)$_4$HF] (**3**) and *trans*-[Ru(IMe$_2$)$_4$HF] (**4**) respectively (Scheme 2.1) within the time of mixing.[ii] As expected, analysis of the reaction volatiles

[ii] Both species were also formed cleanly upon reaction of corresponding dihydride complexes with the less fluorinated substrate 1,2,4-$C_6F_3H_3$, although more slowly.

by ^{19}F NMR spectroscopy revealed the presence of three sets of resonances at δ -138.3 (m), -153.3 (t, $^{3}J_{FF}$ = 20.7 Hz) and -161.5 (m), which integrated in a 2:1:2 ratio and were assigned as *ortho*-, *para*- and *meta*-fluorines of the HDF product, C_6F_5H.

Single-crystal X-ray structures of **3** and **4** are presented in Figure 2.3. The molecules resided on crystallographic C_2 and C_{4i} axes respectively and showed retention of an octahedral coordination sphere at ruthenium comprising of four NHC ligands and the mutually *trans* hydride and fluoride substituents. Table 2.1 shows a comparison of selected metrics. The Ru-C bond distances in both **3** and **4** were slightly elongated compared to their parent dihydride complexes. In contrast to **1** and **3**, the H1-Ru1-C1-N1 torsion angle in **4**, defining the twist of the NHC plane with respect to the H-Ru-F axis, was markedly reduced compared to that in **2**. This could be a consequence of weak hydrogen bonding between the N-Me protons and the fluoride ligand (C-H···F 2.144(4) Å; C···F 3.013(3) Å; C-H-F 149.9(5)°) that helps to lock the carbene positions. Some degree of H-bonding was also observed in **3** (C-H···F 2.132(17) Å; C···F 3.055(4) Å; C-H-F 157.0(3)°). Of particular interest were the long ruthenium-fluorine distances (2.3070(18) Å for **3** and 2.384(4) Å for **4**), which were comparable to the value of 2.284(5) Å found in *trans*-[Ru(dmpe)$_2$H(FHF)], the only other example of a structurally characterised *trans*-H-Ru-F complex in the literature.[2] The Ru-H (and Ru-F) NMR resonances in **3** and **4** appeared at δ -23.19 (δ -281.6) and δ -22.94 (δ -302.4) respectively. The number of proton NHC resonances doubled on going from the ruthenium dihydride complexes (**1** and **2**) to the corresponding hydride fluoride species (**3** and **4**) which reflected both the decrease in symmetry at Ru, as well as the restricted rotation about the Ru-C_{NHC} bonds.

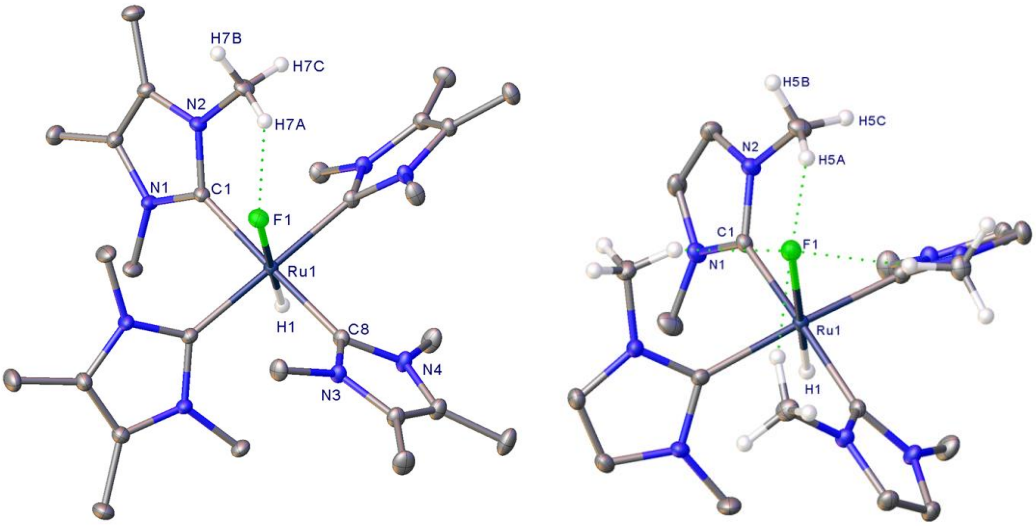

Figure 2.3: Molecular structures of [Ru(IMe$_4$)$_4$HF] (**3**, left) and [Ru(IMe$_2$)$_4$HF] (**4**, right). Thermal ellipsoids are represented at 30% probability. Hydrogen atoms, with the exception of hydride ligands and those on the N-methyl groups showing H-bonding contacts to Ru-F, have been omitted for clarity.

Table 2.1: Selected bond lengths (Å) and angles (°) for complexes **1**-**4**.

	1[1]	**2**	**3**	**4**
Ru-C	2.058(2), 2.064(2)	2.056(2)	2.0741(15), 2.0631(15)	2.069(2)
H-Ru-C-N	42.3, 44.0	40.4	42.6, 40.2	33.7
trans-C-Ru-C	178.13(8)	180.00(7)	178.15(6)	174.6(3)
cis-C-Ru-C	87.41(11)	90.0	87.65(8)	89.874(15)
Ru-F	-	-	2.3070(18)	2.384(4)
C-H···F	-	-	2.144(4)	2.132(12)

It is worth noting that ^{13}C NMR analysis of **4** was not possible due to its insolubility in common organic solvents such as THF, C_6FH_5, DMSO, pyridine or CH_2Cl_2. Although **4** dissolved readily in acetonitrile, it reacted to give a mixture of

fluoride and bifluoride salts of $[Ru(IMe_2)_4H(MeCN)]^+$,[3] which was assigned through comparison of the spectroscopic data for the cation to that of the known IMe_4 analogue, $[Ru(IMe_4)_4H(MeCN)][BAr^F_4]$.[4] Thus, the Ru-H resonated at δ -15.20 in the ^{1}H NMR spectrum, while the $[F]^-$ and $[HF_2]^-$ anions appeared as a broad singlet at δ -70.2 and a doublet at δ -147.2 ($^1J_{FH}$ = 121 Hz) in the ^{19}F NMR spectrum respectively.

Employment of THF as the reaction solvent had a perplexing effect on the appearance of the reaction between **1** and C_6F_6 or C_6F_5H. Thus, upon addition of 1 equiv of hexa- or pentafluorobenzene to a THF-d_8 solution of **1**, the instantaneous formation of black solid was observed. Immediate analysis of the reaction mixture by ^{1}H and ^{19}F NMR spectroscopy revealed complete loss of signals for **1** and the presence of **3** along with the HDF products, C_6F_5H and 1,2,4,5-$C_6F_4H_2$ (δ -138.6, t, J_{FH} = 8.6 Hz) respectively. Following separation of the solid and mother liquor, the precipitate proved to be insoluble in organic solvents, as well as H_2O, but dissolved in aqua regia, implying that the generated heterogeneous suspension consisted of metal particles. No further attempts were made to elucidate the nature of the isolated solid. Nonetheless, we speculated that the unexpected deposition of black material could result from radical processes taking place. To probe this, the reaction was repeated in the presence of TEMPO (5 equiv), a common radical trap. Although no change in colour or sample homogeneity was observed, a yellow precipitate, along with a small amount of yellow crystals were formed after leaving the reaction mixture at room temperature overnight. ^{1}H and ^{19}F NMR spectra were broad and did not show any signals for **1** or **3**. Unfortunately, subsequent X-ray diffraction analysis of the isolated crystalline material proved elusive. Preliminary refinement of the obtained crystal structure indicated that the unit cell comprised of half a molecule of $[Ru(IMe_4)_4HF]$, albeit with a significantly shorter Ru-F bond (ca. 1.990 Å). However, the high disorder and the presence of

significant residual electron density in the lattice impeded the final refinement. Dissolution of the crystals in acetonitrile suggested the formation of a bifluoride salt with a molecule of MeCN coordinated *trans* to the Ru-H, $[Ru(IMe_4)_4H(MeCN)][HF_2]$, analogous to the aforementioned IMe_2 complex. The same difficulties were encountered upon repeating the experiment several times. The fate of TEMPO remains unknown, although given the absence of black precipitate, it is reasonable to assume that the reaction between **1** and C_6F_5H in THF might proceed *via* a radical pathway. Perutz and co-workers reported the formation of *trans*-$[Ru(dmpe)_2(C_6F_5)H]$ from the reaction of *cis*-$[Ru(dmpe)_2H_2]$ and C_6F_6 at -78°C in THF.[5] The authors postulated a mechanism involving electron transfer from the electron rich metal dihydride to hexafluorobenzene to generate a solvent caged radical pair $\{[RuH_2]^{+\cdot}\ [C_6F_6]^{-\cdot}\}$. The resulting radical anion would then lose F^-, which would deprotonate the radical cation to liberate a molecule of HF as a thermodynamic sink. Radical recombination would account for the product formation. Attempts to provide support for an electron transfer process through use of 9,10-dihydroanthracene (DHA) as a radical trap gave disappointingly only trace amounts of anthracene. This was postulated to be due to radicals being trapped in the solvent cage. It might be desirable in future studies on **1** to investigate the effect of other radical quenchers such as DHA or galvinoxyl, as well as repeat the reaction in the presence of TEMPO at lower temperatures.

Interestingly, addition of stoichiometric amounts of C_6F_6 or C_6F_5H to a THF solution of **2** led to an instantaneous precipitation of orange solid, most likely **4**, and no deposition of black solid was observed. As expected, ^{19}F NMR analysis of the reaction mixture confirmed the formation of the HDF products C_6F_5H and 1,2,4,5-$C_6F_4H_2$ respectively.

2.3. Catalytic HDF of fluoroarenes using *trans*-[Ru(NHC)$_4$H$_2$] complexes

In light of the facile conversion of complexes **1** and **2** to **3** and **4** upon reaction with C_6F_6 under stoichiometric conditions, catalytic HDF of aromatic fluorocarbons was explored. The activity of complexes **1** and **2** was screened at 5 mol% loading in C_6H_6 with 50 equiv of Et_3SiH (with respect to catalyst) as a reductant. The outcomes of HDF reactions are summarised in Table 2.2. Complex **1** proved to be a remarkably active catalyst, capable of converting C_6F_6 to 1,2,4,5-$C_6F_4H_2$ within ca. 5 minutes at room temperature, which translates to a TOF value exceeding 480 h^{-1} (Scheme 2.2). The mild reaction conditions and observed *para*-regioselectivity were in a striking contrast to the observations with complexes **I** and **II**, that required elevated temperatures to promote *ortho*-C-F activation of C_6F_5H to give 1,2,3,4-$C_6F_4H_2$. Two subsequent HDF steps on 1,2,4,5-$C_6F_4H_2$ by **1** were complete over ca. 1 month to yield 1,4-$C_6F_2H_4$ (identified by the appearance of a ^{19}F NMR resonance at δ -118.7) in quantitative yield (Table 2.2, entry 1). Increasing the reaction temperature to 90°C significantly reduced the reaction time to just 10 h (Table 2.2, entry 1; Figure 2.4).

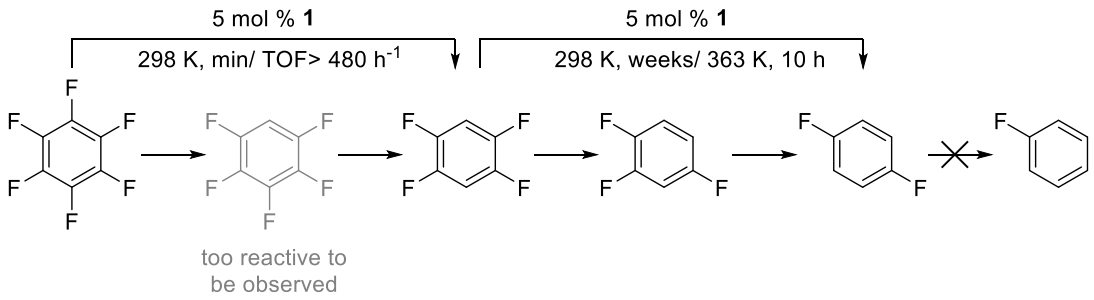

Scheme 2.2: Catalytic HDF by *trans*-[Ru(IMe$_4$)$_4$H$_2$] (**1**).

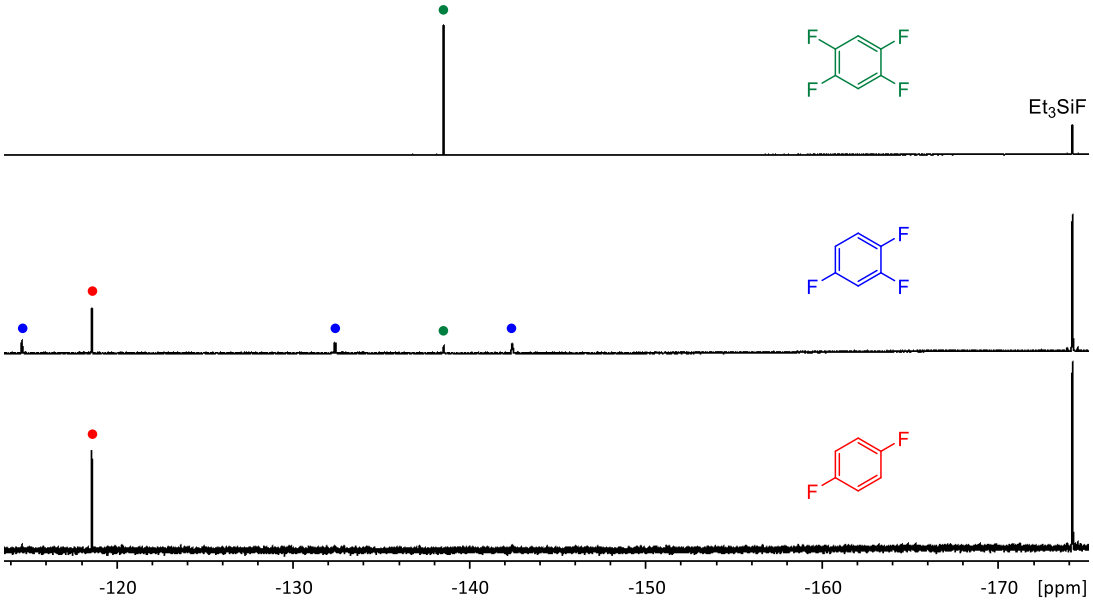

Figure 2.4: ^{19}F NMR spectra (470 MHz, 25°C) showing the progression of a catalytic HDF reaction of C_6F_6 with **1** (5 mol%) and Et_3SiH (100 equiv) in C_6H_6 after 10 min at 25°C (top), 4 h heating at 90°C (middle) and a total of 10 h at 90°C (bottom).

In order to define the scope and regioselectivity of HDF, catalysis was carried out with a range of low fluorine containing substrates (entries 2-5). As anticipated, HDF of 1,2,4,5-$C_6F_4H_2$ first afforded 1,2,4-$C_6F_3H_3$, which was then converted to 1,4-$C_6F_2H_4$ (entries 2 and 3). HDF of 1,4-$C_6F_2H_4$ to fluorobenzene did not occur, although C_6FH_5 could be formed from both 1,2- and 1,3- isomers of $C_6F_2H_4$ (entries 4 and 5). No further reduction to C_6H_6 was observed, consistent with the general paucity of catalytic systems able to react with monofluorinated substrates.[6] Nonetheless, the catalyst was still active as shown by the further propagation of HDF following the addition of more C_6F_6 (20 equiv) at the end of a catalytic run using 1,3-$C_6F_2H_4$ of 539 h duration at 120°C. However, a drop in activity was apparent as full conversion to 1,2,4,5-$C_6F_4H_2$ was achieved only in ca. 1 h (i.e. TOF ≈ 40 h^{-1}), rather than <5 minutes (i.e. TOF ≈ 480 h^{-1}).

The study was further extended to investigate the effect of the silane reductant on the catalytic activity of **1** (entries 6-10). It was established that silanes containing mixed aryl/alkyl substituents ($PhMe_2SiH$ and Ph_2MeSiH), as well as secondary alkyl silanes (Et_2SiH_2) performed comparably to Et_3SiH, although a drop in activity was observed upon switching to the aryl silanes Ph_3SiH or Ph_2SiH_2.

Complex **2** turned out to be less effective for catalytic HDF, requiring longer reaction times to achieve similar conversions (entries 11-12). This is perhaps due to the poor solubility of the fluoride derivative **4**, as indicated by the presence of a fine yellow precipitate in catalytic reactions carried out at 90°C.

Table 2.2: *trans*-[Ru(NHC)$_4$H$_2$] catalysed HDF.[a]

Entry	Cat.	Substrate	Reductant	Product	T [°]	t [h]	TON
1	**1**	C_6F_6	Et_3SiH	1,4-$C_6F_2H_4$	25	740	80
					25/90[b]	10	80
2	**1**	1,2,4,5-$C_6F_4H_2$	Et_3SiH	1,4-$C_6F_2H_4$	90	10	40
3	**1**	1,2,4-$C_6F_3H_3$	Et_3SiH	1,4-$C_6F_2H_4$	90	9	20
4[c]	**1**	1,2-$C_6F_4H_2$	Et_3SiH	C_6FH_5	120	157	20
5[c]	**1**	1,3-$C_6F_4H_2$	Et_3SiH	C_6FH_5	120	539	20
6	**1**	C_6F_6	$PhMe_2SiH$	1,4-$C_6F_2H_4$	25	740	80
7	**1**	C_6F_6	Ph_2MeSiH	1,4-$C_6F_2H_4$	90	17	80
8[d]	**1**	C_6F_6	Ph_3SiH	C_6F_5H (79%) + 1,2,4,5-$C_6F_4H_2$ (21%)	25	740	18.5
9	**1**	C_6F_6	Et_2SiH_2	1,4-$C_6F_2H_4$	25/90[b]	9	80

10	**1**	C_6F_6	Ph_2SiH_2	1,2,4,5-$C_6F_4H_2$	25	264	40
11	**2**	C_6F_6	Et_3SiH	1,2,4,5-$C_6F_4H_2$	25	6	40
12	**2**	C_6F_6	Et_3SiH	1,4-$C_6F_2H_4$	90	103	80

[a] Reaction conditions: 0.1 M fluoroarene, 0.5 M silane, 5 mol% **1** or **2**, 0.5 mL C_6H_6, conversions determined by ^{19}F NMR spectroscopy. [b] Temperature raised to 90°C after ca. 5 min at 25°C. [c] Solvent = $C_6H_5CH_3$. [d] Product distribution is % of main products/total % of all HDF products.

2.4. Mechanistic studies of catalytic HDF

2.4.1. Reactivity of *trans*-[Ru(IMe)$_4$HF] (4) with silanes

The dependence of catalytic conversion on the employed silane suggested that the regeneration of the parent dihydride species from the corresponding fluoride complex, necessary to close the catalytic cycle, might be the rate-limiting step in the HDF of fluoroarenes. Thus, the reactivity of **3** towards $HSiR_3$ (R = Et, Ph) was investigated (Scheme 2.1).

Addition of 5 equiv of Et_3SiH to a C_6H_6 solution of **3** resulted in the immediate and clean reformation of **1**. Since aryl silanes were shown to significantly impair the rate of catalytic HDF, **3** was similarly reacted with Ph_3SiH. Upon addition of 1.5 equiv of C_6F_6 to a C_6H_6 solution of **1** and Ph_3SiH (1:5 ratio), an immediate change in colour from pale yellow to deep purple was apparent,[iii] indicative of the formation of the 16 electron cationic species, $[Ru(IMe_4)_4H]^+$.[4] Addition of pentane to the reaction mixture led to the precipitation of $[Ru(IMe_4)_4H][Ph_3SiF_2]$ (**5**), which was fully characterised by NMR spectroscopy and single crystal X-ray diffraction. The Ru-H chemical shift (δ -40.16) matched the value of δ -40.71 reported for $[Ru(IMe_4)_4H][BAr^F{}_4]$,[4] while the $[Ph_3SiF_2]^-$ anion gave rise to a sharp singlet (with Si satellites) in the ^{19}F NMR spectrum at δ -103.0 ($^1J_{FSi}$ = 259 Hz), consistent with data reported for previously isolated [K([2.2.2.]cryptand)][Ph_3SiF_2] (δ -102.2, $^1J_{FSi}$ = 259 Hz)[7] and [K([18]crown-6)][Ph_3SiF_2] (δ -101.7, $^1J_{FSi}$ = 255 Hz)[8] salts. The molecular structure of **5** is shown in Figure 2.5. The hypervalent pentacoordinate

[iii] It is worth noting that in all catalytic HDF reactions with aryl silanes (Ph_3SiH, Ph_2SiH_2, Ph_2MeSiH), a pink-purple tinge to the reaction mixture was observed.

difluorosilicate anion contains an approximately linear F-Si-F unit (177.1(2)°) with three phenyl groups occupying the equatorial positions of the trigonal bipyramid. There was no significant deviation of bond lengths (Si-F, Si-C) or angles (F-Si-F, C-Si-C) from other known $[Ph_3SiF_2]^-$ compounds.[7,8]

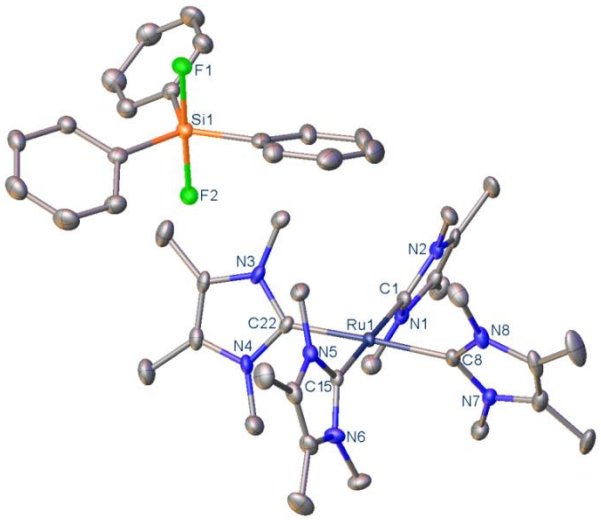

Figure 2.5: Molecular structure of $[Ru(IMe_4)_4H][Ph_3SiF_2]$ (**5**). Thermal ellipsoids are represented at 30% probability. Hydrogen atoms have been omitted for clarity. Selected bond lengths (Å) and angles (°) for the anion: Si(1)-F(1) 1.736(4), Si(1)-F(2) 1.731(4), Si(1)-C(64) 1.896(6), Si(1)-C(70) 1.909(8), Si(1)-C(76) 1.898(6), F(1)-Si(1)-F(2) 177.1(2), C(64)-Si(1)-C(70) 120.5(3), C(64)-Si(1)-C(76) 114.9(3), C(70)-Si(1)-C(76) 124.6(3).

A proposed mechanism for the formation of **5** is presented in Scheme 2.3 and involves two HDF steps of C_6F_6 to give $C_6F_4H_2$ and **3**, which subsequently undergoes fluoride abstraction by the in-situ generated Ph_3SiF to yield **5**. Addition of excess Ph_3SiH to a C_6H_6 suspension of **5** and vigorous shaking of the reaction mixture at room temperature overnight resulted in a clean reformation of **1** and Ph_3SiF. Related reactivity has been observed previously with [(IPr)CuF], which was

activated by fluorosilanes R_3SiF to generate a tight ion pair between $[(IPr)Cu]^+$ and a difluorosilicate $[R_3SiF_2]^-$.[9] The formed species were assumed to assist the hydride transfer from the silane to the copper atom to afford [(IPr)CuH].

Trialkyldifluorosilicates are not known, presumably due to the low Lewis acidity/ fluorophilicity of the silicon centre when substituted with electron donating alkyl groups. Consequently, efforts to isolate or observe a triethylsilicate analogue of **5** in the reaction with Et_3SiH proved unsuccessful. The findings from the stoichiometric experiments with Ph_3SiH and Et_3SiH may help to rationalise the variations seen with silanes in the catalytic HDF experiments in Table 2.2 simply on the basis of different reactivity in the first instance with the hydride fluoride complex **3**. The results certainly do suggest that the reaction of the H-Ru-F with R_3SiH is more complex than a simple bond metathesis reaction of Ru-F and Si-H.

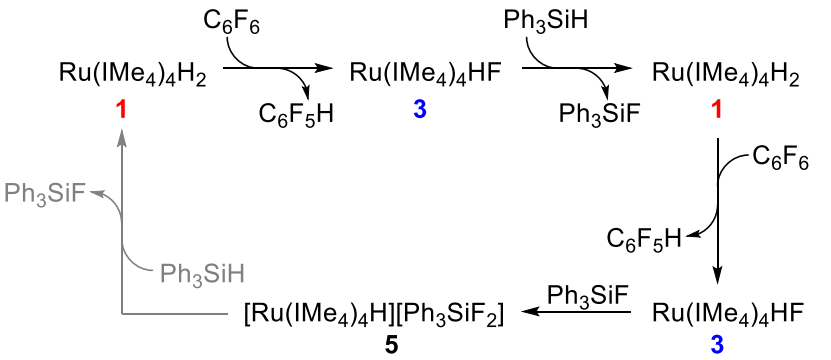

Scheme 2.3: Putative reaction scheme and a balanced reaction (below) for the formation of $[Ru(IMe_4)_4H][Ph_3SiF_2]$ (**5**) (black) and its reaction with Ph_3SiH (grey).

Having shown that alkyl and mixed alkyl/aryl silanes (Table 2.2, entries 6-10) impacted HDF very similarly, and that it is only aryl silanes that showed markedly different behaviour, additional studies aimed at elucidating the effect of

silane concentration on the rate of HDF were conducted. Figure 2.6 shows kinetic profiles of two catalytic HDF experiments starting with 1,2,4-$C_6F_3H_3$ and **1** at 90°C in the presence of 20 equiv of Et_3SiH in one case, and 100 equiv of Et_3SiH in the second case. The results clearly demonstrate that the 5-fold change in silane concentration has no impact on the rate of conversion of 1,2,4-$C_6F_3H_3$ to 1,4-$C_6F_2H_4$ suggesting that the rate-determining step for the catalytic HDF of fluorobenzenes is the C-F bond activation.

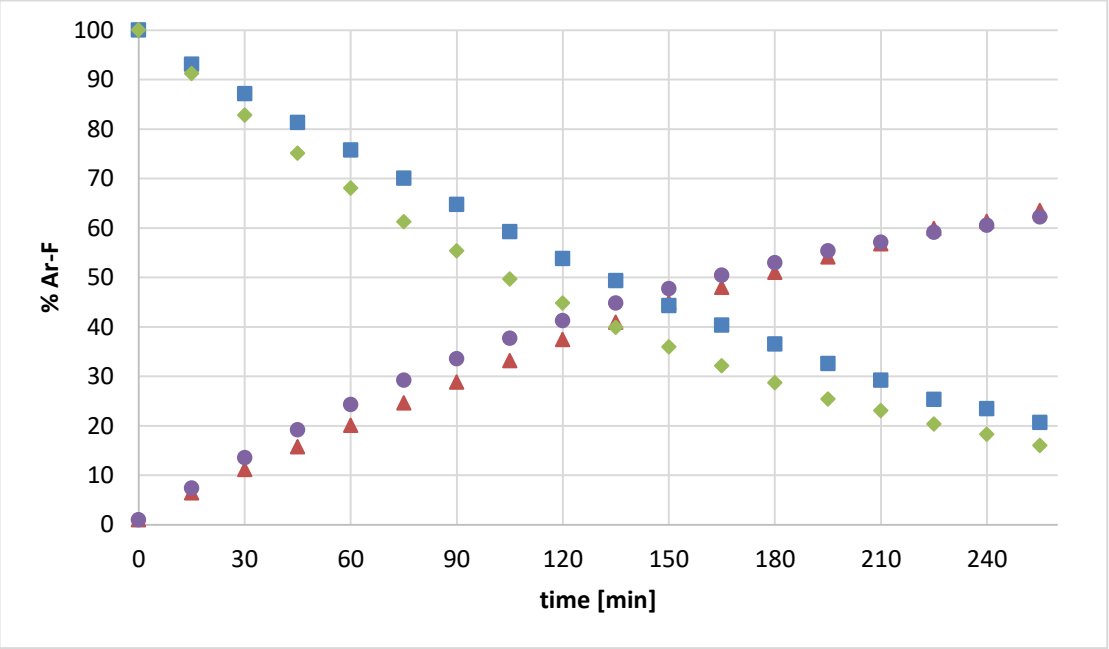

Figure 2.6: Time course plots of the catalytic HDF of 1,2,4-$C_6F_3H_3$ by **1** (5 mol%, $C_6H_5CH_3$, 90°C) showing the consumption profiles (■, ♦) of 1,2,4-$C_6F_3H_3$ and the formation profiles (▲, ●) of 1,4-$C_6F_2H_4$ upon varying the concentrations of Et_3SiH. (■, ▲ = 100 equiv Et_3SiH; ●, ♦ = 20 equiv Et_3SiH).

2.4.2. Probing NHC dissociation in catalytic C-F activation

NHCs have been demonstrated to play an important role in their own right in organofluorine chemistry,[10] mediating catalytic fluorination reactions,[11–13] as well as stoichiometric C-F bond activations of simple fluoroarenes and fluoroalkenes.[14,15]

For example, Kuhn and co-workers reported that N-alkyl carbenes (tetraalkylimidazol-2-ylidenes) effect nucleophilic aromatic substitution in pentafluoropyridine[16] and hexafluorobenzene[17] to afford perfluoroaryl-substituted imidazolium salts (Scheme 2.4A). Kim and Lee[18] described a sequential reaction of an N-aryl carbene (IPr) with two molecules of octafluorotoluene to give a tetrasubstituted imidazolium salt with perfluoro substituents bound at both the C2 and C4 positions (Scheme 2.4B). However, employment of the more electron-rich and thus less activated 1-fluoro-4-trifluoromethylbenzene as a substrate led to just one C-F activation step at the C2 site in IPr or IMes. In contrast, the more nucleophilic (σ-donating) and more electrophilic (π-accepting) cyclic alkyl amino carbenes (CAACs) displayed different reactivity to their diamino counterparts and inserted into the C-F bonds of C_5F_5N (Scheme 2.4C)[19] and C_6F_5X (X = F, H; Scheme 2.4D)[20] to afford single and double C-F activation adducts respectively.[21] The group of Chaplin discovered that the bioxazoline-derived carbene $IBioxMe_4$ enacted selective single and double C-F bond activation of octafluorotoluene and hexafluorobenzne, respectively (Scheme 2.4E).[22] The postulated mechanism for the formation of the fluoroarene substituted zwitterionic imidazoliumolate products involved nucleophilic aromatic substitution by the NHC ligand and concurrent oxazoline ring opening by the liberated fluoride.

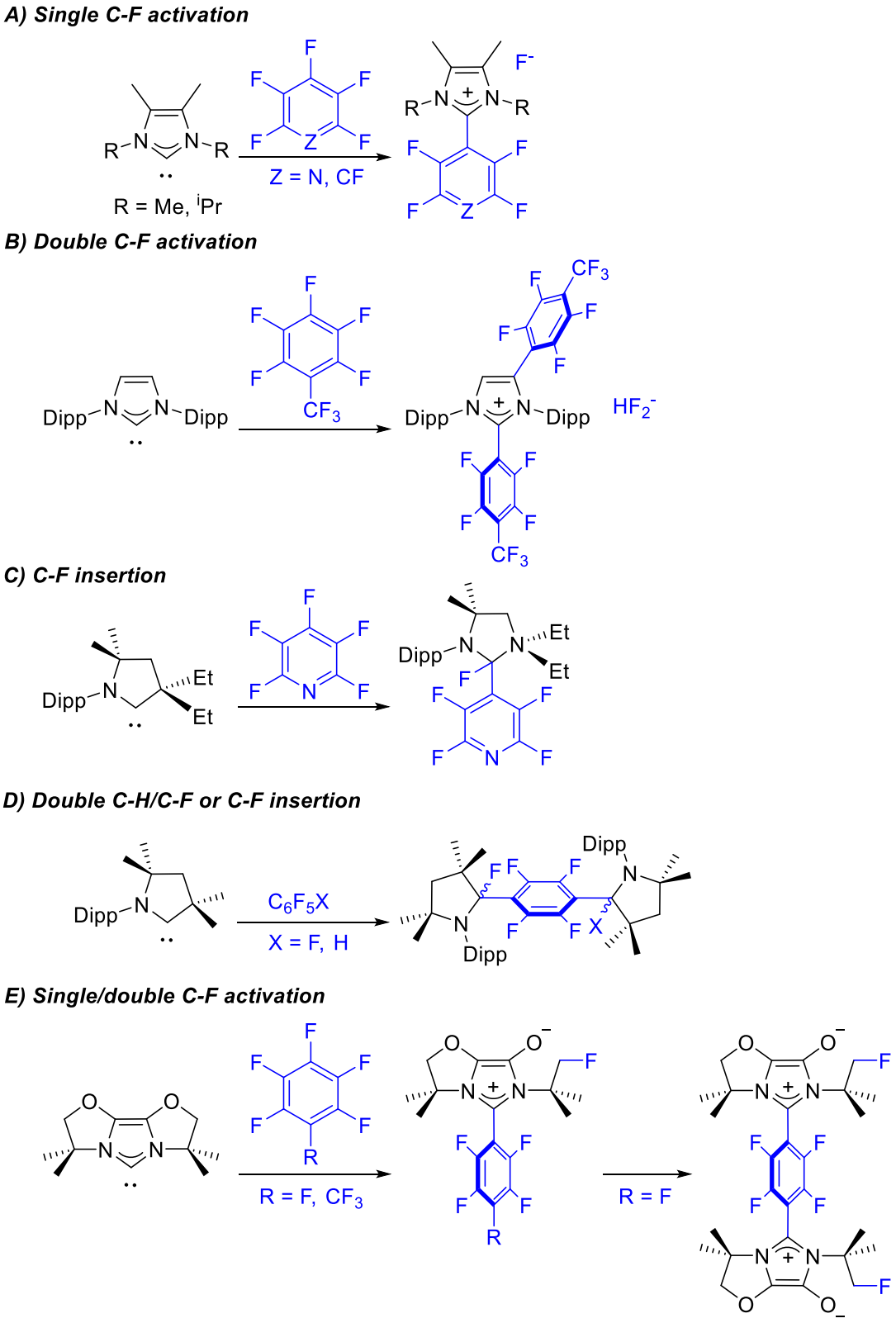

Scheme 2.4: Known examples of C-F activation of perfluoroarenes by NHCs.

The remarkable electron donating properties of NHCs have led to them being regarded as innocent spectator ligands, which bind strongly to late-transition metals and do not dissociate readily from metal centres.[23–27] This was also found to be true for coordinatively saturated **1**, which was probed for carbene loss. No exchange between **1** and IEt_2Me_2 (3 equiv) was observed at room temperature. This indicated that any involvement of a five-coordinate species (such as $[Ru(IMe_4)_3H_2]$) in the HDF reactions carried out at room temperature could be discounted, i.e. room temperature HDF took place at a six-coordinate species *via* a concerted mechanism. However, upon elevating the temperature to 90°C, new hydride resonances appeared in the same δ ~ -8 ppm hydride region of the ^{1}H NMR spectrum as **1**, suggesting that NHC dissociation and exchange was possible at higher temperature.

To investigate if IMe_4 could itself enact C-F bond activation of fluorobenzenes without the need for ruthenium, the free carbene was heated with 1,2,4-$C_6F_3H_3$ (1 equiv) at 70-90°C in the presence of 6 equiv of Et_3SiH. This led to the formation of the addition product, $(IMe_4)C_6F_2H_3(H)$ (**6**) (Scheme 2.5) and Et_3SiF in a 1:1 ratio. **6** was isolated as pale yellow oil and fully characterised by multinuclear NMR spectroscopy (Table 2.3) and mass spectrometry. The backbone methyl groups and the N-Me protons resonated at δ 1.50 and 2.16 respectively. A very small doublet splitting of the latter ($^6J_{HF}$ = 0.7 Hz) was a consequence of coupling to the *ortho*-fluorine in the difluorophenyl ring. The N*C*N bound proton coupled to both *ortho*- and *meta*-fluorine substituents and appeared as a doublet of doublets at δ 4.46 ($^4J_{HF}$ = 2.4 Hz, $^5J_{HF}$ = 0.8 Hz). The aromatic proton signals were unambiguously assigned on the basis of ^{1}H and ^{1}H{^{19}F} NMR spectra. Thus, the *ortho*-H gave rise to a high frequency (δ 7.87) doublet of doublet of doublets due to coupling to *meta*- and *ortho*-fluorines ($^3J_{HF}$ = 9.2 Hz, $^4J_{HF}$ = 5.4 Hz), as well as

N(C*H*)N proton ($^{4}J_{HH}$ = 3.2 Hz). The *meta*- and *para*-protons appeared as multiplets at δ 6.57 and 6.54 respectively, which collapsed into a doublet ($^{3}J_{HH}$ = 9.0 Hz) and a doublet of doublets ($^{3}J_{HH}$ = 9.0 Hz, $^{4}J_{HH}$ = 3.2 Hz) upon ^{19}F decoupling. The *meta*- and *ortho*-fluorines resonated as multiplets at δ -118.1 and -128.4 respectively, which resolved into doublets ($^{5}J_{FF}$ = 18.1 Hz) in the ^{19}F{^{1}H} NMR spectrum. ^{13}C-^{1}H HSQC and HMBC experiments allowed for an unequivocal assignment of all ^{13}C{^{1}H} resonances, with the most pertinent resonances perhaps arising from the NC*N* (δ 86.5, s) and *ipso*-$C_6F_2H_3$ (δ 131.0, dd, $^{2}J_{CF}$ = 17.2 Hz, $^{3}J_{CF}$ = 6.4 Hz) carbons.

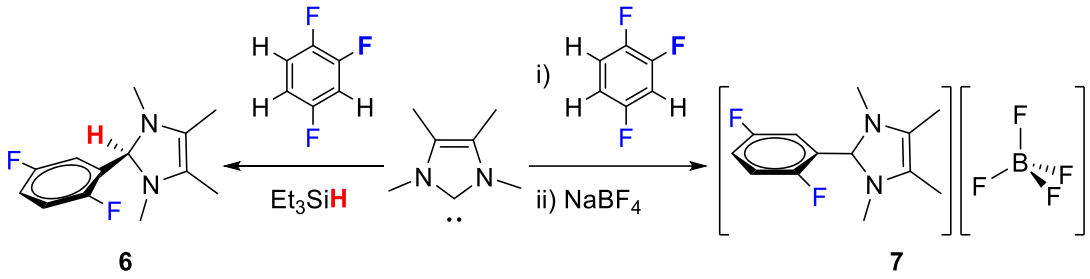

Scheme 2.5: Formation of (IMe_4)($C_6F_2H_3$)(H) (**6**) and [$IMe_4C_6F_2H_3$][BF_4] (**7**) from stoichiometric C-F activation reactions of 1,2,4-$C_6F_3H_3$ with IMe_4.

Table 2.3: ^{1}H, ^{19}F and selected $^{13}C\{^{1}H\}$ NMR data for $(IMe_4)C_6H_3F_2(H)$ (**6**) and $[IMe_4C_6H_3F_2][BF_4]$ (**7**).

		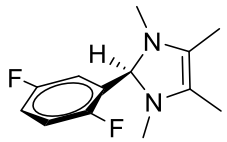 **6**	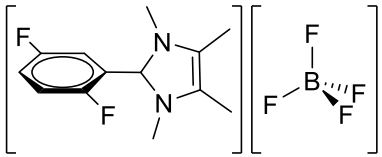 **7**
^{1}H	NCC*H*$_3$	1.50 (s)	2.33 (s)
	NC*H*$_3$	2.16 (d, $^{6}J_{HF}$ = 0.7 Hz)	3.56 (d, $^{6}J_{HF}$ = 0.6 Hz)
	NC*H*N	4.46 (dd, $^{4}J_{HF}$ = 2.4 Hz, $^{5}J_{HF}$ = 0.8 Hz)	-
	o-C$_6$F$_2$*H*$_3$	7.87 (ddd, $^{3}J_{HF}$ = 9.2 Hz, $^{4}J_{HF}$ = 5.4 Hz, $^{4}J_{HH}$ = 3.2 Hz)	7.49 (m, $^{4}J_{HH}$ = 3 Hz)
	m-C$_6$F$_2$*H*$_3$	6.57 (m, $^{3}J_{HH}$ = 9.0 Hz)	7.36 (m, $^{3}J_{HH}$ = 9.2 Hz)
	p-C$_6$F$_2$*H*$_3$	6.54 (m, $^{3}J_{HH}$ = 9.0 Hz, $^{4}J_{HH}$ = 3.2 Hz)	7.45 (m, $^{3}J_{HH}$ = 9.2 Hz, $^{4}J_{HH}$ = 3 Hz)
^{19}F	*m*-C$_6$*F*$_2$H$_3$	-118.1 (m, $^{5}J_{FF}$ = 18.1 Hz)	-114.9 (dtd, $^{5}J_{FF}$ = 17.2 Hz, $^{3}J_{FH}$ = 7.8 Hz, $^{4}J_{FH}$ = 4.3 Hz)
	p-C$_6$*F*$_2$H$_3$	-128.4 (m, $^{5}J_{FF}$ = 18.1 Hz)	-117.5 (m, $^{5}J_{FF}$ = 17.2 Hz)
$^{13}C\{^{1}H\}$	*ipso*-*C*$_6$F$_2$H$_3$	131.0 (dd, $^{2}J_{CF}$ = 17.2 Hz, $^{3}J_{CF}$ = 6.4 Hz)	111.3 ($^{2}J_{CF}$ = 17.2 Hz, $^{3}J_{CF}$ = 9.2 Hz)
	NC*N*	86.5 (s)	136.9 (s)

Although **6** could not be isolated for structural verification, activation at the C2 position was confirmed by an X-ray structure of the imidazolium salt, $[IMe_4C_6F_2H_3][BF_4]$ (**7**) (Figure 2.7), which was obtained upon thermolysis of IMe_4 and 1,2,4-$C_6F_3H_3$ in the absence of any silane (to afford $(IMe_4)(C_6F_2H_3)(F)$), followed by halide extraction with $NaBF_4$.[iv] Similarly to **6**, compound **7** was fully characterised by NMR spectroscopy and all relevant ^{1}H, ^{19}F and $^{13}C\{^{1}H\}$ resonances and coupling constants are listed in Table 2.3. The change in N*C*N hybridisation from sp^3 in **6** to sp^2 in **7** was reflected in a significant shift of the $^{13}C\{^{1}H\}$ NMR signal to higher frequency (from δ 86.5 to 136.9), consistent with decreased shielding.

[iv] Ion exchange was carried out in order to overcome any potential issues arising from the presence of different anions as indicated by ^{1}H and ^{19}F NMR analysis, which implied that at least some of the anion accompanying the cation was bifluoride $[HF_2]^-$, presumably formed by hydrolysis. Selected NMR data for "$[IMe_4C_6H_3F_2][HF_2]$": ^{1}H NMR (500 MHz, CD_2Cl_2, 25°C): δ 16.08 (t, J_{HF} = 121.6 Hz, HF_2^-). ^{19}F NMR (470 MHz, CD_2Cl_2, 25°C): δ -156.5 (d, J_{FH} = 121.6 Hz, HF_2^-). c.f. δ -156.7 for the imidazolium salt shown in Scheme 2.5B.

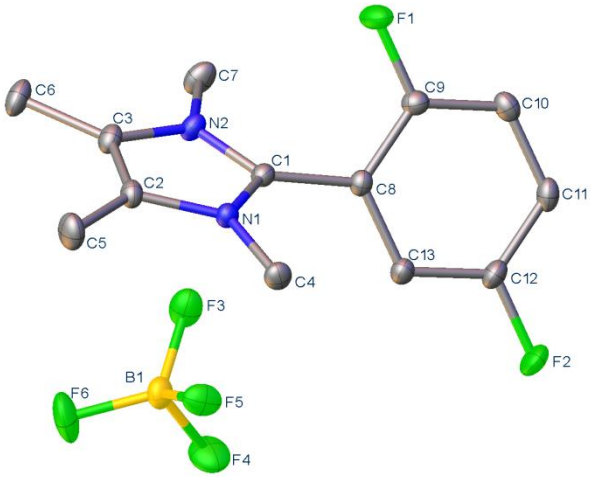

Figure 2.7: Molecular structure of $[IMe_4C_6F_2H_3][BF_4]$ (**7**). Thermal ellipsoids are represented at 30% probability. Hydrogen atoms have been omitted for clarity. Selected bond lengths (Å) and angles (°) for the cation: C1-N1 (1.335(2)), C1-N2 (1.386(2)), C1-C8 (1.469(2)), N1-C2 (1.386(2)), N2-C3 (1.385(2)), C2-C3 (1.356(2)), N2-C1-N1 (107.72(13)), C1-N1-C2 (109.31(13)), N1-C2-C3 (106.91(14)), C2-C3-N2 (106.91(14)), C3-N2-C1 (109.15(13)).

To address the possibility that **6** could eliminate 1,4-$C_6F_2H_4$ and hence catalyse the HDF of 1,2,4-$C_6F_3H_3$, an isolated sample of **6** was heated at 90°C in both the presence and absence of Et_3SiH. In both cases ^{19}F NMR analysis showed <15% conversion to 1,4-$C_6F_2H_4$, implying only a very low level of NHC-mediated stoichiometric HDF. In addition, the absence of any **6** resulting from carbene loss at the end of catalytic runs with **1** provided further evidence that the coordinatively unsaturated species, $[Ru(IMe_4)_3H_2]$, was not catalytically relevant even in the high temperature HDF experiments.

The abovementioned studies were reinforced by monitoring the consumption of 1,2,4-$C_6F_3H_3$ in the presence of **1** by ^{19}F NMR spectroscopy in a series of kinetic experiments summarised in the time course plots shown in Figure 2.8. These revealed

that the rate of HDF of 1,2,4-$C_6F_3H_3$was increased by the presence of 10 equiv of IMe_4 (---), compared to a reference experiment where only **1** and Et_3SiH were used (**XXX**). However, in a substoichiometric reaction between IMe_4 and 1,2,4-$C_6F_3H_3$(1:2 ratio = 50 mol% [IMe_4] loading; ▲▲▲) only one equiv of fluoroarene was consumed (50% conversion), and so the faster decay profile for the experiment with both **1** and IMe_4 resulted from synergistic catalytic and stoichiometric C-F activation, respectively.

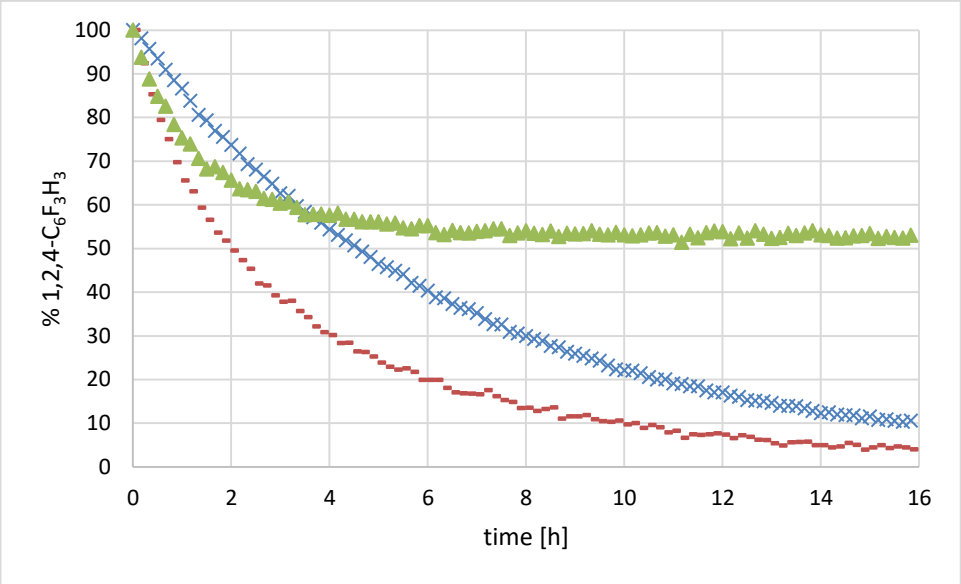

Figure 2.8: Time course plots showing the consumption profile of 1,2,4-$C_6F_3H_3$ in a catalytic HDF reaction using **1** (5 mol%, 100 equiv Et_3SiH, C_6H_6, 70°C) in the absence of any additional IMe_4 (**XXX**), a catalytic HDF reaction using **1** (5 mol%, 100 equiv Et_3SiH, C_6H_6, 70°C) in the presence of 10 equiv IMe_4 (---) and the stoichiometric reaction of 1,2,4-$C_6F_3H_3$ and IMe_4 (2:1 ratio) in C_6H_6 at 70°C (▲▲▲).

2.4.3. DFT study of catalytic HDF

DFT calculations were undertaken by McKay and Macgregor (Heriot-Watt University) to account for the selectivity of the catalytic HDF by **1** of fluoroarenes observed experimentally and to survey the scope of HDF of other fluorobenzenes across

the range C_6F_{6-n} (n = 0-5). Given the importance of the NHC ligand architecture in both facilitating HDF and determining the selectivity of the process, the study employed the full experimental system, i.e. using IMe_4 ligands. Having discounted experimentally a stepwise HDF process involving NHC/fluoroarene substitution, the study focused on the concerted mechanism using 1,2,4-$C_6F_3H_3$ as a model substrate. The full reaction profile is presented in Figure 2.9. The most accessible pathway, with a free energy barrier of +16.2 kcal mol^{-1}, involved attack of the hydride ligand of **1** at the C2 position of 1,2,4-$C_6F_3H_3$. The corresponding transition state (**TS(1-3)$_{2F}$**) showed a slight bending of the {Ru···H^a···C2} moiety (171.9°) and an elongation of Ru···H^a and C2-F2 bonds to 1.90 Å and 1.41 Å respectively. At this point, the new C2-H^a bond formation (1.64 Å) and the contraction of the Ru-H^b (1.65 Å) distance occured, the latter being a consequence of a weakening Ru-H^a interaction. The approaching fluoroarene, defined by the C6 plane, was tilted towards the best-fit plane containing Ru and four carbenic carbons of the NHC ligands. The $\{C_6F_3H_4\}^-$ moiety resembled a Meisenheimer intermediate featuring elongated C_{ipso}-C_{ortho} distances, although H-transfer onto C2 was more advanced than the F-displacement, as indicated by negligible increase in the C2-F2 bond length with respect to the free 1,2,4-$C_6F_3H_3$, as well as the long Ru···F2 distance (3.70 Å). Nonetheless, characterisation *via* IRC calculations confirmed direct migration of F2 onto Ru to form **3** and release 1,4-$C_6F_2H_4$. Overall, the HDF process proved to be highly exothermic (ΔG = -49.9 kcal mol^{-1}).

To assess the overall regioselectivity of 1,2,4-$C_6F_3H_3$ at **1**, the reactions at C1 and C4 were also considered. These proceeded *via* transition states **TS(1-3)$_{1F}$** and **TS(1-3)$_{4F}$** at +19.7 kcal mol^{-1} and +21.4 kcal mol^{-1}, respectively. The geometry of both transition states were similar to **TS(1-3)$_{2F}$**, although with slightly longer Ru···H^a (1.93 Å) and shorter C1/C4···H^a distances (1.58 and 1.56 Å respectively), in line with higher

calculated energy barriers. Thus, formation of 1,4-$C_6F_2H_4$ was a consequence of a clear kinetic preference for the Ru-H attack to occur at the 2-position, as borne out experimentally (Table 2.2, entry 3).

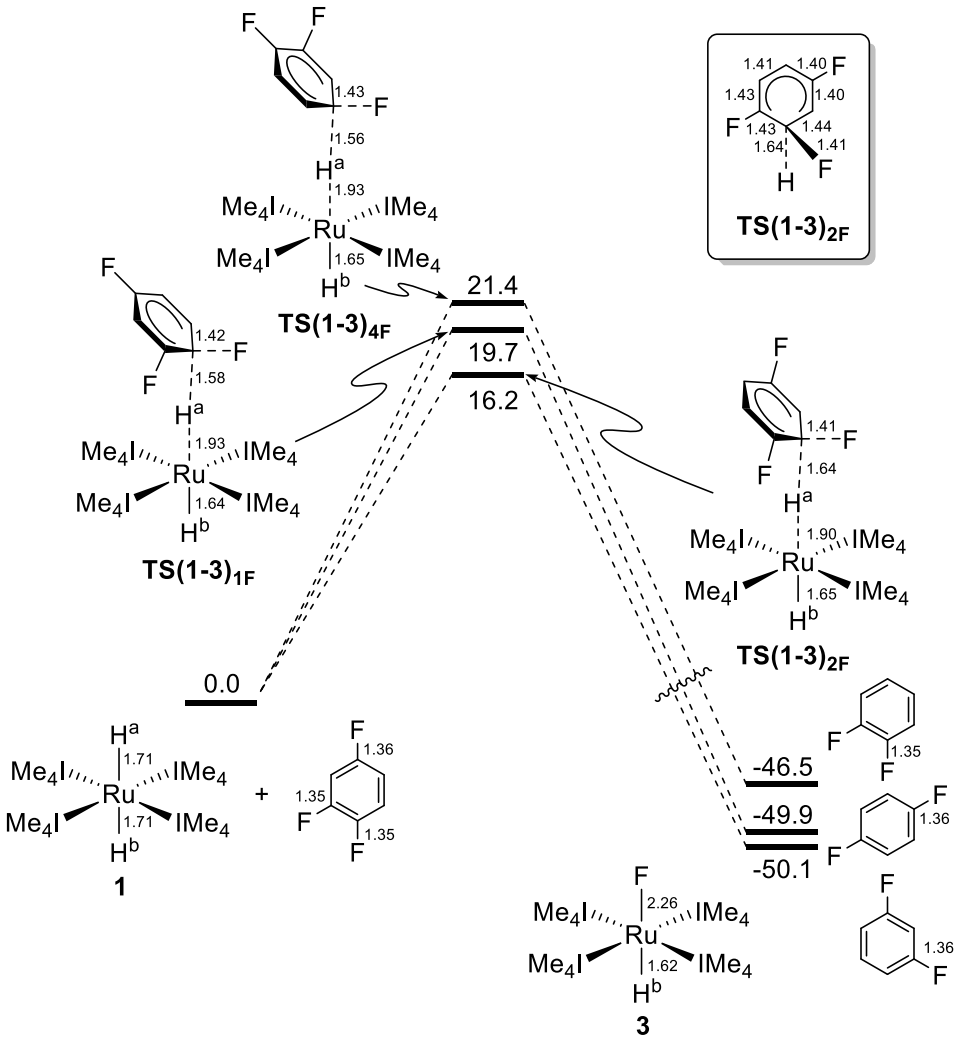

Figure 2.9: Computed reaction profile for HDF of 1,2,4-$C_6F_3H_3$ at *trans*-[Ru(IMe$_4$)$_4$H$_2$] (**1**). Energies (kcal mol^{-1}) are quoted relative to **1** and 1,2,4-$C_6F_3H_3$ computed separately. Selected distances are shown in Å.

Figure 2.10 shows the computed scope of HDF for a range of fluoroarenes at **1**. Consistent with previous reports,[28,29] the C-F bond energy increased as the number of fluorine substituents was reduced. Moreover, the substitution pattern on the aromatic ring dictated the selectivity of HDF and the process was mostly facilitated by the

presence of *ortho*-substituents, which lowered the strength of the target C-F bond. *meta*-F substituents had the same effect, although to a lesser extent, while *para*-F substitution led to higher energy barriers. These predicted trends were supported experimentally, with more forcing conditions required for the HDF of lower fluorinated substrates. Thus, for C_6F_5H (Figure 2.10a), reaction at the C4-position (*para* to H and adjacent to two *ortho*- and two *meta*-F substituents) was favoured over the C2-position with only one *ortho*- and one *para*-F substituent (9.7 vs 13.2 kcal mol^{-1}, respectively). Both 1,2,3,4- and 1,2,3,5- isomers of $C_6F_4H_2$ were calculated to give 1,2,4-$C_6F_3H_3$ and ultimately 1,4-$C_6F_2H_4$ (Figure 2.10b), which did not undergo further HDF due to the unfavourable *para*-arrangement and consequently high barrier of 25.6 kcal mol^{-1}. For 1,2,3,5-$C_6F_4H_3$, reaction at C1-position ($\Delta G^{\dagger}$ = 13.0 kcal mol^{-1}) was only marginally favoured over the C2-position ($\Delta G^{\dagger}$ = 13.6 kcal mol^{-1}), which again reflected a subtle balance of directing effects i.e. the combination of one *ortho*- and two *meta*-substituents at the C1 position led to a decreased barrier, while the presence of two *ortho*-F substituents at C2 was mitigated by one *para*-F substituent. Figure 2.10c suggests that HDF of 1,2,3- and 1,3,5-$C_6F_3H_3$ was possible (barriers of 15.4 kcal mol^{-1} and 18.6 kcal mol^{-1}, respectively) and proceeded to form 1,3-$C_6F_2H_4$. In contrast to 1,4-$C_6F_2H_4$, the HDF of the 1,3 isomer to C_6FH_5 was predicted to occur *via* a barrier of 21.9 kcal mol^{-1}, thanks to the *meta*-arrangement of F-substituents in this isomer. The formation of fluorobenzene was predicted to be even more accessible starting from 1,2-$C_6F_2H_4$ (barrier of 20.3 kcal mol^{-1}), which contained F-substituents in the most favourable *ortho*-disposition. Reduction of fluorobenzene to benzene was too energetically expensive ($\Delta G^{\dagger}$ = 26.1 kcal mol^{-1}) and did not take place.

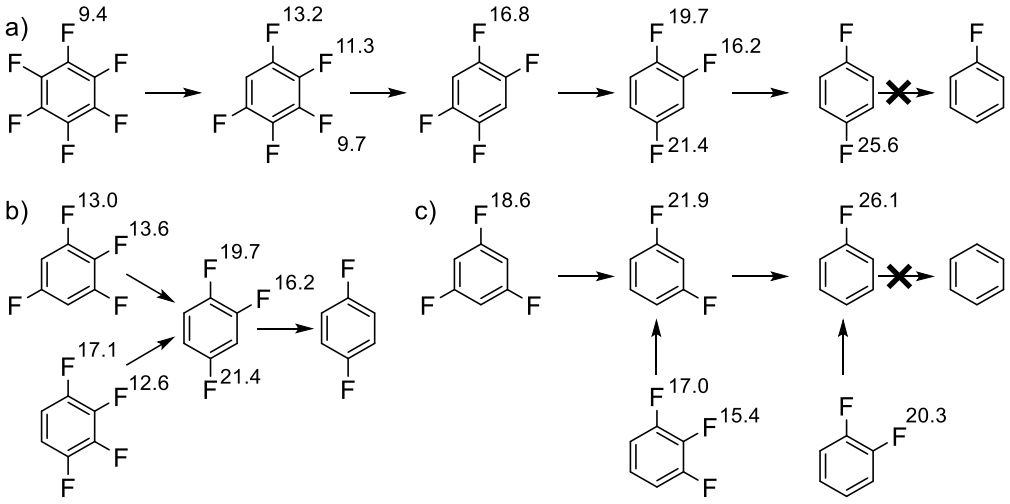

Figure 2.10: Scope of HDF for a range of fluorobenzene substrates. Calculated barriers are in kcal mol^{-1} and were calculated relative to **1** and the appropriate fluoroarene.

2.5. Summary

In conclusion, a joint experimental and computational study of the catalytic HDF of aromatic fluorocarbons at highly electron rich *trans*-[$Ru(NHC)_4H_2$] complexes has been attempted. The *trans*-[$Ru(IMe_4)_4H_2$] complex **1** exhibits outstanding activity and is capable of converting C_6F_6 to 1,4-$C_6F_2H_4$ at room temperature in the presence of alkyl silanes. 1,2- and 1,3- isomers of $C_6F_2H_4$ could be further reduced to fluorobenzene albeit only at 120°C. The high *para*-regioselectivity observed on going from C_6F_5H to 1,2,4,5-$C_6F_4H_2$ contrasts with that of the original system [$Ru(IPr)(PPh_3)_2(CO)H_2$] (**I**)[28–30] and can be rationalised by the DFT calculations, which show that HDF proceeds *via* a concerted nucleophilic attack mechanism at a six-coordinate species. No role for free carbene promoted HDF was proven by the absence of any appreciable elimination of 1,4-$C_6F_2H_4$ from (IMe_4)$C_6H_3F_2$(H) (**6**) and the absence of the latter at the end of catalytic runs with **1**. Selective reduction of 1,2,4-$C_6F_3H_3$ to 1,4-$C_6F_2H_4$ is attributed to the kinetic proclivity for HDF at the C2 position. The rate of catalytic HDF reactions was unaffected by the concentration of the terminal silane reductant, indicating that the

rate-limiting step in the catalytic cycle involved activation of the fluoroarene. However, lower conversions were observed with aryl silanes, most likely due to their propensity to form charge separated species such as the structurally characterised $[Ru(IMe_4)_4H][Ph_3SiF_2]$ (**5**). The remarkable performance of **1** clearly illustrates the importance of rational catalyst design in controlling the mechanism and thus the synthetic outcome of the HDF reaction.

2.6. References for Chapter 2

(1) Wolf, R.; Plois, M.; Hepp, A. *Eur. J. Inorg. Chem.* **2010**, 918.

(2) Whittlesey, M. K.; Perutz, R. N.; Greener, B.; Moore, M. H. *Chem. Commun.* **1997**, 2, 187.

(3) Christe, K. O.; Wilson, W. W. *J. Fluorine Chem.* **1990**, *47*, 117.

(4) Burling, S.; Häller, L. J. L.; Mas-Marzá, E.; Moreno, A.; Macgregor, S. A.; Mahon, M. F.; Pregosin, P. S.; Whittlesey, M. K. *Chem. – Eur. J.* **2009**, *15*, 10912.

(5) Whittlesey, M. K.; Perutz, R. N.; Moore, M. H. *Chem. Commun.* **1996**, 6, 787.

(6) Gianetti, T. L.; Bergman, R. G.; Arnold, J. *Chem. Sci.* **2014**, *5*, 2517.

(7) Yamaguchi, S.; Akiyama, S.; Tamao, K. *Organometallics* **1999**, *18*, 2851.

(8) Prince, P. D.; Bearpark, M. J.; McGrady, G. S.; Steed, J. W. *Dalton Trans.* **2007**, *2*, 271.

(9) Vergote, T.; Nahra, F.; Peeters, D.; Riant, O.; Leyssens, T. *J. Organomet. Chem.* **2013**, *730*, 95.

(10) Reddy, V. P.; Vadapalli, A.; Sinn, E.; Hosmane, N. *J. Organomet. Chem.* **2013**, *747*, 43.

(11) Dong, X.; Yang, W.; Hu, W.; Sun, J. *Angew. Chem. Int. Ed.* **2015**, *54*, 660.

(12) Li, F.; Wu, Z.; Wang, J. *Angew. Chem. Int. Ed.* **2015**, *54*, 656.

(13) Wang, X.; Wu, Z.; Wang, J. *Org. Lett.* **2016**, *18*, 576.

(14) Leclerc, M. C.; Gorelsky, S. I.; Gabidullin, B. M.; Korobkov, I.; Baker, R. T. *Chem. – Eur. J.* **2016**, *22*, 8063.

(15) Arduengo III, A. J.; Calabrese, J. C.; Dias, H. V. R.; Davidson, F.; Goerlich, J. R.; Jockisch, A.; Kline, M.; Marshall, W. J.; Runyon, J. W. *Phosphorus Sulfur Silicon Relat. Elem.* **2016**, *191*, 527.

(16) Kuhn, N.; Fahl, J.; Boese, R.; Henkel, G. *Z. Für Naturforschung B* **1998**, *53*, 881.

(17) Mallah, E.; Kuhn, N.; Maichle-Mößmer, C.; Steimann, M.; Ströbele, M.; Zeller, K.-P. *Z. Für Naturforschung B* **2009**, *64*, 1176.

(18) Kim, Y.; Lee, E. *Chem. Commun.* **2016**, *52*, 10922.

(19) Styra, S.; Melaimi, M.; Moore, C. E.; Rheingold, A. L.; Augenstein, T.; Breher, F.; Bertrand, G. *Chem. – Eur. J.* **2015**, *21*, 8441.

(20) Turner, Z. R. *Chem. – Eur. J.* **2016**, *22*, 11461.

(21) Paul, U. S. D.; Radius, U. *Chem. – Eur. J.* **2017**, *23*, 3993.

(22) Emerson-King, J.; Hauser, S. A.; Chaplin, A. B. *Org. Biomol. Chem.* **2017**, *15*, 787.

(23) Weskamp, T.; Kohl, F. J.; Hieringer, W.; Gleich, D.; Herrmann, W. A. *Angew. Chem. Int. Ed.* **1999**, *38*, 2416.

(24) Schwarz, J.; Böhm, V. P. W.; Gardiner, M. G.; Grosche, M.; Herrmann, W. A.; Hieringer, W.; Raudaschl-Sieber, G. *Chem. – Eur. J.* **2000**, *6*, 1773.

(25) Huang, J.; Jafarpour, L.; Hillier, A. C.; Stevens, E. D.; Nolan, S. P. *Organometallics* **2001**, *20*, 2878.

(26) Hu, X.; Castro-Rodriguez, I.; Olsen, K.; Meyer, K. *Organometallics* **2004**, *23*, 755.

(27) Dorta, R.; Stevens, E. D.; Scott, N. M.; Costabile, C.; Cavallo, L.; Hoff, C. D.; Nolan, S. P. *J. Am. Chem. Soc.* **2005**, *127*, 2485.

(28) Panetier, J. A.; Macgregor, S. A.; Whittlesey, M. K. *Angew. Chem. Int. Ed.* **2011**, *50*, 2783.

(29) Macgregor, S. A.; McKay, D.; Panetier, J. A.; Whittlesey, M. K. *Dalton Trans.* **2013**, *42*, 7386.

(30) Reade, S. P.; Mahon, M. F.; Whittlesey, M. K. *J. Am. Chem. Soc.* **2009**, *131*, 1847.

-

CHAPTER THREE

C-F bond activation using $[Ru(NHC)_2L_2H_2]$ complexes

3.1. Introduction

Our group has previously reported the synthesis and small molecule reactivity of *trans*-dihydride isomers of $[Ru(NHC)_2(PPh_3)_2H_2]$ (NHC = IEt_2Me_2 (**cct-8**), IMe_4 (**ttt-9**)).[i,1] Both complexes were shown to react similarly with CO and CO_2 to give $[Ru(NHC)_2(CO)_3]$ and $[Ru(NHC)_2(PPh_3)(OCHO)H]$ respectively, demonstrating facile phosphine loss from Ru (Scheme 3.1). The *trans*-arrangement of the two hydride ligands in **cct-8** and **ttt-9** imparted highly nucleophilic character of Ru-H, which was evidenced by the formation of $[Ru(NHC)_2(PPh_3)_2H][I]$ and CH_4 in the reactions with electrophile MeI. This suggested that **cct-8** and **ttt-9** could act as (pre)catalysts for the HDF of fluoroarenes. It was anticipated that mixed NHC/PPh_3 *trans*-dihydride species would show enhanced HDF activity over the original system, $[Ru(IPr)(PPh_3)_2(CO)H_2]$ (**I**), but display poorer control of HDF regioselectivity than the corresponding tetracarbene species, $[Ru(NHC)_4H_2]$ (**1** and **2**), as the process could proceed *via* both concerted and stepwise pathways at five-coordinate species, i.e. $[Ru(NHC)_2(PPh_3)H_2]$, as well as along a concerted pathway at six-coordinate complexes.

[i] cct- and ttt- stand for *cis,cis,trans*- and *trans,trans,trans*- respectively and correspond to the relative arrangement of carbene, phosphine and hydride (or hydride/ fluoride) ligands respectively. Figure 3.10 summarises all possible isomers of complex **9**.

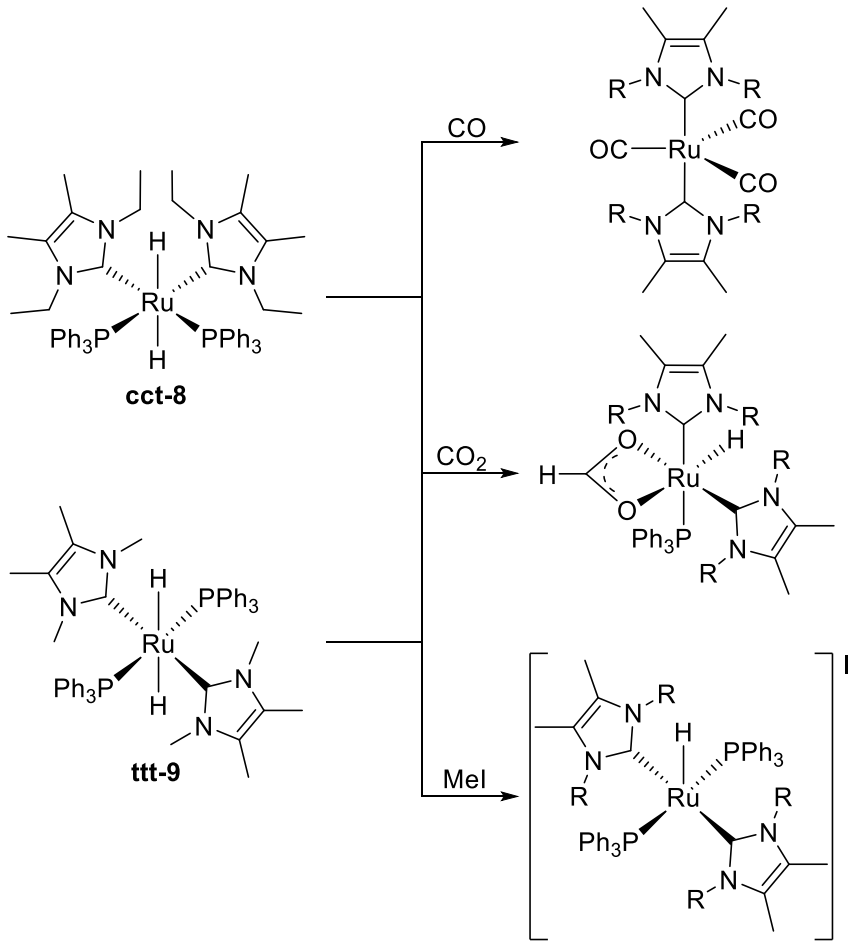

Scheme 3.1: Reactivity of $[Ru(IEt_2Me_2)_2(PPh_3)_2H_2]$ (**cct-8**) and $[Ru(IMe_4)_2(PPh_3)_2H_2]$ (**ttt-9**) with CO, CO_2 and MeI.

3.2. Stoichiometric C-F and C-H activation of C_6F_6 and C_6F_5H using $[Ru(IEt_2Me_2)_2(PPh_3)_2H_2]$ (cct-8)

The reaction of **cct-8** with 10 equiv of either C_6F_6 or C_6F_5H in a C_6H_6 solution[ii] proceeded at room temperature with full consumption of the starting material after ca. 5 h, as indicated by ^{31}P NMR spectroscopy. This showed the appearance of two new product peaks at δ 45 and 59, in an approximate ratio of 1:0.2 from C_6F_6 and 1:0.5 with C_6F_5H. These were assigned to the hydride fluoride

[ii] C_6D_6 needs to be avoided due to the facile H/D exchange in **8**.

complex [Ru(IEt_2Me_2)$_2$(PPh_3)$_2$HF] (**cct-10**) and the biscarbene pentafluorophenyl complex [Ru(IEt_2Me_2)$_2$(PPh_3)(C_6F_5)H] (**11**) respectively (Scheme 3.2).

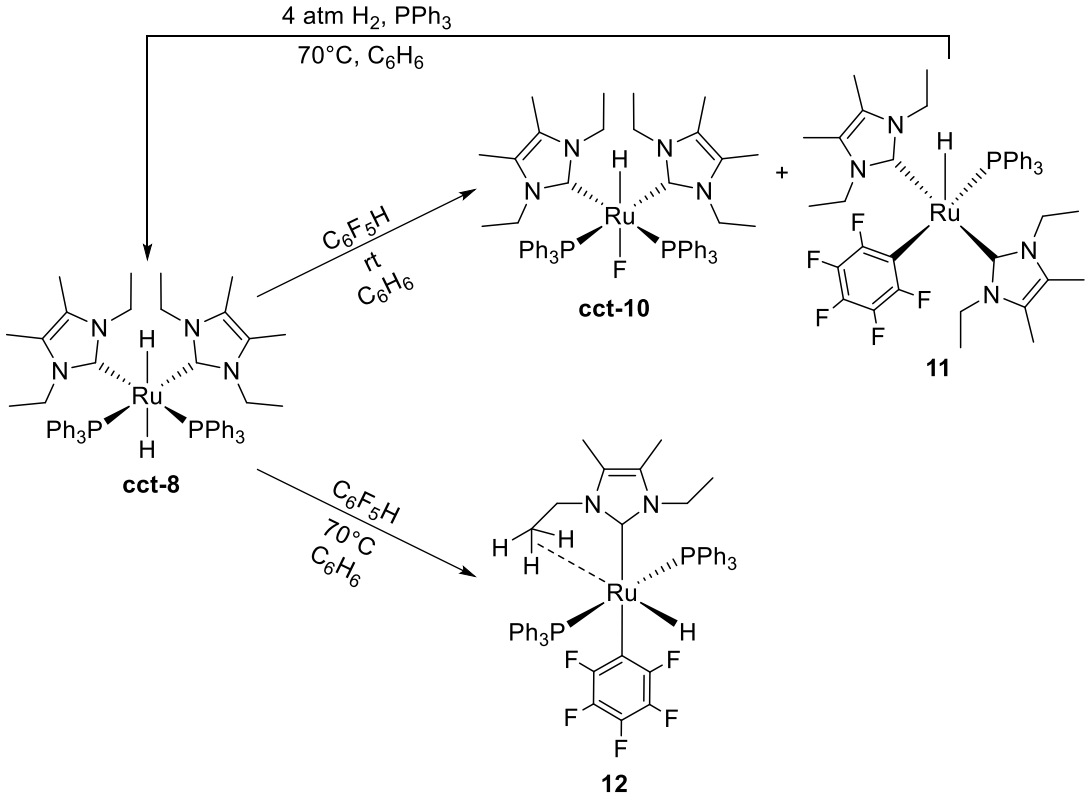

Scheme 3.2: Stoichiometric C-F and C-H activation of C_6F_5H using [Ru(IEt_2Me_2)$_2$(PPh)$_2$$H_2$] (**cct-8**).

Formation of **cct-10** and **11** arose from competing C-F and C-H activation respectively. The latter process could be reversed, as shown by subjecting an *in situ* generated mixture of **cct-10**, **11** and PPh_3 to 4 atm H_2, which brought about disappearance of **11** over ca. 4 h at room temperature. The reversibility of the C-H activation pathway was proven categorically in a more controlled experiment whereby a solution containing an isolated, crystalline sample of **11** and an equivalent of PPh_3 was exposed to 4 atm H_2. This led to the complete conversion of **1** to a mixture of **cct-8** and **cct-10** within 4 h at room temperature.

Analysis of the volatile materials from the reaction of **cct-8** with C_6F_6 by ^1H and ^{19}F NMR spectroscopy helped to explain the observed stoichiometric bond activation steps. The presence of the HDF products C_6F_5H, as well as both 1,2,3,4- and 1,2,4,5-$C_6F_4H_2$, indicated that **cct-8** initially activates the C-F bond in C_6F_6 to give the hydride fluoride complex **cct-10** and C_6F_5H. The released C_6F_5H displayed comparable reactivity as a substrate to C_6F_6 and could undergo C-F activation to generate $C_6F_4H_2$ isomers (and additional **cct-10**), as well as C-H activation to yield **11**. Attempts to accelerate the reaction of **cct-8** with C_6F_5H by employing higher temperatures led to formation of the new bisphosphine pentafluorophenyl complex, $[Ru(IEt_2Me_2)(PPh_3)_2(C_6F_5)H]$ (**12**). The corresponding resonance at δ 52 in the ^{31}P NMR spectrum could also be observed in room temperature experiments, although only after significantly longer times (ca. 100 h) and in negligible amounts (<7% of all Ru containing species). Efforts to convert **11** to its bisphosphine analogue **12** by heating in the presence of PPh_3 (2 equiv) proved unsuccessful, implying that simple NHC/phosphine substitution is not responsible for the formation of the latter. As described in the following sections, all of the organometallic species were isolated and fully characterised by X-ray diffraction and multinuclear NMR spectroscopy.

3.2.1. Isolation and characterisation of $[Ru(IEt_2Me_2)_2(PPh_3)_2HF]$ (cct-10) and $[Ru(IEt_2Me_2)_2(PPh_3)_2H][H_2F_3]$ (13)

Although **cct-10** was initially isolated from the reaction of **cct-8** with C_6F_5H, a more efficient, higher yielding route involved treatment of a C_6H_6 solution of **cct-8** with precisely 0.33 equiv of $Et_3N{\cdot}3HF$ (TREAT-HF). Use of a full equivalent of TREAT-HF instead resulted in the formation of the previously reported cation,[1] $[Ru(IEt_2Me_2)_2(PPh_3)_2H]^+$ with the relatively uncommon $[H_2F_3]^-$ present as

the anion (**13**).[2–6] An optimised synthetic procedure that allowed use of excess TREAT-HF involved *in situ* generation of **13** followed by subsequent salt metathesis with CsF (Scheme 3.3).

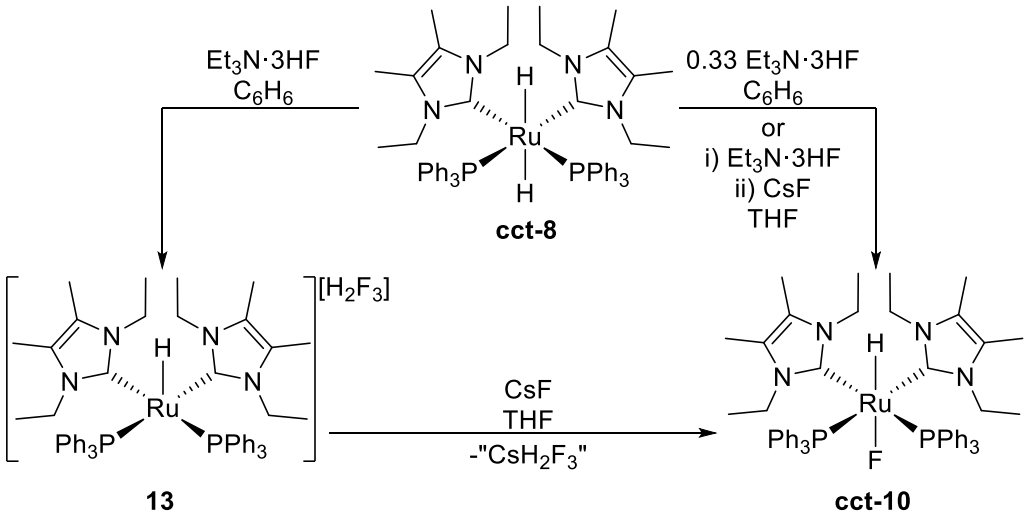

Scheme 3.3: Synthesis of [Ru(IEt$_2$Me$_2$)$_2$(PPh$_3$)$_2$HF] (**cct-10**) and [Ru(IEt$_2$Me$_2$)$_2$(PPh$_3$)$_2$H][H$_2$F$_3$] (**13**).

The hydride fluoride complex (**cct-10**) is isostructural with the parent dihydride **cct-8** and hence there is very little change in either Ru-C/Ru-P distances or C-Ru-C/P-Ru-P angles. The X-ray structure of **cct-10** (Figure 3.1) confirmed the same *trans*-H-Ru-F geometry as found in the [Ru(NHC)$_4$HF] complexes, **3** and **4**, albeit with a shortening of the Ru-F distance (**cct-10**: 2.264(2) Å; **3**: 2.3070(18) Å; **4**: 2.384(4) Å). A diagnostic hydride resonance was recorded in the room temperature ^{1}H NMR spectrum in toluene-d_8 at δ -21.70 as a doublet of triplets with couplings of 52.0 Hz ($^2J_{HF}$) and 19.7 Hz ($^2J_{HP}$). The IEt$_2$Me$_2$ resonances were broad and overlapping, but resolved upon cooling to -45°C into eight sets of methylene (NC*H*$_2$) and four sets of methyl (NCH$_2$C*H*$_3$) signals (Figure 3.2). At this temperature, the hydride resonance was split into a doublet of doublets of doublets ($^2J_{HF}$ = 51.6 Hz, $^2J_{HP}$ = 25.0 Hz, $^2J_{HP}$ = 14.1 Hz), indicating that the two PPh$_3$ ligands are inequivalent

at low temperature. In accordance with this were the changes observed in the $^{31}P\{^{1}H\}$ NMR spectrum. A broad singlet at room temperature was replaced by two very broad, overlapping multiplets at -45°C, with no distinct J_{PP} or J_{PF} splittings. The room temperature ^{19}F NMR spectrum in toluene-d_8 exhibited a broad RuF resonance at δ -354, which partially resolved into a doublet ($^{2}J_{FH}$ = 52.0 Hz) when the solvent was changed to THF-d_8.

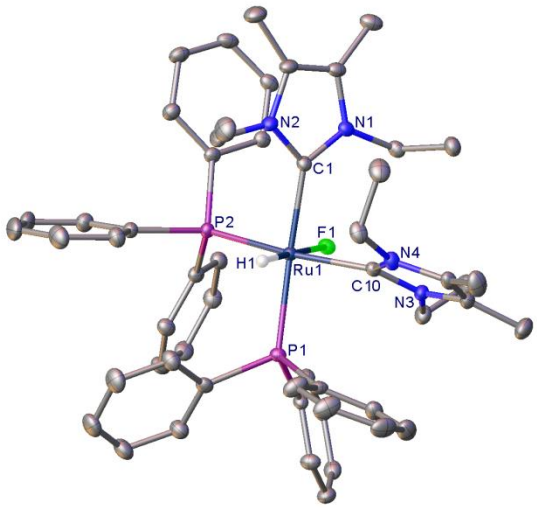

Figure 3.1: Molecular structure of $[Ru(IEt_2Me_2)_2(PPh_3)_2HF]$ (**cct-10**). Thermal ellipsoids are represented at 30% probability. Hydrogen atoms, with the exception of the hydride ligand, have been omitted for clarity. Selected bond lengths and angles are listed in Table 3.1.

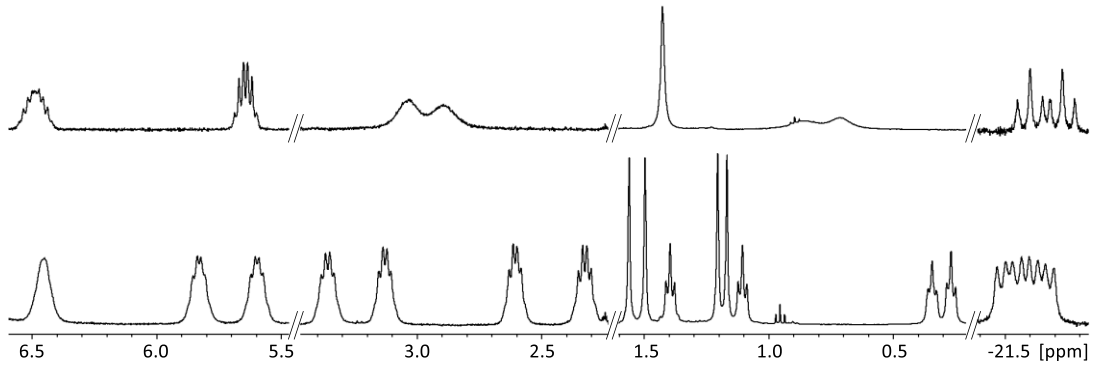

Figure 3.2: Sections of ^{1}H NMR spectra ($C_6D_5CD_3$, 400 MHz; not to scale) of **cct-10** at 25°C (top) and -45°C (bottom).

The molecular structure of **13** is shown in Figure 3.3. The Ru-C and Ru-P bond lengths were almost identical to those found in $[Ru(IEt_2Me_2)_2(PPh_3)_2H][I]$, while the P-Ru-P and C-Ru-C angles were somewhat more acute (161.13(2)° and 165.39(10)° for **13** vs. 165.56(3)° and 169.02(12)° for the iodide counterpart respectively), which is most likely due to different crystal packing of the complexes as in both cases the ions are fully charge separated. The F···F···F bond angle in the anion (124.77(16)°) was found to be smaller than in the simple salt KH_2F_3,[7] which contained two inequivalent $[H_2F_3]^-$ ions with F···F···F angles of ca. 130 and 139°. The F···F bond distances in **13** were 2.281(5) and 2.294(4) Å, within the range of F···F bond lengths reported for KH_2F_3 (2.29-2.35 Å). Since two hydrogen atoms associated with three fluorines could not be reliably located for refinement of the crystal structure, it is not possible to comment on the H···F separations expected in the trifluorodihydrogen anion.

Despite previous solid-state characterisation of the iodide salt of $[Ru(IEt_2Me_2)_2(PPh_3)_2H]^+$, in solution, the complex rearranged to the neutral mono-

PPh_3 hydride iodide complex $[Ru(IEt_2Me_2)_2(PPh_3)HI]$, as indicated by the appearance of a doublet splitting ($^2J_{HP}$ = 41 Hz) on the low frequency hydride resonance (δ -30.45). The room temperature ^{1}H NMR spectrum of **13** in THF-d_8 showed a triplet ($^2J_{HP}$ = 24.0 Hz) signal at δ -29.65, confirming the coordination of two phosphine ligands to the Ru centre. The IEt_2Me_2 ligands were equivalent and gave rise to six resonances at δ 0.44 and 0.88 (t, $^3J_{HH}$ = 7.3 Hz; NCH_2CH_3), 1.81 and 2.01 (s, $NCCH_3$), and 2.75 and 3.36 (q, $^3J_{HH}$ = 7.3 Hz, NCH_2CH_3), which can be accounted for by restricted rotation about the Ru-C_{NHC} bonds. A broad singlet at δ 13.68 was attributed to the $[H_2F_3]^-$ anion and integrated in a 2:1 ratio with Ru-H signal. The downfield chemical shift of the anion matched the value of δ 13.8 reported for $[Mn(dmpe)_2(alkynyl)_2][H_2F_3]$ complexes.[4] The ^{19}F NMR spectrum consisted of a single broad resonance at δ -115.2, which contrasts with the chemical shift of δ -172.2 for the aforementioned manganese compounds.

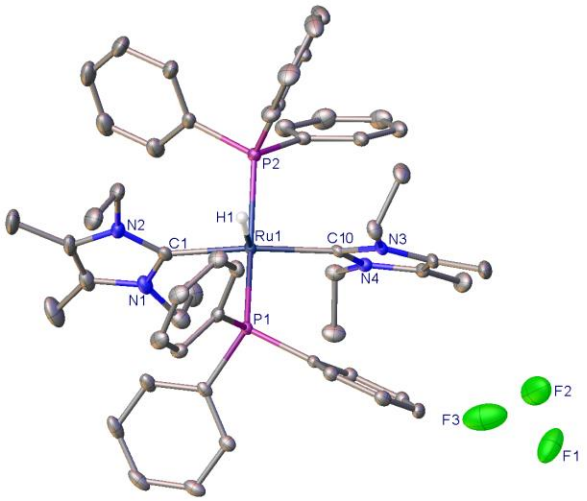

Figure 3.3: Molecular structure of $[Ru(IEt_2Me_2)_2(PPh_3)_2H][H_2F_3]$ (**13**). Thermal ellipsoids are represented at 30% probability. Hydrogen atoms, with the exception of the hydride ligand, have been omitted for clarity. Selected bond lengths (Å) and angles (°): Ru1-C1 2.072(3), Ru1-C10 2.094(2), Ru1-P1 2.3473(6), Ru1-P2 2.3219(6), P1-Ru1-P2 161.13(2), C1-Ru1-P1 90.84(7), C1-Ru1-C10 165.39(10).

3.2.2. Isolation and characterisation of $[Ru(IEt_2Me_2)_2(PPh_3)(C_6F_5)H]$ (11)

The selective preparation of **11** was achieved upon vigorous stirring of a hexane suspension of **cct-8** in the presence of C_6F_5H at room temperature for 24 h, which gave the product as a dark orange precipitate. Recrystallisation from C_6H_6/hexane gave **11** in crystalline form. The X-ray structure (Figure 3.4) revealed that the mutually *trans* NHC ligands (C-Ru-C 173.39(15)°) were arranged at the base of a square pyramid, with the hydride ligand in the apical position. Consequently, the C_6F_5 substituent was positioned opposite PPh_3 (C-Ru-P 172.21(12)°). The angle

formed between the plane of the fluorophenyl ring and the base of the square pyramid was 69.93°, while the Ru-$C_{fluoroaryl}$ bond measured 2.136(4) Å.[iii]

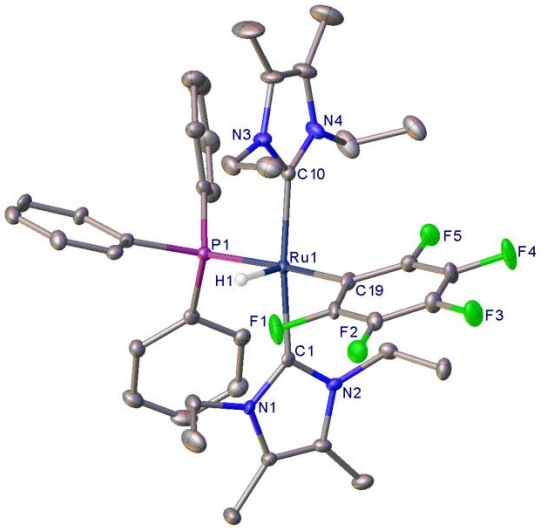

Figure 3.4: Molecular structure of [Ru(IEt_2Me_2)$_2$(PPh_3)(C_6F_5)H] (**11**). Thermal ellipsoids are represented at 30% probability. Hydrogen atoms, with the exception of the hydride ligand, have been omitted for clarity. Selected bond lengths (Å) and angles (°): Ru1-C1 2.090(3), Ru1-C10 2.088(3), Ru1-C19 2.136(4), Ru1-P1 2.2783(11), C1-Ru1-C10 173.39(15), C1-Ru1-C19 88.43(14).

The ^{1}H NMR spectrum of **11** revealed a highly shielded doublet of triplets hydride resonance at δ -33.0 ($^2J_{HP}$ = 30.6 Hz, $^4J_{HF}$ = 7.2 Hz), reflecting the positioning of the hydride ligand opposite a vacant coordination site. ^{19}F NMR spectroscopy revealed three sets of resonances at δ -111.5, -165.6 and -166.4 in a

[iii] The Ru-$C_{fluoroaryl}$ distance in **11** was comparable to those found in the related ruthenium NHC hydride complexes bearing a perfluorinated aryl ligand, such as [Ru(ICy)(dppp)(CO)(Ar^F)H] (Ar^F = C_6F_5, $C_6F_4CF_3$, C_5F_4N)[8] or [Ru(IMes)(PPh_3)(CO)(C_5F_4N)H].[9]

2:2:1 ratio, consistent with a freely rotating C_6F_5 ligand. ^{19}F COSY and ^{1}H-^{19}F HMBC experiments allowed for an unequivocal assignment of the peaks to *ortho*-, *meta*- and *para*-fluorines on the pentafluorophenyl ring respectively. In line with this, the phosphorus signal resolved into a triplet of triplets ($^{4}J_{PF}$ = 20.7 Hz, $^{5}J_{PF}$ = 9.7 Hz), arising from the coupling to *ortho*- and *meta*-fluorines respectively. The appearance of a single doublet signal at 195.9 ($^{2}J_{CP}$ = 4.4 Hz) in the $^{13}C\{^{1}H\}$ NMR spectrum confirmed the equivalence of the two NHC ligands.

3.2.3. Isolation and characterisation of [Ru(IEt$_2$Me$_2$)(PPh$_3$)$_2$(C$_6$F$_5$)H] (12)

The structure of **12** displayed a distorted octahedral geometry, due to the presence of an agostic interaction to the CH_3 group of the N-ethyl arm, occupying the site opposite the Ru-H (Figure 3.5). The agostic distances, Ru···C (2.754(0) Å) and Ru···H (2.065(1) Å), were shorter than the corresponding values found in the previously reported chloride complex [Ru(IEt$_2$Me$_2$)(PPh$_3$)$_2$HCl] (2.823(4) and 2.083(4) Å respectively),[10] suggestive of a strong interaction.[11,12] The angle between the fluoroaryl ring and the mean-plane subtended by the ruthenium centre, the carbenic carbon, the *ipso*-carbon of the fluoroaryl ring and the phosphorus atoms was 85.71°, which contrasted with the corresponding angle found in **11** (69.93°), suggesting that the position of the pentafluorophenyl substituent was locked and enforced by the sterically demanding PPh_3 ligands. The presence of bulky phosphines and the *trans*-arrangement of IEt$_2$Me$_2$ and C_6F_5 ligands accounted for the elongation of the Ru-$C_{fluoroaryl}$ distance to 2.160(2) Å.

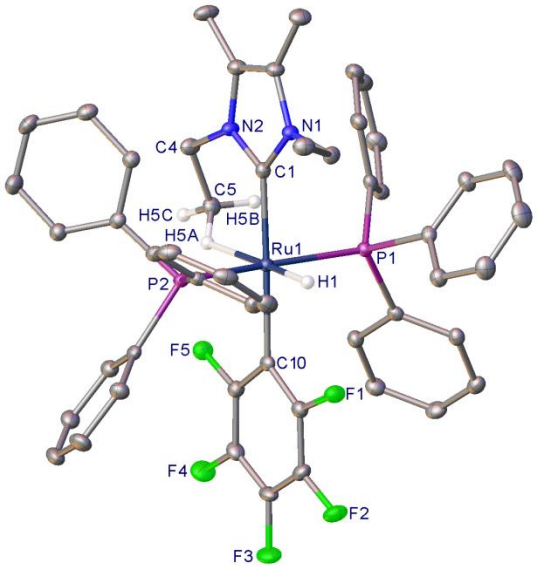

Figure 3.5: Molecular structure of [Ru(IEt$_2$Me$_2$)(PPh$_3$)$_2$(C$_6$F$_5$)H] (**12**). Thermal ellipsoids are represented at 30% probability. Hydrogen atoms, with the exception of the hydride ligand and those on the N-methyl group involved in the agostic interaction, have been omitted for clarity. Selected bond lengths (Å) and angles (°): Ru1-C1 2.060(2), Ru1-C10 2.160(2), Ru1-P1 2.3452(6), Ru1-P2 2.318(6), P1-Ru1-P2 168.093(19), C10-Ru1-P1 91.56(6), C1-Ru1-P2 89.41(6).

The restricted rotation about the Ru-C$_{fluoroaryl}$ bond was substantiated further by ^{19}F NMR spectroscopy, which revealed five distinct resonances at δ -105.5, -111.8, -168.9, -170.1 and -171.5 in a 1:1:1:1:1 ratio. The agostic interaction was retained in solution as evidenced by a low frequency triplet of doublets Ru···H-C resonance at δ 0.48 ($^3J_{HH}$ = 7.3 Hz, $^4J_{HF}$ = 1.5 Hz) and a corresponding doublet signal at δ 6.4 ($^3J_{CP}$ = 7.2 Hz) in the ^{1}H and ^{13}C{^{1}H} NMR spectra respectively (Figure 3.6). The four bond J_{HF} splitting of the methyl agostic protons by one of the *ortho*-fluorines (δ -111.8) on the C$_6$F$_5$ ring was established by ^{1}H-^{19}F HMBC spectroscopy (Figure 3.7). The hydride signal appeared as a triplet of doublets ($^2J_{HP}$ = 23.5 Hz, $^4J_{HF}$ = 6.9 Hz; Figure 3.6) and resonated at a higher frequency (δ -24.7)

than in the case of the five-coordinate, non-agostic **11** (δ -33.0). The J_{HF} splitting was a consequence of coupling to the other *ortho*-F (δ -105.5) as shown by correlation spectroscopy (Figure 3.7).

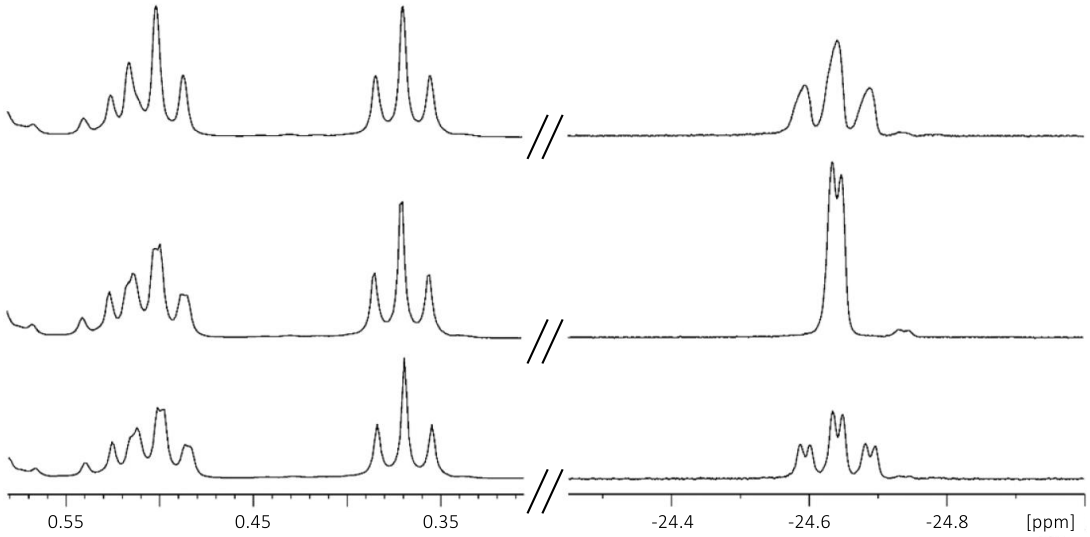

Figure 3.6: Expanded regions of the ^{1}H NMR spectra of [Ru(IEt$_2$Me$_2$)(PPh$_3$)$_2$(C$_6$F$_5$)H] (**12**) (THF-d_8, 500 MHz, 25°C) under a variety of multinuclear decoupling conditions: ^{1}H only (top), ^{1}H{^{31}P} (middle), ^{1}H{^{19}F} (bottom).

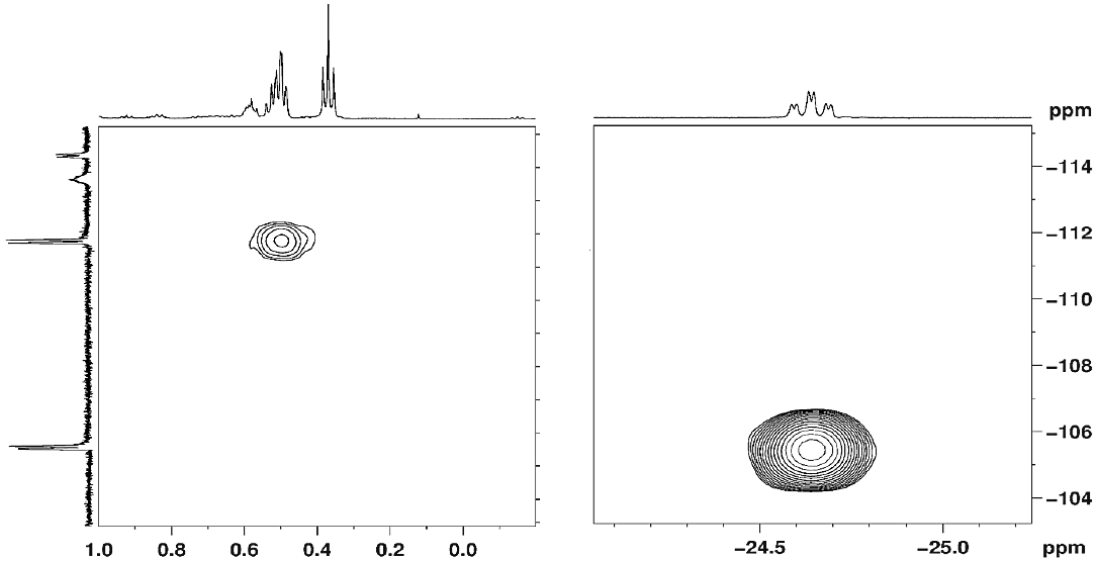

Figure 3.7: Expanded regions of the ^{1}H-^{19}F HMBC (THF-d_8, 500 MHz, 25°C) spectrum of [Ru(IEt_2Me_2)$(PPh_3)_2(C_6F_5)H$] (**12**) showing contacts between methyl protons at δ 0.48 and fluorine at δ -112, and between hydride at δ -24.7 and fluorine at δ -105 ppm.

3.3. Stoichiometric C-F and C-H activation of C_6F_5H using *trans*-[Ru(IMe_4)$_2$(PPh_3)$_2H_2$] (ttt-9)

In contrast to **cct-8**, the reaction of the analogous N-Me carbene derivative **ttt-9** with C_6F_5H (2 equiv) in C_6H_6 required longer reaction times and more forcing conditions to bring about the complete disappearance of the starting dihydride complex. Thus, only after 48 h at 70°C, **ttt-9** was fully converted to [Ru(IMe_4)$_2$(PPh_3)$_2$HF] (**ttt-14**), as established by ^{1}H, $^{31}P\{^{1}H\}$, ^{19}F and $^{13}C\{^{1}H\}$ NMR spectra. ^{1}H-$^{31}P\{^{1}H\}$ HSQC spectroscopy showed a clear correlation between a hydride signal at δ -21.0 ($^{2}J_{HF}$ = 48.0 Hz, $^{2}J_{HP}$ = 22.4 Hz) assigned to **ttt-14** and a doublet resonance at δ 50.1 ($^{2}J_{PF}$ = 18 Hz). The number of NCH_3 and CCH_3 signals was doubled with respect to **ttt-9**, consistent with the reduced symmetry at ruthenium. The corresponding ^{19}F NMR spectrum revealed a broad, low frequency

Ru-F signal at δ -332, while the carbenic carbon was resolved into a triplet ($^2J_{CP}$ = 15 Hz) in the $^{13}C\{^1H\}$ NMR spectrum, consistent with the presence of two equivalent, mutually *trans* IMe_4 ligands situated *cis* to the two phosphines.

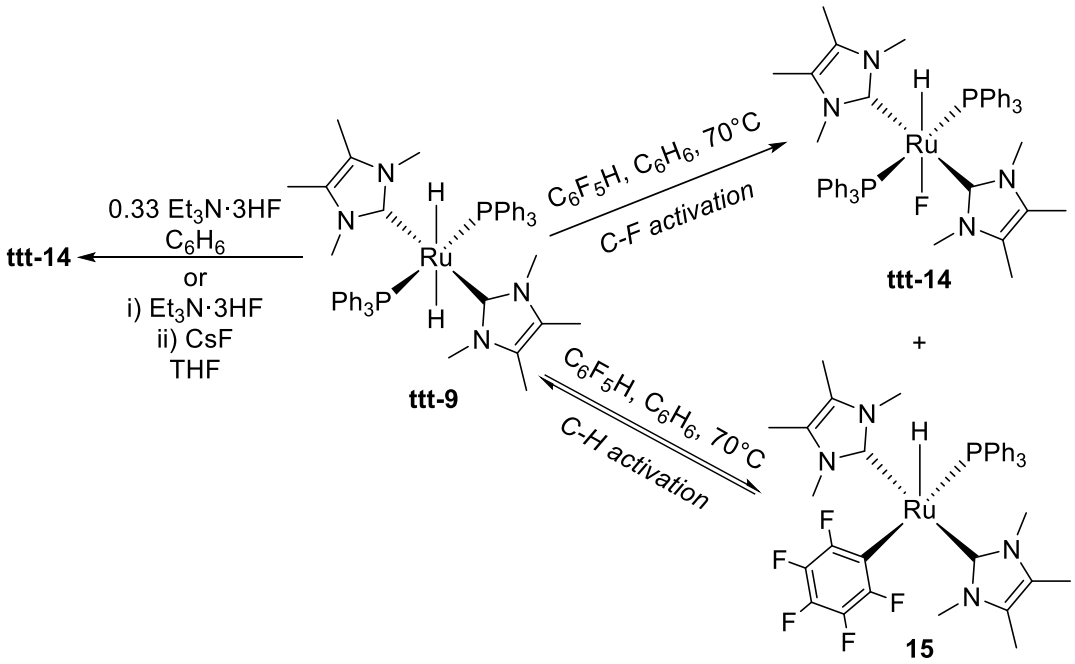

Scheme 3.4: Stoichiometric C-F and C-H activation of C_6F_5H using $[Ru(IMe_4)_2(PPh_3)_2H_2]$ (**ttt-9**) and synthesis of $[Ru(IMe_4)_2(PPh_3)_2HF]$ (**14**) from **ttt-9** and TREAT-HF.

Monitoring the reaction at earlier stages by both ^1H and $^{31}P\{^1H\}$ NMR spectroscopy revealed that the C-F activation of C_6F_5H to give **ttt-14** was accompanied by C-H activation of the substrate to afford another ruthenium containing species, assigned as $[Ru(IMe_4)_2(PPh_3)(C_6F_5)H]$ (**15**) on the basis of the similarity of its NMR spectra to that of the structurally characterised IEt_2Me_2 counterpart, **11** (Scheme 3.4). Thus, the Ru-H signal appeared in the low frequency region of the ^1H NMR spectrum (δ -34.0) as a doublet of triplets ($^2J_{HP}$ = 32.0 Hz, $^4J_{HF}$ = 7.3 H), while the phosphorus signal was observed as a broad singlet at δ 59.5. The absence of **15** at the end of reaction, together with the fact that its formation was

suppressed when **ttt-9** was heated with C_6F_5H under 4 atm H_2, implied that the C-H activation process was reversible, corroborating the previous findings on **cct-8**.

3.4. Isolation of *trans*-[Ru(IMe$_4$)$_2$(PPh$_3$)$_2$HF] (ttt-14)

The hydride fluoride complex (**ttt-14**) could also be conveniently prepared in the same manner as its IEt_2Me_2 analogue (**cct-10**) upon treatment of **ttt-14** with 1 equiv TREAT-HF (to generate *in situ* the ionic complex, $[Ru(IMe_4)_2(PPh_3)_2H][H_2F_3]$)[iv] followed by anion exchange with CsF. Figure 3.8 shows the molecular structure of **ttt-14**, which confirmed retention of the same *trans*-carbene/*trans*-phosphine geometry as in **ttt-9**. The Ru-F distance (2.2694(18) Å) was comparable to those in **3**, **4** and **cct-10**.

[iv] Selected ^{1}H NMR (THF-d_8, 500 MHz, 25°C): δ 13.36 (br s, 2H, $[H_2F_3]^-$), -30.33 (t, $^2J_{HP}$ = 22.4 Hz, 1H, Ru*H*); ^{31}P{^{1}H} NMR (THF-d_8, 202 MHz, 25°C): δ 49.1 (s); ^{19}F NMR (THF-d_8, 470 MHz, 25°C): δ -114.3 (m, $[H_2F_3]^-$).

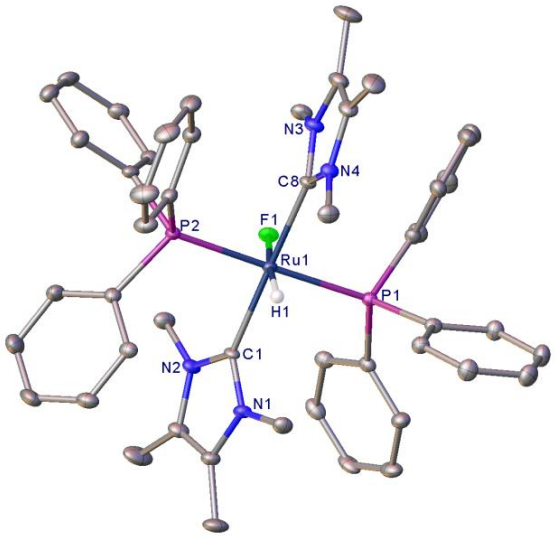

Figure 3.8: Molecular structure of $[Ru(IMe_4)_2(PPh_3)_3HF]$ (**ttt-14**). Thermal ellipsoids are represented at 30% probability. Hydrogen atoms, with the exception of the hydride ligand, have been omitted for clarity. Selected bond lengths and angles are listed in Table 3.1.

3.5. Reactivity of $[Ru(NHC)_2(PPh_3)_2HF]$ with silanes

In order to establish the potential of **cct-8** and **ttt-9** for catalysing HDF of fluoroarenes, the back reaction of the hydride fluoride compounds **cct-10** and **ttt-14** with silanes was investigated. Spectroscopic monitoring by $^{31}P\{^1H\}$ NMR revealed that treatment of **ttt-14** with excess Et_3SiH (3 equiv) led to the full consumption of the former within 20 min at room temperature to afford two new species, neither of which was the parent dihydride **ttt-9** (Figure 3.9). The two products were identified as the ctc-isomer of **9** (Figure 3.10) and the silyl trihydride complex, $[Ru(IMe_4)_2(PPh_3)(SiEt_3)H_3]$ (**16**, δ 58.8, *vide infra*). Over a course of two days, both species disappeared, while a series of new resonances arising from cct-, tcc- and ttt-isomers of **9** were observed. Elevating the temperature to 70°C resulted in full conversion to the latter after 2 h.

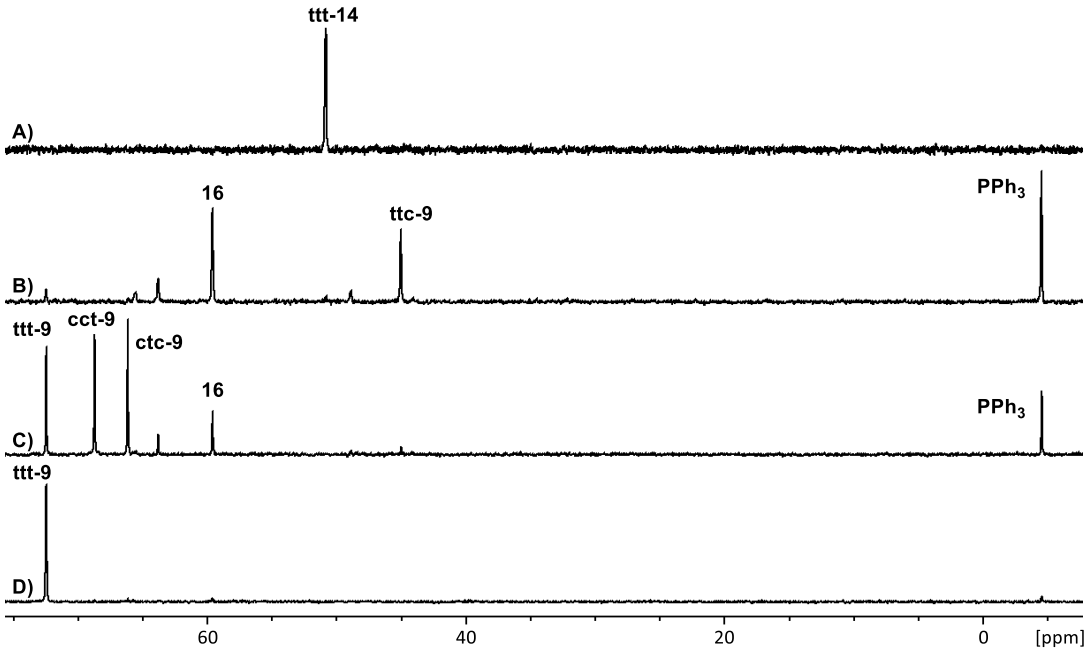

Figure 3.9: $^{31}P\{^{1}H\}$ NMR spectra (C_6H_6, 202 MHz, 25°C) of A) $[Ru(IMe_4)_2(PPh_3)_2HF]$ (**ttt-14**) prior to the room temperature addition of Et_3SiH, B) 20 min after addition of Et_3SiH, C) ca. 12 h after addition of Et_3SiH and D) after heating at 70°C for 2 h.

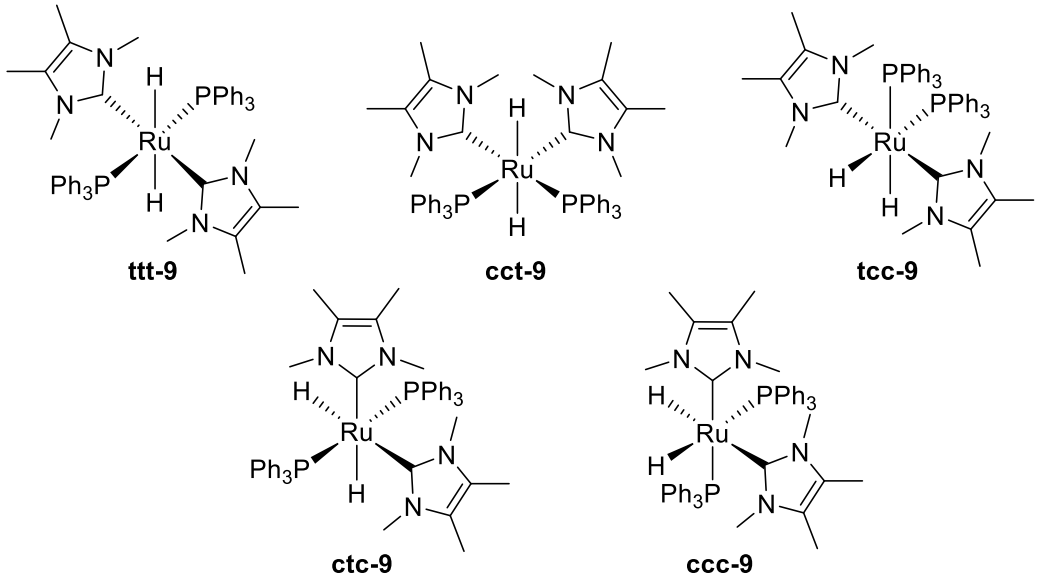

Figure 3.10: Possible isomers of $[Ru(IMe_4)_2(PPh_3)_2H_2]$ (**9**). The prefix indicates the relative arrangement of IMe_4, PPh_3 and H ligands respectively.

3.5.1. Characterisation of $[Ru(IMe_4)_2(PPh_3)(SiR_3)H_3]$ complexes

The presence of both **16** and **tcc-9** at early reaction times indicated that the former species might result from the PPh_3/Et_3SiH substitution at **tcc-9**. This hypothesis was reinforced by the absence of **16** upon immediate addition of Et_3SiH to a mixture of cct- and ctc-isomers of **9** generated *in-situ* in the reaction of $[Ru(PPh_3)_4H_2]$ with IMe_4. It was only after 12 h at room temperature that trace amounts of **16** were detected by both $^{31}P\{^1H\}$ and ^1H NMR spectroscopy (δ -6.00, d, $^2J_{HP}$ = 12.0 Hz, 1H; δ -6.86, d, $^2J_{HP}$ = 11.3 Hz, 2H), consistent with slow isomerisation of either **cct-9** and/or **ctc-9** to **tcc-9**, followed by a rapid phosphine/silane exchange. **16** could not be accessed directly from **ttt-9**, even in the presence of a large excess of Et_3SiH, use of high temperatures (120°C) or long reaction times. However, changing the R-groups on silicon from ethyl to phenyl allowed the isolation of the triphenylsilyl analogue, $[Ru(IMe_4)_2(PPh_3)(SiPh_3)H_3]$ (**17**), following thermolysis of **ttt-9** with Ph_3SiH (3 equiv) at 90° C overnight. **17** exhibited a similar set of upfield proton NMR resonances and coupling constants to **16** (δ -4.82, $^2J_{HP}$ = 10.8 Hz; δ -6.07, $^2J_{HP}$ = 9.2 Hz).

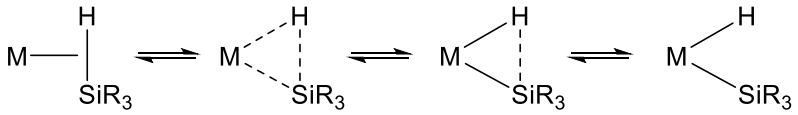

Scheme 3.5: Si-H bond activation: a continuum between σ-silane complex and the product of oxidative addition, silyl hydride complex.

The coordination mode of a Si-H bond to a transition metal complex can range from weak, nonclassical σ-silane interaction (generally three-centre, two-electron bond; η^2-$HSiR_3$) to classical silyl hydride species with two-centre, two-electron M-H and M-Si bonds formed upon complete oxidative addition to the metal

(Scheme 3.5).[13–17] In order to evaluate where along this continuum a particular complex lies, a whole range of analytical methods must be employed, including NMR and IR spectroscopy, as well as diffraction techniques.[18,19] In the case of **17**, the combined experimental data suggested that the compound was best formulated as the silyl trihydride, $[Ru(IMe_4)_2(PPh_3)(SiPh_3)H_3]$, rather than the σ-silane dihydride complex, $[Ru(IMe_4)_2(PPh_3)(Ph_3SiH)H_2]$. By extension, **16** was formulated the same way. The classical nature of the hydride and silyl ligands in **17** was supported by the -40°C ^{1}H-^{29}Si HSQC spectrum, which showed a clear coupling from the doublet ^{29}Si resonance at δ 22.7 ($^{2}J_{SiP}$ = 29.3 Hz) to the two low frequency proton resonances at δ -4.82 and -6.07 with respective J_{SiH} values of 45 Hz and 16 Hz (Figure 3.11). The magnitude of the couplings is below the lower limit of 65 Hz proposed by Sabo-Etienne for the presence of an intact σ Si-H bond.[13] The possibility of **17** being a silyl hydride dihydrogen complex, i.e. $[Ru(IMe_4)_2(PPh_3)(SiPh_3)(\eta^2\text{-}H_2)H]$ was discounted on the basis of the magnitude of the T_1 values measured at both 25 and -50°C (25°C, 400 MHz, 350 ms (δ -4.77), 361 (δ -6.16); -50°C, 400 MHz, 387 ms (δ -4.82), 432 ms (δ -6.06)).

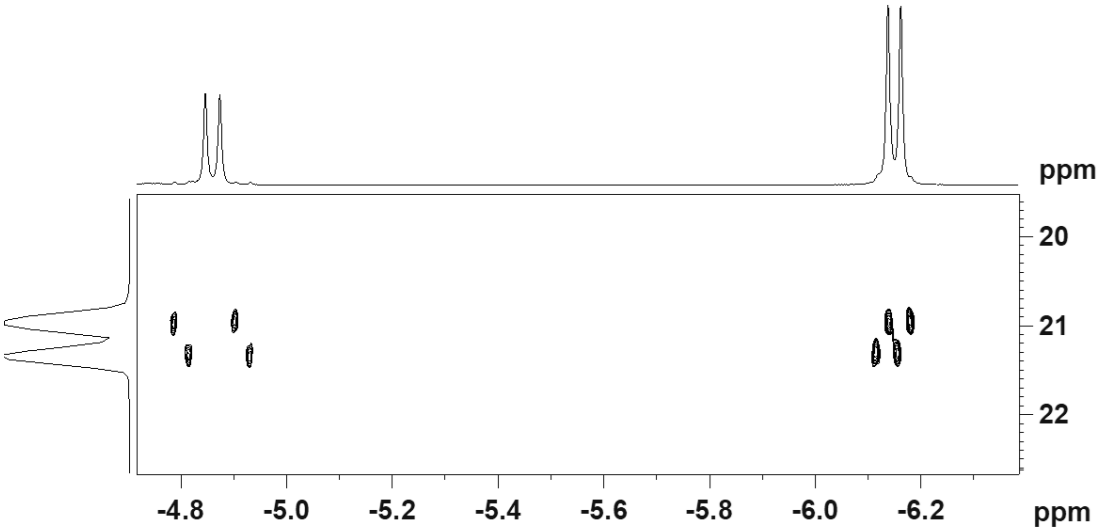

Figure 3.11: ^{1}H-^{29}Si HMBC spectrum ($C_6D_5CD_3$, 400 MHz, -50°C) of $[Ru(IMe_4)_2(PPh_3)(SiPh_3)H_3]$ (**17**).

Single crystal X-ray diffraction (Figure 3.12) was less informative as it was impossible to differentiate the $SiPh_3$ ligand from PPh_3. Nonetheless, closer inspection of the molecular structure revealed that the shortest possible Si···H distance could be 2.075 Å, outside the 1.7-1.9 Å range considered to support σ-bond coordination.[13] However, this value was also significantly shorter than the sum of the Si and H van der Waals radii (3.4 Å), indicating some degree of interaction between the two centres in the H_3SiPh_3 fragment, akin to that seen in $[Ru(PMe_3)_3(SiMe_3)H_3]$.[20–23] On the basis of the review by Sabo-Etienne, the presence of a band at 1776 cm^{-1} in the IR spectrum of **17** was consistent with the existence of a Si··H interaction.

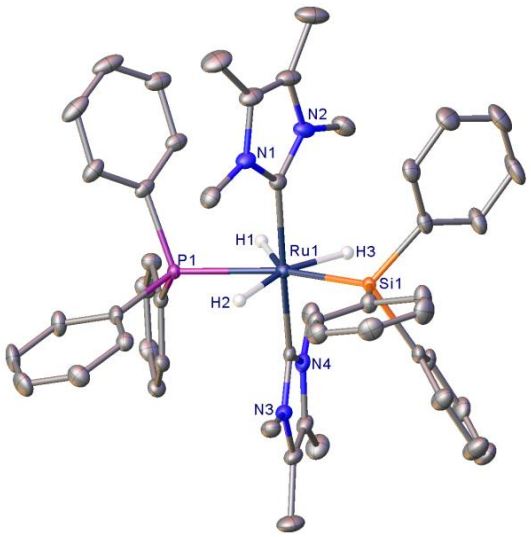

Figure 3.12: Molecular structure of [Ru(IMe$_4$)$_2$(PPh$_3$)(SiPh$_3$)H] (**17**). Hydrogen atoms, with the exception of hydride ligands, have been omitted for clarity. Ellipsoids are shown at the 30% probability level. Selected bond lengths (Å) and angles (°): Ru1-P1 2.430(5), Ru1-Si1 2.311(6), Ru1-P1 2.414(5), Ru1-Si1 2.318(6), Ru1-C1 2.091(3), Ru1-C8 2.082(2), P1-Ru1-Si1 155.72(14), C1-Ru1-C8 173.48(10), C8-Ru1-Si1 95.96(13).

It is perhaps worth reiterating that the bonding types formed by the 3-membered Si, H, M molecular moiety span a continuum with the M(σ-silane) and M-silyl hydride species representing the two extremes. In the presence of other hydrogen atoms in the coordination sphere of the metal, as in the case of **17**, secondary interactions between silicon and hydrogen atoms become increasingly important in the exchange processes that are often present in these highly dynamic systems.[24] Although the solid state study on **17** indicated the presence of weak remanent Si···H interaction, their direct observation by solution spectroscopic techniques was not possible, most likely due to the fast exchange of hydride ligands at the ruthenium metal centre.

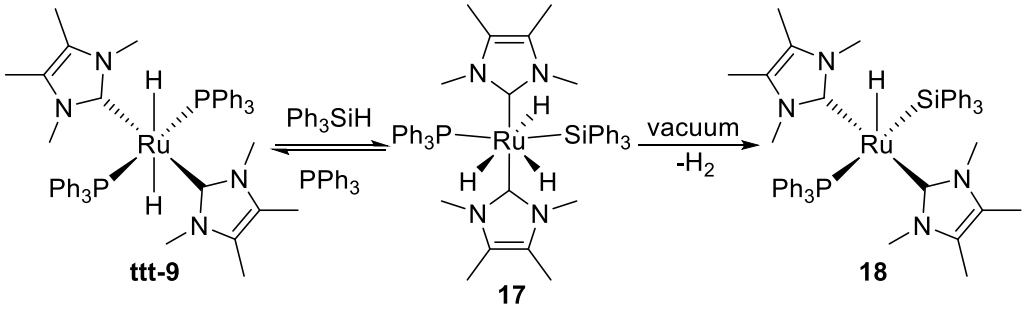

Scheme 3.6: Synthesis of $[Ru(IMe_4)_2(PPh_3)(SiPh_3)H_3]$ (**17**) from $[Ru(IMe_4)_2(PPh_3)_2H_2]$ (**ttt-9**) and Ph_3SiH, and subsequent H_2 loss to afford $[Ru(IMe_4)_2(PPh_3)(SiPh_3)H]$ (**18**).

Interestingly, prolonged exposure of an isolated sample of **17** to vacuum and subsequent analysis by both ^1H and $^{31}P\{^1H\}$ NMR spectroscopy revealed the formation of a new species resonating at δ -33.0 (d, $^2J_{HP}$ = 15.5 Hz) and δ 41.3 respectively. The doublet splitting of the upfield shifted hydride signal and the purple colouration of the sample supported the formation of the five-coordinate 16 electron species, $[Ru(IMe_4)_2(PPh_3)(SiPh_3)H]$ (**18**; Scheme 3.6), resulting from reductive elimination of H_2. This process is consistent with the ability of silicon to labilise other ligands as described in the chemistry of $[Ru(PMe_3)_3(SiR_3)H_3]$.[25]

3.5.2. Characterisation of $[Ru(IEt_2Me_2)_2(PPh_3)(SiR_3)H_3]$ complexes

Analogous experiments of **cct-10** with silanes were less conclusive than for **ttt-14**. Thus, addition of Et_3SiH (1 equiv) to **cct-10** led to the rapid regeneration of **cct-8**. Although no intermediate species or alternative isomers of **8** were observed, increasing the silane concentration led to the appearance of a 1:1:1 ratio of three low frequency doublet Ru-H signals at δ -5.48 (d, $^2J_{HP}$ = 34.7 Hz), -5.77 (d, $^2J_{HP}$ = 9.0 Hz) and -10.38 (dd, *J* = 16.8 Hz, *J* = 6.2 Hz), all of which correlated to a singlet phosphorus resonance at δ 61.1 by ^{31}P-^1H HSQC. This, together with a release of

free PPh_3, implied that phosphine/silane exchange was taking place and suggested that the new species was most likely $[Ru(IEt_2Me_2)_2(PPh_3)(SiEt_3)H_3]$ (**19**). The appearance of three inequivalent hydrides contrasted with the appearance of the IMe_4 complex **16** perhaps due to the different geometry at the metal centre, with a retained *cis*-arrangement of IEt_2Me_2 ligands from **cct-8**. However, as in the case of **16**, full structural assignment of **19** could not be confirmed in the solid state as the complex was only ever present as a part of a mixture of species.

Unlike with **ttt-9**, **cct-8** reacted with Ph_3SiH (3 equiv) at room temperature to afford a single new ruthenium species within 2 h, which could be crystallised from toluene/pentane at -40°C. The isolated complex was tentatively assigned as $[Ru(IEt_2Me_2)_2(PPh_3)(SiPh_3)H_3]$ (**20**). The room temperature ^1H NMR spectrum of the crystalline sample in toluene-d_8 revealed two doublets at δ -4.56 and -4.88, both with $^2J_{HP}$ couplings of 10.2 Hz, and a broad singlet at δ -6.27, all of which correlated to a sharp singlet phosphorus resonance at δ 59.5. However, the three low frequency signals showed a non-integer ratio (1:0.7:1.4), which was initially thought to result from H/D exchange with the solvent. This was discounted since the relative integration of the three hydride signals was virtually unchanged over ca. two weeks in toluene-d_8 solution at room temperature, and the fact that it was only when the sample was heated at 50°C overnight that the H/D scrambling and the formation of H/D isotopologues became apparent (Figure 3.13).

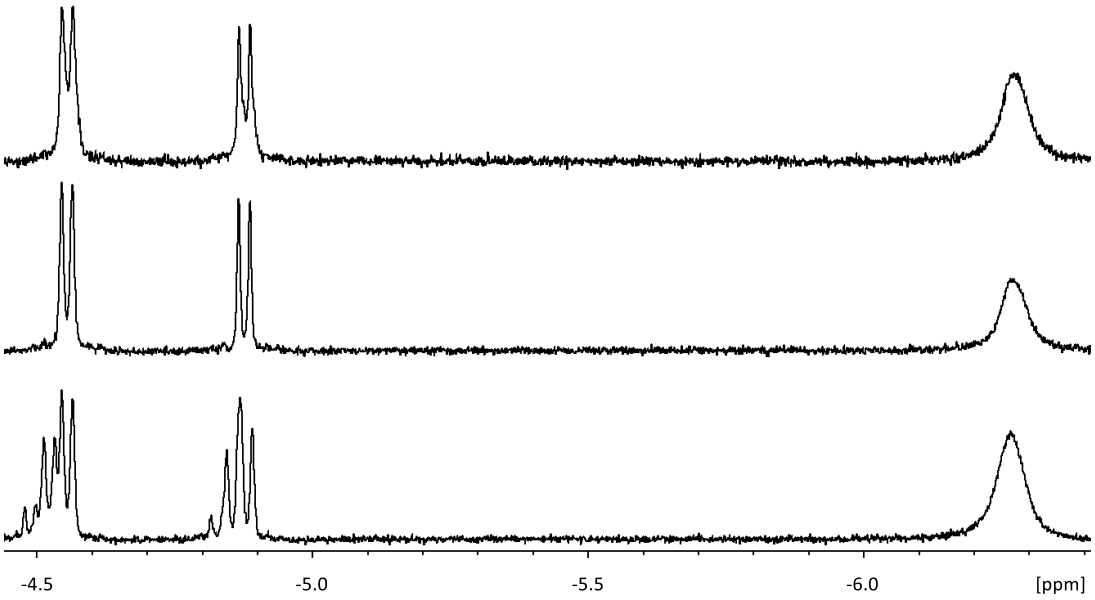

Figure 3.13: Sections of the ^{1}H NMR spectrum ($C_6D_5CD_3$, 500 MHz, 25°C) of $[Ru(IEt_2Me_2)_2(PPh_3)(SiPh_3)H_3]$ (**20**) immediately after dissolution (top), after ca. two weeks at room temperature (middle), after heating the sample at 50°C overnight (bottom).

To rule out any possibility of **20** being fluxional on the NMR timescale, a toluene-d_8 solution was cooled to -65°C in the hope of restricting any potential exchange processes. Unfortunately, the experiment proved unsuccessful as the employment of low temperatures resulted in overall broadening of the low frequency signals in the ^{1}H NMR spectrum and emergence of additional, new low frequency peaks.

Single crystal X-ray diffraction analysis did not provide any additional insight into the exact nature of the isolated species due to the highly disordered nature of the crystal. This prevented unambiguous differentiation of PPh_3 and $SiPh_3$ ligands and location of the hydride components. The full characterisation of **20** remains to be carried out.

3.6. Reactivity of $[Ru(IEt_2Me_2)_2(PPh_3)(C_6F_5)H]$ (11) and $[Ru(IEt_2Me_2)(PPh_3)_2(C_6F_5)H]$ (12) with Et_3SiH

Given the mixture of C-F and C-H activation products furnished in the stoichiometric reactions of **cct-8** and C_6F_6 or C_6F_5H, the individual stoichiometric reactions of the Ru-fluoroaryl complexes **11** and **12** with Et_3SiH were also investigated to establish the viability of the return reduction steps necessary to complete the catalytic HDF cycle. There was no reaction between the bis-NHC pentafluorophenyl complex **11** and Et_3SiH (5 equiv) in C_6D_6 at room temperature or upon heating at 70°C. Similarly, the bis-PPh_3 analogue **12** also proved unreactive towards Et_3SiH at ambient temperature overnight. However, addition of free IEt_2Me_2 to the latter reaction mixture resulted in a rapid formation of both $C_6F_4H_2$ and Et_3SiF at room temperature by ^{19}F NMR spectroscopy. Over the period of ca. 2 h at room temperature, deposition of black solid material was observed, indicating sample decomposition.

3.7. Synthesis and stoichiometric reactivity of $[Ru(NHC)_2(P\text{-}P)HF]$ complexes

Given the presence of free PPh_3 and the formation of biscarbene fluoroaryl species **11** and **15** in the stoichiometric reactions of both **cct-8** and **ttt-9** with C_6F_6 and C_6F_5H, it was assumed that the five-coordinate intermediate species, $[Ru(NHC)_2(PPh_3)H_2]$, were generated and that these were responsible for the competing C-H activation process. Moreover, the coordinative unsaturation of these transient moieties suggested they could also access both stepwise and concerted C-F activation pathways. For these reasons, it was anticipated that the resulting mixture of five- and six-coordinate Ru species in solution and the possibility of unselective

bond activation would impact on both the activity and the overall regioselectivity of the HDF of fluorinated aromatics. In order to assess and try to circumvent this, the synthesis of a series of complexes bearing chelating phosphines, $[Ru(NHC)_2(P\text{-}P)H_2]$ (P-P = dppe, dppp, dppm), was targeted (Scheme 3.7).

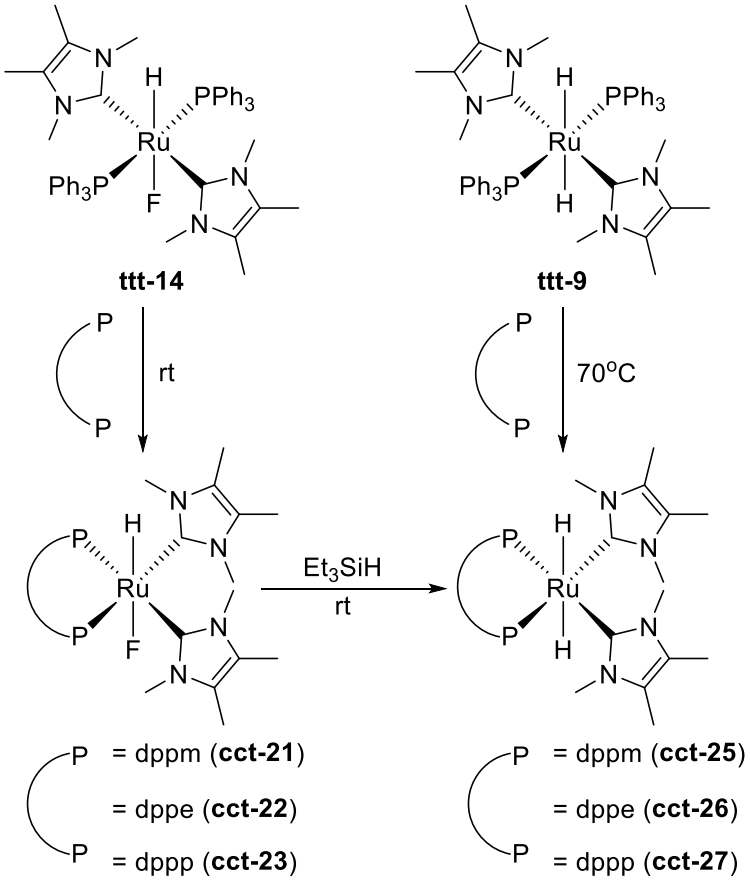

Scheme 3.7: Synthesis of cct-$[Ru(IMe_4)_2(P\text{-}P)HX]$ complexes (P-P = dppe, dppp, dppm; X = H, F).

Preliminary substitution reactions of **ttt-9** with dppm, dppe and dppp were monitored by ^1H and $^{31}P\{^1H\}$ NMR spectroscopy. Although prolonged heating of samples in the presence of 5 equiv of the appropriate chelating phosphine in C_6D_6 at 70°C led to complete conversion to the desired P-P substituted products, their isolation was hampered by their high solubility in hexane, employed initially to remove the eliminated PPh_3 and excess free P-P. In contrast, stirring the hydride

fluoride complex **ttt-14** with a single equivalent of chelating phosphine at room temperature provided an effective route to the corresponding hydride fluoride derivatives [Ru(IMe_4)$_2$(P-P)HF] (P-P = dppm (**cct-21**), dppe (**cct-22**), dppp (**cct-23**)), which could be easily isolated upon precipitation from toluene/pentane in low to moderate yields (49, 64 and 31 % respectively). The preparation of [Ru(IEt_2Me_2)$_2$(dppe)HF] (**cct-24**) was also achieved by substituting both PPh_3 ligands in **cct-8** by dppe.

All cct-[Ru(NHC)$_2$(P-P)$_2$HF] complexes (**21-24**) reacted cleanly with 2 equiv of Et_3SiH in C_6H_6 to afford the *trans*-dihydride complexes, cct-[Ru(NHC)$_2$(P-P)$_2$H$_2$] (NHC = IMe_4, P-P = dppm (**cct-25**), dppe (**cct-26**), dppp (**cct-27**); NHC = IEt_2Me_2, P-P = dppe (**28**)), over the course of two days at room temperature. Of note is complex **26**, which underwent slow isomerisation from the initial cct-isomer to the highly insoluble ccc-isomer in C_6D_6 solution.[v] This was characterised by single crystal X-ray diffraction and is described further in Section 3.8 (*vide infra*). In the case of its IEt_2Me_2 counterpart (**28**), both cct- and ccc-isomers were present in a 1:1 ratio in solution as indicated by ^{1}H and ^{31}P{^{1}H} NMR spectroscopy.[vi]

---

[v] Isomerisation could be accelerated by heating the sample at 70°C, which led to the precipitation of crystalline **26** from the reaction mixure.

[vi] Selected NMR data for complex [Ru(IEt_2Me_2)$_2$(dppe)H$_2$] (**28**): ^{1}H NMR (500 MHz, C_6D_6, 25°C): δ -7.34 (t, $^2J_{HP}$ = 19.2 Hz, cct-RuH_2), -7.91 (dd, $^2J_{HP}$ = 92.1 Hz, $^2J_{HP}$ = 28.1 Hz, ccc-RuH_2), -11.86 (dd, $^2J_{HP}$ = 32.7 Hz, $^2J_{HP}$ = 22.9 Hz, ccc-RuH_2). ^{31}P NMR (C_6D_6, 202 MHz, 25°C): δ 88.9 (s, ccc-RuH_2), 82.2 (s, cct-RuH_2), 47.1 (s, ccc-RuH_2).

3.8. Characterisation of [Ru(NHC)$_2$(P-P)HX] complexes

The molecular structures of compounds **21-24** are illustrated in Figure 3.14. The most pertinent features are the *trans*-H-Ru-F geometry and the *cis*-arrangement of the NHC ligands which is imposed by the presence of the chelating phosphines. A distorted octahedral geometry at the ruthenium centre is observed in all cases and stems from the different bite angles of the utilised P-P ligands. As shown in Table 3.1, the Ru-F bond is elongated as the P-Ru-P angle increases (compounds **21**-**23**), however changing the N-alkyl carbene substituent from methyl (**cct**-**22**) to ethyl (**cct-24**) results in shortening of this distance. Closer investigation of the X-ray structures of complexes **21-24** suggested some degree of hydrogen bonding between methyl hydrogen atoms and the fluoride ligands. Most indicative were weak H···F interactions in **cct-23** (C-H···F 1.955(4) Å, 2.059(5) Å; C···F 2.887(3) Å, 2.990(3) Å; C-H-F 157.8(7)°, 158.0(1)°). Key bond lengths and angles are summarised in Table 3.1.

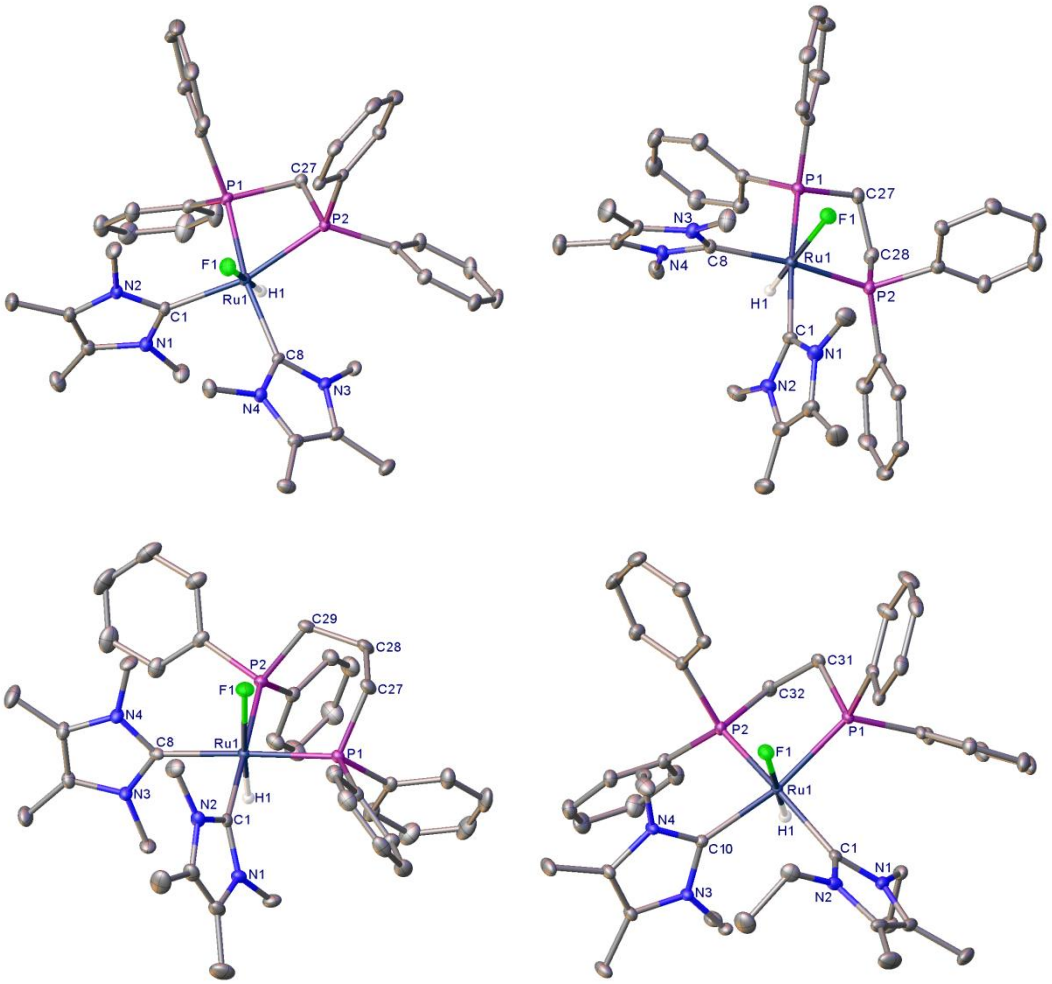

Figure 3.14: Molecular structures of [Ru(IMe$_4$)$_2$(dppm)HF] (**cct-21**, top left), [Ru(IMe$_4$)$_2$(dppe)HF] (**cct-22**, top right), [Ru(IMe$_4$)$_2$(dppp)HF] (**cct-23**, bottom left) and [Ru(IEt$_2$Me$_2$)$_2$(dppe)HF] (**cct-24**, bottom right). Thermal ellipsoids are represented at 30% probability. Hydrogen atoms, with the exception of hydride ligands, have been omitted for clarity. Selected bond lengths and angles are listed in Table 3.1.

Table 3.1: Selected single crystal X-ray data for cct-[Ru(NHC)$_2$(P-P)$_2$HF] complexes (**21-24**). Data for compounds **cct-10** and **ttt-14** are included for comparison.

	Ru-F [Å]	Ru-C [Å]	Ru-P [Å]	P-Ru-P [°]	C-Ru-C [°]
cct-21	2.2109(16)	2.092(3), 2.113(3)	2.2585(7), 2.3135(8)	70.92(3)	94.32(11)
cct-22	2.250(17)	2.123(3), 2.146(3)	2.2594(7), 2.2745(7)	83.71(2)	90.03(10)
cct-23	2.2684(13)	2.103(2), 2.107(2)	2.2833(6), 2.2861(6)	88.72(2)	85.04(8)
cct-24	2.1841(12)	2.1076(17), 2.1379(19)	2.2464(5), 2.3095(5)	82.723(18)	92.50(7)
ttt-14	2.2684(18)	2.112(3), 2.115(3)	2.2891(7), 2.3404(7)	178.78(3)	176.04(11)
cct-10	2.264(2)	2.109(2), 2.115(2)	2.3343(6), 2.3493(6)	98.66(2)	88.61(8)

In solution, all four complexes displayed a characteristic doublet of triplets Ru-H NMR resonance at δ -21 ±2 ppm ($^2J_{HF}$ = 50 ± 2 Hz, $^2J_{HP}$ = 20 ±2 Hz), along with a Ru-F signal in the range δ -330 to δ -342 (Table 3.2). The chemical shifts and coupling constants were in agreement with the NMR metrics for the parent bis-PPh$_3$ compounds (**cct-10** and **ttt-14**). Some degree of fluxional behaviour was apparent for the dppm complex **cct-21**, as the NCH_3 and NCCH_3 resonances of the two NHC ligands were averaged to a broad peak at δ 3.62 and a sharp signal at δ 1.55 respectively, indicating unrestricted rotation around the Ru-C$_{NHC}$ bond (Figure 3.15). Upon cooling a toluene-d_8 solution of **cct-21** to -45°C, the N-methyl protons resolved into three singlets at δ 4.18, 4.17 and 3.14, integrating in a 3:3:6 ratio,

whereas the backbone protons appeared as two distinct signals at δ 1.48 and 1.38 (6:6 ratio).

Table 3.2: Selected NMR data for cct-[Ru(NHC)$_2$(P-P)$_2$HF] complexes (**21-24**). Data for compounds **cct-10** and **ttt-14** are included for comparison.

	^{1}H δ [ppm]	$^2J_{HF}$ [Hz]	$^2J_{HP}$ [Hz]	^{31}P δ [ppm]	^{19}F δ [ppm]
cct-21	-19.68	52.8	20.3	3.5	-342.2
cct-22	-22.90	51.9	22.1	64.8	-330.4
cct-23	-21.90	52.7	20.0	32.9	-332.9
cct-24	-22.32	54.5	21.6	63.8	-348.1
ttt-14	-21.94	48.0	21.0	50.1	-331.5
cct-10	-21.70	51.6	18.7	43.1	-354.4

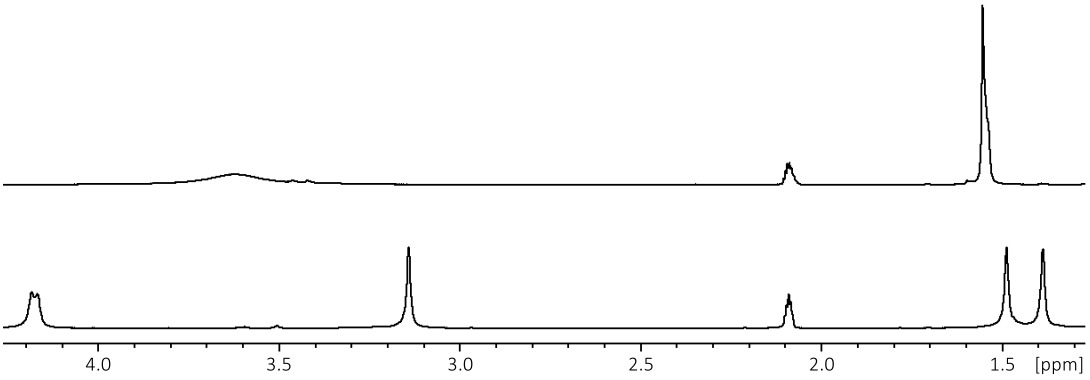

Figure 3.15: Sections of the ^{1}H NMR spectrum ($C_6D_5CD_3$, 400 MHz) of [Ru(IMe$_4$)$_2$(dppm)HF] (**cct-21**) showing NC*H*$_3$ and NCC*H*$_3$ resonances at 25°C (top) and -45°C (bottom).

The corresponding cct-[Ru(NHC)$_2$(P-P)H$_2$] complexes **25-28** were characterised by multinuclear NMR spectroscopy. ^{1}H and ^{31}P{^{1}H} NMR chemical shifts, along with J_{HP} coupling constants, are listed in Table 3.3. All metrics were consistent with the corresponding data for **cct-8** and **ttt-9** and fully supported the

presence of *trans*-dihydride geometries in solution. Compounds **cct-25** and **26** were additionally analysed by X-ray diffraction studies (Figure 3.16). The structure of the former confirmed the original NMR assignment of a cct-isomer, while the latter revealed the mutual *cis*-arrangement of both IMe_4 and hydride ligands. In both cases, a slight increase in the P-Ru-P bite angle, with respect to the fluoride counterparts, was observed.

Table 3.3: Selected NMR data for cct-[Ru(NHC)$_2$(P-P)H$_2$] complexes (**24**-**27**). Data for compounds **cct-8** and **ttt-9** are included for comparison.

	^{1}H δ [ppm]	$^{2}J_{HP}$ [Hz]	^{31}P δ [ppm]
cct-25	-5.37	16.9	10.9
cct-26	-7.20	19.1	86.0
cct-27	-6.64	19.2	47.0
cct-28	-7.34	19.2	82.2
ttt-9	-6.54	20.4	72.4
cct-8	-6.74	20.4	69.7

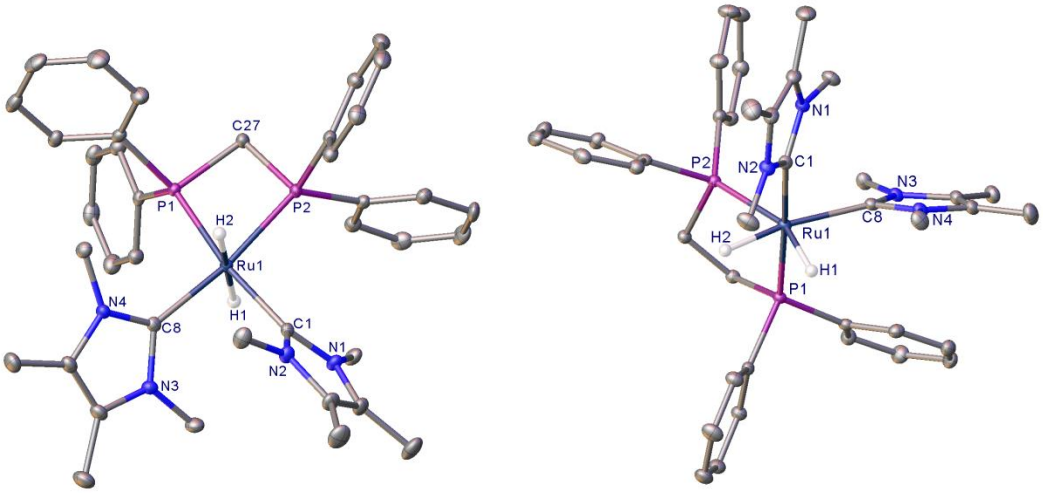

Figure 3.16: Molecular structures of cct-[Ru(IMe$_4$)$_2$(dppm)H$_2$] (**cct-25**, left) and ccc-[Ru(IMe$_4$)$_2$(dppe)H$_2$] (**ccc-26**, right). Thermal ellipsoids are represented at 30% probability. Hydrogen atoms, with the exception of hydride ligands, have been omitted for clarity. Selected bond lengths (Å) and angles (°) for **cct-25**: Ru1-C1 2.088(2), Ru1-C8 2.090(2), Ru1-P1 2.2860(6), Ru1-P2 2.2740(6), P1-Ru1-P2 72.31(2), C1-Ru1-P1 169.80(6), C1-Ru1-C8 87.66(9). Selected bond lengths (Å) and angles (°) for **cct-26**: Ru1-C1 2.098(2), Ru1-C8 (2.123(2), Ru1-P1 2.2526(5), Ru1-P2 2.2874(5), P1-Ru1-P2 85.676(17), C1-Ru1-P1 174.65(5), C1-Ru1-C8 90.96(7).

3.9. Catalytic HDF of C_6F_6 using [Ru(NHC)$_2$L$_2$H$_2$] complexes

In light of the stoichiometric studies described in previous sections, catalytic HDF of C_6F_6 by the various ruthenium precursors was attempted. The results are summarised in Table 3.4. The activity of all complexes was screened at 10 mol% catalyst loading in toluene,[vii] and quantified by TON and TOF values. An

[vii] Toluene, rather than benzene, was used due to the much better solubility of **17** in the former.

elevated temperature (90°C) and a large excess of reductant (80 equiv wrt catalyst) were employed in an effort to afford reasonable reaction rates and to maximise the conversions to low fluorine containing products. Remarkably, both **cct-8** and **ttt-9** were capable of performing up to five HDF steps to generate fluorobenzene (entries 1-3). The formation of less C_6FH_5 with **cct-8** (25%, c.f. 52% for **ttt-9**) might be a consequence of one or more of the following factors; (i) intrinsically lower activity (ii) relative stability of the precursor or (iii) more facile formation of catalytically inactive Ru-fluoroaryl species (**11** and **12**). It might also reflect a difference in regioselectivity to give larger amounts of 1,4-$C_6F_2H_4$, which has a higher predicted barrier for HDF compared to the 1,2- and 1,3- isomers (Section 2.4.3) and might therefore be regarded as a catalytic dead-end. For these reasons, **ttt-9** was selected for further studies.

Table 3.4: $Ru(NHC)_2L_2H_2$ catalysed HDF of C_6F_6.[a]

Entry	Ru source	t (h)	Silane	Product distribution (%)[d]					TON	TOF (h^{-1})
				1,2-$C_6F_2H_4$	1,3-$C_6F_2H_4$	1,4-$C_6F_2H_4$	C_6FH_5	Other products		
1	**ttt-9**	72	Et_3SiH	65	4	10	16	1,2,3- $C_6F_3H_3$ (5 %)	41.1	0.57
2	**ttt-9**	144	Et_3SiH	36	3	9	52	-	45.2	0.31
3	**cct-8**	144	Et_3SiH	32	11	32	25	-	42.6	0.30
4[b]	**ttt-9**	144	Et_3SiH	25	-	10	65	-	46.5	0.32
5[c]	**ttt-9**	144	Et_3SiH	10	-	-	-	1,2,3,4- $C_6F_4H_2$ (36 %), 1,2,4,5- $C_6F_4H_2$ (1 %), 1,2,3- $C_6F_3H_3$ (45 %), 1,2,4- $C_6F_3H_3$ (8 %)	27.2	0.19
6	**ttt-9**	144	$^{i}Pr_3SiH$	66	-	4	24	1,2,3- $C_6F_3H_3$ (6 %)	41.8	0.29
7	**17**	72	Et_3SiH	42	4	34	20	-	42.0	0.58
8	**cct-23**	24	Et_3SiH	3	-	2	95	-	49.5	2.06

9	**cct-23**	24	$^{i}Pr_3SiH$	-	-	1	99	-	49.9	2.08
10	**cct-22**	24	Et_3SiH	10	-	5	85	-	48.5	2.02
11	**cct-22**	24	$^{i}Pr_3SiH$	-	-	3	97	-	49.7	2.07
12	**cct-21**	24	Et_3SiH	49	4	29	18	-	41.8	1.74
13	**cct-21**	24	$^{i}Pr_3SiH$	12	-	5	-	C_6F_6 (1 %), 1,2,3,4- $C_6F_4H_2$ (31 %), 1,2,4,5- $C_6F_4H_2$ (4 %), 1,2,3- $C_6F_3H_3$ (27 %), 1,2,4- $C_6F_3H_3$ (20 %)	44.2	0.61
14	**cct-24**	24	Et_3SiH	6	-	9	85	-	48.5	2.02
15	**cct-24**	24	$^{i}Pr_3SiH$	38	-	8	54	-	45.4	1.89

[a]Reaction conditions: 10 mol% Ru, 0.005 mmol substrate, 0,04 mmol silane, toluene, 90°C. [b]Reaction run under 4 atm H_2. [c]Reaction performed in presence of 10 equiv PPh_3. [d]Product assignments and yields determined by ^{19}F NMR spectroscopy.

HDF of C_6F_6 under 4 atm H_2 resulted in an increased yield of C_6FH_5 (entry 4), consistent with reduction in the extent of competing C-H activation. Retardation of catalysis was observed upon addition of PPh_3 (entry 5), which supports the premise that at least some HDF occurred at a five-coordinate intermediate, most likely the previously postulated mono-phosphine species $[Ru(IMe_4)_2(PPh_3)H_2]$ (Sections 3.1 and 3.6). However, the presence of tetra-, tri- and difluorobenzenes indicated that ligand dissociation is not necessary for the catalysis to propagate. The triphenylsilyl trihydride precursor (**17**) performed comparably to **ttt-9** (entries 1 and 7). The results obtained with chelating phosphine complexes **21-24** can be roughly correlated with the P-Ru-P bite angles measured in their crystal structures. Thus, the dppp derivative **cct-23** proved to be the most active of all of the NHC/phosphine precursors, affording fluorobenzene in an exceptionally high 95% yield (entry 8) over only 24 h, **cct-22** showed slightly lower activity with 85% conversion to C_6FH_5 (entry 10), while the dppm analogue **cct-21** gave a mixture of $C_6F_2H_4$ isomers and C_6FH_5 (18%, entry 12). Changing the N-alkyl substituents on the NHC ligands from methyl to ethyl had a negligible effect on catalysis (entry 14). Replacement of Et_3SiH by $^iPr_3SiH$ accelerated the HDF with **cct-23** and **cct-22** as demonstrated by almost quantitative formation of C_6FH_5 (entries 9 and 11 compared to entries 8 and 10). In contrast, a drop in catalytic activity was apparent for **cct-21** and **cct-24** (entries 13 and 15). This could be due to the more bulky isopropyl groups on silicon and hence greater steric encumbrance upon approaching a crowded ruthenium centre with a narrow P-Ru-P bite angle (70.92(3)°) or larger IEt_2Me_2 ligands respectively. HDF with **ttt-9** was also affected upon changing the silane to $^iPr_3SiH$ (entry 6). In this case, the slightly reduced catalytic performance might reflect the ability of different silanes to form catalytically competent ruthenium silyl trihydride complexes, akin to **16**, **17**, **19** and **20**. However, these hypotheses should be considered

as mere speculation only since variations in catalytic performance as a function of terminal reductant can be difficult to rationalise.

As noted earlier (Section 3.7), the chelating phosphines were utilised with hope of rendering their ruthenium complexes coordinatively saturated and hence driving HDF along a concerted pathway. The high concentration of C_6FH_5 formed with complexes **22-24** implied that either (i) the assumption was correct, although 1,4-$C_6F_2H_4$ (predicted by DFT to be the most favoured isomer of difluorobenzene formed along a concerted pathway; Section 2.4.3) was then required to undergo a further HDF step to fluorobenzene (contradicting the findings with **1** under similar reaction conditions; Section 2.3) or (ii) the assumption was incorrect and catalysis proceeded along a stepwise pathway necessitating ligand dissociation from **22-24**, to give 1,2-$C_6F_2H_4$ and subsequently C_6F_5H. A third interpretation is that there could be other factors influencing the regioselectivity of C-F bond activation (such as subtle F···HC interactions in the key C-F bond breaking transition state during HDF with **II**; Section 1.4) or that the DFT findings on the related $[Ru(NHC)(PPh_3)_2(CO)H_2]$[26,27] (**I** and **II**) and $[Ru(NHC)_4H_2]$[28] (**1**-**2**) systems cannot be extrapolated to explain the observed product distributions with **22-24**. The ^{19}F NMR spectrum of a catalytic run with **cct-22** (5 mol%) stopped after 7 h at 90°C showed the presence of C_6F_6 (9%), 1,2,3,4-$C_6F_4H_2$ (12%) and most importantly 1,2,3-$C_6F_3H_3$ (35%) and 1,2-$C_6F_2H_4$ (41%), with very small amounts of 1,2,4-$C_6F_3H_3$ (2%) and 1,4-$C_6F_2H_4$ (1%) (Scheme 3.8). This result was in accordance with a stepwise pathway,[27] which could occur *via* dissociation of an NHC, but most likely involved temporary unhooking of one end of the chelating phosphine[29–31] to create a catalytically active five-coordinate ruthenium centre. Alternatively, HDF could proceed along a concerted pathway at six-coordinate species albeit with *ortho*-selectivity.

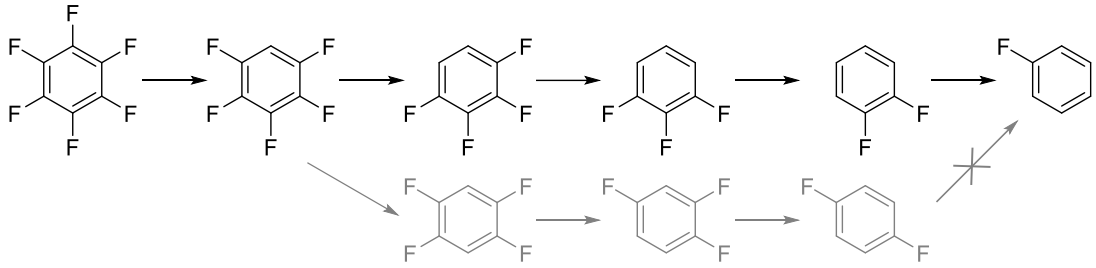

Scheme 3.8: Catalytic HDF products generated with cct-[Ru(NHC)$_2$(P-P)HF] (**21-24**). The major reaction pathway is shown in black.

3.10. Summary

A series of cct-[Ru(NHC)$_2$(L$_2$)H$_2$] complexes (NHC = IMe$_4$, IEt$_2$Me$_2$; L$_2$ = (PPh$_3$)$_2$, dppm, dppe, dppp) have proven capable of performing up to 5 hydrodefluorination (HDF) steps on C_6F_6 substrate to afford C_6FH_5. In the case of the bis-PPh$_3$ complexes **cct-8** and **ttt-9**, facile PPh$_3$ dissociation lowered the regioselectivity of HDF as the reaction could take place through both five- and six-coordinate pathways. Moreover, mechanistic considerations suggested that C-F bond activation could be further complicated by competitive C-H activation to generate catalytically inactive Ru-fluoraryl species (**11**, **12** and **15**), as well as the involvement of seven-coordinate Ru-silyl complexes, such as **16**, **17**, **19** and **20**. Enhanced activity and regioselectivity was observed upon incorporation of bidentate phosphines, in particular dppe and dppp. This was attributed to the very effective formation of coordinatively unsaturated ruthenium species, which were formed *via* dechelation of one of the P-P arms and operated along the stepwise pathway. Overall, these results show that the nature of metal coordination environment plays a crucial role in dictating the regioselectivity of the HDF process and highlight how subtle changes to ancillary ligands affect catalytic activity.

3.11. References for Chapter 3

(1) Davies, C. J. E.; Lowe, J. P.; Mahon, M. F.; Poulten, R. C.; Whittlesey, M. K. *Organometallics* **2013**, *32*, 4927.

(2) Bourosh, P. N.; Bologa, O. A.; Simonov, Y. A.; Bocelli, G.; Gerbeleu, N. V. *Russ. J. Coord. Chem.* **2005**, *31*, 641.

(3) Mathieson, T.; Schier, A.; Schmidbaur, H. *Z. Für Naturforschung B* **2000**, *55*, 1000.

(4) Fernández, F. J.; Alfonso, M.; Schmalle, H. W.; Berke, H. *Organometallics* **2001**, *20*, 3122.

(5) Harvey, B. G.; Arif, A. M.; Glöckner, A.; Ernst, R. D. *Organometallics* **2007**, *26*, 2872.

(6) Bernal, I.; Watkins, S. F. *Comptes Rendus Chim.* **2014**, *17*, 586.

(7) Forrester, J. D.; Senko, M. E.; Zalkin, A.; Templeton, D. *Acta. Cryst.* **1963**, *16*, 58.

(8) Reade, S. P.; Acton, A. L.; Mahon, M. F.; Martin, T. A.; Whittlesey, M. K. *Eur. J. Inorg. Chem.* **2009**, *2009*, 1774.

(9) McKay, D.; Riddlestone, I. M.; Macgregor, S. A.; Mahon, M. F.; Whittlesey, M. K. *ACS Catal.* **2015**, *5*, 776.

(10) Burling, S.; Mas-Marzá, E.; Valpuesta, J. E. V.; Mahon, M. F.; Whittlesey, M. K. *Organometallics* **2009**, *28*, 6676.

(11) Baratta, W.; Herdtweck, E.; Rigo, P. *Angew. Chem. Int. Ed.* **1999**, *38*, 1629.

(12) Baratta, W.; Mealli, C.; Herdtweck, E.; Ienco, A.; Mason, S. A.; Rigo, P. *J. Am. Chem. Soc.* **2004**, *126*, 5549.

(13) Lachaize, S.; Sabo-Etienne, S. *Eur. J. Inorg. Chem.* **2006**, *2006*, 2115.

(14) Nikonov, G. I. In *Advances in Organometallic Chemistry*; Elsevier, 2005; Vol. 53, pp 217–309.

(15) Corey, J. Y. *Chem. Rev.* **2011**, *111*, 863.

(16) Hauf, C.; Barquera-Lozada, J. E.; Meixner, P.; Eickerling, G.; Altmannshofer, S.; Stalke, D.; Zell, T.; Schmidt, D.; Radius, U.; Scherer, W. *Z. Für Anorg. Allg. Chem.* **2013**, *639*, 1996.

(17) Scherer, W.; Meixner, P.; Barquera-Lozada, J. E.; Hauf, C.; Obenhuber, A.; Brück, A.; Wolstenholme, D. J.; Ruhland, K.; Leusser, D.; Stalke, D. *Angew. Chem. Int. Ed.* **2013**, *52*, 6092.

(18) Alcaraz, G.; Sabo-Etienne, S. *Coord. Chem. Rev.* **2008**, *252*, 2395.

(19) Scherer, W.; Meixner, P.; Batke, K.; Barquera-Lozada, J. E.; Ruhland, K.; Fischer, A.; Eickerling, G.; Eichele, K. *Angew. Chem. Int. Ed.* **2016**, *55*, 11673.

(20) Kono, H.; Wakao, N.; Ito, K.; Nagai, Y. *J. Organomet. Chem.* **1977**, *132*, 53.

(21) Haszeldine, R. N.; Malkin, L. S.; Parish, R. V. *J. Organomet. Chem.* **1979**, *182*, 323.

(22) Dioumaev, V. K.; Procopio, L. J.; Carroll, P. J.; Berry, D. H. *J. Am. Chem. Soc.* **2003**, *125*, 8043.

(23) Dioumaev, V. K.; Yoo, B. R.; Procopio, L. J.; Carroll, P. J.; Berry, D. H. *J. Am. Chem. Soc.* **2003**, *125*, 8936.

(24) Atheaux, I.; Delpech, F.; Donnadieu, B.; Sabo-Etienne, S.; Chaudret, B.; Hussein, K.; Barthelat, J.-C.; Braun, T.; Duckett, S. B.; Perutz, R. N. *Organometallics* **2002**, *21*, 5347.

(25) Dioumaev, V. K.; Procopio, L. J.; Carroll, P. J.; Berry, D. H. *J. Am. Chem. Soc.* **2003**, *125*, 8043.

(26) Panetier, J. A.; Macgregor, S. A.; Whittlesey, M. K. *Angew. Chem. Int. Ed.* **2011**, *50*, 2783.

(27) Macgregor, S. A.; McKay, D.; Panetier, J. A.; Whittlesey, M. K. *Dalton Trans.* **2013**, *42*, 7386.

(28) Cybulski, M. K.; McKay, D.; Macgregor, S. A.; Mahon, M. F.; Whittlesey, M. K. *Angew. Chem. Int. Ed.* **2017**, *56*, 1515.

(29) Crumpton, D. M.; Goldberg, K. I. *J. Am. Chem. Soc.* **2000**, *122*, 962.

(30) Crumpton-Bregel, D. M.; Goldberg, K. I. *J. Am. Chem. Soc.* **2003**, *125*, 9442.

(31) Arthur, K. L.; Wang, Q. L.; Bregel, D. M.; Smythe, N. A.; O'Neil, B. A.; Goldberg, K. I.; Moloy, K. G. *Organometallics* **2005**, *24*, 4624.

CHAPTER FOUR

C-O Bond Activation of DPEphos *via* Attack of Nucleophilic Ru-H in RuL_4H_2

4.1. Introduction

Following on from the high activity of the cct-[$Ru(NHC)_2$(P-P)HX] complexes for the catalytic HDF of fluoroarenes described in Chapter 3, the scope of PPh_3/P-P substitution reactions was extended by inclusion of xanthene-based phosphines such as xantphos and DPEphos (Figure 4.1). Due to the serendipitous discovery of unprecedented C-O bond activation of the latter, the studies focused almost exclusively on its reactivity with ruthenium dihydride complexes. Experimental investigations were supplemented by DFT calculations to define the mechanism of reaction and probe the factors promoting unusual ligand activation.

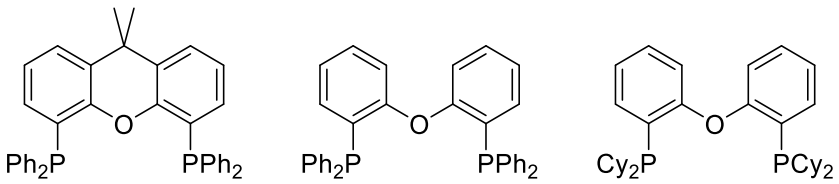

Figure 4.1: Structures of xantphos (left), DPEphos (middle) and DCEphos (right).

4.2. Reactivity of $[Ru(IMe_4)_2(PPh_3)_2H_2]$ (ttt-9)

4.2.1. Reaction of $[Ru(IMe_4)_2(PPh_3)_2H_2]$ (ttt-9) with DPEphos

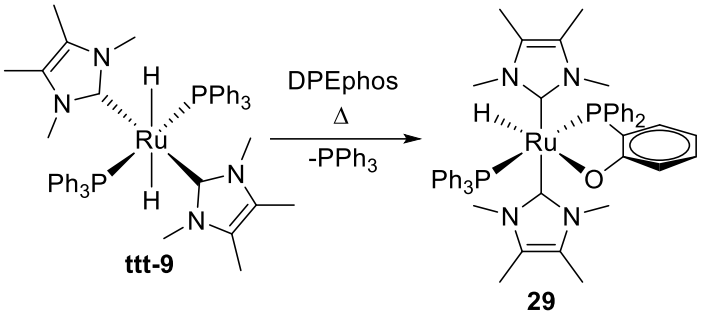

Scheme 4.1: Synthesis of $[Ru(IMe_4)_2(PPh_3)(Ph_2PC_6H_4O)H]$ (**29**) from $[Ru(IMe_4)_2(PPh_3)_2H_2]$ (**ttt-9**).

Upon heating a C_6D_6 solution of **ttt-9** and DPEphos (1.2 equiv) at 90°C overnight, ^{1}H NMR spectroscopy revealed complete disappearance of the hydride signal of the starting complex at δ -6.53 and the formation of a single new Ru-H containing product with a distinctive signal at δ -18.40 ("t", $^2J_{HP}$ = 22.0 Hz). This integrated in a 1:6:6:6:6 ratio with four IMe_4 resonances at δ 1.23, 1.34, 3.03 and 3.79. The hydride resonance is perhaps best described as a pseudotriplet or an overlapping doublet of doublets and its appearance is most likely due to the magnetic similarity of two phosphorus environments. In line with this was a single, possibly coincidental, $^{31}P\{^1H\}$ NMR signal at δ 51.3 and a single high frequency triplet ^{13}C carbene resonance at δ 192.1 ($^2J_{CP}$ = 15 Hz). A characteristic doublet of doublets at δ 178.4 ($^2J_{CP}$ = 14 Hz, $^3J_{CP}$ = 12 Hz) was assigned as the carbon adjacent to the oxygen atom.[1] Yellow crystals of the product were obtained from toluene/pentane. A subsequent X-ray diffraction study revealed the product to be $[Ru(IMe_4)_2(PPh_3)(Ph_2PC_6H_4O)H]$ (**29**; Figure 4.2) resulting from C-O bond activation of the DPEphos ligand. The molecular structure was consistent with the NMR data. The low frequency Ru-H chemical shift most likely

reflected its position opposite the phenolic oxygen atom of the bidentate diphenylphosphinophenolate.[i] The Ru-O was involved in C-H··O interactions with N-methyl protons (C-H···O 2.0414(16) Å, 2.1471(16) Å; C···O 2.976(3) Å, 2.977(3) Å; C-H-O 141.43(14)°, 158.72(15)°). The strong *trans*-influence of the hydride ligand led to the significant elongation of the Ru-O bond with respect to other Ru(II) complexes bearing a $Ph_2PC_6H_4O^-$ ligand (Table 4.1). The phosphine terminus of the 5-membered metallacycle (P1) was bound *trans* to PPh_3 (P1-Ru1-P2 176.94(2) Å), whereas the two IMe_4 ligands retained their same *trans*-arrangement (C1-Ru1-C8 172.97(8) Å) as in **ttt-9**. The Ru-P($Ph_2C_6H_4O$) distance was slightly longer than the corresponding values found in the related species (Table 4.1).

In an attempt to observe any intermediate species on the pathway for C-O bond cleavage, the C_6D_6 solution of **ttt-9** and DPEphos (1.2 equiv) was left at room temperature for a period of 20 days. Subsequent ^{1}H NMR analysis revealed that the major component of the reaction mixture was the unreacted starting material **ttt-9** (ca. 73%), while the amount of the C-O activated product **29** was negligible (ca. 5%). Interestingly, the Ru-H resonance of **ttt-9** was flanked by two small, new triplet signals

[i] Recent studies show that the large variations in the ^{1}H NMR chemical shift of transition-metal hydrides with *trans*-ligands are dominated by the spin-orbit and paramagnetic effects.[2–4] For the ruthenium d^6 systems, $[Ru(NHC)_4(L)H]^{0/+}$ and $[Ru(R_2PCH_2CH_2PR_2)_2(L)H]^+$, the observed trends were rationalised by means of changes in the energies of the occupied Ru d_π orbitals and the unoccupied $\sigma^*_{Ru\text{-}H}$ orbital, and their contribution to the paramagnetic term, which determines the shielding of the ^{1}H nucleus. Thus, the hydride chemical shift in **29** can only be fully accounted for with an aid of relativistic DFT calculations.

at δ -6.40 ($^2J_{HP}$ = 20.6 Hz) and -6.60 ($^2J_{HP}$ = 20.0 Hz). The former arose from the monodeuteride isotopologue of **ttt-9** formed by H/D exchange with C_6D_6,[5] while the latter was likely to be the anticipated PPh_3/DPEphos substitution species, *trans*-[$Ru(IMe_4)_2$(DPEphos)H_2], generated prior to C-O exchange. A new doublet of doublet hydride resonance ($^2J_{HP}$ = 25.4 Hz, $^2J_{HP}$ = 15.3 Hz) was also observed at a slightly higher frequency (δ -17.66) than that of **29** and was tentatively assigned as the *cis* carbene isomer of **29** (*vide infra*).

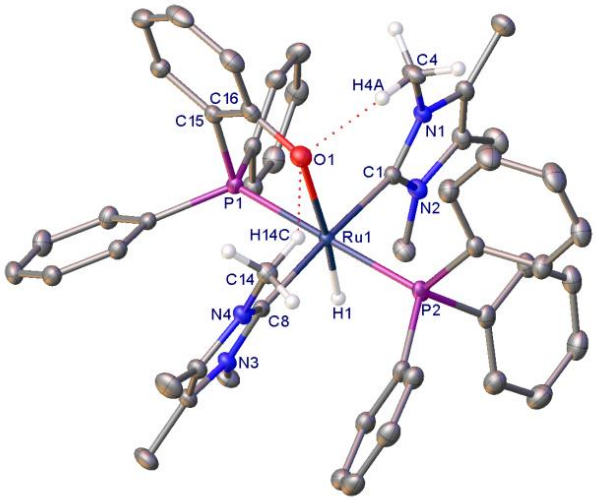

Figure 4.2: Molecular structure of [$Ru(IMe_4)_2(PPh_3)(Ph_2PC_6H_4O)H$] (**29**). Thermal ellipsoids are represented at 30 % probability. All hydrogen atoms, with the exception of the hydride ligand and those on the N-methyl groups involved in the H···O interaction, have been omitted for clarity. Selected bond lengths (Å) and angles (°): Ru1-O1 2.2720(16), Ru-P1 2.3181(5), Ru1-P2 2.2891(5), Ru1-C1 2.121(2), Ru1-C8 2.088(2), O1-Ru1-P1 78.64(4), P1-Ru1-P2 176.94(2), C1-Ru1-C8 172.97(8), P1-Ru1-C1 88.48(5), P2-Ru1-C8 91.42(5).

Table 4.1: Ru-P and Ru-O distances of Ru(II) complexes containing a diphenylphosphinophenolate ($Ph_2PC_6H_4O^-$) ligand.

Complex	Ru-P [Å]	Ru-O [Å]	O-Ru-P [°]	Reference
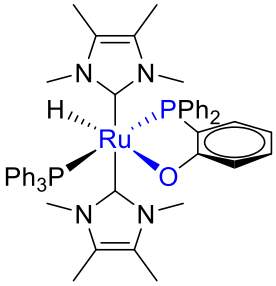 **29**	2.3181(5)	2.2720(16)	78.64(4)	this work
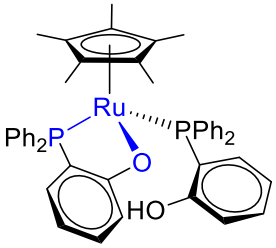	2.307(1)	2.133(2)	80.49(7)	6
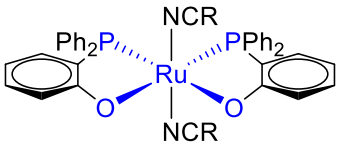	R = Me 2.2663(9), 2.2734(10) R = Et 2.2769(8), 2.2660(9)	R = Me 2.116(2), 2.2132(2) R = Et 2.119(2), 2.125(2)	R = Me 86.86(10), 82.85(7) R = Et 86.00(8), 82.99(7)	7
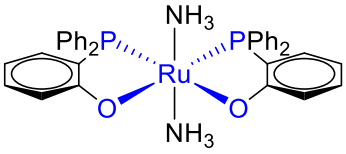	2.2389(6), 2.2487(6)	2.1175(2), 2.1350(2)	82.64(6), 83.10(5)	8

It is noteworthy that none of the complexes shown in Table 4.1 were made *via* C-O activation of DPEphos. The synthesis of [Cp*Ru($Ph_2PC_6H_4O$)($PPh_2C_6H_4OH$)] (Scheme 4.2, top row) was achieved through reduction of [{Cp^*RuCl_2}$_2$] with zinc in MeOH, followed by addition of $PPh_2(C_6H_4OH)$ to the reaction mixture.[6] [Ru($Ph_2PC_6H_4O$)$_2$(NCR)$_2$] (R = Me, Et) (Scheme 4.2, middle row) were synthesised

upon thermolysis of $[Ru(Ph_2PC_6H_4OMe)_2Cl_2]$ in the appropriate solvent, which resulted in the dealkylation of the phosphine-ether ligand *via* CH_3Cl elimination.[7] A similar process was postulated to account for the formation of the amino analogue $[Ru(Ph_2PC_6H_4O)_2(NH_3)_2]$, obtained upon heating an acetone solution of $[Ru(COD)(NH_3)_2(NH_2NMe_2)Cl][BPh_4]$ in the presence of $PPh_2(C_6H_4OMe)$ (Scheme 4.2, bottom row).[8]

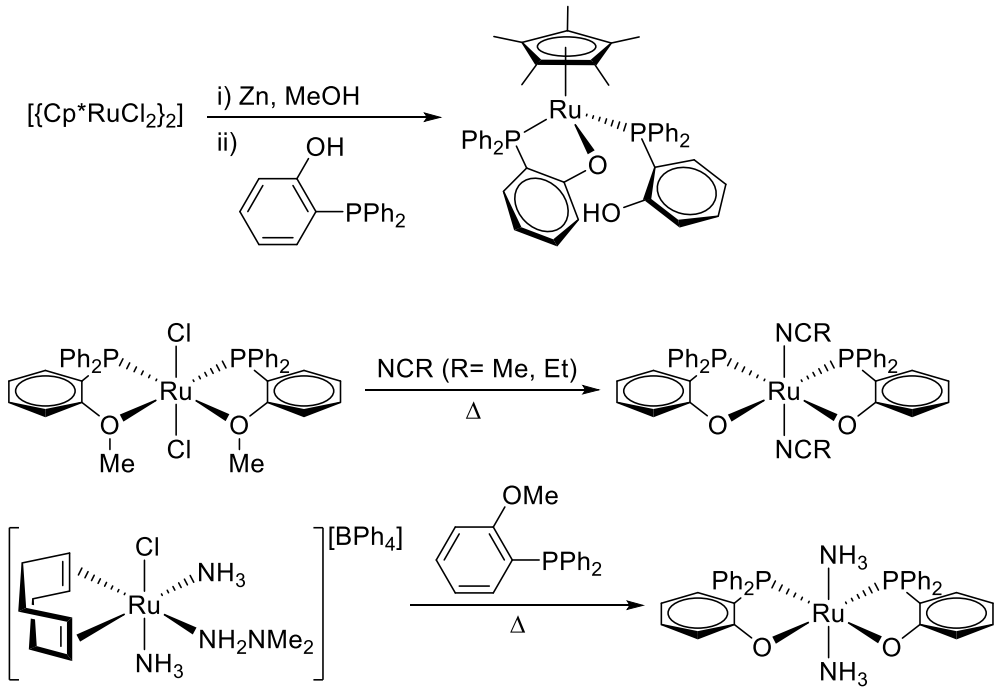

Scheme 4.2: Synthesis of complexes containing a $PPh_2(C_6H_4O)$ ligand.

4.2.2. Reaction of $[Ru(IMe_4)_2(PPh_3)_2H_2]$ (ttt-9) with diphenyl(2-methoxyphenylphosphine)

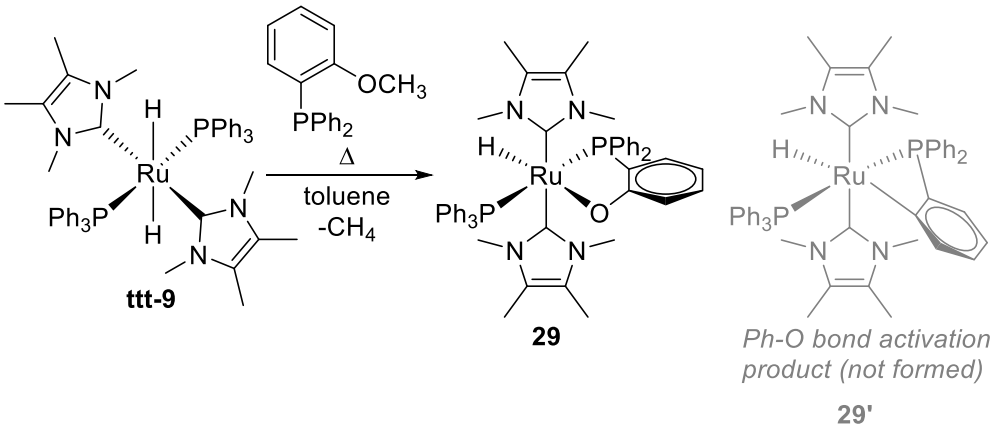

Scheme 4.3: Synthesis of $[Ru(IMe_4)_2(PPh_3)(Ph_2PC_6H_4O)H]$ (**29**) from $Ru(IMe_4)_2(PPh_3)_2H_2]$ (**ttt-9**) and diphenyl(2-methoxyphenylphosphine).

Diphenyl(2-methoxyphenylphosphine) ($PPh_2(2\text{-}C_6H_4OCH_3)$; Scheme 4.3) can be considered as a monodentate analogue of DPEphos containing both aryl (Ph-O) and alkyl (O-CH_3) C-O bonds. It was therefore employed to a) probe if ligand chelation is necessary to facilitate nucleophilic Ru-H attack, and b) determine the selectivity of the reaction, i.e. the preference for either C-O activation of the Csp^2-O or Csp^3-O bond. It was found that heating a toluene solution of **ttt-9** and $PPh_2(2\text{-}C_6H_4OCH_3)$ (1.2 equiv) overnight at 100°C, i.e. conditions comparable to the reaction between **ttt-9** and DPEphos (Section 4.2.1), led to the selective formation of just **29** as indicated by both ^1H and ^{31}P NMR spectroscopy. This shows that bidentate coordination is not required for the nucleophilic attack of Ru-H on a C-O to take place and also shows that activation of the weaker sp^3 C-O bond[ii] takes place, presumably with loss of CH_4. The

[ii] Bond dissociation energies (BDE) of Ph-OCH_3 and PhO-CH_3 bonds in anisole are 91 and 80 kcal mol^{-1} respectively.[9]

origin of this selectivity was most likely thermodynamic as the formation of the 5-membered metallacycle in **29**, as well as the release of methane provides stronger driving force than the alterative strained 4-membered ring in the sp^2 C-O activated product **29'** and elimination of MeOH. Further discussion of selectivity in C-O activation steps is provided in Section 4.6.

4.2.3. Reaction of $[Ru(IMe_4)_2(PPh_3)_2H_2]$ (ttt-9) with DCEphos

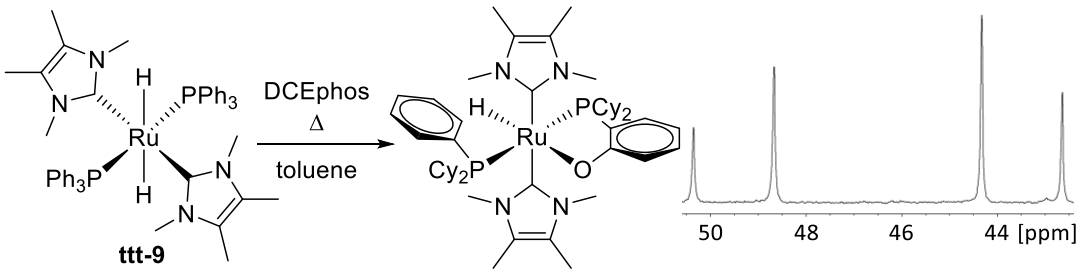

Scheme 4.4: Reaction between $[Ru(IMe_4)_2(PPh_3)_2H_2]$ (**ttt-9**) and DCEphos (left), and a section of the $^{31}P\{^1H\}$ NMR spectrum ($C_6H_5CH_3$, 162 MHz, 25°C) showing product resonances (right).

The reaction between **ttt-10** and $(Cy_2PC_6H_4)_2O$ (DCEphos; Scheme 4.4) was carried out to examine the effect of the PR_2 substituents on the reaction outcome. It was assumed that the replacement of phenyl groups in DPEphos by more electron donating cyclohexyl substituents would render the sp^2 C-O bonds of the P-O-P ligand less activated and make nucleophilic attack by Ru-H less likely. This premise proved to be correct as the C-O cleavage only took place under far more forcing conditions. Thus, after 2 days at 120°C in toluene almost complete conversion of **ttt-9** to a new species was observed by ^1H and $^{31}P\{^1H\}$ NMR spectroscopy. This was assigned tentatively as $[Ru(IMe_4)_2(P(Cy)_2Ph)(Cy_2PC_6H_4O)H]$ due to the appearance of a single new Ru-H resonance at a very similar chemical shift (δ -19.69, $^2J_{HP}$ = 27.3 Hz, $^2J_{HP}$ = 14.5 Hz) to

that of **29**, as well as the presence of two doublet phosphorus signals at δ 49.5 and 43.4 with a large *trans*-$^2J_{PP}$ coupling constant of ca. 272 Hz.[iii] The presence of two phosphorus resonances suggested that $P(Cy)_2Ph$ and $Cy_2PC_6H_4O$ represent two distinct and hence magnetically inequivalent ligand environments, which is in striking contrast to **29**. The DCEphos derivative could not be isolated and fully characterised as prolonged heating of the reaction mixture did not lead to full conversion but instead product decomposition was observed as suggested by loss of the product resonances.

4.2.4. Reaction of $[Ru(IMe_4)_2(PPh_3)_2H_2]$ (ttt-9) with xantphos

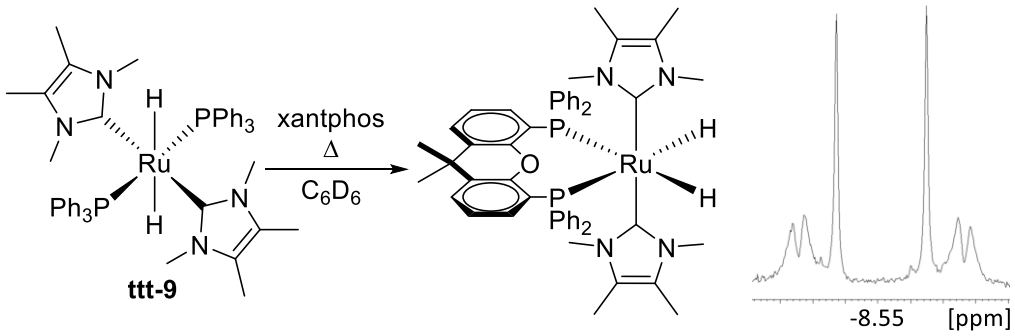

Scheme 4.5: Reaction of $[Ru(IMe_4)_2(PPh_3)_2H_2]$ (**ttt-9**) and xantphos (left), and a section of the ^1H NMR spectrum (C_6D_6, 500 MHz, 25°C) showing the hydride resonance of the product (right).

In comparison to DPEphos, the presence of the dimethyl bridge in the 10-position of xantphos widens its bite angle and enhances the overall ligand backbone

[iii] Approximate chemical shifts and J_{PP} values are given as the coupling pattern resembled a second order AB system (Scheme 4.4).

rigidity,[iv] which is considered to be the main reason for the remarkable stability of the formed chelates. Although C-O activation of DPEphos proved to be relatively facile, it was anticipated that due to the additional constraint within xantphos, a similar reaction would not proceed but rather that a conventional PPh_3/xantphos substitution reaction would take place. Indeed, NMR analysis of a C_6D_6 solution of **ttt-9** and xantphos (5 equiv) heated at 70°C for 3 days revealed formation of a new second order hydride resonance at δ -8.55, which was assigned to ccc-isomer of $[Ru(IMe_4)_2(xantphos)H_2]$ (Scheme 4.5). The $^{31}P\{^1H\}$ NMR spectrum comprised a singlet resonance at δ 26.9. No efforts to isolate and fully characterise the complex were made on the basis that there was no evidence of C-O activation taking place.

[iv] The natural bite angle, defined as the preferred chelation angle determined only by ligand backbone constraints and not by metal valence angles, displayed by xantphos is 111.7°, while its flexibility range, defined as the accessible range of bite angles within less than 3 kcal mol^{-1} excess strain energy from the calculated natural bite angle, ranged from 97 to 135°. DPEphos was calculated to exhibit a natural bite angle of 102.2° and a flexibility range of 86-120°.[10,11]

4.3. Reaction of $[Ru(IEt_2Me_2)_2(PPh_3)_2H_2]$ (cct-8) with DPEphos

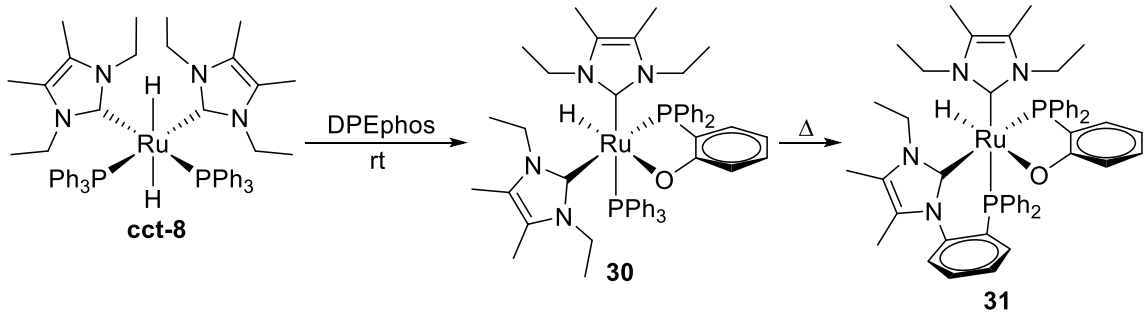

Scheme 4.6: Synthesis of $[Ru(IEt_2Me_2)(IEtMe_2(C_6H_4)PPh_2)(Ph_2PC_6H_4O)H]$ (**31**) from $[Ru(IEt_2Me_2)_2(PPh_3)_2H_2]$ (**cct-8**) and DPEphos *via* $[Ru(IEt_2Me_2)_2(PPh_3)Ph_2PC_6H_4O)H]$ (**30**).

As noted in Chapter 3, $[Ru(IEt_2Me_2)_2(PPh_3)_2H_2]$ (**cct-8**) exhibited higher stoichiometric reactivity towards sp^2 C-F bonds than its IMe_4 counterpart (**ttt-9**) and facilitated HDF of fluoroarenes at room temperature. It was therefore reasonable to assume that **cct-8** would also cleave the C-O bond of DPEphos but perhaps under milder conditions. The reaction shown in Scheme 4.6 was first monitored by ^1H and ^{31}P NMR spectroscopy in C_6D_6, which revealed slow conversion of **cct-8** to **ttt-8** (δ -6.49 (t, $^2J_{HP}$ = 21.9 Hz) and δ 58.2 respectively), along with other species (assigned to **ctc-8** and **tcc-8** on the basis of the similarity of the Ru-H chemical shifts to those for the IMe_4 analogues) over a period of 3 weeks. In addition, there was a new doublet of doublets Ru-H signal at δ -17.21 ($^2J_{HP}$ = 26.2 Hz and $^2J_{HP}$ = 12.3 Hz), which was tentatively assigned to the product of C-O activation, $[Ru(IEt_2Me_2)_2(PPh_3)Ph_2PC_6H_4O)H]$ (**30**). The sample was subsequently reduced to dryness and recystallised from toluene/ pentane at -40°C to afford a very small amount of crystals which confirmed assignment of **30**. The molecular structure of **30** is shown in Figure 4.3. The complex retained a *cis*- (90.6(2)°) arrangement of carbene ligands from **cct-8**, with one IEt_2Me_2 positioned *trans* to PPh_3

(165.44(17)°) and the other *trans* to the P terminus of the chelating diphenylphosphinophenolate (169.26(19)°). As expected, the hydride was located opposite the oxygen atom. Similarly to **29**, there was evidence of hydrogen bonding between Ru-O and one of the methylene (NCH_2) groups (C-H···O 2.137(4) Å; C···O 3.067(7) Å; C-H-O 155.7(4) Å). Despite a different disposition of the NHC ligands with respect to **29**, the Ru-P, Ru-C and Ru-O bond lengths, as well as the O-Ru-P bond angle, were comparable. Unfortunately, in spite of repeated efforts, attempts not only to crystallise **30** again but also to generate it again in higher yield proved impossible, precluding additional characterisation or reactivity studies from being undertaken.

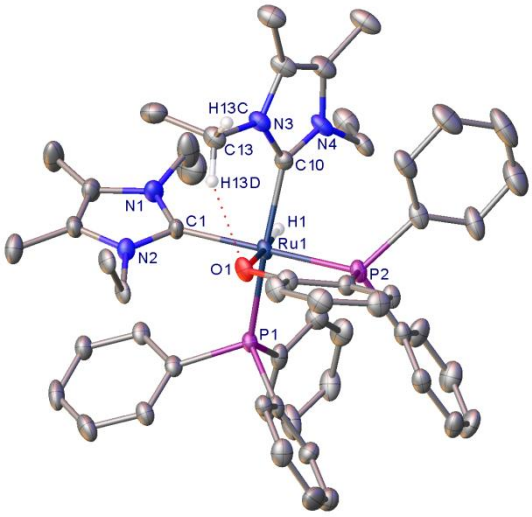

Figure 4.3: Molecular structure of [Ru(IEt_2Me_2)$_2$(PPh_3)$Ph_2PC_6H_4O$)H] (**30**). Thermal ellipsoids are represented at 30 % probability. Hydrogen atoms, with the exception of the hydride ligand and H13C/D, have been omitted for clarity. Selected bond lengths (Å) and angles (°): Ru1-O1 2.276(3), Ru-P1 2.3153(15), Ru1-P2 2.3477(12), Ru1-C1 2.2099(5), Ru1-C10 2.095(6), O1-Ru1-P2 77.95(10), P1-Ru1-P2 94.93(5), C1-Ru1-C10 90.6(2), C1-Ru1-P1 89.38(18), P2-Ru1-C10 87.68(14).

In an attempt to accelerate the reaction of **cct-8** with DPEphos to afford **30**, a reaction mixture was heated at 90°C in toluene.[v] Surprisingly, employment of higher temperatures led to the isolation of [Ru(IEt_2Me_2)($IEtMe_2(C_6H_4)PPh_2$)($Ph_2PC_6H_4O$)H] (**31**, Figure 4.4) featuring an unexpected chelating NHC-phosphine ligand, generated *via* a combination of C-O activation, cleavage of an N-Et carbene linkage and formation of a new N-C bond. Related C-N bond activation of $I^iPr_2Me_2$ and $I^iPr_2Ph_2$ at Ru has been shown to generate N-bound tautomers and propene.[12–14] Cleavage of the C-N bond in IEt_2Me_2 ligand has been observed upon treatment of [Fe(IEt_2Me_2)$_2Cl_2$] with PhLi or ^{n}BuLi to generate a mixture of dinuclear complexes containing a ligated $IEtMe_2$ fragment.[15]

[v] The reaction was cleaner and better yields were obtained when refluxing Et_2O was used as a solvent.

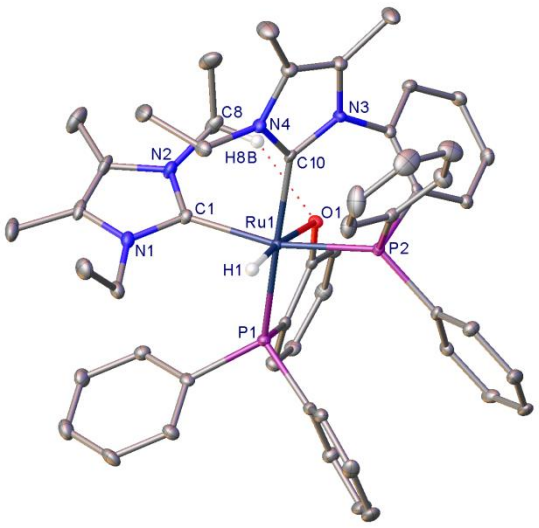

Figure 4.4: Molecular structure of [Ru(IEt$_2$Me$_2$)(IEtMe$_2$(C$_6$H$_4$)PPh$_2$)(Ph$_2$PC$_6$H$_4$O)H] (**31**). Thermal ellipsoids are represented at 30 % probability. All hydrogen atoms, with the exception of the hydride ligand and H8B, have been omitted for clarity. Selected bond lengths (Å) and angles (°): Ru1-O1 2.265(2), Ru-P1 2.3198(9), Ru1-P2 2.3089(8), Ru1-C1 2.104(3), Ru1-C10 2.071(3), O1-Ru1-P1 79.45(6), P1-Ru1-P2 102.88(3), C1-Ru1-C10 88.36(12), C1-Ru1-P1 91.42(9), P2-Ru1-C10 77.19(8).

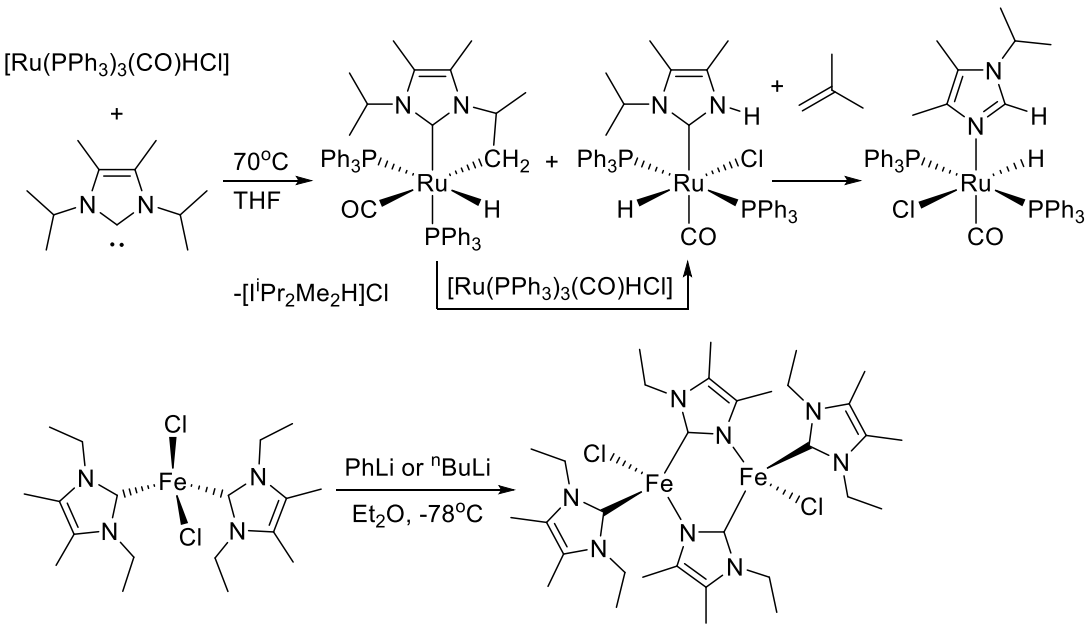

Scheme 4.7: Two examples of C-N bond activation of NHC ligands.

Chauvin and co-workers reported the synthesis of a dinuclear copper complex bearing analogous, N-methyl substituted phosphinocarbene ligands (Scheme 4.8).[16] This involved complexation of an imidazolio-diphosphine salt (formed upon phosphinylation of 1-(1-phenyl)-1*H*-imidazole to imidazole-diphosphine followed by N-methylation) to give a dicationic dinuclear copper complex, which subsequently underwent dephosphinylation upon treatment with $Et_4N^+Cl^-$ to afford the final product. The phosphinylation/dephosphinylation pathway is in contrast to the N-C coupling/ethane elimination, which is likely to take place upon going from **30** to **31**.

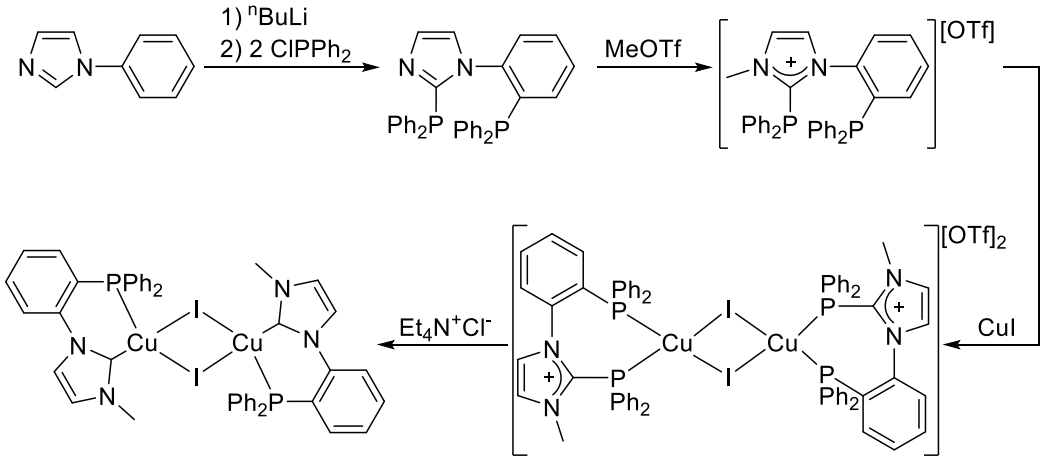

Scheme 4.8: Synthesis of a dinuclear copper complex featuring NHC-phosphine ligands.[16]

Selected X-ray diffraction data for compounds **30** and **31** are summarised in Table 4.2. Apart from the anticipated decrease in the highlighted C-Ru-P angle upon the formation of the new 6-membered metallacycle, perhaps most germane was slight widening of the O-Ru-P_{PO} bite angle and shortening of the involved Ru-O and Ru-P_{PO} bonds. The C-H···O interaction observed in **30** was also present in the N-C activated product **31** (C-H···O 2.126(2) Å; C···O 2.998(4) Å; C-H-O 145.9(2)°).

Table 4.2: Selected bond lengths (Å) and bond angles (°) for compounds **30** and **31**.

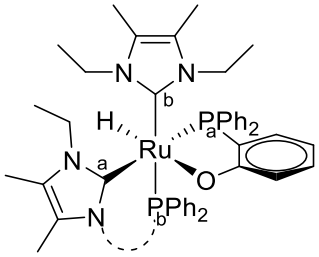	**30**	**31**
Ru-O	2.276(3)	2.252(2)
Ru-P_a	2.3477(12)	2.3198(9)
Ru-P_b	2.3153(15)	2.3089(8)
Ru-C_a	2.099(5)	2.071(3)
O-Ru-P_a	77.95(10)	79.45(6)
C_a-Ru-C_b	90.6(2)	88.36(12)
C_a-Ru-P_b	89.38(18)	77.19(8)
C_a-Ru-P_a	169.26(19)	175.11(9)

The hydride signal of **31** appeared as a doublet of doublets at δ -17.71 with $^2J_{HP}$ coupling constants of 20.0 and 15.0 Hz. The presence of only three NCH_2CH_3 resonances at δ 0.48, 0.85 and 1.12, along with six multiplets at higher frequency arising from the diastereotopic methylene protons was consistent with cleavage of one of the four original N-Et groups. The four backbone CH_3 groups gave rise to four singlets at δ 1.42, 1.46, 1.53 and 1.59, whereas the downfield region of the spectrum contained overlapping aryl-H resonances, which integrated to the expected 28 protons with respect to Ru-H. The inequivalence of two P atoms was apparent from the $^{31}P\{^1H\}$ NMR spectrum, which displayed two doublet signals at δ 59.3 and 54.6 with $^2J_{PP}$ = 28.4 Hz. Two different carbenic carbon resonances were observed and appeared as doublet of doublets at δ 194.6 ($^2J_{CP}$ = 80 Hz, $^2J_{CP}$ = 21 Hz) and 191.5 ($^2J_{CP}$ = 88 Hz, $^2J_{CP}$ = 15

Hz). A doublet signal at δ 179.2 ($^2J_{CP}$ = 23 Hz) was attributed to the C1 carbon (ArO) of the P-O ligand.

4.4. Reaction of $[Ru(PPh_3)_4H_2]$ (32) with DPEphos

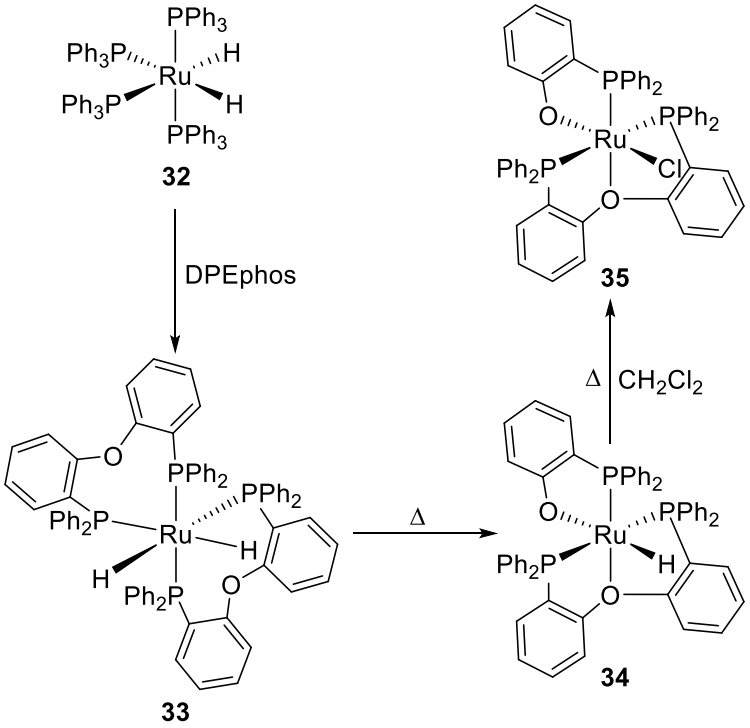

Scheme 4.9: Synthesis of $[Ru(DPEphos)_2H_2]$ (**33**) from $[Ru(PPh_3)_4H_2]$ (**32**) and DPEphos, conversion of **33** to $[Ru(DPEphos)(Ph_2PC_6H_4O)H]$ (**34**) and its subsequent chlorination to $[Ru(DPEphos)(Ph_2PC_6H_4O)Cl]$ (**35**).

In light of the DPEphos C-O activation at **cct-8** and **ttt-9**, the studies were extended to investigate if the reaction was limited only to dihydride complexes containing electron donating NHC ligands. Thus, $[Ru(PPh_3)_4H_2]$ (**32**), was reacted directly with DPEphos (2 equiv) to afford the new bis-DPEphos complex, $[Ru(DPEphos)_2H_2]$ (**33**; Scheme 4.9) in high yield (88%) after 8 h at room temperature. The ^{1}H NMR spectrum of **33** showed a pseudo doublet of triplets at δ -9.80 (J = 48.3 Hz, 34.3 Hz) corresponding to the XX' part of an AA'MM'XX'spin system (where

AA'MM' were the four phosphorus atoms) confirming the formation of the *cis*-dihydride isomer. Similar spectra have been observed for the analogous *cis*-[Ru(P-P)$_2$H$_2$] complexes (P-P = dppe,[17] dppf,[18] sixantphos, homoxantphos).[19,20] The ^{31}P{^{1}H} NMR spectrum consisted of two apparent triplets at δ 41.1 and 35.3 ($^2J_{PP}$ = 18 Hz). The X-ray crystal structure (Figure 4.5) showed a highly distorted octahedral geometry with the widest P1-Ru1-P4 angle of 138.806(18)°. The bite angles adopted by the two DPEphos ligands were equal to 99.355(17)° and 101.863(18)°, while the Ru-P distances ranged from 2.3156(5) to 2.4108(5) Å. The deviation from linearity in *trans*-P-Ru-P angle has been previously observed in [Ru(PPh$_3$)$_3$(CO)H$_2$], which exhibited an intramolecular hydrogen bond between one of the hydride ligands and an adjacent, symmetry generated *ortho*-C-H proton of a phenyl group of one of the PPh$_3$ ligands.[21] A survey of crystallographic structures of other ruthenium hydride species with coordinated triphenylphoshine ligand revealed that such H···H interactions are in fact a common feature of such systems.

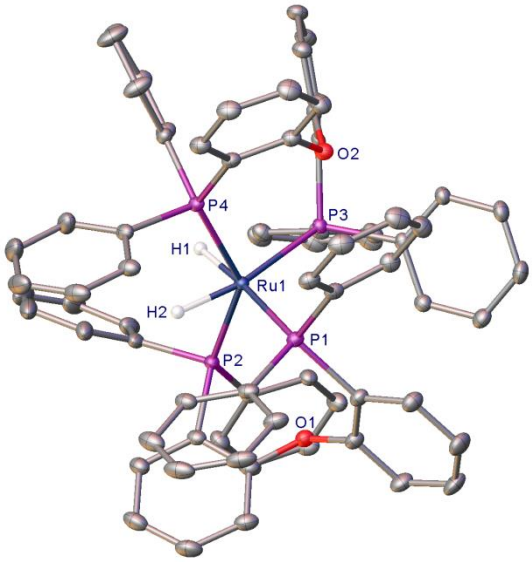

Figure 4.5: Molecular structure of *cis*-[Ru(DPEphos)$_2$H$_2$ (**33**). Thermal ellipsoids are represented at 30 % probability. All hydrogen atoms, with the exception of hydride ligands, have been omitted for clarity. Selected bond lengths (Å) and angles (°): Ru1-P1 (2.4108(5)), Ru1-P2 (2.3179(5)), Ru1-P3 (2.3827(5)), Ru1-P4 (2.3156(5)), P1-Ru1-P2 (101.863(18)), P3-Ru1-P4 (99.355(17)), P1-Ru1-P3 (104.960(17)), P2-Ru1-P4 (138.806(18)).

Heating an isolated sample of **33** in benzene, THF or toluene overnight at 80°C resulted in C-O bond activation of one of the coordinated DPEphos ligands to give the new diphenylphosphinophenolate hydride complex, [Ru(DPEphos)(Ph$_2$PC$_6$H$_4$O)H] (**34**). The ^{1}H NMR spectrum of **34** revealed a low frequency quartet Ru-H signal at δ -13.95 ($^2J_{HP}$ = 21.7 Hz), consistent with a *cis*-H-Ru-P/*trans*-H-Ru-O arrangement and the presence of three phosphorus atoms bound to the metal centre. The corresponding ^{31}P{^{1}H} NMR spectrum comprised of a triplet resonance at δ 76.8 ($^2J_{PP}$ = 30.1 Hz) along with a very broad signal at δ 49.6, which integrated in a ca. 1:2 ratio (Figure 4.6). These were attributed to Ph$_2$PC$_6$H$_4$O$^-$ and DPEphos ligands respectively, the broadness of the latter most likely arising from a rapid dissociation/coordination of the P-*O*-P

linker. Upon cooling a toluene-d_8 solution of **34** to -15°C, the broad resonance resolved into two doublets at δ 49.6 and 48.8 with a $^2J_{PP}$ coupling constant of 30.1 Hz, indicating that the two diphenylphosphine ends of DPEphos became inequivalent. The signals began to merge at -45°C before full coalescence at -75°C, accompanied by the broadening of the $Ph_2PC_6H_4O^-$ resonance.

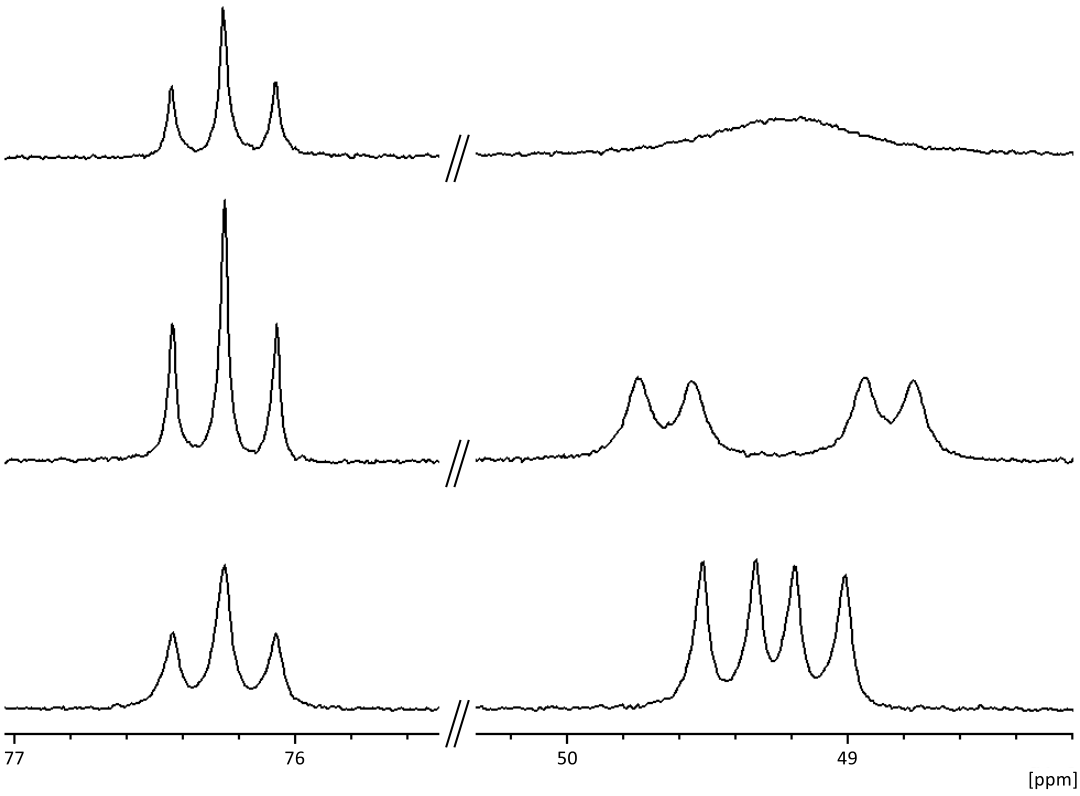

Figure 4.6: Sections of $^{31}P\{^1H\}$ NMR ($C_6D_5CD_3$, 400 MHz) spectra of [Ru(DPEphos)($Ph_2PC_6H_4O$)H] (**34**) recorded at 25°C (top), -15°C (middle) and -45°C (bottom).

Attempted crystallisation of **34** from CH_2Cl_2/pentane resulted in the chlorination of the Ru-H bond to afford the chloride derivative, [Ru(DPEphos)($Ph_2PC_6H_4O$)Cl] (**35**), which was structurally characterised as shown in Figure 4.7. The Ru-P (2.2066(7) Å) and Ru-O (2.099(2) Å) bond distances and the P-Ru-O bond angle (85.36(7)°) of the 5-membered diphenylphosphinophenolate

metallacycle were similar to those measured in the complexes shown inTable 4.1, rather than those found in complexes **29**-**31**, which were in turn closer in value to the related bond lengths and angles of the intact tricoordinated DPEphos ligand (Ru-O: 2.247(2) Å; Ru-P: 2.3136(7) and 2.3326(7)Å; P-Ru-O: 77.58(5) and 81.39(5)°). The $^{31}P\{^{1}H\}$ NMR spectrum consisted of a well-resolved triplet at δ 64.5 ($^{2}J_{PP}$ = 29.5 Hz) and two broad resonances at δ 35.0 and 30.7. No attempts were made to resolve the signals at low temperature. On the basis of comparison to **34**, the former higher frequency signal was assigned as the $Ph_2PC_6H_4O^-$ ligand, while the hemilabile DPEphos gave rise to the latter two.

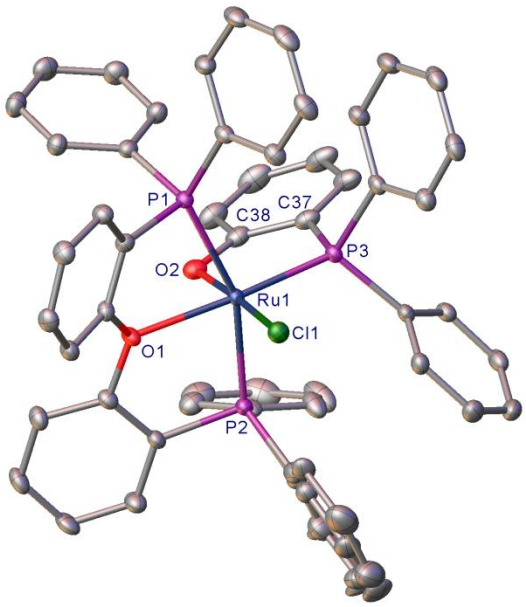

Figure 4.7: Molecular structure of [Ru(DPEphos)($Ph_2PC_6H_4O$)Cl] (**35**). Thermal ellipsoids are represented at 30 % probability. All hydrogen atoms, with the exception of hydride ligands, have been omitted for clarity. Selected bond lengths (Å) and angles (°): Ru1-Cl1 2.4368(9), Ru1-O1 2.247(2), Ru1-O2 2.099(2), Ru1-P1 2.3326(7), Ru1-P2 2.3136(7), Ru1-P3 2.2066(7), P1-Ru1-O1 77.58(5), P2-Ru1-O1 81.39(5), P3-Ru1-O2 85.36(7).

4.5. DFT studies of C-O activation by $[Ru(IMe_4)_2(PPh_3)_2H_2]$ (ttt-9)

Preliminary computational studies of the activation of DPEphos by **ttt-9** have undertaken by Macgregor and Beattie at Heriot-Watt University to establish the mechanism of the C-O bond cleavage in the reaction between **ttt-9** and DPEphos and determine the factors controlling the process. Replacement of the two PPh_3 ligands by DPEphos led to the formation of $[Ru(IMe_4)_2(DPEphos)H_2]$ (**INT(9-29)**), which was predicted to be most stable as the cct-isomer (**cct-INT(9-29)**; ΔG = +2.6 kcal mol^{-1} relative to $[Ru(IMe_4)_2(PPh_3)_2H_2]$ (**ttt-9**) and free DPEphos). The mutual *trans*-arrangement of strong *trans*-influence hydride ligands led to elongated Ru-H bonds (1.68 and 1.69 Å) and accumulation of negative charge (H^1: -0.098, Mulliken). The tcc- (**tcc-INT(9-29)**) and ccc- (**ccc-INT(9-29)**) isomers were calculated to be at higher energies with values of +3.7 and +6.8 kcal mol^{-1} respectively. In all cases, these species were lower in energy when the 8-membered Ru-P-C-C-O-C-C-P ring adopted a boat-boat conformation. Moreover, two possible conformers were identified for the ccc-isomer; one where the C-O-C linker is positioned anti to the hydride in the central H-Ru-IMe_4, and the other where the two moieties are in a syn arrangement (**ccc-INT'(9-29)**). Although the former was computed to be thermodynamically favourable (ΔG = +6.8 kcal mol^{-1}), it is the latter form (ΔG = +10.4 kcal mol^{-1}) that was located on the C-O bond cleavage pathway.

Several mechanisms for the C-O bond activation step were considered. Oxidative addition or σ-bond metathesis were discounted as both processes would necessitate highly unfavourable dissociation of an IMe_4 ligand (to free up a vacant coordination site on Ru) with an energy barrier exceeding 37 kcal mol^{-1}. Thus, a direct

nucleophilic attack of a hydride ligand at the sp^2 carbon of the C-O bond seemed to be the most viable mechanistic scenario.

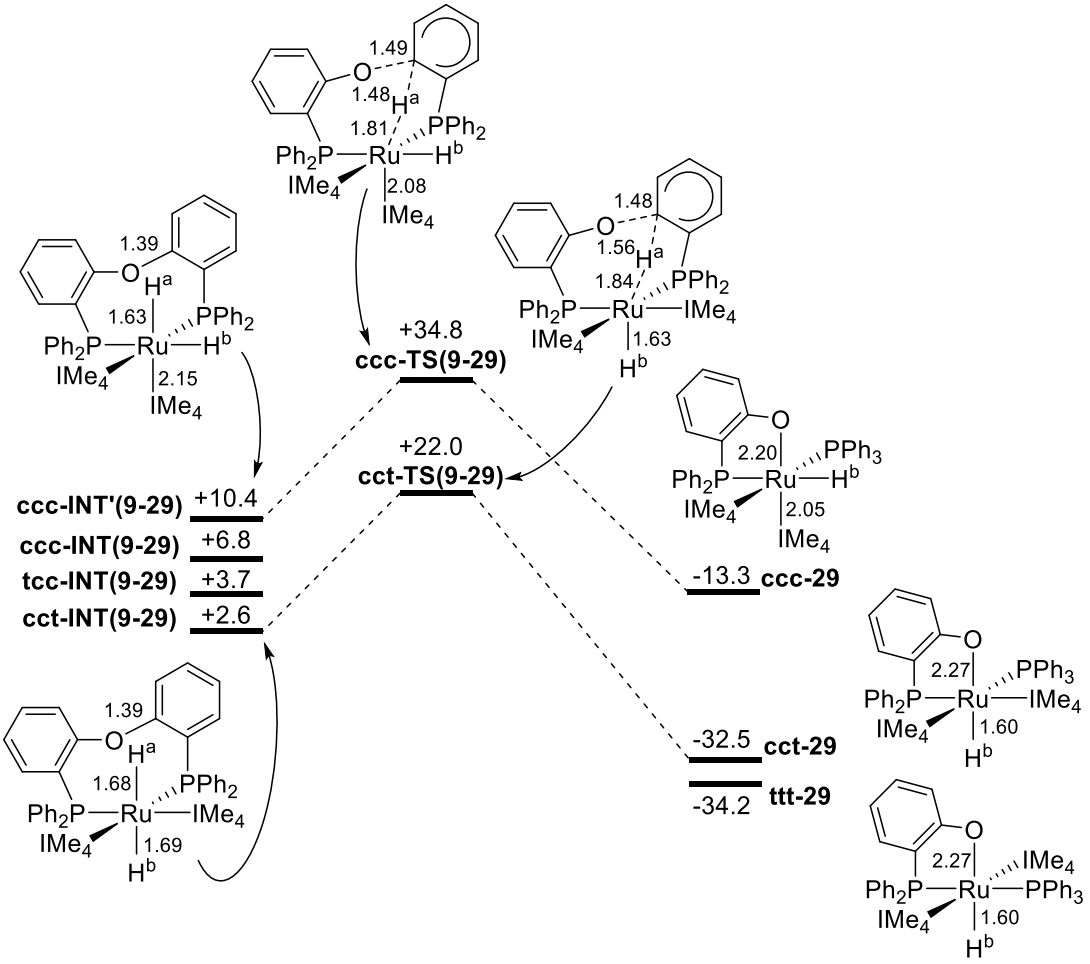

Figure 4.8: Computed free energy profiles (kcal mol^{-1}; BP86 (C_6H_6, D3BJ)) for the nucleophilic hydride attack in **cct-INT(9-29)** and **ccc-INT(9-29)** with selected distances in Å.

Computed reaction profiles for hydride attack in **cct-INT(9-29)** and **ccc-INT(9-29)** are shown in Figure 4.8. The nucleophilic attack of the hydride ligand in **cct-INT(9-29)** proceeded in a single step *via* **cct-TS(9-29)** (ΔG = 22.0 kcal mol^{-1}; Figure 4.9) in which the H^a···C2 distance has shortened from over 3 Å in **cct-INT(9-29)** to 1.56 Å and the C2···O bond lengthened to 1.48 Å (c.f. 1.39 Å in **cct-INT(9-29)**). The elongation of the Ru···H^a distance to 1.84 Å was accompanied by a slight contraction of the Ru-H^b

bond to 1.63 Å. The $\{C_6H_4\}$ moiety resembled a Meisenheimer-type intermediate formed in an aromatic substitution (S_NAr) reaction. Consistent with this picture was the lengthening of C1-C2 (1.46 Å) and C2-C3 (1.43 Å) distances. The Ru···O distance was long (3.34 Å) but full characterisation *via* IRC calculations confirmed that O moves onto the metal centre to give **cct-29** (ΔG = -32.5 kcal mol^{-1}) containing a *P,O*-ruthenacycle. The isomer isolated experimentally, **ttt-29** was predicted to be 1.7 kcal mol^{-1} lower in energy than the cct-form, showing a good agreement between the experimental and computational data.

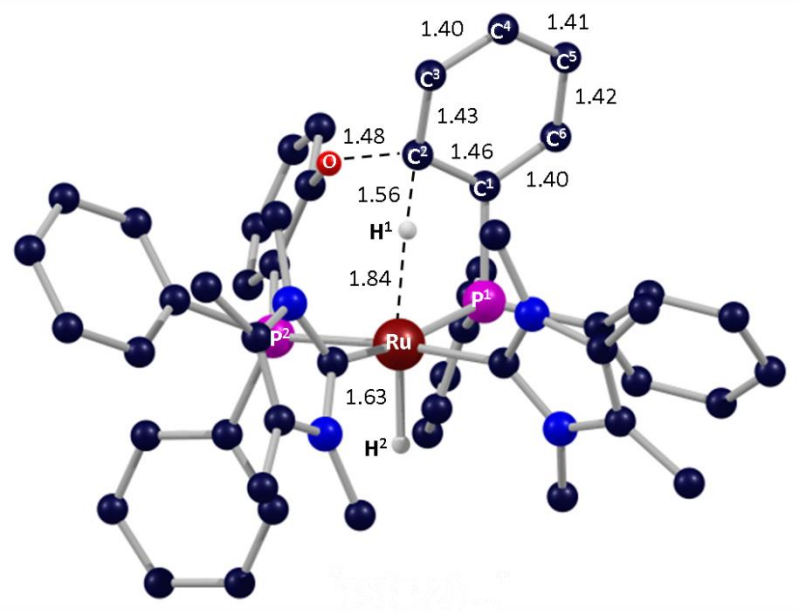

Figure 4.9: Computed structure of **cct-TS(9-29)** with key distances (Å). Hydrogen atoms, with the exception of hydride ligands, have been omitted for clarity.

The alternative C-O bond cleavage in **ccc-INT'(9-29)** (preceded by conformational rearrangement from **ccc-INT(9-29)**) involved a nucleophilic attack *via* a different transition state, **ccc-TS(9-29)**, at +34.8 kcal mol^{-1} to ultimately give **ccc-29** at -13.3 kcal mol^{-1}. **ccc-TS(9-29)** displayed a similar geometry to **cct-TS(9-29)** albeit with shorter Ru···H^a (1.81 Å) and C1···C2 (1.48 Å) distances. Consequently, there was a

clear kinetic preference for the C-O bond activation in **cct-INT(9-29)**. This was due to the positioning of H^a in **ccc-INT'(9-29)** opposite IMe_4, resulting in decreased nucleophilicity when compared to **cct-INT(9-29)**. In line with this was a shorter Ru-H^a bond (1.63 Å) and lower computed negative charge (-0.02, Mulliken; c.f. **cct-INT(9-29)**). The resulting ccc-isomer of **29** (**ccc-29**) was strongly disfavoured over both **cct-29** and **ttt-29**.

4.6. Discussion

The bidentate phosphine ligands based on xanthene-like backbones have been shown to have a pronounced effect on the rate and selectivity of multiple metal catalysed reactions, such as rhodium[10,11,22,23] and platinum catalysed hydroformylation,[24,25] nickel catalysed hydrocyanation[26–28] and palladium catalysed cross coupling.[29,30] Their prevalence in many industrial processes arises from a wide range of bite angles that can be adopted through subtle alterations to the bridge in the 10-position of the xanthene unit. Moreover, the presence of both phosphorus and oxygen donor sites within the rigid diphenylether backbone allows the ligands to coordinate to the metal centre in both tridentate ("O" linker in) and bidentate ("O" linker out) modes and to form either *cis*- or *trans*-isomers. Temporary dissociation of either the linker or one of the phosphine arms can result in hemilabile behaviour,[31] which can in turn provide additional stabilisation of the metal coordination sphere during catalytic transformations.[32–34] Other appealing and important properties of this class of ligands include high thermal stability and apparent resistance to bond degradation reactions. Although decomposition pathways of P-donor ligands have received a great deal of attention,[35–41] the cleavage of an unreactive sp^2-sp^3 hybridised carbon-oxygen bond of the DPEphos ligand has no literature precedence. The most

common deactivation routes of homogeneous catalysts containing monodentate tertiary phosphine ligands are shown in Figure 4.10.[41] Cyclometalation and P-C bond cleavage have been identified as degradation pathways in the hydroformylation of 1-hexene using $[Rh(PPh_3)_3(CO)H]$.[42] Interestingly, despite highly reductive conditions, phosphine oxidation has also been observed in a related rhodium catalysed hydroformylation system where a mixture of supercritical CO_2 and ionic liquid were used as the reaction medium.[43]

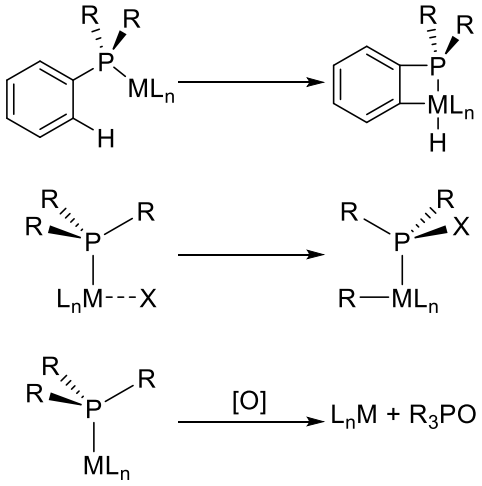

Figure 4.10: Common phosphine decomposition pathways: cyclometalation (C-H bond cleavage; top), intra/intermolecular nucleophilic attack (P-C bond cleavage; middle), phosphine oxidation (M-P bond cleavage; bottom).

In terms of xanthene-based diphosphines, Johnson and Weller described P-C activation of a xantphos ligand bound to Rh(I) centre during amine-borane dehydrocoupling reactions to afford the phosphide-bridged Rh_2 dimer **i** shown in Figure 4.11.[44] Ligand activation was also observed in a more controlled experiment in which two low-coordinate Rh fragments $\{Rh(\kappa^3\text{-}_{P,O,P}\text{-xantphos})\}^+$ and $\{Rh(\kappa^3\text{-}_{P,O,P}\text{-xantphos})(H)_2\}^+$ combined *in situ* in the presence of trimethyl amine borane to form the hydride bridged complex, $[Rh_2(xantphos)_2(\mu\text{-}H)_2(H_3B{\cdot}NMe_3)_n][BAr^F{}_4]_2$, which

underwent P-aryl bond rupture to give $[Rh_2(\kappa^3\text{-P,O,P-xantphos'})_2(\eta^1\text{-}H_3B{\cdot}NMe_3)_2][BAr^F{}_4]_2$ (**ii**, Figure 4.11) accompanied by benzene or biphenyl/H_2 elimination. P-C bond activation of xantphos was also observed in the reaction of the stanna-*closo*-dodecaborate $[Bu_3NH][SnB_{11}H_{11}]$ and $[Pd(xantphos)Cl_2]$ (Scheme 4.10).[45] The initially formed substitution product, $[Pd(SnB_{11}H_{11})(xantphos)]$ (**iii**), readily converted to a dinuclear Pd(I)-Pd(I) complex (**iv**), which featured a P-B bond formed *via* B-H and P-C bond cleavage. In both cases, the C_{aryl}-O-C_{aryl} oxo linker of the xantphos ligand remained intact.

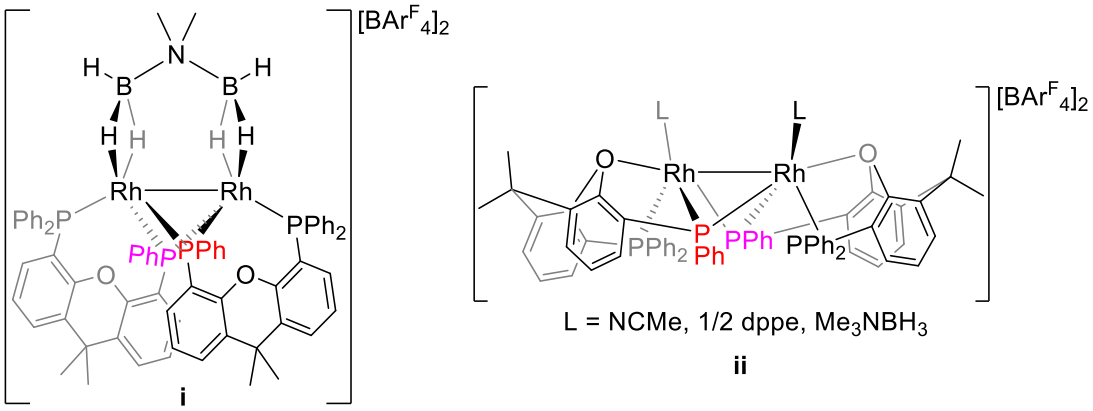

Figure 4.11: P-C activated dimeric complexes based upon the $\{Rh_2(xantphos')_2\}^{2+}$ motif: $[Rh_2(\kappa^2\text{-P,P-xantphos'})_2(\eta^2,\ \eta^2\text{-}H_3BNMe_2BH_3)][BAr^F{}_4]_2$ (**i**; left) and $[Rh_2(\kappa^3\text{-P,O,P-xantphos'})_2(L)_2][BAr^F{}_4]_2$ (**ii**; right).[44]

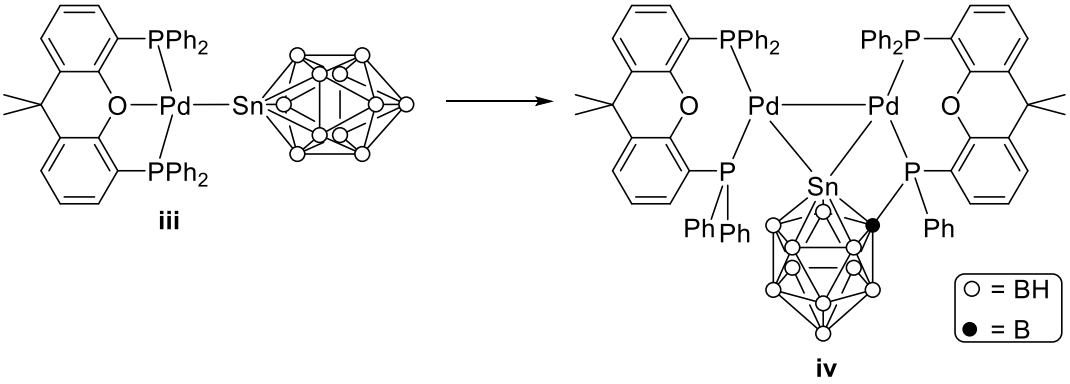

Scheme 4.10: P-C and B-H bond activation in [Pd($SnB_{11}H_{11}$)(xantphos)] (**iii**) leading to the formation of a dinuclear palladium complex **iv**.[45]

Although functionalisation of C-O bonds of ethers into C-H, C-C or C-B bonds has been achieved previously with organometallic complexes through hydrogenolysis,[46–49] cross-coupling[50–55] and borylation[56,57] reactions respectively, a clear understanding of the mechanisms that underpin cleavage of C-O bonds remains underdeveloped. Almost two decades ago, Milstein and co-workers reported metal insertion into the C-O bond of an aryl alkyl ether tethered to two pendant phosphines under mild conditions (Scheme 4.11).[26,27] The selectivity of C-O bond activation was shown to be dependent on both transition metal (Rh, Ni, Pd) and the exact alkyl group involved. Thus, metals in low oxidation states (e.g. Rh(I)) favoured activation of the strong aryl-O bond, whereas more electrophilic centres (Pd(II) or Ni(II)) facilitated cleavage of the weaker alkyl-O moiety, affording stable PCP and POP pincer complexes respectively. Importantly, the initially formed Ar-Rh-OCH_3 unit could not even be detected spectroscopically and was proposed to only be an intermediate prior to rapid β-H elimination to afford the final isolated Ar-Rh-H species (**v**) and formaldehyde. The observation of competitive aryl and alkyl-O bond activation [Pd(CF_3CO_2)$_2$] and an aryl ethoxy ether unit (Ar-O-Et) implied that the processes were kinetically controlled. Since C-O bond cleavage reactions were observed with both acidic and basic d^8 metal centres,

the reactivity of the studied complexes was most likely not of purely electronic origin but should be predominately associated with their low coordination number, which allows facile chelation of the bidentate phosphine predisposing the C-O bond towards activation.

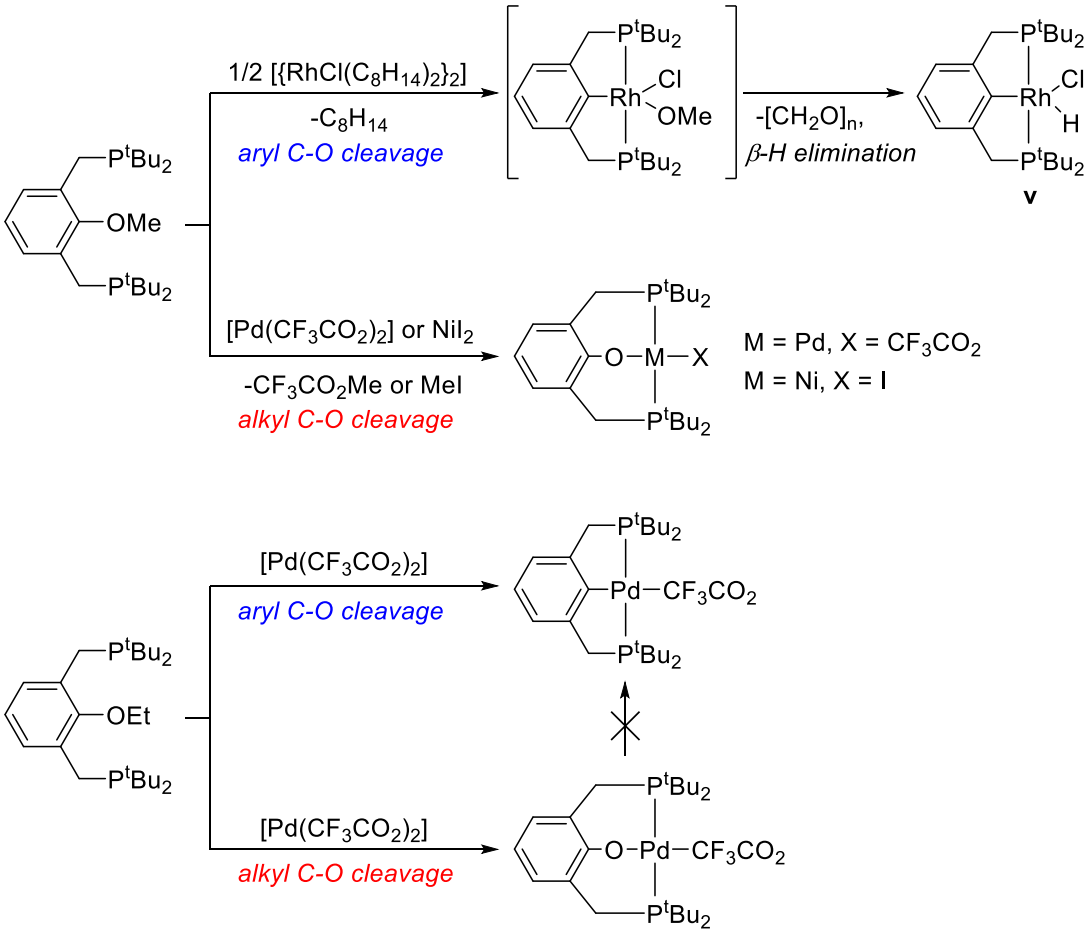

Scheme 4.11: Aryl- and alkyl-oxygen bond activation of phosphinoethers by Rh(I), Pd(II) and Ni(II) complexes.[9,58]

More recently, Agapie et al. observed hydrogenolysis of an unreactive aryl-O bond in (diphosphine)aryl methyl ethers with $Ni(COD)_2$.[59] The studies were later extended to investigate the mechanism of stoichiometric C-O bond breaking in a series of aryl alkyl and diaryl ethers by group 9 and 10 transition metals in different oxidation states (Scheme 4.12).[60] Pd(0) and Pt(0) were found to activate C-O bonds of diaryl

ethers but exhibited selectivity for the weaker, yet more distant, alkyl C-O bond in the reactions with aryl alkyl substrates. In contrast, Ni(0) and Rh(0) reacted preferentially with the aryl C-O bond, which was explained in terms of stronger metal-arene interaction preceding C-O cleavage. Ir(I) was unselective, cleaving aryl and alkyl C-O bonds simultaneously. All reactions proceeded *via* a redox pathway and involved oxidative addition of the C-O bond to the low valent metal centre (M(0)/M(II) or M(I)/M(III)). This is in striking contrast to the DPEphos C-O activation reactions with our Ru(II) dihydride complexes, which proceed with a net retention of the oxidation state. In the case of aryl-methyl ether activation with Ni(0) and Rh(I), the C-O cleavage step was followed by β-H elimination to liberate formaldehyde, reductive elimination of an aryl C-H bond and finally decarbonylation of CH_2O to afford the Ni(0) and Rh(I) carbonyl complexes respectively. The cleavage of alkyl C-O bonds was also promoted by more oxidised M(II) dihalide complexes (Ni, Pd and Pt) to afford new M-phenoxide-chloride-diphosphine species (**vi**) and MeCl *via* Lewis acid-base mechanism.

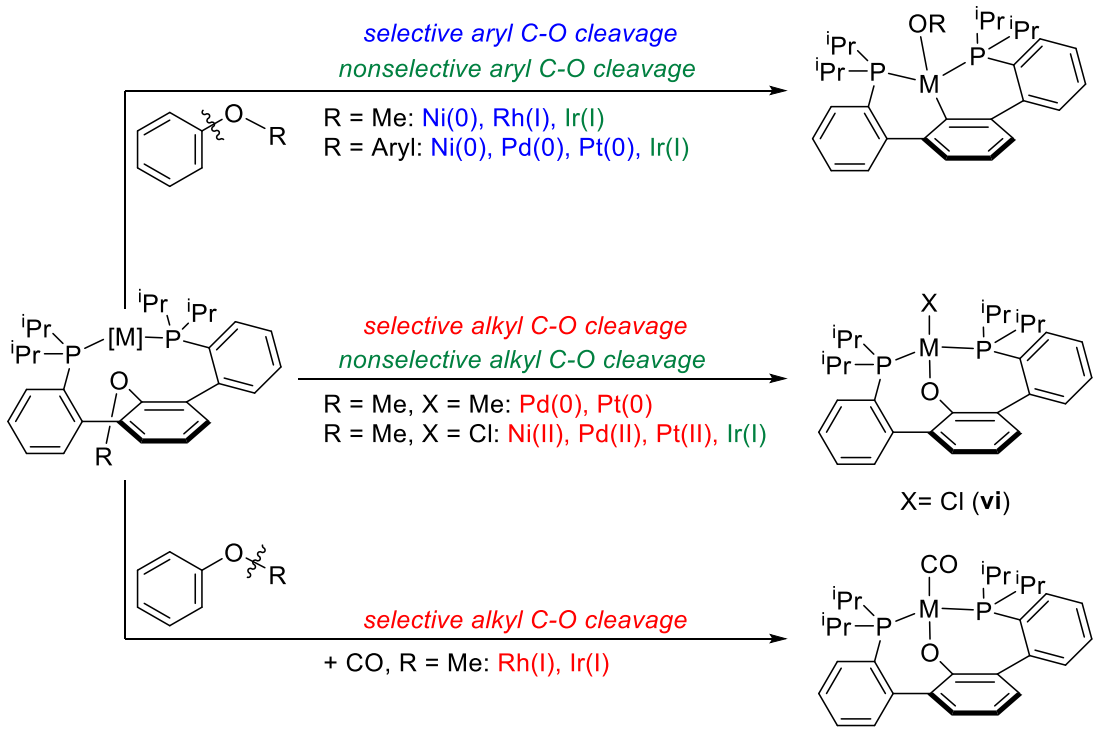

Scheme 4.12: Reactivity of terphenyl diphosphines bearing aryl-methyl ether or aryl-aryl ether moieties with group 9 and 10 metal centres in different oxidation states.[60]

In 2004, Kakiuchi et at.[61] described a chelation-assisted ruthenium catalysed coupling reaction of aromatic ethers with boronic acid esters *via* aryl C-O bond cleavage (Scheme 4.13). Subsequent mechanistic studies revealed that $[Ru(PPh_3)_3(CO)H_2]$, used as a catalyst, underwent reductive elimination of H_2 to generate the putative Ru(0) fragment, "$Ru(PPh_3)_3(CO)$", which in the first instance reacted with an aromatic C-H bond of the substrate to give the new Ru(II) hydride complex **vii**. This interconverted to the aryloxy species **viii** upon heating at 80°C for 3 h, indicating that the Ru-H and R-OAr complexes were the kinetic and thermodynamic products respectively. The catalytic cycle was completed following transmetallation with the organoboronate and concurrent reductive elimination of the cross coupled product. Employment of the bulky 2,2-dimethyl-1-(2-*p*-tolylphenyl)propan-1-one **ix** as a substrate afforded the isolable ruthenium aryloxide complex **x**, representing the first

example of the direct observation of an oxidative addition of an aryl C-O bond to a transition metal complex.[62] A few years later, Zhao and Snieckus showed that the reactivity of $[Ru(PPh_3)_3(CO)H_2]$ was not limited to ketones and that C-OMe activation could be achieved by means of amide[63] and ester chelation.[64]

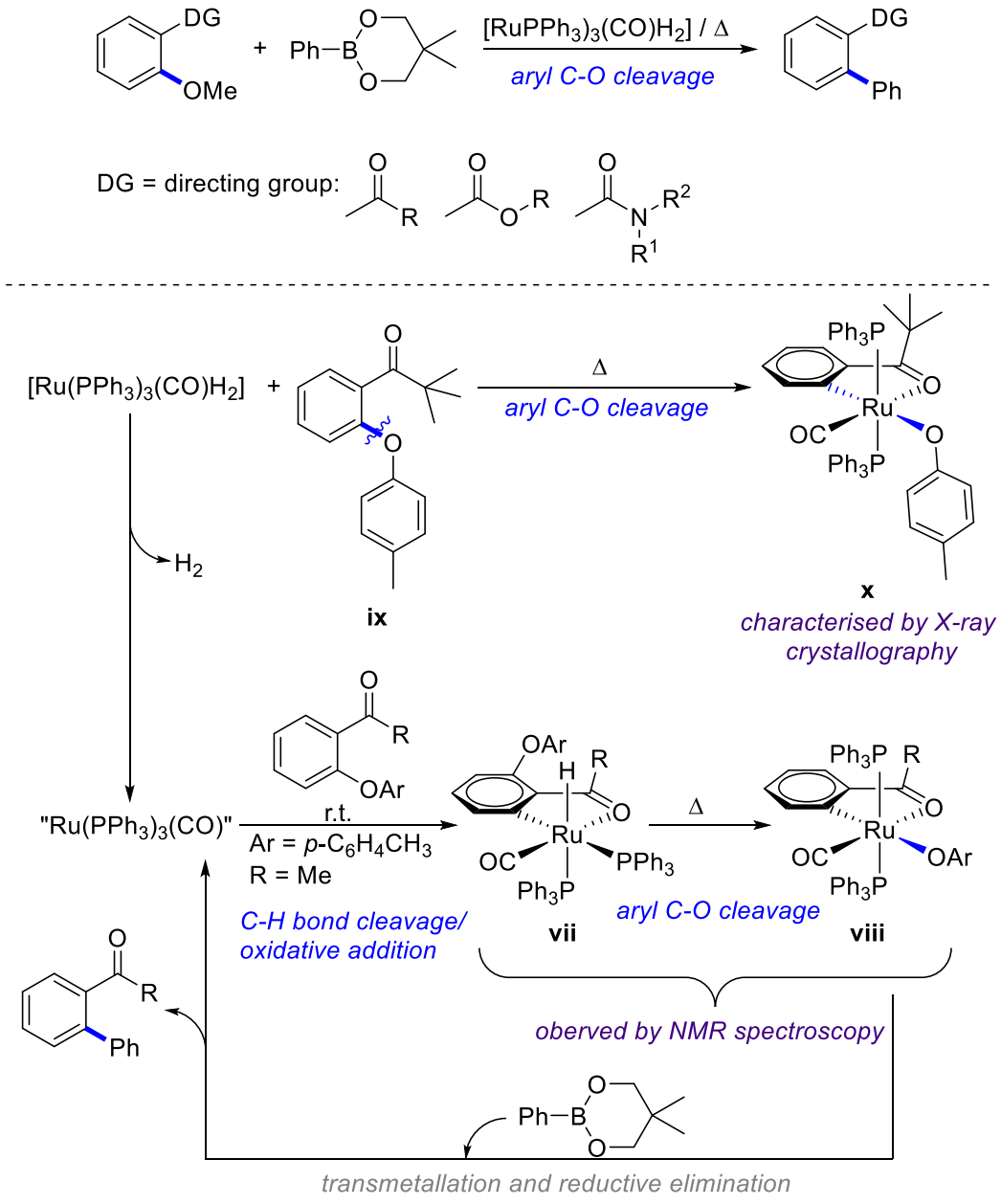

Scheme 4.13: Summary of aryl C-O cleavage reactions with $[Ru(PPh_3)_3(CO)H_2]$.[61–64]

$[Ru(PPh_3)_3(CO)H_2]$ has been also utilised in the depolymerisation of lignin related polymers through tandem dehydrogenation/ reductive ether cleavage.[65–67]

Noteworthy were the quantitative yield and conversion for the C-O bond breaking step attained by the *in situ* generated [Ru(xantphos)(PPh_3)(CO)H_2] system, which has been also shown to catalyse alkylation of alcohols with ketonitriles through a hydrogen transfer process.[68] Interestingly, the DPEphos derivative [Ru(DPEphos)(PPh_3)(CO)H_2] proved completely inactive in either of the reactions. In light of the C-O activation chemistry at [Ru(PPh_3)$_3$(CO)H_2] and joint experimental and computational results described in this chapter, the lack of activity with [Ru(DPEphos)(PPh_3)(CO)H_2] may have been a consequence of nucleophilic hydride attack at the coordinated DPEphos ligand to generate the catalytically inactive complex, [Ru(PPh_3)$_2$($PPh_2C_6H_4O$)(CO)H]. The findings presented in this chapter should raise questions about the generally assumed inertness and suitability of DPEphos in catalytic processes.

4.7. Summary

C-O bond activation of DPEphos has been shown to take place upon thermolysis of the phosphine with [Ru(IMe_4)$_2$(PPh_3)$_2H_2$] (**ttt-9**) to give [Ru(IMe_4)$_2$(PPh_3)($Ph_2PC_6H_4O$)H] (**29**) featuring a 5-membered *P,O*-ruthenacycle. DFT calculations revealed that initial PPh_3/DPEphos substitution was followed by a nucleophilic attack of the ruthenium bound hydride on the aromatic sp^2 hybridised carbon atom of the chelated P-P ligand. In the reaction of [Ru(IEt_2Me_2)$_2$(PPh_3)$_2H_2$] (**cct-8**) and DPEphos, C-O cleavage was accompanied by C-N activation of one of the NHC ligands to afford [Ru(IEt_2Me_2)($IEtMe_2(C_6H_4)PPh_2$)($Ph_2PC_6H_4O$)H] (**31**), containing a N-phosphino functionalised carbene. DPEphos activation was not restricted to ruthenium NHC complexes as demonstrated by the formation of [Ru(DPEphos)($Ph_2PC_6H_4O$)H] (**34**) upon mild heating of [Ru(DPEphos)$_2H_2$] (**33**). The results presented in this chapter illustrate the first example of degradative C-O bond

activation of DPEphos and indicate that similar ligand deactivation pathways might account for the decreased activity sometimes observed in transition metal catalysed reactions mediated by DPEphos.

4.8. References for Chapter 4

(1) Heinicke, J.; Peulecke, N.; Kindermann, M. K.; Jones, P. G. *Z. Für Anorg. Allg. Chem.* **2005**, *631*, 67.

(2) Hrobárik, P.; Hrobáriková, V.; Meier, F.; Repiský, M.; Komorovský, S.; Kaupp, M. *J. Phys. Chem. A* **2011**, *115*, 5654.

(3) Greif, A. H.; Hrobárik, P.; Hrobáriková, V.; Arbuznikov, A. V.; Autschbach, J.; Kaupp, M. *Inorg. Chem.* **2015**, *54*, 7199.

(4) Häller, L. J. L.; Mas-Marzá, E.; Cybulski, M. K.; Sanguramath, R. A.; Macgregor, S. A.; Mahon, M. F.; Raynaud, C.; Russell, C. A.; Whittlesey, M. K. *Dalton Trans.* **2017**, *46*, 2861.

(5) Davies, C. J. E.; Lowe, J. P.; Mahon, M. F.; Poulten, R. C.; Whittlesey, M. K. *Organometallics* **2013**, *32*, 4927.

(6) Canestrari, M.; Chaudret, B.; Dahan, F.; Huang, Y.-S.; Poilblanc, R.; Kim, T.-C.; Sanchez, M. *J. Chem. Soc. Dalton Trans.* **1990**, *4*, 1179.

(7) Hsu, S. C. N.; Hu, S.-C.; Wu, Z.-S.; Chiang, M. Y.; Hung, M.-Y. *J. Organomet. Chem.* **2009**, *694*, 1912.

(8) Malan, F. P.; Noh, J.-H.; Naganagowda, G.; Singleton, E.; Meijboom, R. *J. Organomet. Chem.* **2016**, *825–826*, 139.

(9) Van Der Boom, M. E.; Liou, S.-Y.; Ben-David, Y.; Shimon, L. J.; Milstein, D. *J. Am. Chem. Soc.* **1998**, *120*, 6531.

(10) Kranenburg, M.; van der Burgt, Y. E. M.; Kamer, P. C. J.; van Leeuwen, P. W. N. M.; Goubitz, K.; Fraanje, J. *Organometallics* **1995**, *14*, 3081.

(11) Casey, C. P.; Whiteker, G. T.; Melville, M. G.; Petrovich, L. M.; Gavney, J. A.; Powell, D. R. *J. Am. Chem. Soc.* **1992**, *114*, 5535.

(12) Burling, S.; Mahon, M. F.; Powell, R. E.; Whittlesey, M. K.; Williams, J. M. J. *J. Am. Chem. Soc.* **2006**, *128*, 13702.

(13) Häller, L. J. L.; Page, M. J.; Erhardt, S.; Macgregor, S. A.; Mahon, M. F.; Naser, M. A.; Vélez, A.; Whittlesey, M. K. *J. Am. Chem. Soc.* **2010**, *132*, 18408.

(14) Häller, L. J. L.; Macgregor, S. A. *Eur. J. Inorg. Chem.* **2009**, 2000.

(15) Xiang, L.; Xiao, J.; Deng, L. *Organometallics* **2011**, *30*, 2018.

(16) Abdellah, I.; Canac, Y.; Mboyi, C. D.; Duhayon, C.; Chauvin, R. *J. Organomet. Chem.* **2015**, *776*, 149.

(17) Bautista, M. T.; Cappellani, E. P.; Drouin, S. D.; Morris, R. H.; Schweitzer, C. T.; Sella, A.; Zubkowski, J. *J. Am. Chem. Soc.* **1991**, *113*, 4876.

(18) Chin, B.; Lough, A. J.; Morris, R. H.; Schweitzer, C. T.; D'Agostino, C. *Inorg. Chem.* **1994**, *33*, 6278.

(19) Kamer, P. J.; van Leeuwen, P. N.; others. *Chem. Commun.* **1997**, *4*, 373.

(20) Almeida Leñero, K.; Kranenburg, M.; Guari, Y.; Kamer, P. C. J.; van Leeuwen, P. W. N. M.; Sabo-Etienne, S.; Chaudret, B. *Inorg. Chem.* **2003**, *42*, 2859.

(21) Junk, P. C.; Steed, J. W. *J. Organomet. Chem.* **1999**, *587*, 191.

(22) van der Veen, L. A.; Keeven, P. H.; Schoemaker, G. C.; Reek, J. N. H.; Kamer, P. C. J.; van Leeuwen, P. W. N. M.; Lutz, M.; Spek, A. L. *Organometallics* **2000**, *19*, 872.

(23) van der Veen, L. A.; Keeven, P. K.; Kamer, P. C. J.; van Leeuwen, P. W. N. M. *J. Chem. Soc. Dalton Trans.* **2000**, *13*, 2105.

(24) Kawabata, Y.; Hayashi, T.; Ogata, I. *J. Chem. Soc. Chem. Commun.* **1979**, *10*, 462.

(25) Hayashi, T.; Kawabata, Y.; Isoyama, T.; Ogata, I. *Bull. Chem. Soc. Jpn.* **1981**, *54*, 3438.

(26) Kranenburg, M.; Kamer, P. C. J.; van Leeuwen, P. W. N. M.; Vogt, D.; Keim, W. *J. Chem. Soc. Chem. Commun.* **1995**, *21*, 2177.

(27) Goertz, W.; Kamer, P. C.; van Leeuwen, P. W.; Vogt, D. *Chem. Commun.* **1997**, *16*, 1521.

(28) Boele, M. K.; van der Veen, L.; Kamer, P. J.; van Leeuwen, P. N.; others. *J. Chem. Soc. Dalton Trans.* **1998**, *18*, 2981.

(29) Hayashi, T.; Tamao, K.; Katsuro, Y.; Nakae, I.; Kumada, M. *Tetrahedron Lett.* **1980**, *21*, 1871.

(30) Hayashi, T.; Konishi, M.; Kobori, Y.; Kumada, M.; Higuchi, T.; Hirotsu, K. *J. Am. Chem. Soc.* **1984**, *106*, 158.

(31) Braunstein, P.; Naud, F. *Angew. Chem. Int. Ed.* **2001**, *40*, 680.

(32) Moxham, G. L.; Randell-Sly, H. E.; Brayshaw, S. K.; Woodward, R. L.; Weller, A. S.; Willis, M. C. *Angew. Chem. Int. Ed.* **2006**, *45*, 7618.

(33) Moxham, G. L.; Randell-Sly, H.; Brayshaw, S. K.; Weller, A. S.; Willis, M. C. *Chem. – Eur. J.* **2008**, *14*, 8383.

(34) Ohshima, T.; Miyamoto, Y.; Ipposhi, J.; Nakahara, Y.; Utsunomiya, M.; Mashima, K. *J. Am. Chem. Soc.* **2009**, *131*, 14317.

(35) Garrou, P. E. *Chem. Rev.* **1985**, *85*, 171.

(36) Michman, M. *Isr. J. Chem.* **1986**, *27*, 241.

(37) Bruce, M. I. *Angew. Chem. Int. Ed. Engl.* **1977**, *16*, 73.

(38) Albrecht, M. *Chem. Rev.* **2010**, *110*, 576.

(39) Parkins, A. W. *Coord. Chem. Rev.* **2006**, *250*, 449.

(40) Macgregor, S. A. *Chem. Soc. Rev.* **2007**, *36*, 67.

(41) van Leeuwen, P. W. N. M. *Appl. Catal. Gen.* **2001**, *212*, 61.

(42) Deshpande, R. M.; Divekar, S. S.; Gholap, R. V.; Chaudhari, R. V. *J. Mol. Catal.* **1991**, *67*, 333.

(43) Webb, P. B.; Sellin, M. F.; Kunene, T. E.; Williamson, S.; Slawin, A. M. Z.; Cole-Hamilton, D. J. *J. Am. Chem. Soc.* **2003**, *125*, 15577.

(44) Johnson, H. C.; Weller, A. S. *Angew. Chem. Int. Ed.* **2015**, *54*, 10173.

(45) Dimmer, J.-A.; Hornung, M.; Wütz, T.; Wesemann, L. *Organometallics* **2012**, *31*, 7044.

(46) Sergeev, A. G.; Hartwig, J. F. *Science* **2011**, *332*, 439.

(47) Atesin, A. C.; Ray, N. A.; Stair, P. C.; Marks, T. J. *J. Am. Chem. Soc.* **2012**, *134*, 14682.

(48) Sawatlon, B.; Wititsuwannakul, T.; Tantirungrotechai, Y.; Surawatanawong, P. *Dalton Trans* **2014**, *43*, 18123.

(49) Xu, L.; Chung, L. W.; Wu, Y.-D. *ACS Catal.* **2016**, *6*, 483.

(50) Wenkert, E.; Michelotti, E. L.; Swindell, C. S. *J. Am. Chem. Soc.* **1979**, *101*, 2246.

(51) Cornella, J.; Martin, R. *Org. Lett.* **2013**, *15*, 6298.

(52) Yonova, I. M.; Johnson, A. G.; Osborne, C. A.; Moore, C. E.; Morrissette, N. S.; Jarvo, E. R. *Angew. Chem. Int. Ed.* **2014**, *53*, 2422.

(53) Rosen, B. M.; Quasdorf, K. W.; Wilson, D. A.; Zhang, N.; Resmerita, A.-M.; Garg, N. K.; Percec, V. *Chem. Rev.* **2011**, *111*, 1346.

(54) Tobisu, M.; Chatani, N. *Acc. Chem. Res.* **2015**, *48*, 1717.

(55) Wang, C.; Ozaki, T.; Takita, R.; Uchiyama, M. *Chem. – Eur. J.* **2012**, *18*, 3482.

(56) Kinuta, H.; Tobisu, M.; Chatani, N. *J. Am. Chem. Soc.* **2015**, *137*, 1593.

(57) Zarate, C.; Manzano, R.; Martin, R. *J. Am. Chem. Soc.* **2015**, *137*, 6754.

(58) van der Boom, M. E.; Liou, S.-Y.; Ben-David, Y.; Vigalok, A.; Milstein, D. *Angew. Chem. Int. Ed. Engl.* **1997**, *36*, 625.

(59) Kelley, P.; Lin, S.; Edouard, G.; Day, M. W.; Agapie, T. *J. Am. Chem. Soc.* **2012**, *134*, 5480.

(60) Edouard, G. A.; Kelley, P.; Herbert, D. E.; Agapie, T. *Organometallics* **2015**, *34*, 5254.

(61) Kakiuchi, F.; Usui, M.; Ueno, S.; Chatani, N.; Murai, S. *J. Am. Chem. Soc.* **2004**, *126*, 2706.

(62) Ueno, S.; Mizushima, E.; Chatani, N.; Kakiuchi, F. *J. Am. Chem. Soc.* **2006**, *128*, 16516.

(63) Zhao, Y.; Snieckus, V. *J. Am. Chem. Soc.* **2014**, *136*, 11224.

(64) Zhao, Y.; Snieckus, V. *Chem. Commun.* **2016**, *52*, 1681.

(65) Nichols, J. M.; Bishop, L. M.; Bergman, R. G.; Ellman, J. A. *J. Am. Chem. Soc.* **2010**, *132*, 12554.

(66) Wu, A.; Patrick, B. O.; Chung, E.; James, B. R. *Dalton Trans.* **2012**, *41*, 11093.

(67) Chmely, S. C.; Kim, S.; Ciesielski, P. N.; Jiménez-Osés, G.; Paton, R. S.; Beckham, G. T. *ACS Catal.* **2013**, *3*, 963.

(68) Ledger, A. E. W.; Slatford, P. A.; Lowe, J. P.; Mahon, M. F.; Whittlesey, M. K.; Williams, J. M. J. *Dalton Trans.* **2009**, *4*, 716.

CHAPTER FIVE

Reactivity of ruthenium dihydride complexes with $P(C_6F_5)_3$

5.1. Introduction

As described in Chapter 3, $[Ru(IMe_4)_2(PPh_3)_2H_2]$ (**ttt-9**) was shown to undergo facile substitution reactions of both PPh_3 ligands by bidentate phosphines to yield a series of $[Ru(IMe_4)_2(PP)H_2]$ (P-P = dppm (**cct-25**), dppe (**cct-26**), dppp (**cct-27**)) complexes. The propensity of **ttt-9** to undergo phosphine dissociation was also manifested in the reactions with P(*o*-tolyl)$_3$ and $P(C_6D_5)_3$ previously shown by Davies,[1] the latter also leading to the generation of monodeuteride (**ttt-9-HD**) and dideuteride (**ttt-9-D_2**) complexes, consistent with Ru-H/C-D exchange taking place.

The results presented in this chapter arose completely serendipitously in the reactions of ruthenium dihydride complexes, **ttt-9** and $[Ru(PPh_3)_4H_2]$ (**32**) with tris(pentafluorophenyl)phosphine ($P(C_6F_5)_3$ abbreviated to PCF), an electron deficient analogue of PPh_3.

5.2. Reaction of $[Ru(IMe_4)_2(PPh_3)_2H_2]$ (ttt-9) with PCF

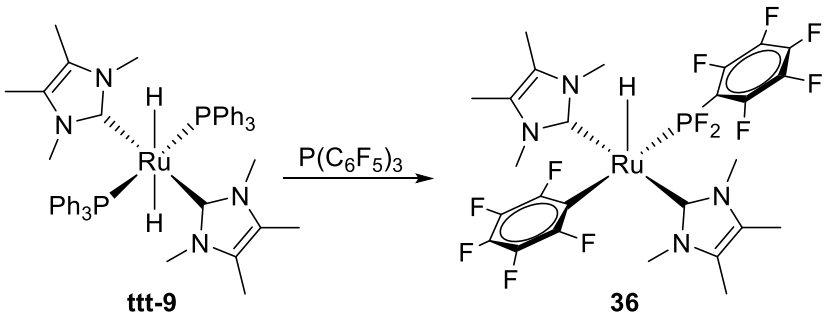

Scheme 5.1: Formation of $[Ru(IMe_4)_2(PF_2(C_6F_5))(C_6F_5)H]$ (**36**) from $[Ru(IMe_4)_2(PPh_3)_2H_2]$ (**ttt-9**) and PCF.

Heating a C_6H_6 solution of **ttt-9** and PCF (2 equiv) at 50°C for 2 days led to the formation of one major new ruthenium hydride complex, which was assigned as the remarkable, five-coordinate complex $[Ru(IMe_4)_2(PF_2(C_6F_5))(C_6F_5)H]$ (**36**, Scheme 5.1) on the basis of multinuclear NMR spectroscopy. The ^{1}H NMR spectrum exhibited four distinct IMe_4 singlet resonances at δ 3.39, 3.28, 1.32 and 1.25, and a Ru-H doublet of triplets signal at δ -29.62 ($^2J_{HP}$ = 46.1 Hz, $^3J_{HF}$ = 6.1 Hz; Figure 5.1) in a 6:6:6:6:1 ratio. The very low frequency chemical shift of the hydride was consistent with its positioning opposite a vacant site (c.f. δ -30.33 in $[Ru(IMe_4)_2(PPh_3)(C_6F_5)H]$ (**15**)). The ^{31}P NMR signal of the ligated pentafluorophenyldifluorophosphine, $PF_2(C_6F_5)$ appeared at a very high frequency (δ 161.4; Figure 5.1) as a triplet of multiplets with a large J_{PF} coupling constant of 1125 Hz.[2–4] The PF_2 group appeared as a doublet of triplets in the ^{19}F NMR spectrum at δ -31.1 (J_{FP} = 1125 Hz, $^4J_{FF}$ = 16 Hz), with the triplet splitting arising from interaction with two *ortho*-fluorine atoms of the pentafluorophenyl ring attached to phosphorus. The *ortho*-, *para*- and *meta*-F signals of P(C_6F_5) were observed at δ -137.3, -154.4 and -162.7 respectively, while the corresponding signals for the Ru bound pentafluorophenyl group appeared at δ -114.5, -163.2 and -163.4. All ^{19}F signals were assigned unambiguously with the aid of ^{19}F COSY spectroscopy (Figure 5.2). The doublet splitting of the C_{NHC} resonance (δ 188.3, $^2J_{CP}$ = 16 Hz) was further proof for the presence of just a single phosphine ligand in the complex.

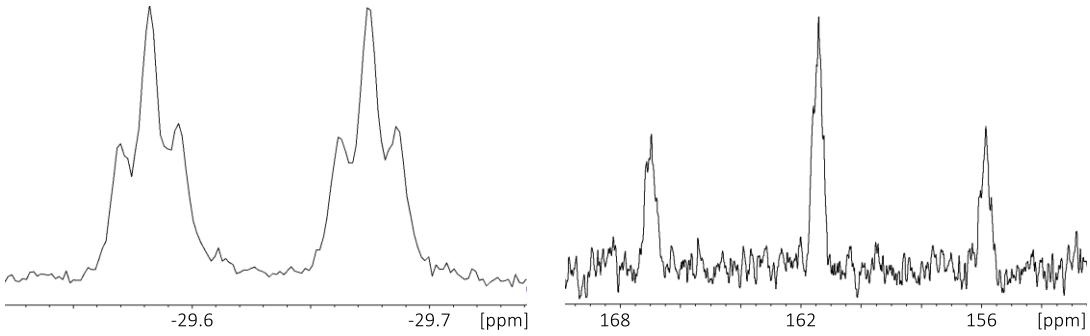

Figure 5.1: Sections of ^{1}H (500 MHz; left) and ^{31}P{^{1}H} (202 MHz; right) NMR spectra (C_6D_6, 25°C) of [Ru(IMe$_4$)$_2$(PF$_2$(C$_6$F$_5$))(C$_6$F$_5$)H] (**36**).

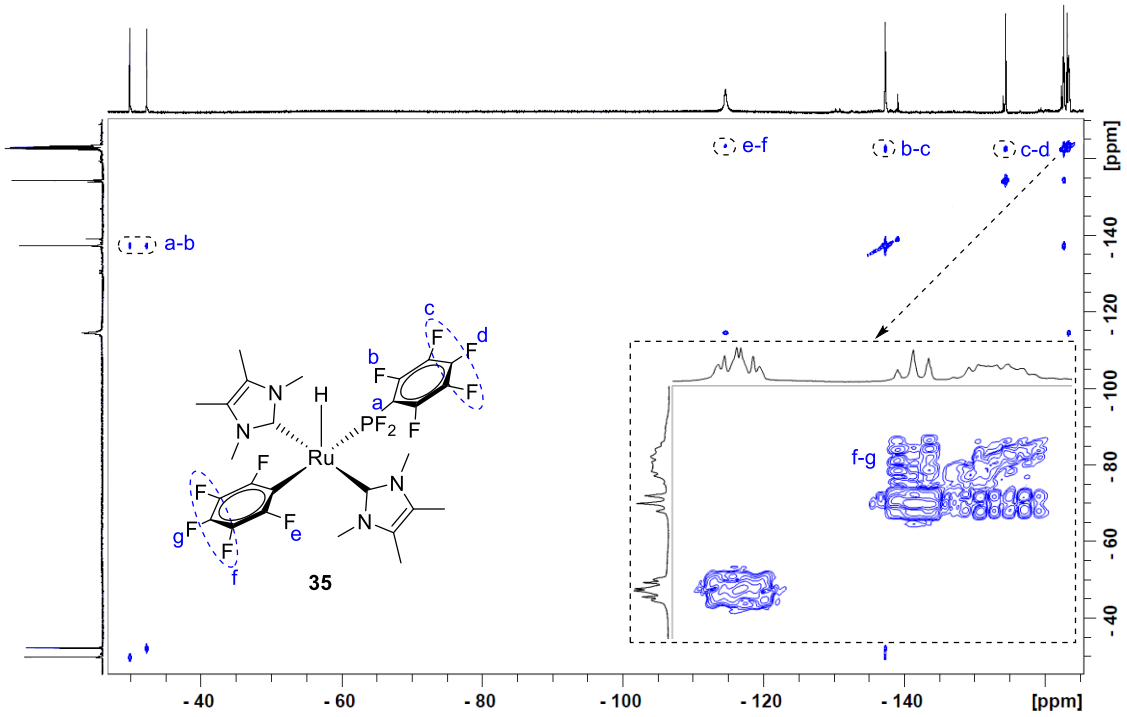

Figure 5.2: ^{19}F COSY spectrum of [Ru(IMe$_4$)$_2$(PF$_2$(C$_6$F$_5$))(C$_6$F$_5$)H] (**36**) in C_6D_6.

Spectroscopic monitoring of the room temperature reaction of **ttt-9** with just 1.2 equiv PCF over the course of 2 days revealed the presence of [Ru(IMe$_4$)$_2$(PPh$_3$)(C$_6$F$_5$)H] (**15**, Section 3.3), **36**, an additional unknown Ru-H containing species (^{1}H NMR: δ -29.95, dm, $^{2}J_{HP}$ = 48.5 Hz; ^{31}P{^{1}H} NMR: δ 125.8, "t", $^{2}J_{PF}$ = 1265 Hz) and unreacted starting material (Figure 5.3). The absence of any

remaining free PCF indicated that more than 1 equiv of the substrate was required to bring about full consumption of the ruthenium starting material. The corresponding ^{19}F NMR spectrum consisted of a sharp doublet resonance at δ -6.74 ($^{2}J_{FP}$ = 1265 Hz) and a set of three signals arising from C_6F_5H. The former might correspond to ruthenium coordinated $PF_2(C_6H_5)$ and could be related to the unknown species observed by ^{1}H and $^{31}P\{^{1}H\}$ NMR spectroscopy. Addition of further 1.2 equiv of PCF and vigorous shaking of the reaction mixture overnight led to the complete disappearance of **ttt-9**. Identification of fluorophosphorus by-products was not achievable by NMR spectroscopy as no other distinct ^{31}P or ^{19}F resonances could be detected.

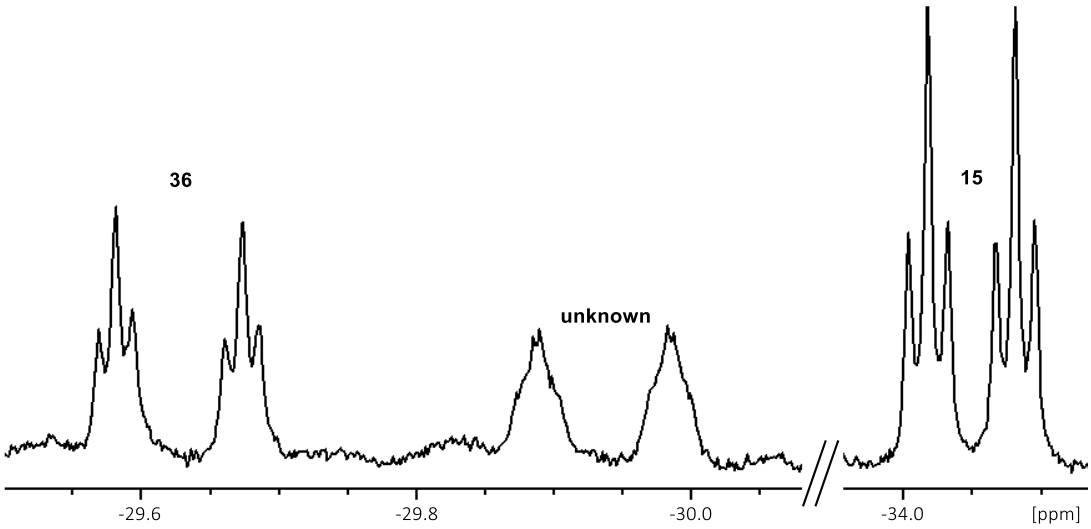

Figure 5.3: Section of the ^{1}H NMR spectrum (C_6D_6, 500 MHz, 25°C) of the reaction between $[Ru(IMe_4)_2(PPh_3)_2H_2]$ (**ttt-9**) and PCF (1.2 equiv) after 2 days at room temperature.

Despite very exhaustive efforts, the high solubility of **36** in common organic solvents, as well as poorly solvating hexamethyldisiloxane, precluded its isolation and structural verification at the time. Efforts to crystallise chloro, carbonyl and isocyanide derivatives of **36** prepared by (i) dissolution of the complex in CH_2Cl_2, (ii) treatment with 1 atm CO and (iii) addition of 1-pentyl or cyclohexyl isocyanides failed. Attempts

to detect **36** by mass spectrometry were also unsuccessful as the spectrum did not contain the anticipated isotope pattern for the $C_{26}H_{27}F_{12}N_4PRu$ molecular ion of m/z = 756.08 or any other signals that could be attributed to plausible fragments formed upon ionisation of **36**.

Given the possibility of multiple P-C/F exchange reactions and phosphine decomposition, no mechanism for the reaction between **ttt-9** and PCF can be proposed sensibly without additional experimental and/or computational studies. In an effort to circumvent extensive bond breaking and forming processes seen with **ttt-9** and to shed some light in terms of mechanistic information on the cleavage reactions of PCF, the ruthenium precursor was changed to $[Ru(PPh_3)_4H_2]$ (**32**).

5.3. Reaction of $[Ru(PPh_3)_4H_2]$ (32) with PCF and characterisation of $[Ru(PPh_3)_3HF]$ (37)

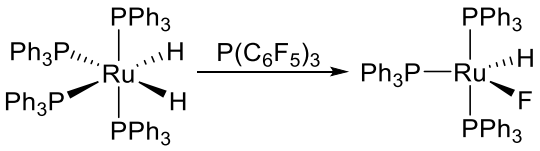

32 **37**

Scheme 5.2: Synthesis of $[Ru(PPh_3)_3HF]$ (**37**) from $[Ru(PPh_3)_4H_2]$ (**32**) and PCF.

Stirring $[Ru(PPh_3)_4H_2]$ (**32**) with PCF (0.35 equiv) in C_6H_6 at room temperature overnight afforded a dark red solution, which upon layering with pentane yielded crystals of the hydride fluoride complex $[Ru(PPh_3)_3HF]$ (**37**, Scheme 5.2). This species is the last of the hydride halide complexes, $[Ru(PPh_3)_3H(halide)]$, to be prepared.[5] An X-ray crystal structure of **37** (Figure 5.4) revealed a distorted trigonal bipyramidal geometry at the ruthenium centre with the two *axial* phosphines highly distorted away from a *trans*-P-Ru-P arrangement with an angle of 153.023(15)°. The Ru-F distance (2.0652(12) Å) lies in the range reported for the related Ru-F complexes,

$[Ru(PPh_3)_3(CO)HF]$ (2.0986(15) Å)[6] or $[Ru(PPh_3)_2(CO)_2F_2]$ (2.011(4) Å).[7] The room temperature ^1H NMR spectrum in CD_2Cl_2 revealed a sharp quartet resonance at δ -22.33 ($^2J_{HP}$ = 28.0 Hz) indicating magnetic equivalence of the phosphine ligands (splitting by Ru-F was too hard to resolve; Figure 5.5). As known for $[Ru(PPh_3)HCl]$, no apparent signal was observed in the room temperature $^{31}P\{^1H\}$ NMR spectrum, consistent with the complex being fluxional. The Ru-F resonance appeared as a broad singlet at δ -214 (w_h = 79 Hz) in the 25°C ^{19}F NMR spectrum, but upon lowering the temperature to -25°C, this resolved into a doublet ($^2J_{FP}$ = 79 Hz), resulting from interaction with just one of the phosphine ligands. The origin of the coupling was confirmed in the corresponding -25°C $^{31}P\{^1H\}$ NMR spectrum, which showed a doublet signal at δ 88.9 with an identical $^2J_{PF}$ coupling constant, as well as a singlet resonance at δ 39.6. The two peaks were in an approximate 1:2 ratio. Although the Ru-H signal became broader at -25°C, the $^1H\{^{31}P\}$ decoupled NMR spectrum exhibited a $^2J_{HF}$ coupling of 10.8 Hz, which was presumably lost in the line width of the ^{19}F signal. These observations suggested rearrangement of the ligands at the metal centre and locking of the conformation akin to that determined by X-ray crystallography.

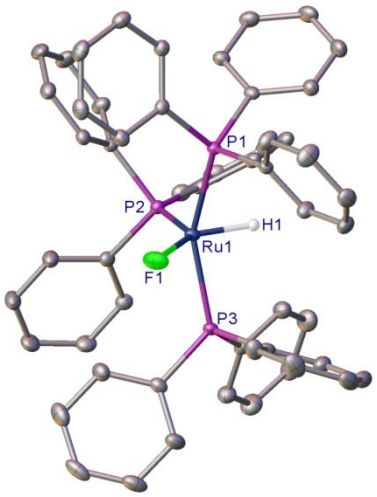

Figure 5.4: Molecular structure of $[Ru(PPh_3)_3HF]$ (**37**). Thermal ellipsoids are represented at 30 % probability. Hydrogen atoms, with the exception of the hydride ligand, have been omitted for clarity. Selected bond lengths (Å) and angles (°): Ru1-F1 2.0652(12), Ru1-P1 2.3423(4), Ru1-P2 2.1996(5), Ru1-P3 2.3201(5); P1-Ru1-F1 88.19(4), P2-Ru1-F1 133.51(5), P3-Ru1-F1 89.10(4), P1-Ru1-P2 102.333(17), P2-Ru1-P3 98.963(17), P1-Ru1-P3 153.023(17).

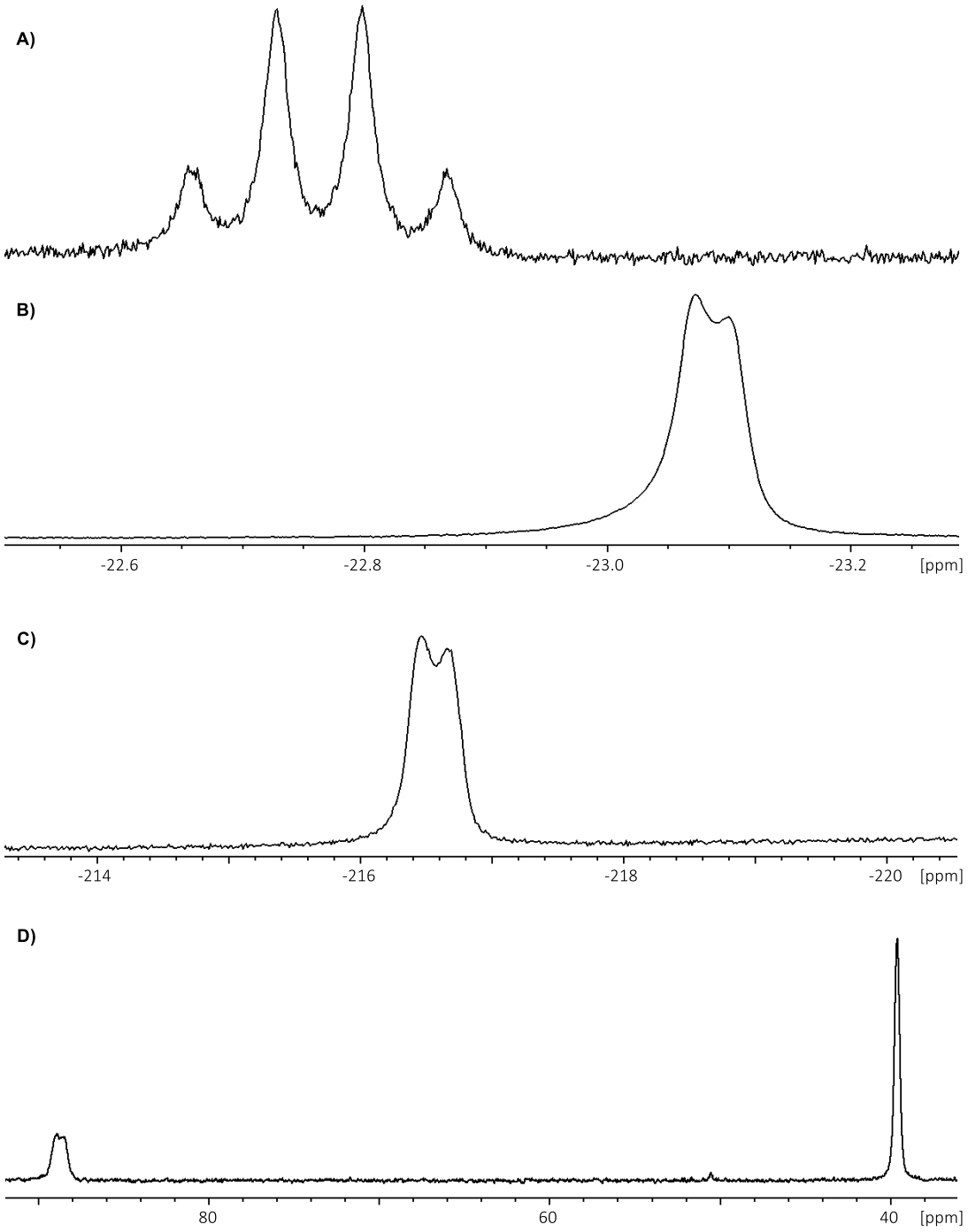

Figure 5.5: Sections of the ^{1}H (400 MHz, 25°C; A), $^{1}H\{^{31}P\}$ (400 MHz, -25°C; B), ^{19}F (376 MHz, -25°C; C) and $^{31}P\{^{1}H\}$ (162 MHz, -25°C; D) NMR spectra of $[Ru(PPh_3)_3HF]$ (**37**) in CD_2Cl_2.

Cooling a toluene-d_8 solution of **37** brought about better resolved ^{1}H and $^{31}P\{^{1}H\}$ NMR signals. Thus, upon ^{31}P decoupling, the doublet of multiplets ^{1}H NMR

signal at -45°C resolved into a doublet at δ -22.01 with a $^{2}J_{HF}$ splitting of 16.1 Hz (Figure 5.6), while the high frequency phosphorus resonance at δ 91.4 appeared as a doublet of triplets with $^{2}J_{PF}$ and $^{2}J_{PP}$ coupling constants of 83.1 and 24.3 Hz respectively (Figure 5.7). The signal at δ 40.5 resembled an AB spin system and hence no *J* values could be obtained. No additional spectroscopic information was gained when THF-d_8 was used as the solvent.

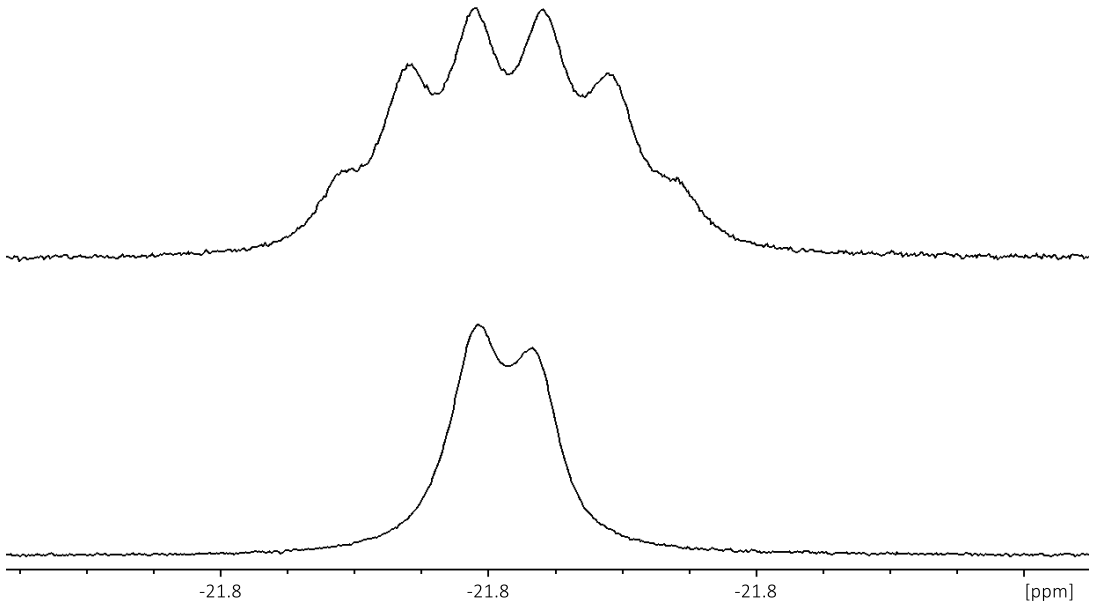

Figure 5.6: Ru-H region of the ^{1}H (top) and $^{1}H\{^{31}P\}$ NMR spectra ($C_6D_5CD_3$, 400 MHz, -45°C) of $[Ru(PPh_3)_3HF]$ (**37**).

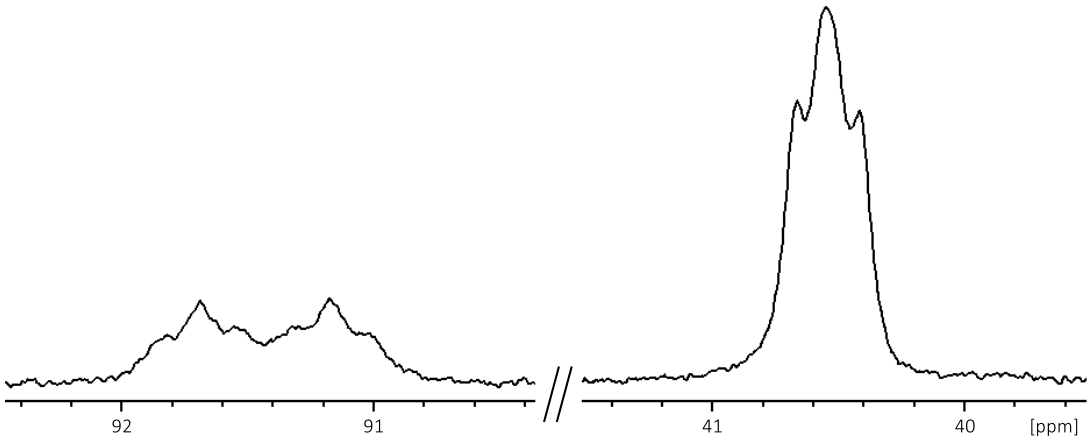

Figure 5.7: Sections of the $^{31}P\{^{1}H\}$ NMR spectrum ($C_6D_5CD_3$, -45°C, 162 MHz) of [$Ru(PPh_3)_3HF$] (**37**).

The fate of PCF could not be determined unequivocally. In an effort to identify the fluoroarylphosphine by-products, the reaction was repeated with varying amounts of PCF. It was found that full conversion of **32** to **37** and almost complete disappearance of PCF could be achieved with just 0.20 equiv of the phosphine over a period of three days. Further alteration of the reaction stoichiometry to 0.17 or 0.11 equiv of PCF (Figure 5.8A and Figure 5.8B respectively) allowed for the spectroscopic observation of three intermediates, which gave rise to three sets of doublet of doublet and triplet of triplet resonances (Table 5.1), and most likely resulted from replacement of PPh_3 ligand(s) at **32** by *in-situ* generated tris(3,4,5-trifluorophenyl)phosphine, $P(3,4,5\text{-}C_6F_3H_2)_3$,[8] which was also detected by $^{31}P\{^{1}H\}$ NMR spectroscopy (δ -1.8). This premise was further supported by the fact that the same species were generated when **32** was reacted directly with $P(3,4,5\text{-}C_6F_3H_2)_3$ (Figure 5.8C).[i] The absence of **37** suggested

[i] A pure sample of $P(3,4,5\text{-}C_6F_3H_2)_3$ for comparison was kindly provided by Dr Matt Clarke (University of St. Andrews).

that its formation in the reaction between **32** and PCF involved sequential HDF of the six *ortho*-fluorines of the three $C_6F_5)_3$ groups, while the different ratio of intermediate complexes in the reactions with 0.17 and 0.11 equiv PCF indicated that PPh_3/P(3,4,5-$C_6F_3H_2)_3$ substitution at **32** was reversible. Activation of C-F bonds in the *ortho*-position is unusual as normally it is the *para*-fluorines that undergo nucleophilic aromatic substitution.[9]

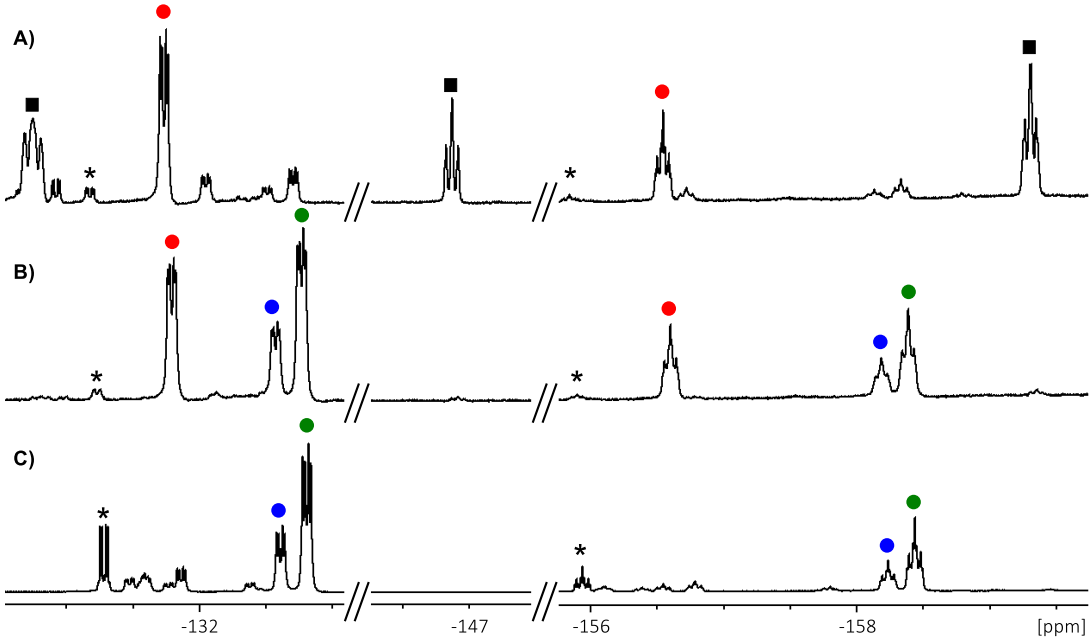

Figure 5.8: Sections of the ^{19}F NMR spectra (C_6D_6, 25°C, 470 MHz) of the room temperature reaction between [Ru($PPh_3)_4H_2$] (**32**) and A) 0.17 equiv PCF, B) 0.11 equiv PCF and C) 1.3 equiv P(3,4,5-$C_6F_3H_2)_3$. ■ and * denote PCF and P(3,4,5-$C_6F_3H_2)_3$ respectively, while ● are used to highlight different substitution products arising from the reaction between **32** with P(3,4,5-$C_6F_3H_2)_3$.

Table 5.1: Comparison of ^{19}F NMR data for the intermediates observed in the reactions between $[Ru(PPh_3)_4H_2]$ (**32**) and PCF or $P(3,4,5\text{-}C_6F_3H_2)_3$. Data for the latter are included for comparison. Colours correspond to NMR resonances of different substitution products highlighted in Figure 5.8.

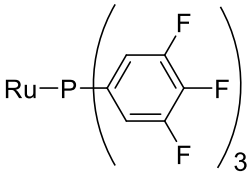	*m*-F (2F)			*p*-F (1F)		
	^{19}F δ [ppm]	$^{3}J_{FF}$ [Hz]	$^{3}J_{FH}$ [Hz]	^{19}F δ [ppm]	$^{3}J_{FF}$ [Hz]	$^{4}J_{FH}$ [Hz]
●	-131.7	21.1	8.0	-156.5	21.1	6.3
●	-132.5	21.6	8.0	-158.1	21.6	7.0
●	-132.7	20.8	8.6	-158.3	20.8	6.8
$P(3,4,5\text{-}C_6F_3H_2)$	-131.2	20.6	7.0	-155.8	20.6	6.3

5.4. Reactivity of $[Ru(PPh_3)_3HF]$ (37)

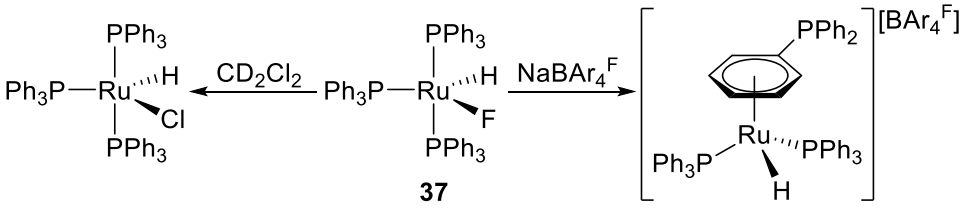

Scheme 5.3: Reaction of $[Ru(PPh_3)_3HF]$ (**37**) with CD_2Cl_2 and $NaBAr_4^F$ resulting in the formation of $[Ru(PPh_3)_3HCl]$ and $[Ru(PPh_3)_2(\eta^6\text{-}C_6H_5PPh_2)H][BAr^F_4]$ respectively.

The reactivity of the Ru-F bond in **37** towards fluorophilic reagents was examined. The fluoride ligand was readily abstracted upon reaction with $NaBAr_4^F$ in CD_2Cl_2 to afford the known cation $[Ru(PPh_3)_2(\eta^6\text{-}C_6H_5PPh_2)]$ (Scheme 5.3). This was identified on the basis of a triplet of doublets Ru-H signal at δ –8.61 ($^{2}J_{HP}$ = 38.6 Hz, $^{3}J_{HP}$ = 8.9 Hz) in the ^{1}H NMR spectrum and two phosphorus resonances at δ 49.0 and -5.2 in a relative ratio of 2:1. The data matched those of the BF_4^- salt of the cation,

previously reported by Wilkinson upon thermolysis of $[Ru(PPh_3)_3(CO_2Me)H]$ in methanol with a large excess of HBF_4.[ii,10]

Slow conversion of **37** to its chloride analogue, $[Ru(PPh_3)_3HCl]$,[5] took place in CD_2Cl_2 at ambient temperature over the course of a few days. Heating benzene, toluene or THF solutions of **37** above 60°C led to sample decomposition, as indicated by the loss of signal intensity in Ru-H resonance. Further studies were carried out with an aim of replacing the Ru-F bond by a Ru-E bond (E = B, C, Si).

5.4.1. Reactivity of $[Ru(PPh_3)_3HF]$ (37) with silanes

5.4.1.1. Reaction of $[Ru(PPh_3)_3HF]$ (37) with R_3SiH (R = Et, Ph) and characterisation of $[Ru(PPh_3)_3(SiR_3)H_3]$ (38, R = Et; 39, R = Ph).

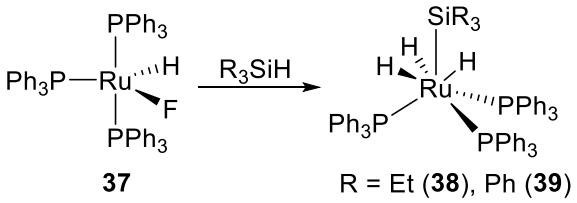

Scheme 5.4: Synthesis of $[Ru(PPh_3)_3(SiR_3)H_3]$ (**38**, R= Et; **39**, R= Ph) from $[Ru(PPh_3)_3HF]$ (**37**) and R_3SiH.

Addition of 2 equiv of R_3SiH (R = Et, Ph) to C_6D_6 solutions of **37** afforded the ruthenium silyl trihydride complexes, $[Ru(PPh_3)_3(SiR_3)H_3]$ (R = Et (**38**), Ph (**39**)) in the time of mixing. Although both complexes were reported 40 years ago as products from the reactions of **32** with appropriate silanes,[11,12] they were not isolated for structural verification and their characterisation was limited to ^1H NMR and IR spectroscopy and elemental analysis. The molecular structures of **37** and **38** are shown in Figure 5.9 and

[ii] The cation was also formed upon chloride abstraction from $[Ru(PPh_3)_3HCl]$ using $NaBAr^F_4$.

confirm a seven-coordinate geometry at Ru with a silyl group capping the face defined by the three readily located hydride ligands in a pseudo octahedral *fac*-$(PPh_3)_3RuH_3$ unit. Alternatively, each hydride ligand could be viewed as capping one of the three SiP_2 faces of a distorted tetrahedron subtended by three phosphines, with the silyl ligand occupying its vertices (average Si-Ru-P 113.8° (**38**) and 113.6° (**39**); average P-Ru-P 104.7° (**38**) and 105.5° (**39**)). The three C atoms bound to Si and the three P atoms were eclipsed, whilst the hydride ligands were staggered with respect to the Si-C and Ru-P bonds. Consequently, the coordination sphere of ruthenium exhibited almost perfect C_3 molecular symmetry about the Ru-Si axis. This ligand disposition is typical for compounds of the type $[L_3M(ER_3)H_3]$.[13–19] Of note were the nonbonding contacts within the $Ru(Si)H_3$ fragment. Although the Ru-H distances (ca. 1.6 Å) were characteristic of terminal ruthenium hydrides,[20,21] the formally nonbonded contacts between the latter and silicon (ca. 2.1 Å) suggested significant Si···H interactions.[22] The H···H separations in **38** lay within the range 2.24- 2.35 Å (ca. 2.33 Å for **39**), considerably longer than those found in dihydrogen complexes[23] and hence consistent with the formulation of the complexes as ruthenium silyl trihydrides, $[Ru(PPh_3)_3(SiR_3)H_3]$ rather than nonclassical ruthenium dihydrogen silyl hydrides, $[Ru(PPh_3)_3(\eta^2\text{-}H_2)(SiR_3)H]$. The Ru-Si distance (2.4110(5) Å) in **38** was slightly longer than the values of 2.3682(6) Å in **39** and 2.376(1) Å determined in $[Ru(PMe_3)_3(SiMe_3)H_3]$.[24] The high *trans*-influence hydride ligands help to rationalise the long Ru-P distances (ca. 2.41 and 2.43Å for **38** and **39** respectively).

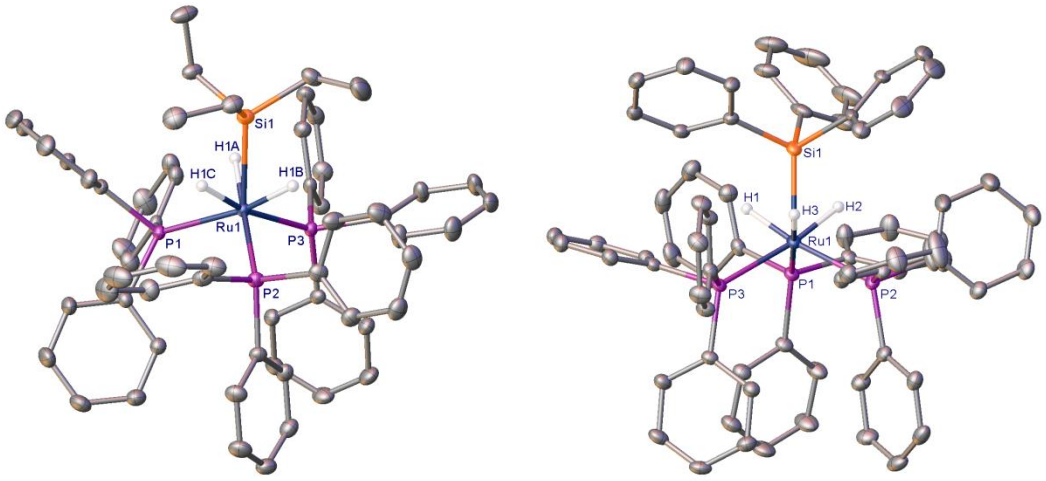

Figure 5.9: Molecular structures of $[Ru(PPh_3)_3(SiEt_3)H_3]$ (**38**, left) and $[Ru(PPh_3)_3(SiPh_3)H_3]$ (**39**, right). Thermal ellipsoids are represented at 30 % probability. Hydrogen atoms, with the exception of hydride ligands, have been omitted for clarity.

The most characteristic feature of the ^{1}H NMR spectra of both **38** and **39** are the complex Ru-H multiplets at δ -10.58 and -9.37 respectively (Figure 5.10). As in the case of the aforementioned $[Ru(PMe_3)_3(SiMe_3)H_3]$ complex, **38** and **39** were not fluxional on the NMR scale (only a slight broadening of the hydride resonance was observed at -55°C) and the line shape of the low frequency signal arose from the AA'A''XX'X'' spin system. The corresponding $^{31}P\{^{1}H\}$ NMR spectra consisted of sharp singlets at δ 41.8 and 37.5 respectively.

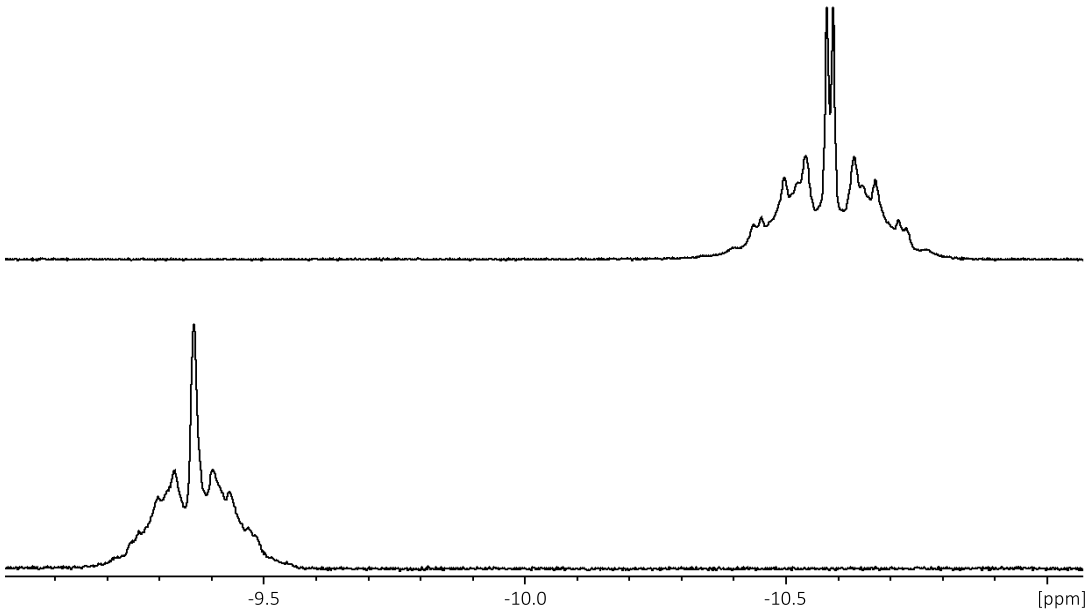

Figure 5.10: Sections of ^{1}H NMR (25°C) spectra showing Ru-H resonances of [Ru(PPh$_3$)$_3$(SiEt$_3$)H$_3$] (**38**, top, THF-d_8, 400 MHz) and [Ru(PPh$_3$)$_3$(SiPh$_3$)H$_3$] (**39**, bottom, C_6D_6, 500 MHz).

Attempts to form Ru(PPh$_3$)$_3$(SiR$_3$)H complexes upon Si-Si cleavage of Si_2Me_6 or Si_2Ph_6 with **37** resulted in no reaction being observed.

5.4.1.2. Reactivity of [Ru(PPh$_3$)$_3$HF] (37) with CF$_3$SiMe$_3$

Trifluoromethyltrimethylsilane (CF_3SiMe_3 or Ruppert-Prakash reagent) is a convenient CF_3 transfer reagent, which in one noteable case has been successfully employed by Caulton and co-workers for the preparation of the difluorocarbene complexes, [Ru(PR$_3$)$_2$(CO)(CF$_2$)HF] (PR$_3$ = P^{i}Pr$_3$, P^{t}Bu$_2$Me) following α-F migration from transient [Ru(PR$_3$)$_2$(CO)(CF$_3$)H] species.[25] Prompted by these results, **37** was reacted with CF_3SiMe_3 (1 equiv) in C_6D_6. The reaction proved to be slow and ultimately resulted in sample decomposition as indicated by the appearance of free PPh_3 and a number of unidentified broad signals of low intensity in the ^{31}P NMR spectrum overnight. A small, but characteristic, ^{19}F doublet resonance arising from CF_3H was

observed at δ -77.6 ($^2J_{FH}$ = 78.4 Hz),[26] suggesting that the F/CF_3 exchange did indeed occur to form [Ru(PPh_3)$_3$(CF_3)H], which we assume is unstable to reductive elimination of fluoroform and "Ru(PPh_3)$_3$". There was no evidence in the $^{31}P\{^1H\}$ NMR spectrum for the presence of a cyclometallated species[27–29] such as [Ru(PPh_3)$_2$($Ph_2PC_6H_4$)H], which might be expected to form from the transient Ru(0) species. This suggested that "Ru(PPh_3)$_3$" simply decomposed.

The use of excess CF_3SiMe_3 (> 2 equiv) accelerated the reaction as all the starting material was consumed after ca. ½ h at room temperature. Changing the solvent from C_6D_6 to either toluene-d_8 or THF-d_8 had no noticeable effect on the outcome of the reaction. Monitoring spectroscopically a THF-d_8 reaction of **37** and CF_3SiMe_3 inserted into the NMR spectrometer at -30°C failed to reveal the formation of any intermediate species.

5.4.2. Reactivity of [Ru(PPh_3)$_3$HF] (37) with boranes

5.4.2.1. Reactivity of [Ru(PPh_3)$_3$HF] (37) with B_2Pin_2

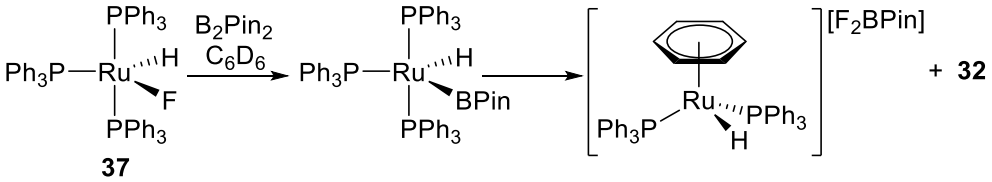

Scheme 5.5: Reaction of [Ru(PPh_3)$_3$HF] (**37**) with B_2Pin_2.

A ^1H NMR spectrum of **37** and equivalent amount of B_2Pin_2 in C_6D_6 (Scheme 5.5) measured after 1 h at room temperature showed the formation of three new Ru-H containing species (Figure 5.11A) with signals at δ -5.49 (dt, $^2J_{HP}$ = 59.7 Hz, $^2J_{HP}$ = 31.9 Hz), δ -9.28 (t, $^2J_{HP}$ = 36.9 Hz) and δ -10.14 (m) that integrated in a 0.5:1.2:0.7 ratio with respect to **37** (integral of 1). These were assigned tentatively as

$[Ru(PPh_3)_3(BPin)H]$, $[Ru(PPh_3)_2(\eta^6\text{-}C_6H_6)H]^+$ and $[Ru(PPh_3)_4H_2]$ (**32**) respectively.[30,iii] In the $^{31}P\{^1H\}$ NMR spectrum, $[Ru(PPh_3)_3(BPin)H]$ gave rise to doublet (δ 55.3, $^2J_{PP}$ = 15.3 Hz) and triplet (δ 43.6, $^2J_{PP}$ = 15.3 Hz) signals, while $[Ru(PPh_3)_2(\eta^6\text{-}C_6H_6)H]^+$ appeared as a sharp singlet at δ 51.8 (Figure 5.11B). After further 2 h at room temperature, the hydride signal for $[Ru(PPh_3)_3(BPin)H]$ disappeared, while the triplet signal for the cation shifted downfield to δ -9.21 ($^2J_{HP}$ = 36.9 Hz). A small change in the chemical shift of the corresponding $^{31}P\{^1H\}$ NMR resonance (to δ 51.9) was also observed. This could be due to the substitution of a benzene substituent by a deuterated solvent molecule and formation of $[Ru(PPh_3)_2(\eta^6\text{-}C_6D_6)H]^+$. The anion was identified by ^{11}B NMR spectroscopy as $[F_2BPin]$ which exhibited a broad triplet at δ 6.7 ($^2J_{BF} \approx 25$ Hz), as well as a ^{19}F signal at δ -141.3.[31]

[iii] $[Ru(PPh_3)_3HF]$ crystallises with one guest molecule of C_6H_6 in the lattice.

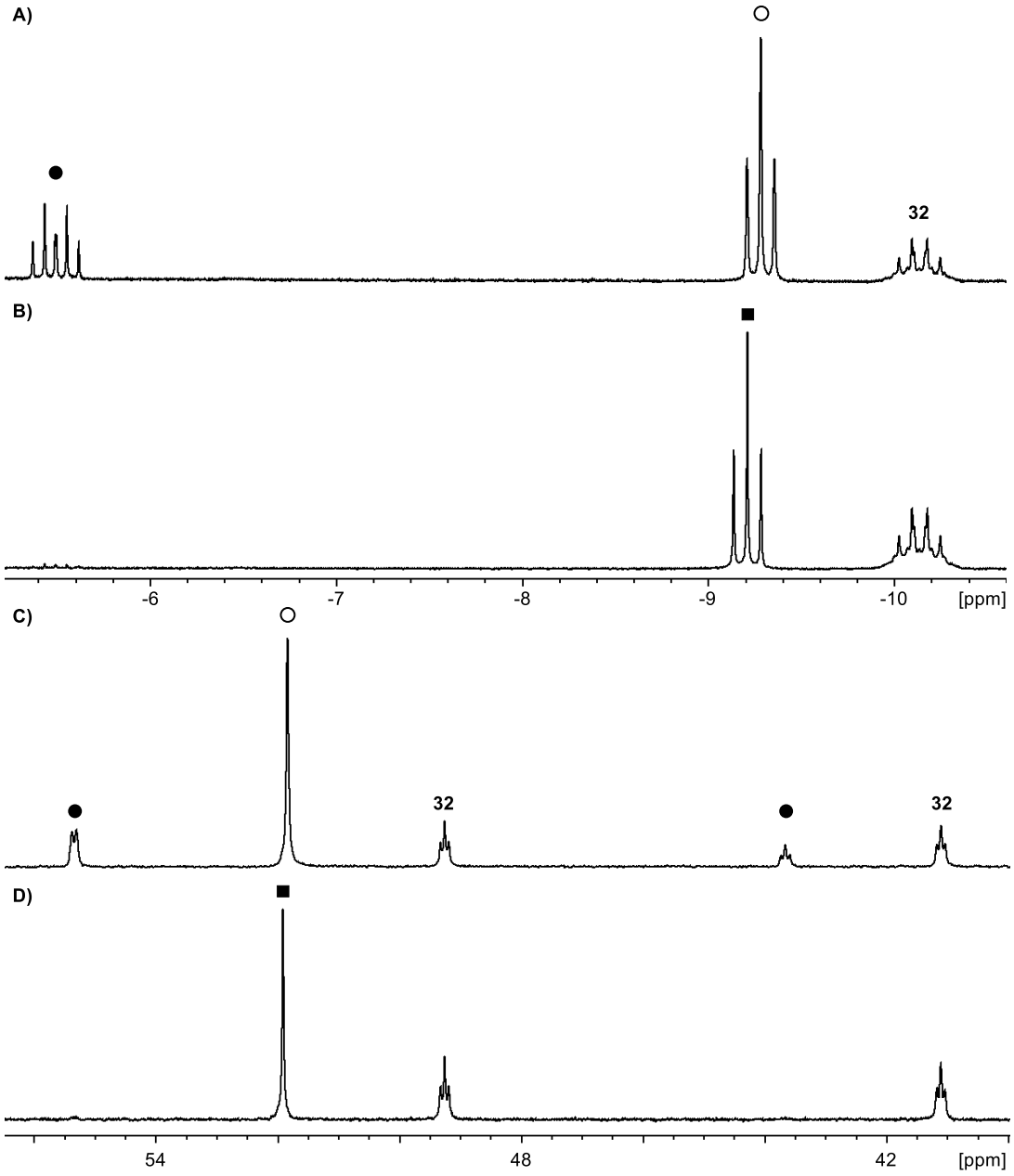

Figure 5.11: Sections of the ^{1}H (500 MHz) and $^{31}P\{^{1}H\}$ (202 MHz) NMR spectra (recorded at 25°C) of the reaction between $[Ru(PPh_3)_3HF]$ (**37**) and B_2Pin_2 (1 equiv) in C_6D_6 after 1h (A and C) and 3 h (B and D) at room temperature. ●, ○ and ■ denote $[Ru(PPh_3)_3(BPin)H]$, $[Ru(PPh_3)_2(\eta^6\text{-}C_6H_6)H][F_2BPin]$ and $[Ru(PPh_3)_2(\eta^6\text{-}C_6D_6)H][F_2BPin]$ respectively.

5.4.2.2. Reactivity of [Ru(PPh$_3$)$_3$HF] (37) with HBPin

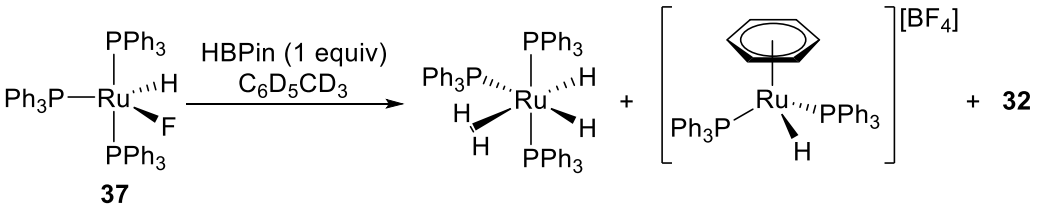

Scheme 5.6: Reaction of [Ru(PPh$_3$)$_3$HF] (**37**) with HBPin (1 equiv).

^{1}H and ^{31}P{^{1}H} NMR spectroscopy showed that treatment of a toluene-d_8 solution of **37** with HBPin (1 equiv) led to the formation of [Ru(PPh$_3$)$_3$(η^2-H$_2$)H$_2$] (^{1}H NMR: δ -7.12; ^{31}P{^{1}H} NMR: δ 57.8),[32] [Ru(PPh$_3$)$_2$(η^6-C$_6$D$_5$CD$_3$)H]$^+$ (^{1}H NMR: δ -9.47, $^2J_{HP}$ = 37.1 Hz; ^{31}P{^{1}H} NMR: 52.4)[30] and [Ru(PPh$_3$)$_4$H$_2$] (**32**) (*vide infra*) in a 1:0.2:0.7 ratio after 45 min at room temperature (Scheme 5.6). The ^{11}B NMR spectrum consisted of two broad and overlapping signals at δ 21.7 and δ 20.8, and a sharp singlet at δ 0.6. The latter two resonances were assigned to FBPin and [BF$_4$]$^-$ respectively, which were also observed by ^{19}F NMR spectroscopy at δ -149.8 and -149.9 ([^{11}BF$_4$]$^-$ and [^{10}BF$_4$]$^-$), and -150.7 (br s, FBPin). After ca. 40 h at room temperature, the signals corresponding to [Ru(PPh$_3$)$_2$(η^6-C$_6$D$_5$CD$_3$)H][BF$_4$] diminished, while the relative ratio of [Ru(PPh$_3$)$_3$(η^2-H$_2$)H$_2$] and **32** was approximately 1:0.7 (Figure 5.12).

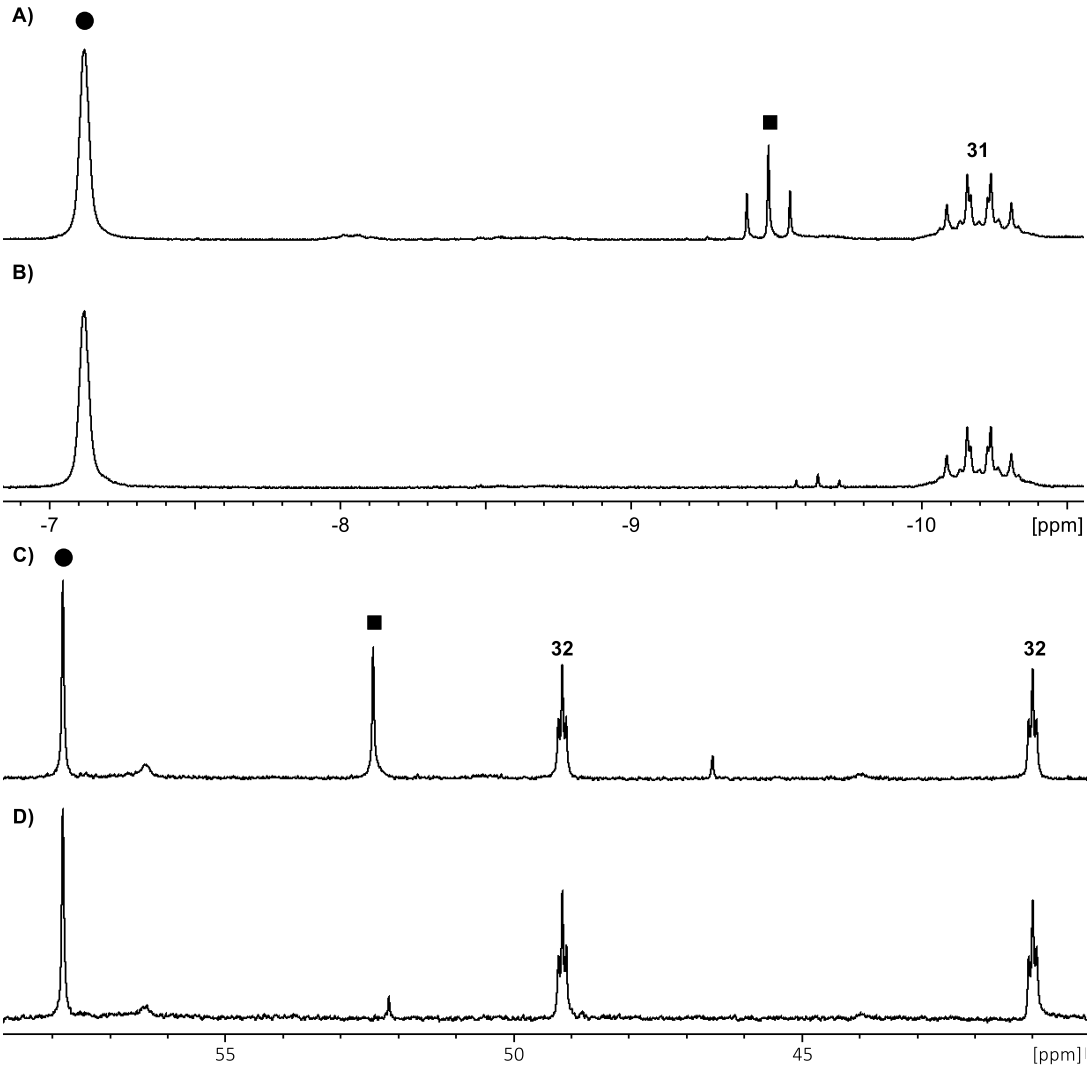

Figure 5.12: Sections of ^{1}H (500 MHz) and $^{31}P\{^{1}H\}$ (202 MHz) NMR spectra (recorded at 25°C) of the reaction between $[Ru(PPh_3)_3HF]$ (**37**) and HBPin (1 equiv) in toluene-d_8 after 45 min (A and C) and 40 h (B and D) at room temperature. ● and ■ denote $[Ru(PPh_3)_3(\eta^2\text{-}H_2)H_2]$ and $[Ru(PPh_3)_2(\eta^6\text{-}C_6D_5CD_3)H]^+$ respectively.

Interestingly, the formation of different species was observed when the reaction was repeated in the presence of excess HBpin (5 equiv) in toluene-d_8. Thus, the room temperature ^{1}H NMR spectrum recorded after 30 min at 25°C revealed four broad Ru-H resonances at δ -6.02, - 8.05, -9.64 and -10.52 in an approximate ratio of 1:1:1:1 (Figure 5.13). The three lowest frequency signals sharpened upon cooling the solution to -15°C; the signal now at δ -8.04 appeared as a triplet of doublets (J = 27.2 Hz, J =

16.3 Hz), that at δ -9.49 was a doublet of multiplets (doublet splitting ≈ 37 Hz) and that at δ -10.46 resolved into a doublet of triplets (J = 59.7 Hz, J = 17.5 Hz) respectively. Exchange spectroscopy (Figure 5.14) at -15°C showed that these were in exchange, while the T_1 values measured at this temperature suggested the presence of three hydride ligands (163 ms (δ -5.93), 291 ms (δ - 8.04),191 ms (δ -10.46)). All three resonances collapsed into singlets upon ^{31}P broad band decoupling. The room temperature $^{31}P\{^1H\}$ NMR spectrum consisted of two broad signals at δ 52.2 and δ 50.4, and a sharp singlet at δ 46.5. At -15°C, the broad resonances resolved into a doublet and a triplet respectively, with an identical coupling constant of 25 Hz. ^1H-^{31}P HMQC spectroscopy at this temperature showed that these coupled to the hydride resonances at δ -5.93, -8.04 and -10.46, suggesting that one of the species formed was the HBPin adduct, $[Ru(PPh_3)_3(HBPin)H_2]$ (**40**), while the lone peak at δ 46.5 correlated to the Ru-H signal at δ -9.49 (T_1 at -15°C = 195 ms). This was tentatively assigned as the Ru(IV) boryl trihydride complex $[Ru(PPh_3)_3(BPin)H_3]$, on the basis of the similarity of its NMR spectra to that of analogous Ru (IV) silyl complexes **38** and **39**. However, further studies are necessary to establish its identity categorically.

Upon removal of all the volatiles and redissolution of the residue in toluene-d_8, the signal corresponding to $[Ru(PPh_3)(\eta^2\text{-}H_2)H_2]$ (*vide supra*) appeared. Over a period of 3 weeks, there was complete conversion to just this species.

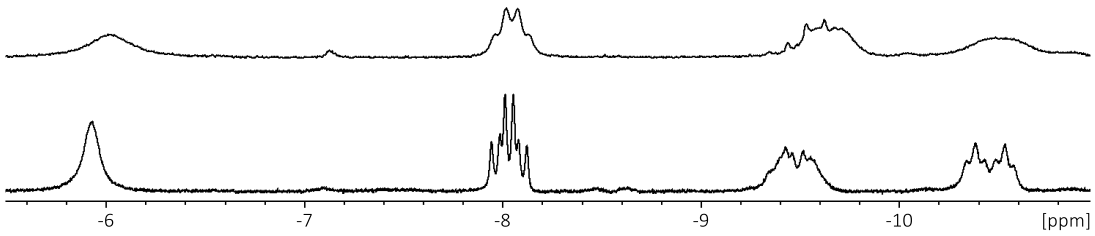

Figure 5.13: Low frequency region of the ^{1}H NMR spectra (400 MHz, $C_6D_5CD_3$) of the reaction between $[Ru(PPh_3)_3HF]$ (**37**) and HBPin (5 equiv) after 30 min at 25°C (top) and -15°C (bottom).

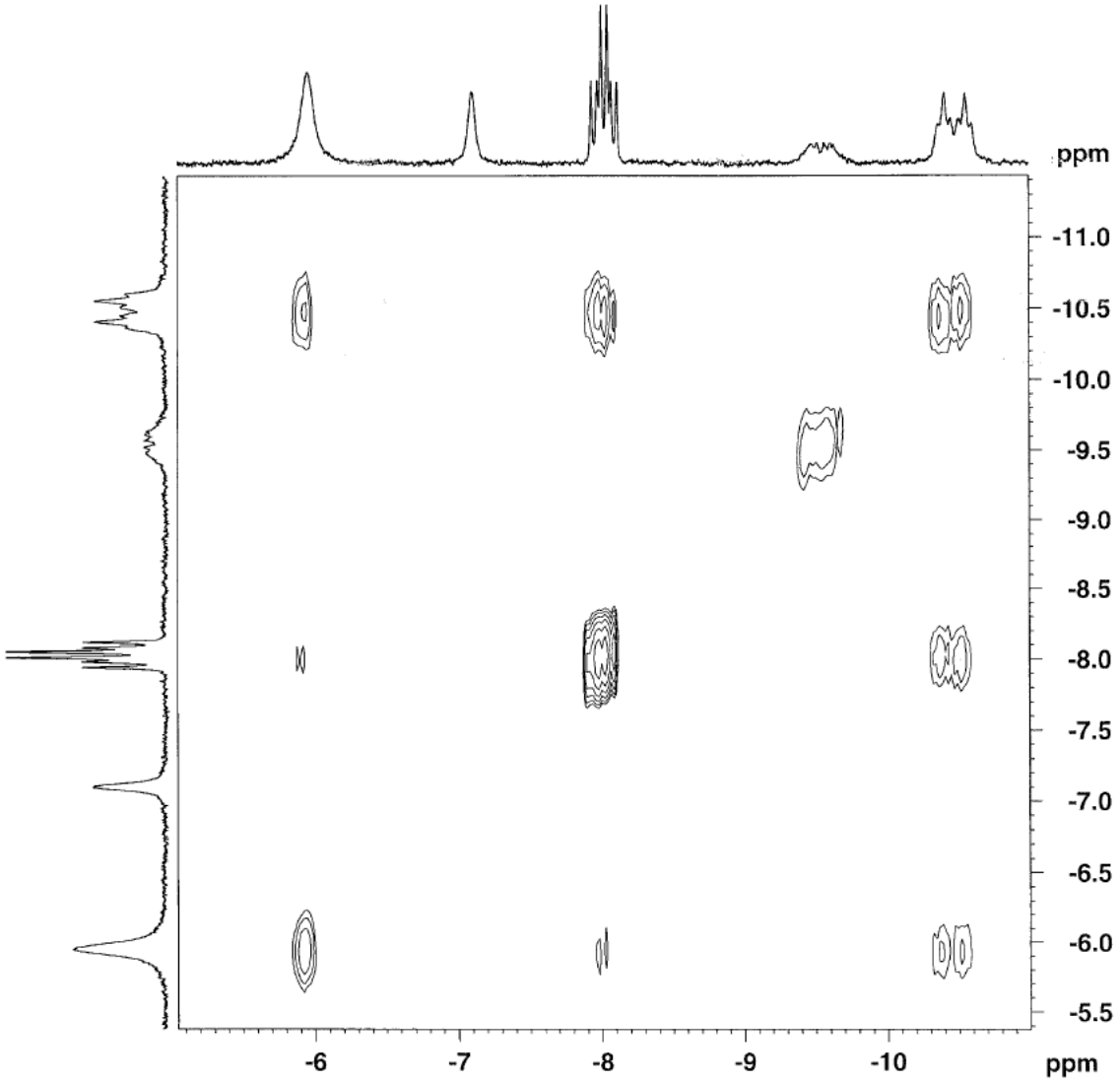

Figure 5.14: EXSY spectrum showing intramolecular H/H exchange in $[Ru(PPh_3)_3(HBPin)H_2]$ (**40**).

Single crystals of **40** suitable for X-ray diffraction were obtained upon layering a C_6H_6 solution of **37** with pentane in the presence of excess (10 equiv) HBpin. The solid state structure (*vide infra*) confirmed the formulation of **40** as a σ-borane dihydride $[Ru(PPh_3)_3(HBPin)H_2]$, rather than hydride dihydroborate ($[Ru(PPh_3)_3[(\mu\text{-}H)_2BPin]H]$) or trihydride boryl ($[Ru(PPh_3)_3(BPin)H_3]$) complexes. **40** represents a trisphosphine analogue of the bisphosphine dihydrogen complex, $[Ru(PCy_3)_2(\eta^2\text{-}H_2)(\eta^2\text{-}HBPin)H_2]$, reported by Sabo-Etienne following treatment of $[Ru(PCy_3)_2(\eta^2\text{-}H_2)_2H_2]$ with HBPin (1 equiv) in THF.[33]

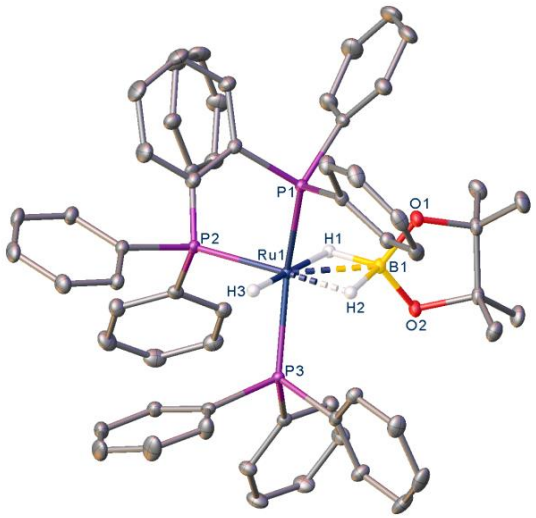

Figure 5.15: Molecular structure of $[Ru(PPh_3)_3(HBPin)H_2]$ (**40**). Thermal ellipsoids are represented at 30 % probability. Hydrogen atoms, with the exception of hydride ligands and that of the coordinated borane have been omitted for clarity. Selected bond lengths (Å) and angles (°): Ru1-B1 2.1747(16), Ru1-P1 2.3337(4), Ru1-P2 2.3885(4), Ru1-P3 2.3398(4); P1-Ru-B1 88.62(5), P2-Ru1-B1 131.21(4), P3-Ru-B1 96.63(5), P1-Ru1-P2 99.278(13), P1-Ru1-P3 152.859(13), P2-Ru1-P3 97.146(13).

The molecular structure of **40** (Figure 5.15) featured a distorted octahedral geometry at the ruthenium centre with two phosphines in axial positions. The four

coordination sites in the equatorial plane were occupied by two hydride ligands (H1and H3), one σ B1-H2 bond and a ligated PPh_3. The B1-H2bond distance (1.36(2) Å)[iv] represented a normal elongation for a σ-borane complex by comparison to the calculated B-H bond distance of 1.17 Å in a free dialkoxyborane.[34] A weak Lewis acid/base interaction between the hydride H1 and the boron atom was reflected by the long distance of 1.57(2) Å and supported σ-borane coordination. Further evidence came from the relative orientation of the BPin group with respect to the metal centre. The angle of 170.05(16)°, measured between the middle of [O, O], B and Ru, showed that the BPin group is not pointing toward the ruthenium atom, as it would be anticipated for a dihydridoborate or dihydride boryl species.[33] The Ru1-B1 bond length of 2.1747(16) Å was very similar to that found in $[Ru(PCy_3)_2(\eta^2\text{-}H_2)(\eta^2\text{-}HBPin)H_2]$ (2.173(2) Å). Relevant metrics for both complexes are listed in Table 5.2.

[iv] The Ru-H ligands in **40** were all located and refined without restraints which, keeping in mind the uncertainties in hydride positions, allowed for approximate analysis of bond distances and angles involving H atoms present in the coordination sphere of the ruthenium centre.

Table 5.2: Selected bond lengths (Å) and angles (°) for $[Ru(PPh_3)_3(HBPin)H_2]$ (**40**) and $[Ru(PCy_3)_2(\eta^2\text{-}H_2)(\eta^2\text{-}HBPin)\ H_2]$.[33]

	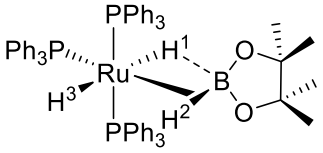	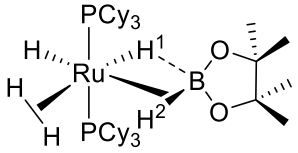
Ru-B	2.1747(16)	2.173(2)
$Ru\text{-}H^1$	1.61(2)	1.57(2)
$Ru\text{-}H^2$	1.73(2)	1.67(2)
$B\text{-}H^2$	1.36(2)	1.30(2)
$B\cdots H^1$	1.57(2)	1.89(2)
B-O	1.401(2), 1.407(2)	1.406(2)
P-Ru-P (axial)	152.859(13)	157.66(1)
Cent[O, O]-B-Ru	170.05(16)	170.0
$H^1\text{-}Ru\text{-}H^2$	84.5(10)	94.7(10)
$Ru\text{-}H^2\text{-}B$	88.7(11)	93.28(6)
$Ru\text{-}B\text{-}H^2$	52.7(9)	50.1(8)
$Ru\text{-}H^1\text{-}B$	86.4(10)	77.2(6)
O-B-O	109.05(12)	109.2(1)

5.5. Discussion

Both $PF_2(C_6F_5)$ and C_6F_5 ligands in **36** could have only been formed as a result of multiple bond cleavage and formation steps and most likely involved inter- or intramolecular nucleophilic Ru-H attack on P followed by sequence of bond breaking and bond forming processes. Transformations involving P-C/F exchange are known and perhaps the best characterised example of such is the F/Ph rearrangement of the fluoro analogue of Wilkinson's catalyst, $[Rh(PPh_3)_3F]$, reported by Grushin and Marshall.[35] The fluorophosphine complex *cis*-$[Rh(PPh_3)_2(PFPh_2)Ph]$ was found to be an

intermediate in the C-Cl bond activation reaction of chlorobenzene yielding *trans*-[Rh(PPh$_3$)$_2$(PFPh$_2$)Cl] (Scheme 5.7A). Kinetic studies showed that the Rh-phenyl complex is formed *via* the facile and reversible intramolecular P-Ph/F exchange process, which was not influenced by added phosphine.[36] Initial DFT calculations on a *cis*-[Rh(PH$_3$)$_2$(PH$_2$Ph)F] model system pointed to two possible mechanisms (Scheme 5.7B): Ph transfer from P to Rh followed by P-F formation (formally an oxidative addition to give a Rh(III)-phosphide species, followed by reductive elimination (Pathway 1); and intramolecular nucleophilic attack of Rh-F to produce a metallophosphorane intermediate from which Ph migration to Rh occurs (Pathway 2). Further theoretical studies on the full [Rh(PPh$_3$)$_3$F] system revealed a clear preference for the latter.[37]

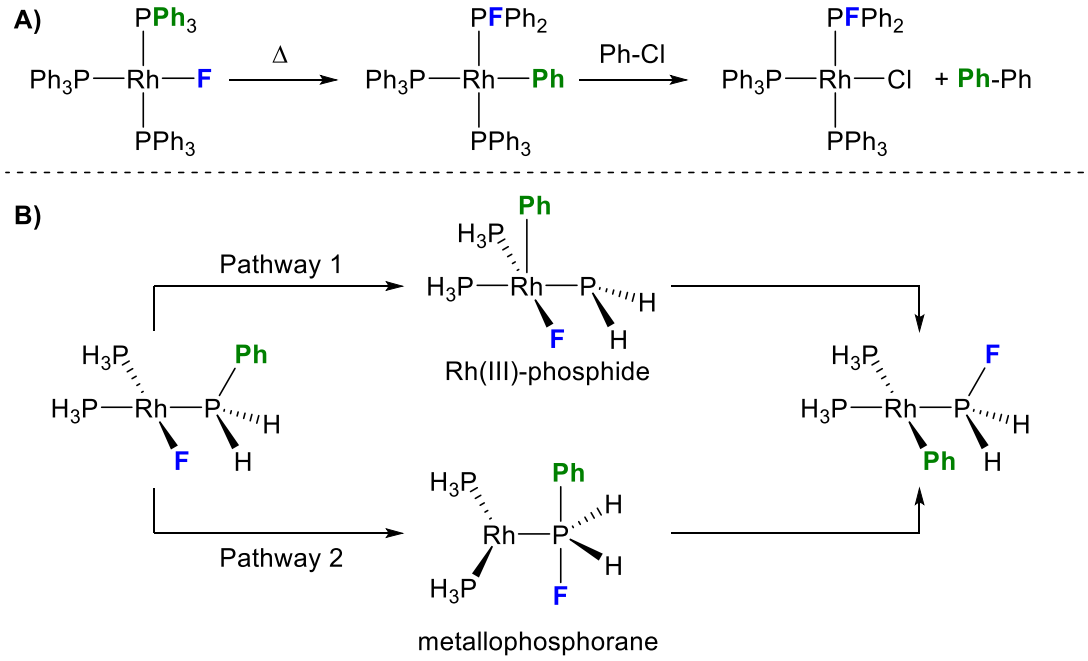

Scheme 5.7: Ph-Cl activation at [Rh(PPh$_3$)$_3$F] (A) and computed mechanism of F/Ph exchange in *cis*-[Rh(PPh$_3$)$_2$(PFPh$_2$)Ph] (B).

Another example of P-C/F exchange was described by Milstein and co-workers,[38] who showed that heating [Ir(PEt$_3$)$_3$Me] in hexafluorobenzene led to the formation of *trans*-[Ir(PEt$_3$)$_2$(PEt$_2$F)(C$_6$F$_5$)], C$_2$H$_4$ and CH$_4$ *via* C-F and P-C bond

cleavage and P-F bond formation (Scheme 5.8A). The reaction was later investigated through DFT calculations using the small PH_3 model complex, *trans*-$[Ir(PH_3)_2(PH_2Et)(Me)]$, to reveal a novel, low-energy phosphine-assisted C-F activation mechanism (Scheme 5.8B).[39] This involved nucleophilic attack of the electron-rich Ir metal centre at C_6F_6 and trapping of the displaced fluoride by a phosphine ligand to generate a metallophosphorane intermediate, $[Ir(PH_3)_2(PH_2EtF)(C_6F_5)(Me)]$. Facile transfer of the ethyl group from P to Ir and subsequent *β*-H elimination of C_2H_4 and reductive elimination of methane accounted for the final products. It was found that the reaction proceeded in a concerted fashion *via* a 4-centered transition state and that the presence of *ortho*-F substituents promoted C-F cleavage. Analogous P-C/F chemistry was also observed during C-F bond activation reactions of fluoropyridines[40,41] and hexafluorobenzene[36] by zerovalent $[Pt(PR_3)_2]$ (R = ^{i}Pr, Cy) complexes.

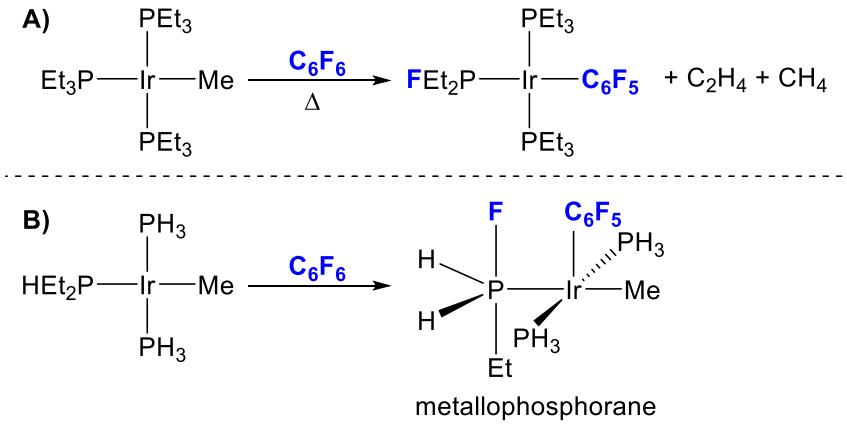

Scheme 5.8: P-C/F exchange observed in the reaction between $[Ir(PEt_3)_3(Me)]$ and C_6F_6 (A), and phosphine-assisted C-F activation generating metallophosphorane intermediate (B).

Complexes containing a difluoropentafluorophenyl ligand, $P(C_6F_5)F_2$ are not known. Although fluorophosphines containing aryl or alkyl groups, such as $P(C_6H_5)_2F$[42] or $P(CH_3)_2F$[43] disproportionate at room temperature in accord with the overall equation

shown in Scheme 5.9,[42–48] their perfluorinated counterparts $P(C_6F_5)_2F$[49] and $P(CF_3)_2F$ are stable.[v] Similarly, $P(C_6H_5)F_2$[48] and $P(CH_3)F_2$[46] undergo redox disproportionation, while their analogues containing electron-withdrawing C_6F_5- or CF_3- groups are readily distillable. Interestingly, despite reduced stability of difluorophenylphosphine, crystallographically characterised transition metal complexes bearing $P(C_6H_5)F_2$ ligands exist.[50–52] The absence of species containing ligated $P(C_6F_5)F_2$ suggests that such i) cannot be made easily or ii) if formed, they are not particularly stable and thus isolable.

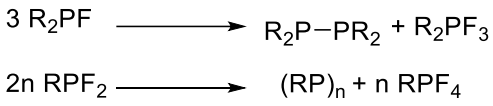

Scheme 5.9: Disproportionation reactions of organofluorophosphines.

5.6. Summary

The reactivity of ruthenium dihydride complexes $[Ru(IMe_4)_2(PPh_3)_2H_2]$ (**ttt-9**) and $[Ru(PPh_3)_4H_2]$ (**32**) towards tris(pentafluorophenyl)phosphine (PCF) has been described. The reaction of **ttt-9** with PCF afforded $[Ru(IMe_4)_2(PF_2(C_6F_5))(C_6F_5)H]$ (**36**), which was fully characterised by NMR spectroscopy. To the best of our knowledge, this is the first example of a transition metal complex containing a $PF_2(C_6F_5)$ ligand. In contrast, employment of a less reactive tetrakisphosphine precursor **32** gave the isolable hydride fluoride complex $[Ru(PPh_3)_3HF]$ (**37**). This formed upon sequential HDF of the *ortho*-C-F bonds in PCF. **37** was shown to react cleanly with tertiary silanes to give the trihydride silyl complexes $[Ru(PPh_3)_3(SiR_3)H_3]$ (R = Et (**38**), Ph (**39**)), whereas reaction with excess HBPin led to the isolation of the σ-borane dihydride complex $[Ru(PPh_3)_3(HBPin)H_2]$ (**40**).

[v] Both $P(C_6F_5)_2F$ and $P(CF_3)_2F$ disproportionate upon heating.

5.7. References for Chapter 5

(1) Davies, C. J. E. PhD Thesis, 2014.

(2) Müller, A.; Niecke, E.; Glemser, O. *Z. Für Anorg. Allg. Chem.* **1967**, *350*, 256.

(3) Kemmitt, R. D. W.; Nichols, D. I.; Peacock, R. D. *J. Chem. Soc. Inorg. Phys. Theor.* **1968**, 1898.

(4) Barlow, M. G.; Green, M.; Haszeldine, R. N.; Higson, H. G. *J. Chem. Soc. B Phys. Org.* **1966**, 1025.

(5) Miloserdov, F. M.; McKay, D.; Muñoz, B. K.; Samouei, H.; Macgregor, S. A.; Grushin, V. V. *Angew. Chem. Int. Ed.* **2015**, *54*, 8466.

(6) Reade, S. P.; Nama, D.; Mahon, M. F.; Pregosin, P. S.; Whittlesey, M. K. *Organometallics* **2007**, *26*, 3484.

(7) Brewer, S. A.; Coleman, K. S.; Fawcett, J.; Holloway, J. H.; Hope, E. G.; Russell, D. R.; Watson, P. G. *J. Chem. Soc. Dalton Trans.* **1995**, *7*, 1073.

(8) Clarke, M. L.; Ellis, D.; Mason, K. L.; Orpen, A. G.; Pringle, P. G.; Wingad, R. L.; Zaher, D. A.; Baker, R. T. *Dalton Trans.* **2005**, *7*, 1294.

(9) Pollock, C. L.; Saunders, G. C.; Sarah Smyth, E. C. M.; Sorokin, V. I. *J. Fluorine Chem.* **2008**, *129*, 142.

(10) McConway, J. C.; Skapski, A. C.; Phillips, L.; Young, R. J.; Wilkinson, G. *J. Chem. Soc., Chem. Commun.* **1974**, *9*, 327.

(11) Kono, H.; Wakao, N.; Ito, K.; Nagai, Y. *J. Organomet. Chem.* **1977**, *132*, 53.

(12) Haszeldine, R. N.; Malkin, L. S.; Parish, R. V. *J. Organomet. Chem.* **1979**, *182*, 323.

(13) Knorr, M.; Gilbert, S.; Schubert, U. *J. Organomet. Chem.* **1988**, *347*, C17.

(14) Gilbert, S.; Knorr, M.; Mock, S.; Schubert, U. *J. Organomet. Chem.* **1994**, *480*, 241.

(15) Schubert, U.; Gilbert, S.; Mock, S. *Chem. Ber.* **1992**, *125*, 835.

(16) Hübler, K.; Hübler, U.; Roper, W. R.; Schwerdtfeger, P.; James Wright, L. *Chem. – Eur. J.* **1997**, *3*, 1608.

(17) Möhlen, M.; Rickard, C. E. F.; Roper, W. R.; Salter, D. M.; Wright, L. J. *J. Organomet. Chem.* **2000**, *593–594*, 458.

(18) Rickard, C. E.; Roper, W. R.; Woodgate, S. D.; Wright, L. J. *J. Organomet. Chem.* **2000**, *609*, 177.

(19) Feldman, J. D.; Peters, J. C.; Tilley, T. D. *Organometallics* **2002**, *21*, 4065.

(20) Lemke, F. R.; Brammer, L. *Organometallics* **1995**, *14*, 3980.

(21) Brammer, L.; Klooster, W. T.; Lemke, F. R. *Organometallics* **1996**, *15*, 1721.

(22) Lachaize, S.; Sabo-Etienne, S. *Eur. J. Inorg. Chem.* **2006**, *2006*, 2115.

(23) Heinekey, D. M.; Oldham, W. J. *Chem. Rev.* **1993**, *93*, 913.

(24) Dioumaev, V. K.; Procopio, L. J.; Carroll, P. J.; Berry, D. H. *J. Am. Chem. Soc.* **2003**, *125*, 8043.

(25) Huang, D.; Koren, P. R.; Folting, K.; Davidson, E. R.; Caulton, K. G. *J. Am. Chem. Soc.* **2000**, *122*, 8916.

(26) Sartori, P.; Habel, W. *J. Fluorine Chem.* **1980**, *16*, 265.

(27) Pez, G. P.; Grey, R. A.; Corsi, J. *J. Am. Chem. Soc.* **1981**, *103*, 7528.

(28) Wilczynski, R.; Fordyce, W. A.; Halpern, J. *J. Am. Chem. Soc.* **1983**, *105*, 2066.

(29) Fordyce, W. A.; Wilczynski, R.; Halpern, J. *J. Organomet. Chem.* **1985**, *296*, 115.

(30) Siedle, A. R.; Newmark, R. A.; Pignolet, L. H.; Wang, D. X.; Albright, T. A. *Organometallics* **1986**, *5*, 38.

(31) Pietsch, S.; Neeve, E. C.; Apperley, D. C.; Bertermann, R.; Mo, F.; Qiu, D.; Cheung, M. S.; Dang, L.; Wang, J.; Radius, U.; Lin, Z.; Kleeberg, C.; Marder, T. B. *Chem. – Eur. J.* **2015**, *21*, 7082.

(32) Samouei, H.; Miloserdov, F. M.; Escudero-Adán, E. C.; Grushin, V. V. *Organometallics* **2014**, *33*, 7279.

(33) Lachaize, S.; Essalah, K.; Montiel-Palma, V.; Vendier, L.; Chaudret, B.; Barthelat, J.-C.; Sabo-Etienne, S. *Organometallics* **2005**, *24*, 2935.

(34) Rablen, P. R.; Hartwig, J. F. *J. Am. Chem. Soc.* **1996**, *118*, 4648.

(35) Marshall, W. J.; Grushin, V. V. *Organometallics* **2004**, *23*, 3343.

(36) Macgregor, S. A.; Roe, D. C.; Marshall, W. J.; Bloch, K. M.; Bakhmutov, V. I.; Grushin, V. V. *J. Am. Chem. Soc.* **2005**, *127*, 15304.

(37) Macgregor, S. A.; Wondimagegn, T. *Organometallics* **2007**, *26*, 1143.

(38) Blum, O.; Frolow, F.; Milstein, D. *J. Chem. Soc. Chem. Commun.* **1991**, *4*, 258.

(39) Erhardt, S.; Macgregor, S. A. *J. Am. Chem. Soc.* **2008**, *130*, 15490.

(40) Jasim, N. A.; Perutz, R. N.; Whitwood, A. C.; Braun, T.; Izundu, J.; Neumann, B.; Rothfeld, S.; Stammler, H.-G. *Organometallics* **2004**, *23*, 6140.

(41) Nova, A.; Erhardt, S.; Jasim, N. A.; Perutz, R. N.; Macgregor, S. A.; McGrady, J. E.; Whitwood, A. C. *J. Am. Chem. Soc.* **2008**, *130*, 15499.

(42) Brown, C.; Murray, M.; Schmutzler, R. *J. Chem. Soc. C Org.* **1970**, *7*, 878.

(43) Seel, F.; Rudolph, K.; Gombler, W. *Angew. Chem. Int. Ed. Engl.* **1967**, *6*, 708.

(44) Seel, F.; Rudolph, K. *Z. Für Anorg. Allg. Chem.* **1968**, *363*, 233.

(45) Pabel, M.; Willis, A. C.; Wild, S. B. *Inorg. Chem.* **1996**, *35*, 1244.

(46) Ang, H. G.; Schmutzler, R. *J. Chem. Soc. Inorg. Phys. Theor.* **1969**, 702.

(47) Riesel, L.; Haenel, J.; Ohms, G. *J. Fluorine Chem.* **1988**, *38*, 335.

(48) Schmutzler, R.; Heuer, L.; Schomburg, D. *Phosphorus Sulfur Silicon Relat. Elem.* **1993**, *83*, 149.

(49) Fild, M.; Schmutzler, R. *J. Chem. Soc. Inorg. Phys. Theor.* **1969**, 840.

(50) Crump, W.; Kruck, T.; Siegers, B.; Tebbe, K.-F. *Acta Crystallogr. C* **1994**, *50*, 1074.

(51) Stelzer, O.; Sheldrick, W. S.; Subramanian, J. *J. Chem. Soc. Dalton Trans.* **1977**, *10*, 966.

(52) Sheldrick, W. S.; Stelzer, O. *Chem. Ber.* **1977**, *110*, 3421.

CHAPTER SIX

Experimental procedures and characterising data

6.1. General procedures

All manipulations were carried out under argon using standard Schlenk, high vacuum and glovebox techniques using dried and degassed solvents, unless otherwise stated. Glassware (ampoules and NMR tubes fitted with a J. Young's resealable PTFE valve, and Schlenk flasks) were oven dried at 140°C overnight and subsequently flame dried under vacuum prior to use. Hexane, toluene, diethyl ether, pentane and dichloromethane were purified using an MBraun solvent purification system. Benzene was distilled from Na dispersion, while THF was kept in contact with KOH or over molecular sieves prior to distillation from Na/benzophenone. Fluorobenzene was distilled from calcium hydride. 1-Hexanol was used as purchased (Fisher). Methanol was refluxed over Mg/I_2 and collected by distillation. Solvents were stored over activated 4 Å molecular sieves (diethyl ether, THF, 2-MeTHF, dichloromethane, methanol, pentane) or over a potassium mirror (benzene, toluene, hexane). Deuterated solvents (Sigma-Aldrich and Euriso-top) were vacuum transferred from potassium (benzene-d_6, toluene-d_8, THF-d_8) or calcium hydride (dichloromethane-d_2, chloroform-d_1). Acetonitrile-d_3 was dried over activated 4 Å molecular sieves. All liquid fluoroaromatic (Fluorochem; C_6F_6, C_6F_5H, $C_6F_4H_2$, $C_6F_3H_3$, $C_6F_2H_4$, C_6FH_5) and silane (Sigma-Aldrich; Et_3SiH, $^iPr_3SiH$, Ph_2MeSiH, $PhMe_2SiH$, Ph_2SiH_2, Et_2SiH_2) reagents were dried over activated 4 Å molecular sieves. $RuCl_3 \cdot xH_2O$ (Johnson Matthey and Precious Metals) was used as received, while PPh_3 (Sigma-Aldrich) was recrystallized twice from hot ethanol. Other phosphines (dppm, dppe, dppp, xantphos, DPEphos, DCEphos, $PPh_2(2\text{-}C_6H_4OCH_3)$, $P(C_6F_5)_3$) were used as received.

6.2. Physical and analytical techniques:

NMR spectra were recorded on Bruker Avance 400/ 500 and Avance III 500 MHz NMR spectrometers at 25°C, unless otherwise stated, and referenced to the residual protio and ^{13}C solvent signals: C_6D_6 (^1H, δ 7.16; ^{13}C, δ 128.0), THF-d_8 (^1H, δ 3.58; ^{13}C, δ 25.4), $C_6D_5CD_3$ (^1H, δ 2.09; ^{13}C, δ 20.4), $CDCl_3$ (^1H, δ 7.26; ^{13}C, δ 77.1), CD_2Cl_2 (^1H, δ 5.32; ^{13}C, δ 53.8), CD_3CN (^1H, δ 1.94; ^{13}C, δ 118.2). ^{31}P {^1H} and ^{19}F NMR spectra were referenced externally to 85 % H_3PO_4 (δ 0.0) and $CFCl_3$ (δ 0.0).

X-ray crystal structures were recorded on a Nonius KappaCCD or Agilent SuperNova and Agilent Excalibur diffractometers, with structural solutions and refinements performed using SHELXS-97 and SHELXL-97 respectively.[1] Hydride ligands, where present, were located and refined at a distance of 1.6 Å from the relevant metal centre. Mass spectra were measured on a Bruker UHR-ESI-QTOF MaXis HD by Dr Anneke Lubben at the University of Bath. IR spectra were recorded as KBr discs on a Nicolet Nexus FTIR spectrometer.

Elemental analyses were performed by the Elemental Microanalysis Limited, Okehampton, Devon.

6.3. Preparation of starting materials

6.3.1. Preparation of NHC precursors

6.3.1.1. 1,3,4,5-tetramethylimidazole-2-thione (IMe_4=S)

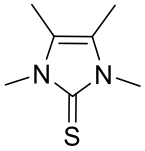

The synthesis of IMe_4=S was carried out according to a modified literature procedure.[2] A stirred 1-hexanol (250 mL) solution of 1,3-dimethyl-2-thiourea (10.4 g,

0.1 mol) and 3-hydroxy-2-butanone (8.8 g, 0.1 mol) was refluxed overnight. The solution was allowed to return to room temperature prior to rapid cooling to -78°C, which resulted in an instantaneous precipitation of a pale yellow solid. This was rapidly filtered and the solid was washed several times with cold H_2O and Et_2O, followed by recrystallization from CH_2Cl_2/Et_2O at 5°C. The colourless block-shaped crystals were separated by filtration, washed twice with cold ether and dried under vacuum. The ether washings and the filtrate were combined and kept at -40°C K for several days to yield a second crop of crystals. Combined yield: 8.4 g (54%). ^{1}H NMR (CD_2Cl_2, 500 MHz, 25°C): δ 3.47 (s, 6H, NC*H*$_3$), 2.06 (s, NCC*H*$_3$, 6H).

6.3.1.2. 1,3-diethyl-4,5-dimethylimidazole-2-thione (IEt_2Me_2=S)

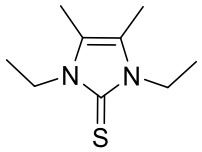

The synthesis of IEt_2Me_2=S was carried out according to a modified literature procedure[2] as above for IMe_4=S using 1,3-diethyl-2-thiourea (13.2 g, 0.1 mol). Combined yield: 8.8 g (48%). ^{1}H NMR ($CDCl_3$, 500 MHz, 25°C): δ 4.07 (q, $^2J_{HH}$ = 7.0 Hz, 4H, NC*H*$_2$CH$_3$), 2.07 (s, 6H, NCC*H*$_3$), 1.25 (t, $^2J_{HH}$ = 7.0 Hz, 6H, NCH$_2$C*H*$_3$).

6.3.1.3. 1,3-di(methyl)imidazolium iodide ([IMe_2H][I])

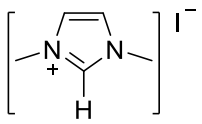

[IMe_2H][I] was prepared according to a literature procedure.[3] Methylimidazole (20.8 g, 0.253 mol) and iodomethane (35.9 g, 0.253 mol) were refluxed in 100 mL toluene overnight. Upon cooling the reaction mixture to room temperature, a white solid precipitated, which was collected by filtration, washed with hexane and dried under

vacuum to afford [IMe_2H][I] as a white hygroscopic powder, which was stored in a glovebox. Yield: 47.0 g (83%). ^{1}H NMR (D_2O, 500 MHz, 25°C): δ 8.62 (s, 1H, NC*H*N), 7.38 (s, 2H, NC*H*), 3.85 (s, 6H, NCH_3).

6.3.2. Preparation of NHC ligands

6.3.2.1. 1,3,4,5-tetramethylimidazol-2-ylidene (IMe_4)

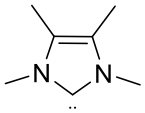

The synthesis of IMe_4 was carried out according to a modified literature procedure.[4] 1,3,4,5-tetramethylimidazole-2-thione (2.1 g, 13.4 mmol) and chopped pieces of potassium (1.15 g, 29.5 mmol) were suspended in 2-MeTHF (45 ml) and heated at 100°C overnight. After cooling, the suspension was filtered through a celite plug (pre-wetted with THF) and the filtercake washed with THF (3 × 10 mL). The combined 2-MeTHF and THF solutions were reduced to dryness to afford a pale yellow solid. Yield: 1.44 g (86 %). ^{1}H NMR (C_6D_6, 500 MHz, 25°C): δ 3.56 (s, 6H, NCH_3), 1.56 (s, 6H, NCCH_3).

6.3.2.2. 1,3-diethyl-4,5-dimethylimidazol-2-ylidene (IEt_2Me_2)

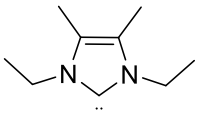

1,3-diethyl-4,5-dimethylimidazole-2H-thione (IEt_2Me_2=S, 1.9 g, 10.4 mmol) and chopped pieces of potassium (0.9 g, 23.0 mmol) were suspended in 2-MeTHF (45 mL) and heated at 100°C overnight. After cooling, the suspension was filtered through a celite plug (pre-wetted with THF) and the filtercake washed with THF (3 × 10 mL). The combined 2-MeTHF and THF solutions were reduced to dryness to afford a pale yellow oil, which solidified in a glovebox freezer. Yield: 1.35 g (85%). ^{1}H NMR (C_6D_6, 500

MHz, 25°C): δ 3.81 (q, $^{2}J_{HH}$ = 7.3 Hz, 4H, NC*H*$_2$CH$_3$), 1.65 (s, NCC*H*$_3$, 6H), 1.22 (t, $^{2}J_{HH}$ = 7.3 Hz 6H, NCH$_2$C*H*$_3$,).

6.3.3. Preparation of ruthenium precursor complexes

[Ru(PPh$_3$)$_3$Cl$_2$] was prepared according to the published method.[5]

6.3.3.1. [Ru(PPh$_3$)$_4$H$_2$] (32)

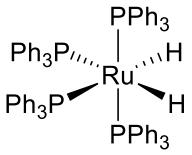

A slightly modified literature procedure was used.[6] A 250 mL three-neck round-bottom flask equipped with a rubber septum was charged with PPh$_3$ (12.0 g, 45.76 mmol), [Ru(PPh$_3$)$_3$Cl$_2$] (2.0 g, 2.08 mmol), C$_6$H$_6$ (60 mL), and MeOH (100 mL). After agitation under argon for 10 min, a MeOH suspension (5 mL) of NaBH$_4$ (3.0 g, 79.30 mmol) was added in portions over a period of 30 min. During the addition, the originally brown reaction mixture turned yellow. After stirring for an additional hour, the mixture was diluted with degassed MeOH (100 mL) and the yellow solid now present was collected on a frit under argon, washed with degassed MeOH (3 × 40 mL), then degassed Et$_2$O (3 × 40 mL) and dried under vacuum overnight. Yield: 2.32 g (96%). ^{31}P{^{1}H} NMR (C$_6$H$_6$, 121.5 MHz, 25°C): δ 49.1 (t, $^{2}J_{PP}$ = 13.8 Hz), 40.9 (t, $^{2}J_{PP}$ = 13.8 Hz).

6.3.3.2. [Ru(IMe$_4$)$_4$Cl$_2$]

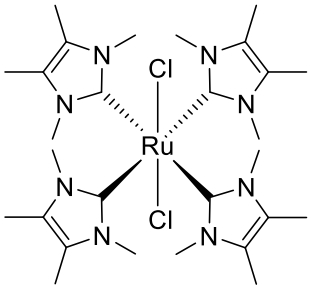

A mixture of [Ru(PPh$_3$)$_3$Cl$_2$] (0.60 g, 0.62 mmol) and IMe$_4$ (0.372 g, 3.00 mmol) was stirred in toluene (3 mL) at 25°C overnight. The pale orange precipitate that was formed was isolated by cannula filtration, washed with Et$_2$O (2 × 5 mL) and dried in vacuo. Yield: 0.34 g (81%). ^{1}H NMR (C$_6$D$_6$, 500 MHz, 25°C): δ 3.70 (s, 6H, NC*H*$_3$), 1.80 (s, 6H, NCC*H*$_3$).

6.3.3.3. [Ru(IMe$_2$)$_4$Cl$_2$]

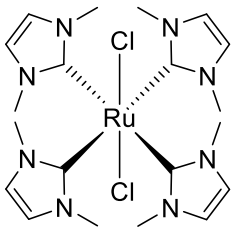

In-situ generation of 1,3-dimethylimidazol-2-ylidene (IMe$_2$) was carried out according to an optimised literature procedure.[7] THF (10 mL) was added to a mixure of 1,3-di(methyl)imidazolium iodide (2.8 g, 12.5 mmol) and KH* (1.0 g, 25.0 mmol) charged into a J.Young's resealable ampoule. Instantaneous evolution of H$_2$ was observed. The suspension was stirred for 1.5 h, after which time gas evolution had ceased and Et$_2$O (10 mL) was added to ensure precipitation of the generated potassium iodide. The THF/Et$_2$O solution of the generated 1,3-dimethylimidazol-2-ylidene was filtered by cannula and added dropwise to a THF (5 mL) suspension of [Ru(PPh$_3$)$_3$Cl$_2$]. The product precipitated immediately as a pale orange solid, which was isolated by

cannula filtration, washed with Et_2O (2 × 10 mL) and dried in vacuo. Yield: 1.12 g (97%). The insolubility of $[Ru(IMe_2)_4Cl_2]$ in common organic solvents precluded NMR analysis.[8]

*Potassium hydride was obtained as a 30 wt % suspension in mineral oil. The mineral oil was washed away with dry hexane and the KH dried under vacuum.

6.3.3.4. $[Ru(IEt_2Me_2)_4Cl_2]$

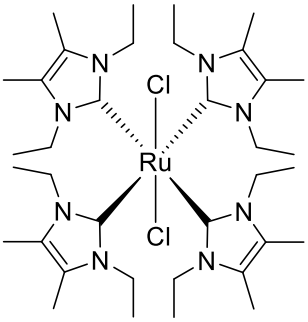

A mixture of $[Ru(PPh_3)_3Cl_2]$ (300 mg, 0.31 mmol) and IEt_2Me_2 (219 mg, 1.14 mmol) was stirred in toluene (3 mL) for 1 h. The resultant deep orange solution was filtered by cannula and the filtrate reduced to dryness. The sticky dark orange residue was suspended in hexane (5 mL) and stirred vigorously for 1 h to afford a pale orange precipitate, which was isolated by cannula filtration, washed with hexane (2 × 3 mL) and dried in vacuo. Yield: 132 mg (55%). NMR data matched those in the literature.[9] ^{1}H NMR (C_6D_6, 500 MHz, 25°C): δ 4.77 (m, $^2J_{HH}$ = 13.6 Hz, $^3J_{HH}$ = 7.1 Hz, 8H, NCH_2CH$_3$), 3.58 (m, $^2J_{HH}$ = 13.6 Hz, $^3J_{HH}$ = 7.1 Hz, 8H, NCH_2CH$_3$), 1.96 (s, 24 H, NCCH_3), 1.35 (t, $^3J_{HH}$ = 7.1 Hz, 24 H, NCH$_2$CH_3).

6.3.4. KC_8

Graphite (2g, 90-150 micron grade, Fluka) was charged into a flame-dried Schlenk tube and heated under vacuum with a heat gun for 1 h to desorb any oxygen

and water. Inside the glove box, a stoichiometric amount of potassium metal (0.82 g) was added in small chunks. The Schlenk tube was subsequently removed from the glove box and placed in an oil bath preheated to 90°C, and the temperature elevated to 200°C over a period of 45 min whilst maintaining vigorous stirring. KC_8 was obtained as a pyrophoric, fine bronze/golden powder in quantitative yield. Yield: 2.8 g.

6.4. Experimental procedures and characterising data for Chapter 2

6.4.1. $[Ru(IMe_4)_4H_2]$ (1)

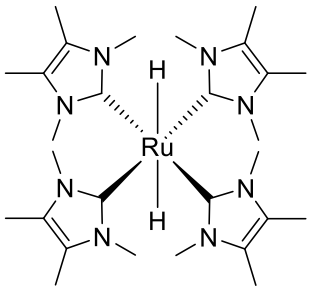

$[Ru(IMe_4)_4Cl_2]$ (255 mg, 0.38 mmol) and KC_8 (154 mg, 1.14 mmol) were charged into a J.Young's resealable ampoule. THF (5 mL, stored over K) was vacuum transferred onto the solids and the resulting suspension was subjected to 1 atm H_2. The dark-green reaction mixture was stirred overnight at 25°C before removing the volatiles in vacuo. In the glovebox, Et_2O (10 mL, stored over K) was syringed into the ampoule and the contents were stirred vigorously for 5 minutes. The suspension was allowed to settle for 1 h before passing the resultant pale yellow solution through a glass microfibre filter (pre-wetted with 5 mL of dry Et_2O). Extraction was repeated two more times (2 x 5 mL) and the combined Et_2O extracts transferred into a J.Young's ampoule. The volatiles were removed in vacuo on a Schlenk line to afford a pale yellow solid. Yield: 182 mg (80%). Spectroscopic data matched those in the original report.[10] Due to the facile H/D exchange observed in C_6D_6, ^{1}H NMR analysis of **1** was carried out in THF-

d_8. ^{1}H NMR (THF-d_8, 500 MHz, 25°C): δ 3.37 (s, 24H, NCH_3), 1.97 (s, 24H, CCH_3), -8.14 (s, 2H, Ru*H*).

6.4.2. [Ru(IMe$_2$)$_4$H$_2$] (2)

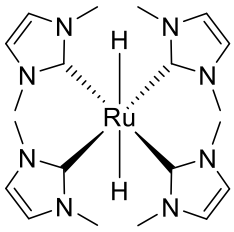

[Ru(IMe$_2$)$_4$Cl$_2$] (300 mg, 0.54 mmol) and KC_8 (218 mg, 1.62 mmol) were charged into a J.Young's resealable ampoule. THF (3 mL, stored over K) was vacuum transferred onto the solids and the resulting suspension was subjected to 1 atm H_2. The reaction mixture was stirred at 60°C for 2 h before removing the volatiles in vacuo. The product was extracted into Et_2O (10 mL), filtered by cannula and reduced to dryness to yield a pale orange solid. Yield: 204 mg (78%). Crystals suitable for X-ray diffraction were obtained upon layering a saturated benzene solution of **2** with pentane. ^{1}H NMR (C_6D_6, 500 MHz, 25°C): δ 6.43 (s, 8H, NCC*H*), 3.49 (s, 24H, NCH_3), -7.45 (s, 2H, Ru*H*). ^{13}C{^{1}H} NMR (C_6D_6, 126 MHz, 25°C): δ 212.6 (s, RuC_{NHC}), 117.9 (s, NC*C*H), 39.0 (s, N*C*H$_3$). Elemental analysis calcd. (%) for $C_{20}H_{34}N_8Ru$ (487.62): C 49.26, H 7.03, N 22.98; found C 49.27, H 7.04, N 23.03.

6.4.3. [Ru(IMe$_4$)$_4$HF] (3)

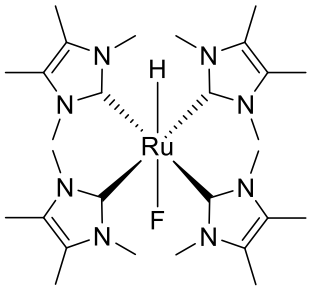

Pentafluorobenzene (8.15 µL, 73.4 µmol) was syringed into an NMR tube fitted with a J. Young's resealable PTFE valve containing a C_6H_6 solution (0.4 mL) of [Ru(IMe$_4$)$_4$H$_2$] (**1**, 22 mg, 36.7 µmol). Immediate ^{1}H and ^{19}F NMR analysis confirmed the formation of **3**. Layering the sample with hexane afforded a small amount of yellow crystals suitable for X-ray diffraction. Yield: 5 mg (22%). ^{1}H NMR (C_6H_6, 500 MHz, 25°C): δ 4.04 (s, 12H, NC*H*$_3$), 3.42 (s, 12H, NC*H*$_3$), 1.80 (s, 12H, CC*H*$_3$), 1.80 (s, 12H, CC*H*$_3$), -23.19 (d, $^2J_{HF}$ = 54.6 Hz, 1H, Ru*H*). ^{19}F NMR (C_6H_6, 470 MHz, 25°C): δ -281.6 (br d, Ru*F*). ^{13}C{^{1}H} NMR (C_6H_6, 126 MHz, 25°C): δ 206.1 (s, Ru*C*$_{NHC}$), 121.5 (s, N*C*CH$_3$), 120.1 (s, N*C*CH$_3$), 34.1 (s, N*C*H$_3$), 33.0 (d, J_{CF} = 22.6 Hz, N*C*H$_3$), 9.4 (NC*C*H$_3$), 8.9 (NC*C*H$_3$). Elemental analysis calcd. (%) for $C_{28}H_{49}FN_8Ru$ (617.78): C 54.44, H 7.99, N 18.13; found C 54.47, H 8.11, N 18.29.

6.4.4. [Ru(IMe$_2$)$_4$HF] (4)

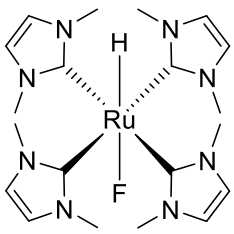

An excess of C_6F_5H (0.1 mL, 0.9 mmol) was allowed to slowly diffuse into a toluene solution (1 mL) of [Ru(IMe$_2$)$_4$H$_2$] (**2**, 37.8 mg, 77.6 µmol). The orange microcrystalline material formed over several days was washed with hexane (1 mL),

Et_2O (2 x 1 mL) and dried in vacuo. Yield: 29 mg (74%). Elemental analysis calcd. (%) for $C_{20}H_{33}FN_8Ru$ (505.57): C 47.51, H 6.58, N 22.16; found C 47.89, H 6.72, N 21.93.

A small amount of crystals suitable for X-ray diffraction were obtained *via* a different method in which a C_6FH_5 solution (0.4 mL) of TREAT-HF (3.47 µL, 21.3 µmol) was allowed to slowly diffuse into a C_6FH_5 solution (1 mL) of **2** (31.2 mg, 64 µmol), separated with a buffer of neat C_6FH_5 (0.5 mL). The insolubility of **4** in common organic solvents (THF, C_6FH_5, DMSO, pyridine, CH_2Cl_2) precluded full NMR analysis, however ^{1}H NMR data for **4** was obtained from a catalytic HDF reaction of C_6F_6 with **2** in the presence of Et_3SiH was carried out in C_6D_6. ^{1}H NMR (C_6D_6, 500 MHz, 25°C): δ 6.37 (s, 4H, NCC*H*), 6.34 (s, 4H, NCC*H*), 3.92 (s, 12H, NCH_3), 3.14 (s, 12H, NCH_3), -22.94 (s, 1H, Ru*H*).^{19}F NMR (C_6D_6, 470 MHz, 25°C): δ -302.2 (br s, Ru*F*).

6.4.5. [Ru(IMe$_2$)$_4$H(MeCN)][F/HF$_2$]

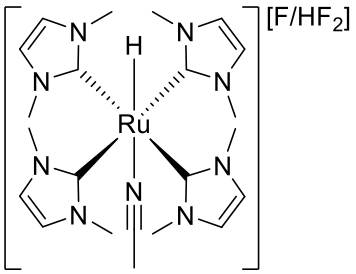

[Ru(IMe$_2$)$_4$HF] (**4**, 40 mg, 79 µmol) was dissolved in CH_3CN (1 mL) and stirred for 5 min before removing the volatiles. The obtained pale brown residue was washed with Et_2O (3 x 3 mL) and dried in vacuo to afford a pale yellow solid. Yield: 24 mg. ^{1}H NMR (CD_3CN, 500 MHz, 25°C): δ 6.86 (s, 8 H, NCC*H*), 3.23 (s, 12H, NCH_3), 2.96 (s, 12H, NCH_3), -15.20 (s, 1H, Ru*H*). ^{19}F NMR (CD_3CN, 470 MHz, 25°C): δ -73.8 (br s, F^-), -149.0 (t, $^2J_{FD}$ = 18.1 Hz, DF_2^-). ^{13}C{^{1}H} NMR (CD_3CN, 126 MHz, 25°C): δ 201.8 (s, RuC_{NHC}), 121.7 (s, NC*C*H), 121.2 (s, NC*C*H), 38.2 (s, NCH_3), 37.2 (s, NCH_3).

Selected NMR data in CH_3CN: ^{1}H NMR (500 MHz, 25°C): δ 16.32 (t, $^2J_{HD}$ = 121.4 Hz, HF_2^-). ^{19}F NMR (470 MHz, 25°C): δ 70.2 (br s, F^-), -147.2 (d, $^2J_{FH}$ = 121.4 Hz, HF_2^-).

6.4.6. [Ru(IMe$_4$)$_4$H][Ph$_3$SiF$_2$] (5)

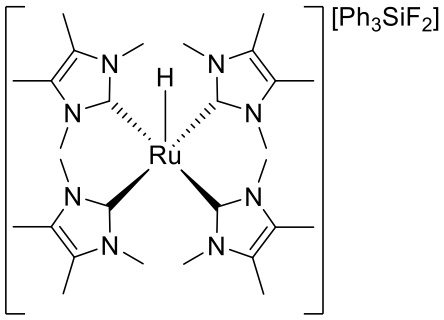

C_6F_6 (10 µL, 87.6 µmol) was added to a C_6H_6 solution (0.4 mL) of [Ru(IMe$_4$)$_4$H$_2$] (**1**, 35 mg, 58.4 µmol) and Ph_3SiH (76 mg, 292 µmol). An immediate colour change from yellow to deep purple was observed. Addition of pentane (2 mL) resulted in the precipitation of a deep purple solid, which was isolated, washed with pentane (3 x 0.5 mL) and dried in vacuo. Yield: 47 mg (90%). Crystals suitable for X-ray diffraction were obtained by layering a concentrated THF sample of **5** with pentane. ^{1}H NMR (THF-d_8, 500 MHz, 25°C): δ 8.03 (m, 6H, C_6H_5), 6.98-6.88 (m, 9H, C_6H_5), 3.10 (s, 12H, NCH_3), 3.03 (s, 12H, NCH_3), 2.01 (s, 12H, $NCCH_3$), 2.00 (s, 12H, $NCCH_3$), -40.16 (s, 1H, Ru*H*). ^{19}F NMR (THF-d_8, 470 MHz, 25°C): δ -103.0 (s, $^1J_{FSi}$ = 259 Hz, Ph_3SiF_2). Elemental analysis calcd. (%) for $C_{46}H_{64}N_8F_2SiRu \cdot 0.5C_4H_8O$: C 61.84, H 7.35, N 12.02; found C 61.93, H 7.36, N 12.32.

6.4.7. $IMe_4HC_6F_2H_3$ (6)

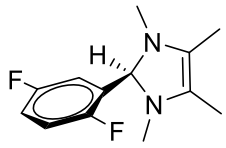

IMe_4 (105 mg, 0.85 mmol) was added to a C_6H_6 solution (3 mL) of 1,2,4-$C_6F_3H_3$ (89 µL, 0.85 mmol) and Et_3SiH (0.8 mL, 5.1 mmol) in an ampoule fitted with a J. Young's resealable tap and the mixture was stirred for 24 h at 70°C. After removal of the volatiles, the oily brown residue was extracted into hexane (3 mL), cannula filtered and the solvent removed in vacuo to yield **6** as a pale yellow oil. Yield: 153 mg (76%). ^{1}H NMR (C_6D_6, 500 MHz, 25°C): δ 7.87 (ddd, $^3J_{HF}$ = 9.2 Hz, $^4J_{HF}$ = 5.4 Hz, $^4J_{HH}$ = 3.2 Hz, 1H, *o*-$C_6F_2H_3$), 6.57 (m, $^3J_{HH}$ = 9.0 Hz, 1H, *m*-$C_6F_2H_3$), 6.54 (m, $^3J_{HH}$ = 9.0 Hz, $^4J_{HH}$ = 3.2 Hz, 1H, *p*-$C_6F_2H_3$), 4.46 (dd, $^4J_{HF}$ = 2.4 Hz, $^5J_{HF}$ = 0.8 Hz, 1H, NC*H*N), 2.16 (d, $^6J_{HF}$ = 0.7 Hz, 6H, NCH_3), 1.50 (s, 6H, NCCH_3). ^{19}F NMR (C_6D_6, 470 MHz, 25°C): δ -118.1 (m, $^5J_{FF}$ = 18.1 Hz, 1F, *m*-$C_6F_2H_3$), -128.4 (m, $^5J_{FF}$ = 18.1 Hz, 1F, o-$C_6F_2H_3$). ^{13}C{^{1}H} NMR (C_6D_6, 126 Hz MHz, 25°C): δ 160.0 (dd, J_{CF} = 104.7 Hz, $^4J_{CF}$ = 2.3 Hz, *m*-$C_6F_2H_3$), 158.0 (dd, J_{CF} = 104.8 Hz, $^4J_{CF}$ = 2.2 Hz, *o*-$C_6F_2H_3$), 131.0 (dd, $^2J_{CF}$ = 17.2 Hz, $^3J_{CF}$ = 6.4 Hz, *i*-$C_6F_2H_3$), 121.5 (N*C*CH_3), 117.2 (dd, $^2J_{CF}$ = 24.8 Hz, $^3J_{CF}$ = 5 Hz, *o*-$C_6F_2H_3$), 116.5 (dd, $^2J_{CF}$ = 24.5 Hz, $^3J_{CF}$ = 9 Hz, *m*-$C_6F_2H_3$), 116.2 (dd, $^2J_{CF}$ = 25.2 Hz, $^3J_{CF}$ = 8.2 Hz, *p*-$C_6F_2H_3$), 86.5 (N*C*N), 37.2 (N*C*H_3), 10.0 (NC*C*H_3). ESI-MS (THF): calcd. for $(IMe_4C_6H_3F_2)^+$, 237.120; obsd., 237.119.

6.4.8. $[IMe_4C_6F_2H_3][BF_4]$ (7)

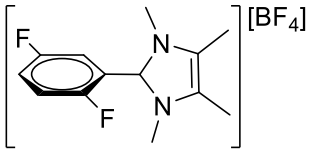

IMe_4 (125 mg, 1.0 mmol) was added to a C_6H_6 solution (3 mL) of 1,2,4-$C_6F_3H_3$ (158 µL, 1.5 mmol) in an ampoule fitted with a J. Young's resealable tap. The reaction mixture was stirred overnight at 80°C to give a deep red oily suspension. The oily residue was isolated by cannula filtration, washed with Et_2O (2 x 3 mL) and dried in vacuo to afford a dark orange/red solid corresponding to $[IMe_4C_6H_3F_2][HF_2]$. Yield: 160 mg. Selected NMR data: ^{1}H NMR (500 MHz, CD_2Cl_2, 25°C): δ 16.08 (t, $^1J_{HF}$ = 121.6 Hz, HF_2^-). ^{19}F NMR (470 MHz, CD_2Cl_2, 25°C): δ -156.5 (d, $^1J_{FH}$ = 121.6 Hz, HF_2^-). A portion of the isolated solid (93.5 mg) was subsequently stirred in the presence of $NaBF_4$ (53 mg, 0.48 mmol) in CH_2Cl_2 (3 mL) for 2 h at 25°C. A colour change from dark red to pale orange was observed. The solution was filtered by cannula and Et_2O added to induce precipitation of an off-white/beige solid. This was reprecipitated from CH_2Cl_2/Et_2O and washed with Et_2O (2 x 3 mL). Yield: 90 mg (48%). Colourless crystals suitable for X-ray diffraction were obtained by slow diffusion of pentane into a concentrated CH_2Cl_2 solution of **7**. The compound could also be efficiently recrystallised using Et_2O instead of pentane. ^{1}H NMR (500 MHz, CD_2Cl_2, 25°C): δ 7.49 (m, $^4J_{HH}$ = 3 Hz, 1H, *o*-$C_6F_2H_3$), 7.45 (m, $^3J_{HH}$ = 9.2 Hz, $^4J_{HH}$ = 3 Hz, 1H, *p*-$C_6F_2H_3$), 7.36 (m, $^3J_{HH}$ = 9.2 Hz, 1H, *m*-$C_6F_2H_3$), 3.56 (d, $^6J_{HF}$ = 0.6 Hz, 6H, NCH_3), 2.33 (s, 6H, NCCH_3). ^{19}F NMR (470 MHz, CD_2Cl_2, 25°C): δ -114.9 (dtd, $^5J_{FF}$ = 17.2 Hz, $^3J_{FH}$ = 7.8 Hz, $^4J_{FH}$ = 4.3 Hz, 1F, *m*-$C_6F_2H_3$), -117.5 (m, $^5J_{FF}$ = 17.2 Hz, 1F, *o*-$C_6F_2H_3$), -153.9 ($^{11}BF_4^-$), -154.0 ($^{10}BF_4^-$). ^{13}C{^{1}H} NMR (126 MHz, CD_2Cl_2, 25°C): δ 159.0 (dd, J_{CF} = 302.8 Hz, $^4J_{CF}$ = 2.6 Hz, *m*-$C_6F_2H_3$), 157.0 (dd, J_{CF} = 303.8 Hz, $^4J_{CF}$= 2.3 Hz, *o*-$C_6F_2H_3$),

136.9 (N*C*N), 126.8 (N*C*CH$_3$), 122.7 (dd, $^2J_{CF}$= 24.8 Hz, $^3J_{CF}$ = 8.9 Hz, *p*-*C*$_6$F$_2$H$_3$), 119.6 (d, $^2J_{CF}$ = 26.4 Hz, *o*-*C*$_6$F$_2$H$_3$), 118.9 (dd, $^2J_{CF}$ = 23.5 Hz, $^3J_{CF}$ = 8.9 Hz, m-*C*$_6$F$_2$H$_3$), 111.3 ($^2J_{CF}$ = 17.2 Hz, $^3J_{CF}$ = 9.2 Hz, *i*-*C*$_6$F$_2$H$_3$), 33.3 (N*C*H$_3$), 9.0 (NC*C*H$_3$). Elemental analysis calcd. (%) for $C_{13}H_{12}BF_6N_2$ (321.23): C 48.15, H 4.66, N 8.64; found C 48.22, H 4.65, N 8.46.

6.5. Experimental procedures and characterising data for Chapter 3

6.5.1. [Ru(IEt$_2$Me$_2$)$_2$(PPh$_3$)$_2$H$_2$] (cct-8)

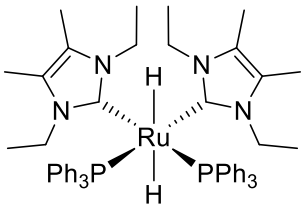

The synthesis of **cct-8** was carried out according to a modified literature procedure.[11] A benzene solution (2 mL) of IEt$_2$Me$_2$ (130 mg, 0.86 mmol) was cannula filtered into a benzene suspension (4 mL) of [Ru(PPh$_3$)$_4$H$_2$] (**32**, 0.45 g, 0.39 mmol) and stirred for 5 min. The solution was subsequently filtered by cannula and reduced to dryness. The resultant sticky residue was washed with pentane (3 x 5 mL) to afford **cct-8** as a pale yellow solid. Yield: 280 mg (77%). NMR data matched those in the literature.[12] ^{1}H NMR (C$_6$D$_6$, 500 MHz, 25°C): δ 7.97−7.91 (br, 10H, PC$_6$*H*$_5$), 7.06−7.02 (br, 3H, PC$_6$*H*$_5$), 6.96−6.90 (br, 17H, PC$_6$*H*$_5$), 6.49 (dq, $^2J_{HH}$ = 13.2 Hz, $^3J_{HH}$ = 6.5 Hz, 4H, NC*H*$_2$CH$_3$), 3.00 (dq, $^2J_{HH}$ = 13.2 Hz, $^3J_{HH}$ = 6.5 Hz, 4H, NC*H*$_2$CH$_3$), 1.40 (s, 12H, NCC*H*$_3$), 0.79 (br t, $^3J_{HH}$ = 6.5 Hz, 12H, NCH$_2$C*H*$_3$), −6.74 (t, $^2J_{HP}$ = 20.4 Hz, 2H, Ru*H*). ^{31}P{^{1}H} NMR (C$_6$D$_6$, 202 MHz, 25°C): δ 69.7 (s).

6.5.2. [Ru(IMe$_4$)$_2$(PPh$_3$)$_2$H$_2$] (ttt-9)

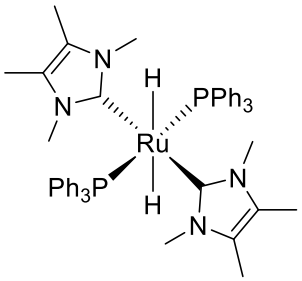

Synthesis of **ttt-9** was carried out according to a modified literature procedure.[12] A benzene solution (2 mL) of IMe_4 (142 mg, 1.14 mmol) was cannula filtered into a benzene suspension (4 mL) of [Ru(PPh$_3$)$_4$H$_2$] (0.6 g, 0.52 mmol) and stirred for 2 days at 50°C. The solution was subsequently filtered by cannula and reduced to dryness. The resultant sticky residue was washed with pentane (3 x 5 mL) to afford **ttt-9** as a pale yellow solid. Yield: 374 mg (82%). NMR data matched those reported in the literature.[12] ^{1}H NMR (C_6D_6, 500 MHz, 25°C): δ 7.80 (br m, 12H, PC$_6$*H*$_5$), 6.99-6.92 (m, 18H, PC$_6$*H*$_5$), 3.74 (s, 12H, NCC*H*$_3$), 1.34 (s, 12H, NC*H*$_3$), −6.74 (t, $^2J_{HP}$ = 20.4 Hz, 2H, Ru*H*). ^{31}P{^{1}H} NMR (C_6D_6, 202 MHz, 25°C: δ 71.6 (s).

6.5.3. [Ru(IEt$_2$Me$_2$)$_2$(PPh$_3$)$_2$HF] (cct-10)

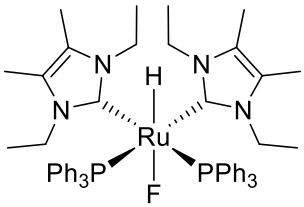

C_6F_6 (50 μL, 0.45 mmol) was added to a benzene (5 mL) solution of [Ru(IEt$_2$Me$_2$)$_2$(PPh$_3$)$_2$H$_2$] (**cct-8**, 140 mg, 0.15 mmol) in a J.Young's resealable ampoule. The reaction mixture was stirred vigorously for 24 h at room temperature, filtered by cannula and evaporated to dryness to afford an oily red residue. Addition of hexane (1 mL) under the action of vigorous stirring resulted in a formation of a deep

orange suspension (of **11**), which was isolated by cannula filration. Leaving the hexane filtrate at room temperature for a few days afforded yellow crystals of **cct-10**, which were manually separated from red needles of residual **11**. Yield: 43 mg (30%). Elemental analysis calcd. (%) for $C_{57}H_{63}N_4FP_2Ru{\cdot}0.5C_6H_{14}$ (993.18): C 68.93, H 7.10, N 5.64; found C 68.99, H 7.15, N 5.62.

A more efficient route to **cct-10** involved treatment of **cct-8** with $Et_3N{\cdot}3HF$ (TREAT-HF). Thus, a benzene solution (2 mL) of IEt_2Me_2 (116 mg, 0.76 mmol) was cannula filtered into a benzene suspension (4 mL) of $Ru(PPh_3)_4H_2$ (**32**) (0.4 g, 0.34 mmol) and stirred for 5 min before adding a THF solution (2 mL) of TREAT-HF (28 µL, 0.17 mmol) and stirring the resultant solution for further 2 h. CsF (105 mg, 0.69 mmol) was then added and the reaction mixture stirred overnight at room temperature, after which time the solution was filtered by cannula and reduced to dryness. The resulting sticky solid was washed with pentane (3 x 5 mL) and dried in vacuo to afford a pale yellow solid. Yield: 170 mg (53%). ^{1}H NMR ($C_6D_5CD_3$, 400 MHz, 25°C): δ 6.80* (br s, 1H, NCH_2CH$_3$), 6.45 (br s, 1H, NCH_2CH$_3$), 5.83 (br m, 1H, NCH_2CH$_3$), 5.60 (br m, 1H, NCH_2CH$_3$), 3.36 (br m, 1H, NCH_2CH$_3$), 3.13 (br m, 1H, NCH_2CH$_3$), 2.61 (br m, 1H, 6.8 Hz, NCH_2CH$_3$), 2.32 (br m, 1H, NCH_2CH$_3$), 1.56 (s, 3H, NCCH_3), 1.49 (s, 3H, NCCH_3), 1.39 (t, 3H, $^3J_{HH}$ = 6.8 Hz, NCH$_2$CH_3), 1.21 (s, 3H, NCCH_3), 1.16 (s, 3H, NCCH_3), 1.10 (t, 3H, $^3J_{HH}$ = 6.8 Hz, NCH$_2$CH_3), 0.34 (t, 3H, $^3J_{HH}$ = 6.8 Hz, NCH$_2$CH_3), 0.26 (t, 3H, $^3J_{HH}$ = 6.8 Hz, NCH$_2$CH_3), -21.58 (ddd, 1H, $^2J_{HF}$ = 51.6 Hz, $^2J_{HP}$ = 25.0 Hz, $^2J_{HP}$ = 14.1 Hz, Ru*H*). *chemical shift established by ^{1}H COSY. ^{31}P{^{1}H} NMR ($C_6D_5CD_3$, 122 MHz, 25°C): δ 43.1 (br s). ^{19}F NMR (THF-d_8, 470 MHz, 25°C): δ -354.4 (br d, $^2J_{FH}$ = 51.6 Hz). ^{13}C{^{1}H} NMR ($C_6D_5CD_3$, 100 MHz, 25°C): δ 191.4 (m, RuC_{NHC}), 124.4 (s, NCCH$_3$), 123.5 (s, NCCH$_3$), 122.9 (s, NCCH$_3$), 122.3 (s, NCCH$_3$), 43.2 (s, NCH$_2$CH$_3$), 42.0 (d, J_{CP} or J_{CF} = 16.4 Hz, NCH$_2$CH$_3$), 40.5 (d, J_{CP} or J_{CF} = 32.2

Hz, NCH_2CH$_3$), 16.2 (s, NCH$_2$*C*H$_3$), 15.0 (s, NCH$_2$*C*H$_3$), 14.2 (s, NCH$_2$*C*H$_3$), 13.6 (s, NCH$_2$*C*H$_3$), 9.4 (s, NC*C*H$_3$), 9.1 (s, NC*C*H$_3$), 8.8 (s, NC*C*H$_3$), 8.7 (s, NC*C*H$_3$).

6.5.4. [Ru(IEt$_2$Me$_2$)$_2$(PPh$_3$)(C$_6$F$_5$)H] (11)

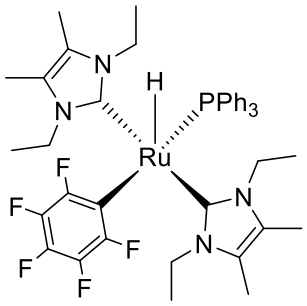

C_6F_5H (120 μL, 1.1 mmol) was syringed into a J. Young's resealable ampoule containing a hexane suspension (5 mL) of [Ru(IEt$_2$Me$_2$)$_2$(PPh$_3$)$_2$H$_2$] (**cct-8**, 100 mg, 0.11 mmol). The reaction mixture was stirred vigorously at room temperature for 24 h to give a dark orange solid, which was isolated by cannula filtration, washed with hexane (2 × 5 mL) and dried in vacuo. Yield: 53 mg (58%). Crystals suitable for X-ray diffraction were obtained upon layering a concentrated toluene solution of **11** with hexane. ^{1}H NMR (C_6D_6, 500 MHz, 25°C): δ 7.43–7.49 (m, 6H, PC$_6$*H*$_5$), 6.90–7.05 (br m, 9H, PC$_6$*H*$_5$), 4.77 (m, 2H, NC*H*$_2$CH$_3$), 3.60 (m, 4H, NC*H*$_2$CH$_3$), 3.05 (m, 2H, NC*H*$_2$CH$_3$), 1.48 (s, 6H, NCC*H*$_3$), 1.45 (s, 6H, NCC*H*$_3$), 1.02 (t, 6H, $^3J_{HH}$ = 7.3 Hz, NCH$_2$C*H*$_3$), 0.98 (t, 6H, $^3J_{HH}$ = 7.3 Hz, NCH$_2$C*H*$_3$), -32.95 (dt, 1H, $^2J_{HP}$ = 30.6 Hz, $^4J_{HF}$ = 7.2 Hz, Ru*H*). ^{31}P{^{1}H} NMR (C_6D_6, 122 MHz, 25°C): δ 59.5 (tt, $^4J_{PF}$ = 20.7 Hz, $^5J_{PF}$ = 9.7 Hz). ^{19}F NMR (C_6D_6, 470 MHz, 25°C): δ -111.5 (br, 2F, *o*-C$_6$F$_5$), -165.6 (m, 2F, *m*-C$_6$F$_5$), -166.4 (1F, t, J_{FF} = 20.3 Hz, *p*-C$_6$F$_5$). ^{13}C{^{1}H} NMR (C_6D_6, 126 MHz, 25°C): δ 195.9 (d, $^2J_{CP}$ = 12.1 Hz, Ru*C*$_{NHC}$), 142.8 (d, J_{CP} = 26.7 Hz, P*C*$_6$H$_5$), 133.6 (d, J_{CP} = 11.0 Hz, P*C*$_6$H$_5$), 127.4 (s, P*C*$_6$H$_5$), 127.1 (d, J_{CP} = 7.3 Hz, P*C*$_6$H$_5$), 123.6 (s, N*C*CH$_3$), 123.2 (s, N*C*CH$_3$), 43.2 (s, NCH$_2$CH$_3$), 42.4 (s, NCH$_2$CH$_3$), 15.4 (s, NC*C*H$_3$), 15.3 (s,

NC*C*H$_3$), 9.2 (s, NCH$_2$*C*H$_3$), 9.0 (s, NCH$_2$*C*H$_3$). Elemental analysis calcd. (%) for $C_{42}H_{48}N_4F_5PRu$ (835.88): C 60.34, H 5.79, N 6.70; found: C 60.36, H 5.74, N 6.72.

6.5.5. [Ru(IEt$_2$Me$_2$)(PPh$_3$)$_2$(C$_6$F$_5$)H] (12)

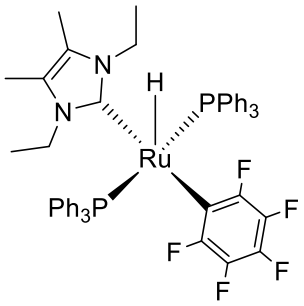

A J. Young's resealable NMR tube containing [Ru(IEt$_2$Me$_2$)$_2$(PPh$_3$)$_2$H$_2$] (**cct-8**, 45 mg, 48 μmol) and C_6F_5H (16 μL, 145 μmol) was heated in C_6H_6 (0.5 mL) at 70°C overnight to afford a deep red solution. This was filtered by cannula and the filtrate evaporated to dryness. After washing with hexane (3 × 0.5 mL), the residue was redissolved in a minimal amount of THF and layered with hexane to afford deep red crystals of **12**. Yield: 13 mg (28%). ^{1}H NMR (THF-d_8, 500 MHz, 25°C): δ 7.02–7.24 (br m, 30H, PC$_6$*H$_5$*), 3.38 (q, $^3J_{HH}$ = 7.3 Hz, 2H, NC*H$_2$*CH$_3$), 2.90 (q, $^3J_{HH}$ = 7.3 Hz, 2H, NC*H$_2$*CH$_3$), 1.96 (s, 3H, NCC*H$_3$*), 1.92 (s, 3H, NCC*H$_3$*), 0.48 (td, $^3J_{HH}$ = 7.3 Hz, $^4J_{HF}$ = 1.5 Hz, 3H, NCH$_2$C*H$_3$*), 0.34 (t, $^3J_{HH}$ = 7.3 Hz, 3H, NCH$_2$C*H$_3$*), −24.66 (td, $^2J_{HP}$ = 23.5 Hz, $^2J_{HF}$ = 6.9 Hz, 1H, Ru*H*). ^{31}P{^{1}H} NMR (THF-d_8, 202 MHz, 25°C): δ 52.3 (s). ^{19}F NMR (THF-d_8, 470 MHz, 25°C): δ −105.5 (m, 1F, *o*-C$_6$F$_5$), −111.8 (m, 1F, *o*-C$_6$F$_5$), −168.9 (m, 1F, *m*-C$_6$F$_5$), −170.1 (m, 1F, *p*-C$_6$F$_5$), −171.5 (t, 1F, $^3J_{FF}$ = 20.2 Hz, *p*-C$_6$F$_5$). ^{13}C{^{1}H} NMR (THF-d_8, 126 MHz, 25°C): δ 194.0 (m, Ru*C$_{NHC}$*), 139.0 ('virtual triplet' ('vt'), *J* = 17 Hz, P*C*$_6$H$_5$), 134.6 ('vt', *J* = 6 Hz, P*C*$_6$H$_5$), 129.0 (s, P*C*$_6$H$_5$), 127.9 ('vt', *J* = 4 Hz, P*C*$_6$H$_5$), 126.2 (s, N*C*CH$_3$), 124.7 (s, N*C*CH$_3$), 44.0 (s, N*C*H$_2$CH$_3$), 42.5 (s, N*C*H$_2$CH$_3$), 14.5 (s, NCH$_2$*C*H$_3$), 9.8 (s, NC*C*H$_3$), 9.4 (s, NC*C*H$_3$), 6.4 (d, J_{CF} = 7.5 Hz,

NCH_2CH_3). Elemental analysis calcd. (%) for $C_{51}H_{47}N_2F_5P_2Ru$ (945.92): C 64.75, H 5.01, N 2.96; found C 64.89, H 4.98, N 3.01.

6.5.6. [Ru(IEt$_2$Me$_2$)$_2$(PPh$_3$)$_2$H][H$_2$F$_3$] (13)

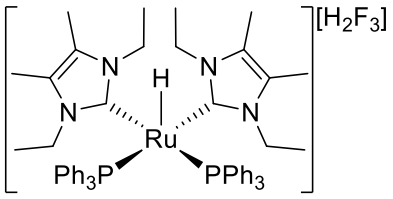

TREAT-HF (17.5 μL, 0.11 mmol) was added to a C_6H_6 (5 mL) solution of [Ru(IEt$_2$Me$_2$)$_2$(PPh$_3$)$_2$H$_2$] (**cct-8**, 100 mg, 0.11 mmol) in a J. Young's resealable ampoule. The reaction mixture was stirred at room temperature for 30 min at room temperature, before the sample was reduced to dryness. The sticky orange/red residue was washed with hexane (2 × 2 mL) and Et_2O (2 × 2 mL) and then redissolved in THF (5 mL). Addition of Et_2O resulted in the precipitation of an orange solid, which was washed further with Et_2O (2 × 5 mL) and then dried in vacuo. Yield: 76 mg (69%). Crystals suitable for X-ray diffraction were obtained upon layering a concentrated THF-d_8 solution with hexane. ^{1}H NMR (THF-d_8, 500 MHz, 25°C): δ 13.68 (br s, 2H, [H_2F_3]$^-$), 7.34–7.16 (m, 30H, PC_6H_5), 3.36 (q, $^3J_{HH}$ = 7.3 Hz, 4H, NCH_2CH_3), 2.75 (q, $^3J_{HH}$ = 7.3 Hz, 4H, NCH_2CH_3), 2.01 (s, 6H, $NCCH_3$), 1.81 (s, 6H, $NCCH_3$), 0.88 (t, $^3J_{HH}$ = 7.3 Hz, 6H, NCH_2CH_3), 0.44 (t, $^3J_{HH}$ = 7.3 Hz, 6H, NCH_2CH_3), −29.65 (t, $^2J_{HP}$ = 24.0 Hz, 1H, Ru*H*). ^{31}P{^{1}H} NMR (THF-d_8, 202 MHz, 25°C): δ 46.1 (s). ^{19}F NMR (THF-d_8, 470 MHz, 25°C): δ −115.2 (br s). Elemental analysis calcd. (%) for $C_{54}H_{65}N_4F_3P_2Ru \cdot 2C_4D_8O$ (1149.75): C 64.71, H 5.70, N 4.87; found C 64.38, H 5.69, N 4.84.

6.5.7. [Ru(IMe$_4$)$_2$(PPh$_3$)$_2$HF] (ttt-14)

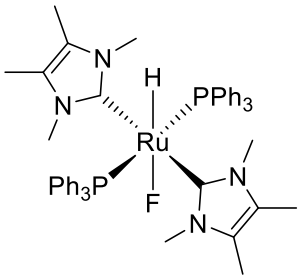

A benzene solution (2 mL) of IMe_4 (142 mg, 1.14 mmol) was cannula filtered into a benzene suspension (4 mL) of $[Ru(PPh_3)_4H_2]$ (0.6 g, 0.52 mmol) and stirred for 2 days at 50°C before adding a THF solution (2 mL) of TREAT-HF (42 µL, 0.26 mmol) and stirring the resultant solution for further 2 h. CsF (158 mg, 1.04 mmol) was then added and the reaction mixture stirred overnight at room temperature, after which time the solution was filtered by cannula and reduced to dryness. The product was washed with Et_2O (3 x 5 mL) and dried in vacuo to afford **ttt-14** as a pale yellow solid. Yield: 376 mg (81%). Crystals suitable for X-ray diffraction were obtained upon layering a saturated THF solution with pentane. ^{1}H NMR (500 MHz, C_6D_6, 25°C): δ 7.85 (br, 12H, PC$_6$*H$_5$*), 6.97 (br, 18 H, PC$_6$*H$_5$*), 3.94 (s, 3H, NC*H$_3$*), 3.92 (s, 3H, NC*H$_3$*), 3.26 (s, 6H, NC*H$_3$*), 1.37 (s, 6H, NCC*H$_3$*), 1.33 (s, 6H, NCC*H$_3$*), -21.94 (dt, 1H, $^2J_{HF}$ = 48.0 Hz, $^2J_{HP}$ = 21.0 Hz, Ru*H*). ^{31}P{^{1}H} NMR (C_6D_6, 162 MHz, 25°C): δ 50.1 (br s). ^{19}F NMR (C_6D_6, 376 MHz, 25°C): δ -331.5 (br, 1F, Ru*F*). ^{13}C{^{1}H} NMR (126 MHz, C_6D_6, 25°C): δ 192.9* (t, $^2J_{CP}$ = 14 Hz, Ru*C*$_{NHC}$), 141.3 ('vt', J_{CP} = 11.1 Hz, P*C*$_6$H$_5$), 135.2 ('vt', J_{CP} = 10.4 Hz, P*C*$_6$H$_5$), 126.5 ('vt', J_{CP} = 7.5 Hz, P*C*$_6$H$_5$), 124.0 (s, N*C*CH$_3$), 122.5 (s, N*C*CH$_3$), 35.5 (s, N*C*H$_3$), 35.4 (s, N*C*H$_3$), 33.4 (s, N*C*H$_3$), 33.0 (s, N*C*H$_3$), 9.9 (s, NC*C*H$_3$), 8.9 (s, NC*C*H$_3$). *Ru*C*$_{NHC}$ resonance recorded at 100 MHz on a more concentrated sample. Elemental analysis calcd. (%) for $C_{50}H_{55}FN_4P_2Ru$ (893.46): C 67.15, H 6.20, N 6.27; found C 66.84, H 6.20, N 6.16.

6.5.8. [Ru(IMe$_4$)$_2$(PPh$_3$)(SiPh$_3$)H$_3$] (17)

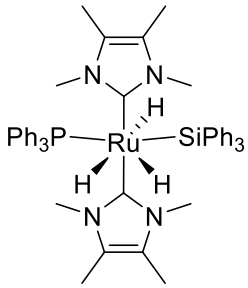

[Ru(IMe$_4$)$_2$(PPh$_3$)$_2$H$_2$] (**ttt-9**, 30 mg, 34.3 µmol) and Ph$_3$SiH (44 mg, 0.17 mmol) were dissolved in C_6H_6 (0.5 mL) in a J. Young's resealable NMR tube and heated overnight at 90°C. Colourless crystals of **17** were obtained after leaving the sample at room temperature for one week. These were recrystallised from toluene/pentane. Yield: 27 mg (91%). Selected ^{1}H NMR ($C_6D_5CD_3$, 500 MHz, 25°C): δ 3.49 (s, 6H, N*CH$_3$*), 3.16 (s, 6H, N*CH$_3$*), 1.59 (s, 6H, NCC*H$_3$*), 1.15 (s, 6H, NCC*H$_3$*), -4.84 (d, $^2J_{HP}$ = 11.0 Hz, 1H, Ru*H*), -6.13 (d, $^2J_{HP}$ = 9.9 Hz, 2H, Ru*H*); ^{31}P{^{1}H} NMR ($C_6D_5CD_3$, 121.5 MHz, 25°C): δ 59.6 (s). Selected ^{13}C{^{1}H} NMR ($C_6D_5CD_3$, 126 MHz, 25°C): δ 192.2 (d, $^2J_{CP}$ = 11 Hz, RuC$_{NHC}$), 150.9 (d, *J* = 2 Hz, *i*-C_6H_5), 141.2 (d, *J* = 30 Hz, *i*-C_6H_5), 123.3 (s, N*C*CH$_3$), 122.6 (s, N*C*CH$_3$), 37.7 (s, N*C*H$_3$), 36.0 (s, N*C*H$_3$), 9.9 (s, NC*C*H$_3$), 9.2 (s, NC*C*H$_3$). Elemental analysis calcd. (%) for $C_{50}H_{57}N_4SiPRu{\cdot}0.5C_6H_5CH_3$ (920.23): C 69.83, H 6.68, N 6.09; found 69.86, H 6.76, N 6.01.

6.5.9. [Ru(IMe$_4$)$_2$(dppm)HF] (cct-21)

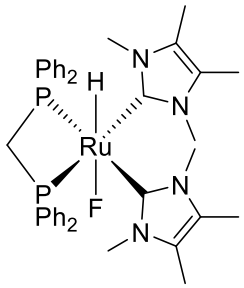

A toluene (0.4 mL) solution of [Ru(IMe$_4$)$_2$(PPh$_3$)$_2$HF] (**ttt-14**, 80 mg, 0.089 mmol) and dppm (41 mg, 0.107 mmol) was shaken vigorously in a J. Young's resealable NMR tube for 1 h at room temperature. The solution was filtered, concentrated and layered with pentane to afford **cct-21** as pale yellow crystals. Yield: 21 mg (31%). ^{1}H NMR ($C_6D_5CD_3$, 400 MHz, -45°C): δ 8.66 (br, 4H, PC$_6$*H*$_5$), 7.41 (br, 4H, PC$_6$*H*$_5$), 7.23-7.15 (m, 6H, PC$_6$*H*$_5$), 7.13-6.96 (m, 6H, PC$_6$*H*$_5$), 4.57 (m, 1H, PC*H*$_2$P), 4.45 (m, 1H, PC*H*$_2$P), 4.18 (s, 3H, NC*H*$_3$), 4.17 (s, 3H, NC*H*$_3$), 3.14 (s, 6H, NC*H*$_3$), 1.48 (s, 6H, NCC*H*$_3$), 1.38 (s, 6H, NCC*H*$_3$), -19.68 (dt, $^{2}J_{HF}$ = 52.8 Hz, $^{2}J_{HP}$ = 20.3 Hz, 1H, Ru*H*). ^{31}P{^{1}H} NMR (C_6D_6, 202 MHz, 25°C): δ -3.7 (s). ^{19}F NMR (C_6D_6, 470 MHz, 25°C): δ -343.6 (t, $^{2}J_{HF}$ = 52.8 Hz). ^{13}C{^{1}H} NMR ($C_6D_5CD_3$, 100 MHz, -45°C): δ 192.4 (dd, $^{2}J_{CP}$ = 115 Hz, $^{2}J_{CP}$ = 33 Hz, Ru*C*$_{NHC}$), 144.6 ('t', J_{CP} = 17 Hz, *i*-P*C*$_6$H$_5$), 142.3 ('t', J_{CP} = 7 Hz, *o*-P*C*$_6$H$_5$), 135.4 (s, *m*-P*C*$_6$H$_5$), 131.8 (s, *p*-P*C*$_6$H$_5$), 123.7 (s, N*C*CH$_3$), 122.1 (s, N*C*CH$_3$), 56.8 (t, $^{1}J_{CP}$ = 19 Hz, P*C*H$_2$P), 35.9 (s, N*C*H$_3$), 33.9 (s, N*C*H$_3$), 33.6 (s, N*C*H$_3$), 9.4 (s, NC*C*H$_3$), 8.8 (s, NC*C*H$_3$). Elemental analysis calcd. (%) for $C_{39}H_{47}N_4FP_2Ru$ (753.40): C 62.14, H 6.28, N 7.43; found C 62.25, H 6.31, N 7.45.

6.5.10. [Ru(IMe$_4$)$_2$(dppe)HF] (cct-22)

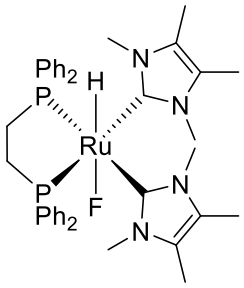

A toluene (0.4 mL) solution of [Ru(IMe$_4$)$_2$(PPh$_3$)$_2$HF] (**ttt-14**, 80 mg, 0.089 mmol) and dppe (42 mg, 0.107 mmol) was shaken vigorously for 1 h at room temperature in a J. Young's resealable NMR tube. The solution was then filtered, concentrated and layered with pentane to afford **cct-22** as pale yellow crystals. Yield: 34 mg (49%). ^{1}H NMR (C_6D_6, 400 MHz, 25°C): δ 8.70 (br, 4H, PC$_6$*H*$_5$), 7.36 (br m, 4H, PC$_6$*H*$_5$), 7.23 (m, 4H, PC$_6$*H*$_5$), 7.09 (m, 2H, PC$_6$*H*$_5$), 6.93 (br, 6H, PC$_6$*H*$_5$), 4.39 (s, 3H, NC*H*$_3$), 4.37 (s, 3H, NC*H*$_3$), 2.91 (s, 6H, NC*H*$_3$), 2.37 (m, 4H, P(C*H*$_2$)$_2$P), 1.47 (s, 6H, NCC*H*$_3$), 1.42 (s, 6H, NCC*H*$_3$), -22.9 (dt, $^{2}J_{HF}$ = 51.9 Hz, $^{2}J_{HP}$ = 22.1 Hz, Ru*H*). ^{31}P{^{1}H} NMR (C_6D_6, 162 MHz, 25°C): δ 64.8 (br s). ^{19}F NMR (C_6D_6, 376 MHz, 25°C): δ -330.4 (br s). ^{13}C{^{1}H} NMR (C_6D_6, 125 MHz, 25°C): δ 191.5 (dd, $^{2}J_{CP}$ = 95 Hz, $^{2}J_{CP}$ = 18 Hz, Ru*C*$_{NHC}$), 146.7 (m, *i*-P*C*$_6$H$_5$), 143.8 (m, *i*-P*C*$_6$H$_5$), 135.7 (br, P*C*$_6$H$_5$), 131.6 (br, P*C*$_6$H$_5$), 124.2 (s, N*C*CH$_3$), 122.7 (s, N*C*CH$_3$), 35.0 (br t, *J* = 10 Hz, N*C*H$_3$), 33.8 (br m, N*C*H$_3$), 33.3 (t, $^{2}J_{CP}$ = 24 Hz, P(*C*H$_2$)$_2$P), 9.7 (s, NC*C*H$_3$), 8.8 (s, NC*C*H$_3$). Elemental analysis calcd. (%) for $C_{40}H_{49}N_4FP_2Ru$ (767.85): C 62.57, H 6.43, N 7.29; found C 62.76, H 6.66, N 6.98.

6.5.11. [Ru(IMe$_4$)$_2$(dppp)HF] (cct-23)

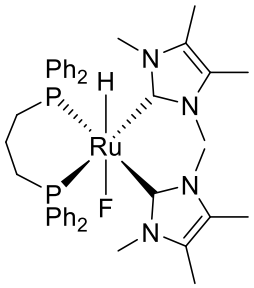

[Ru(IMe$_4$)$_2$(PPh$_3$)$_2$HF] (**ttt-14**, 80 mg, 0.089 mmol) and dppp (44 mg, 0.11 mmol) were dissolved in toluene (0.4 mL) in a J. Young's resealable NMR tube and the mixture shaken vigorously at room temperature for 1 h. After filtration, the filtrate was concentrated and layered with pentane to afford **cct-23** as pale yellow crystals. Yield: 45 mg (64%). ^{1}H NMR (C_6D_6, 500 MHz, 25°C): δ 8.05 (br m, 4H, PC$_6$*H*$_5$), 7.88 (br m, 4H, PC$_6$*H*$_5$), 7.09-6.84 (br m, 12H, PC$_6$*H*$_5$), 4.04 (s, 3H, NC*H*$_3$), 4.02 (s, 3H, NC*H*$_3$), 3.54 (br m, 2H, P(C*H*$_2$)$_3$P), 3.46 (s, 3H, NC*H*$_3$), 2.40 (br m, 2H, P(C*H*$_2$)$_3$P), 1.97 (m, 1H, P(C*H*$_2$)$_3$P), 1.70 (m, 1H, P(C*H*$_2$)$_3$P), 1.40 (s, 6H, NCC*H*$_3$), 1.39 (s, 6H, NCC*H*$_3$), -21.90 (dt, $^{2}J_{HF}$ = 52.7 Hz, $^{2}J_{HP}$ = 20.0 Hz, 1H, Ru*H*). ^{31}P{^{1}H} NMR (C_6D_6, 202 MHz, 25°C): δ 32.9 (s). ^{19}F NMR (C_6D_6, 470 MHz, 25°C): δ -332.9 (br s, Ru*F*). ^{13}C{^{1}H} NMR (C_6D_6, 126 MHz, 25°C): δ 193.0 (dd, $^{2}J_{CP}$ = 102 Hz, $^{2}J_{CP}$ = 30 Hz, Ru*C*$_{NHC}$), 144.7 ('t', J_{CP} = 12 Hz, *i*-P*C*$_6$H$_5$), 142.5 ('t', J_{CP} = 14 Hz, *i*-P*C*$_6$H$_5$), 133.2 (br m, P*C*$_6$H$_5$), 126.9 (br m, P*C*$_6$H$_5$), 123.6 (s, N*C*CH$_3$), 122.0 (s, N*C*CH$_3$), 35.6 (m, NCH$_3$), 33.5 (m, NCH$_3$), 28.8 (br, P(C*H*$_2$)P), 19.9 (br s, P(C*H*$_2$)P), 9.6 (s, NC*C*H$_3$), 8.9 (s, NC*C*H$_3$). Elemental analysis calcd. (%) for $C_{41}H_{51}N_4FP_2Ru$ (781.43): C 62.96, H 6.58, N 7.17; found C 63.14, H 6.50, N 7.43.

6.5.12. [Ru(IEt$_2$Me$_2$)$_2$(dppe)HF] (cct-24)

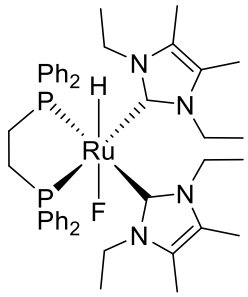

A toluene (0.4 mL) solution of [Ru(IEt$_2$Me$_2$)$_2$(PPh$_3$)$_2$HF] (**cct-8**, 50 mg, 53 µmol) and dppe (25 mg, 63 µmol) was shaken vigorously for 1 h at room temperature in a J. Young's resealable NMR tube. The solution was filtered, concentrated and layered with pentane to afford **cct-24** as pale yellow crystals. Yield: 19 mg (44%). ^{1}H NMR (C_6D_6, 500 MHz, 25°C): δ 8.35 (br m, 4H, PC$_6$*H*$_5$), 7.46 (br m, 4H, PC$_6$*H*$_5$), 7.19-7.13 (br m, 4H, PC$_6$*H*$_5$), 7.09-6.97 (br m, 8H, PC$_6$*H*$_5$), 6.13 (br m, 2H, NC*H*$_2$CH$_3$), 4.69 (m, 2H, NC*H*$_2$CH$_3$), 3.84 (m, 2H, NC*H*$_2$CH$_3$), 3.13 (m, 2H, NC*H*$_2$CH$_3$), 2.38 (m, 4H, P(C*H*$_2$)P), 1.67 (s, 6H, NCC*H*$_3$), 1.61 (s, 6H, NCC*H*$_3$), 1.10 (t, $^3J_{HH}$ = 6.9 Hz, 6H, NCH$_2$C*H*$_3$), 0.62 (t, $^3J_{HH}$ = 6.9 Hz, 6H, NCH$_2$C*H*$_3$), -22.32 (dt, $^2J_{HF}$ = 54.5 Hz, $^2J_{HP}$ = 21.6 Hz, 1H, Ru*H*). ^{31}P{^{1}H} NMR (C_6D_6, 202 MHz, 25°C): δ 63.8 (s). ^{19}F NMR (C_6D_6, 470 MHz, 25°C): δ -348.1 (br s, Ru*F*). ^{13}C{^{1}H} NMR (C_6D_6, 126 MHz, 25°C): δ 191.1 (ddd, $^2J_{CP}$ = 98 Hz, $^2J_{CP}$ = 18 Hz, $^2J_{CF}$ = 4 Hz, Ru*C*$_{NHC}$), 145.8 (m, *i*-P*C*$_6$H$_5$), 143.3 (m, *i*-P*C*$_6$H$_5$), 135.0 (br m, P*C*$_6$H$_5$), 132.2 ('t', J_{CP} = 4 Hz, P*C*$_6$H$_5$), 127.4 ('t', J_{CP} = 4 Hz, P*C*$_6$H$_5$) , 127.3 ('t', J_{CP} = 4 Hz, P*C*$_6$H$_5$), 127.2 (s, P*C*$_6$H$_5$), 124.6 (s, N*C*CH$_3$), 123.1 (s, N*C*CH$_3$), 42.7 (s, N*C*H$_2$CH$_3$), 41.7 (s, N*C*H$_2$CH$_3$), 41.4 (s, N*C*H$_2$CH$_3$), 32.8 ('t', J_{CP} = 23 Hz, P(*C*H$_2$)$_2$P), 17.0 (s, NCH$_2$*C*H$_3$), 14.8 (s, NCH$_2$*C*H$_3$), 9.7 (s, NC*C*H$_3$), 9.1 (s, NC*C*H$_3$). Elemental analysis calcd. (%) for $C_{44}H_{57}N_4FP_2Ru$ (823.96): C 64.14, H 6.97, N 6.80; found C 63.98, H 6.89, N 6.61.

6.5.13. [Ru(IMe$_4$)$_2$(dppm)H$_2$] (cct-25)

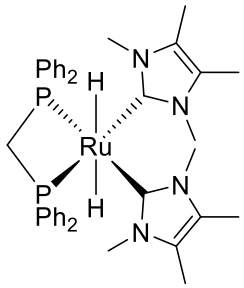

Et_3SiH (8.4 µL, 52.9 µmol) was added to a C_6D_6 solution (0.4 mL) of [Ru(IMe$_4$)$_2$(dppm)HF] (**cct-21**, 20 mg, 26.4 µmol) and the sample left for 2 days at room temperature to afford the *cis*,*cis*,*trans*-isomer of **25** as indicated by NMR spectroscopy. A small number of X-ray quality crystals were isolated upon layering a toluene solution with pentane. ^{1}H NMR (C_6D_6, 500 MHz, 25°C): δ 8.38 (br, 8H, PC$_6$*H*$_5$), 7.12 (m, 6H, PC$_6$*H*$_5$), 7.05 (m, 6H, PC$_6$*H*$_5$), 4.79 (t, $^2J_{HP}$ = 9.1 Hz, 2H, P(C*H*$_2$)P), 3.70 (s, 12H, NC*H*$_3$), 1.52 (s, 12H, NCC*H*$_3$), -5.37 (t, $^2J_{HP}$ = 16.9 Hz, 2H, Ru*H*). ^{31}P{^{1}H} NMR (C_6D_6, 202 MHz, 25°C): δ 10.9 (s). ^{13}C{^{1}H} NMR (C_6D_6, 126 MHz, 25°C): δ 199.3 (dd, $^2J_{CP}$ = 111 Hz, $^2J_{CP}$ = 38 Hz, Ru*C*$_{NHC}$), 146.3 (‘t’, J_{CP} = 11 Hz, *i*-P*C*$_6$H$_5$), 133.3 (‘t’, J_{CP} = 6 Hz, *o*-P*C*$_6$H$_5$), 127.7 (s, *p*-P*C*$_6$H$_5$), 127.5 (‘t’, J_{CP} = 4 Hz, *m*-P*C*$_6$H$_5$), 122.2 (s, N*C*CH$_3$), 61.3 (t, $^1J_{CP}$ = 17 Hz, P*C*H$_2$P), 36.8 (s, NCH$_3$), 9.8 (s, NC*C*H$_3$).

6.5.14. [Ru(IMe$_4$)$_2$(dppe)H$_2$] (cct-26)

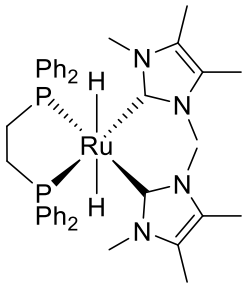

Et_3SiH (6 µL, 38 µmol) was syringed into a J. Young's resealable NMR tube containing a C_6D_6 solution (0.4 mL) of [Ru(IMe$_4$)$_2$(dppe)HF] (**cct-22**, 16 mg, 19 µmol) and the sample left overnight at room temperature to afford the *cis*,*cis*,*trans*-isomer of **26** as indicated by NMR spectroscopy. ^{1}H NMR (C_6D_6, 500 MHz, 25°C): δ 7.90 (t, $^3J_{HP}$ = 7.5 Hz, 8H, PC$_6$*H*$_5$), 7.12 (m, 8H, PC$_6$*H*$_5$), 7.05 (m, 4H, PC$_6$*H*$_5$), 3.82 (s, 12 H, NC*H*$_3$), 2.31 (d, $^2J_{HP}$ = 17.0 Hz, 4H, P(C*H*$_2$)$_2$P), 1.50 (s, 12H, NCC*H*$_3$), -7.20 (t, $^2J_{HP}$ = 19.1 Hz, 2H, Ru*H*). ^{31}P{^{1}H} NMR (C_6D_6, 202 MHz, 25°C): δ 86.0 (s). ^{13}C{^{1}H} NMR (C_6D_6, 126 MHz, 25°C): δ 197.7 (dd, $^2J_{CP}$ = 90 Hz, $^2J_{CP}$ = 20 Hz, Ru*C*$_{NHC}$), 146.1 (m, *i*-P*C*$_6$H$_5$), 133.1 (br m, P*C*$_6$H$_5$), 127.3 (br s, P*C*$_6$H$_5$), 127.2 (br m, P*C*$_6$H$_5$), 122.5 (s, N*C*CH$_3$), 37.0 (s, N*C*H$_3$), 33.9 ('t', J_{CP} = 24 Hz, P(*C*H$_2$)$_2$P), 9.9 (s, NC*C*H$_3$). Leaving the sample to stand at room temperature for further few days afforded a small amount of pale yellow crystals of the all *cis*-isomer of **26**, which proved to be insoluble in all common NMR solvents. Yield: 7 mg (49%). Elemental analysis calcd. (%) for $C_{40}H_{50}N_4P_2Ru$ (749.85): C 64.05, H 6.72, N 7.47; found C 64.39, H 6.76, N 7.35.

6.5.15. [Ru(IMe$_4$)$_2$(dppp)H$_2$] (cct-27)

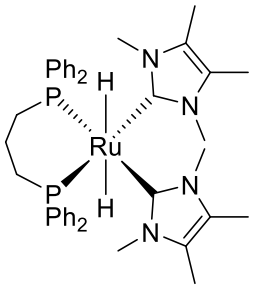

Et_3SiH (8.1 µL, 51.0 µmol) was added to a C_6D_6 solution (0.4 mL) of [Ru(IMe$_4$)$_2$(dppp)HF] (**cct-23**, 20 mg, 25.5 µmol) and the sample left for 2 days at room temperature to afford *cis*,*cis*,*trans*-isomer of **27** as indicated by NMR spectroscopy. No attempt was made to isolate the complex. ^{1}H NMR (C_6D_6, 500 MHz, 25°C): δ 7.99 (br, 8H, PC$_6$*H*$_5$), 7.03 (m, 8H, PC$_6$*H*$_5$), 6.95 (m, 4H, PC$_6$*H*$_5$), 3.87 (s, 12H, NC*H*$_3$), 2.82 (br, 4H, PC*H*$_2$CH$_2$C*H*$_2$P), 1.70 (m, 2H, PCH$_2$C*H*$_2$CH$_2$P), 1.40 (s, 12H, NCC*H*$_3$), -6.64 (t, $^2J_{HP}$ = 19.2 Hz, 2H, Ru*H*). ^{31}P{^{1}H} NMR (C_6D_6, 202 MHz, 25°C): δ 47.0 (s). ^{13}C{^{1}H} NMR (C_6D_6, 126 MHz, 25°C): δ 197.7 (dd, $^2J_{CP}$ = 99 Hz, $^2J_{CP}$ = 32 Hz, Ru*C*$_{NHC}$), 145.0 (‘t’, J_{CP} = 12 Hz, *i*-P*C*$_6$H$_5$), 133.1 (‘t’, J_{CP} = 5 Hz, *o*-P*C*$_6$H$_5$), 126.6 (m, overlapping *m/p*-P*C*$_6$H$_5$), 122.0 (s, N*C*CH$_3$), 37.1 (s, N*C*H$_3$), 35.4 (‘t’, J_{CP} = 14 Hz, P*C*H$_2$CH$_2$*C*H$_2$P), 20.3 (‘t’, J_{CP} = 5 Hz, PCH$_2$*C*H$_2$CH$_2$P), 9.8 (s, NC*C*H$_3$).

6.6. Experimental procedures and characterising data for Chapter 4

6.6.1. [Ru(IMe$_4$)$_2$(PPh$_3$)(Ph$_2$PC$_6$H$_4$O)H] (29)

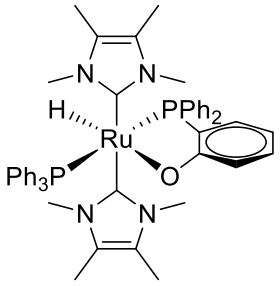

[Ru(IMe$_4$)$_2$(PPh$_3$)$_2$H$_2$] (**ttt-9**, 29.5 mg, 34 µmol) and DPEphos (21.7 mg, 40 µmol) were dissolved in 0.4 mL C_6H_6 in a J. Young's resealable NMR tube and heated at 90°C overnight. Subsequent addition of pentane resulted in precipitation of a pale yellow solid which was further washed with pentane (3 x 0.5 mL) and dried in vacuo. The resultant solid was redissolved in 0.2 mL toluene and layered with pentane to afford **29** as yellow crystals. Yield: 13 mg (43%). ^{1}H NMR (C_6D_6, 500 MHz, 25°C): δ 7.77 (s, 6H, s, ArH), 7.52 (m, 1H, ArH), 7.39 (m, 1H, ArH), 7.32 (s, 4H, ArH), 6.96 (s, 10H, ArH), 6.86 (m, 2H, ArH), 6.80 (m, 4H, ArH), 6.50 (m, 1H, ArH), 3.79 (s, 6H, NC*H*$_3$), 3.03 (s, 6H, NC*H*$_3$), 1.34 (s, 6H, NCC*H*$_3$), 1.23 (s, 6H, NCC*H*$_3$), -18.40 (t, $^2J_{HP}$ = 22.0 Hz, 1H, Ru*H*). ^{31}P{^{1}H} NMR (C_6D_6, 202 MHz, 25°C): δ 51.3 (s). ^{13}C{^{1}H} NMR (C_6D_6, 126 MHz, 25°C): δ 192.1 (t, $^2J_{CP}$ = 15 Hz, N*C*N), 178.4 (dd, $^2J_{CP}$ = 14 Hz, $^3J_{CP}$ = 12 Hz, OAr), 143.1 (dd, J_{CP} = 17 Hz, J_{CP} = 14 Hz, Ar), 141.5 (dd, J_{CP} = 18 Hz, J_{CP} = 15 Hz, Ar), 135.3 (s, Ar), 134.5 (t, J_{CP} = 6 Hz, Ar), 132.6 (t, J_{CP} = 6 Hz, Ar), 131.1 (s, Ar), 127.4 (s, Ar), 126.7 (m, Ar), 123.3 (s, N*C*CH$_3$), 123.2 (s, N*C*CH$_3$), 121.4 (t, J_{CP} = 3 Hz, Ar), 111.5 (t, J_{CP} = 2 Hz, Ar), 35.1 (s, N*C*H$_3$), 22.0 (s, N*C*H$_3$), 10.1 (s, *C*H$_3$), 8.8 (s, *C*H$_3$). Elemental analysis calcd. (%) for $C_{50}H_{54}N_4OP_2Ru$ (889.45): C 67.48, H 6.11, N 6.29; found: C 68.02, H 6.08, N 6.30.

6.6.2. [Ru(IEt$_2$Me$_2$)(IEtMe$_2$(C$_6$H$_4$)PPh$_2$)(Ph$_2$PC$_6$H$_4$O)H] (31)

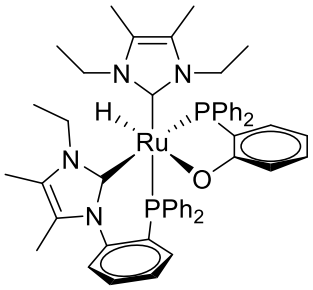

[Ru(IEt$_2$Me$_2$)$_2$(PPh$_3$)$_2$H$_2$] (**cct-8**, 31 mg, 0.033 mmol) and DPEphos (21.5 mg, 40 µmol) were dissolved in Et$_2$O (0.3 mL) in a J. Young's resealable NMR tube and refluxed at 60°C overnight to afford pale orange crystals of **31**, which were isolated by cannula filtration, washed with Et$_2$O (3 x 0.5 mL) and dried in vacuo. Yield: 12 mg (39%). ^{1}H NMR (C$_6$D$_6$, 500 MHz, 25°C): δ 8.97 (br s, 1H, Ar*H*), 8.43 (br s, 2H, Ar*H*), 7.63 (dt, J_{HH} = 7.7 Hz, J_{HH} = 1.6 Hz, 1H, ArH), 7.35-7.20 (m, 4H, ArH), 7.08-6.95 (m, 4H, ArH), 6.91 (br s, 3H, ArH), 6.88-6.74 (m, 5H, ArH), 6.70-6.48 (m, 7H, ArH), 5.72 (m, 1H, NC*H$_2$*CH$_3$), 5.13 (m, 1H, NC*H$_2$*CH$_3$) 5.11 (m, 1H, NC*H$_2$*CH$_3$ of IEtMe$_2$(C$_6$H$_4$)PPh$_2$), 3.82 (m, 1H, NC*H$_2$*CH$_3$ of IEtMe$_2$(C$_6$H$_4$)PPh$_2$), 3.38 (m, 1H, NC*H$_2$*CH$_3$), 2.18 (m, 1H, NC*H$_2$*CH$_3$), 1.59 (s, 3H, NCC*H$_3$* of IEtMe$_2$(C$_6$H$_4$)PPh$_2$), 1.53 (s, 3H, NCC*H$_3$*), 1.46 (s, 3H, NCC*H$_3$*), 1.42 (s, 3H, NCC*H$_3$* of IEtMe$_2$(C$_6$H$_4$)PPh$_2$), 1.12 (t, $^3J_{HH}$ = 7.1 Hz, 3H, NCH$_2$C*H$_3$*), 0.85 (t, $^3J_{HH}$ = 7.0 Hz, 3H, NCH$_2$C*H$_3$* of IEtMe$_2$(C$_6$H$_4$)PPh$_2$), 0.48 (t, $^3J_{HH}$ = 7.0 Hz, 3H, NCH$_2$C*H$_3$*), -17.71 (dd, $^2J_{HP}$ = 20.0 Hz, $^2J_{HP}$ = 15 Hz, 1H, Ru*H*). ^{31}P{^{1}H} NMR (C$_6$D$_6$, 202 MHz, 25°C): δ 59.3 (d, $^2J_{PP}$ = 28.4 Hz), 54.6 (d, $^2J_{PP}$ = 28.4 Hz). ^{13}C{^{1}H} NMR (C$_6$D$_6$, 100 MHz, 25°C): δ 194.6 (dd, $^2J_{CP}$ = 80 Hz, $^2J_{CP}$ = 21 Hz, N*C*N), 191.5 (dd, $^2J_{CP}$ = 88 Hz, $^2J_{CP}$ = 15 Hz, N*C*N), 179.2 (d, $^2J_{CP}$ = 23 Hz, OAr), 149.0 (dd, J_{CP} = 29 Hz, J_{CP} = 4 Hz, *i*-C$_6$H$_5$), 143.4 (d, J_{CP} = 9 Hz, *i*-C$_6$H$_5$), 139.8 (d, J_{CP} = 41 Hz, *i*-C$_6$H$_5$), 135.7 (br, Ar), 135.5 (br, Ar), 135.3 (br, Ar), 134.3 (d, J_{CP} = 11 Hz, *o*-C$_6$H$_5$), 133.8 (d, $^2J_{CP}$ = 31 Hz, *i*-C$_6$H$_5$), 132.3 (s, *p*-C$_6$H$_5$), 130.8

(s, *p*-C_6H_5), 130.2 (s, *p*-C_6H_5), 124.7 (d, *J* = 3 Hz, N*C*CH_3), 124.0 (br t, *J* = 2 Hz, N*C*CH_3), 123.8 (d, *J* = 3 Hz, N*C*CH_3 of IEtMe$_2$(C_6H_4)PPh_2), 123.7 (d, *J* = 2 Hz, N*C*CH_3 of IEtMe$_2$(C_6H_4)PPh_2), 43.8 (s, N*C*H_2CH_3), 43.5 (s, N*C*H_2CH_3), 41.4 (s, N*C*H_2CH_3 of IEtMe$_2$(C_6H_4)PPh_2), 16.1 (s, NCH_2*C*H_3), 14.4 (s, NCH_2*C*H_3), 14.0 (s, NCH_2*C*H_3), 11.1 (s, NC*C*H_3), 10.0 (s, *C*H_3), 9.3 (s, NC*C*H_3), 8.9 (s, NC*C*H_3). Elemental analysis calcd. (%) for $C_{52}H_{56}N_4OP_2Ru$ (915.46): C 68.18, H 6.16, N 6.12; found: C 68.57, H 6.16, N 6.02.

6.6.3. [Ru(DPEphos)$_2$H$_2$] (33)

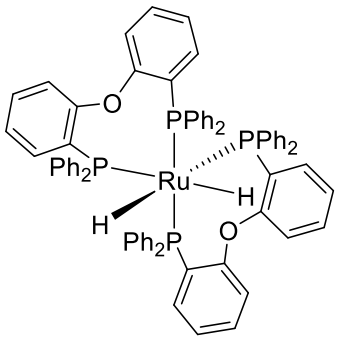

[Ru(PPh_3)$_4$$H_2$] (**32**, 300 mg, 0.26 mmol) and DPEphos (336 mg, 0.62 mmol) were dissolved in C_6H_6 (2 mL) and stirred at 25°C for 8 h. The solution was subsequently filtered by cannula and layered with pentane to afford **33** as yellow crystals. Yield: 270 mg (88%). ^{1}H NMR (C_6D_6, 500 MHz, 25°C): δ 7.78- 7.31 (m, 12 H, ArH), 7.02-6.19 (m, 44 H, ArH), -9.80 (m, 2 H, Ru*H*). ^{31}P{^{1}H} NMR (C_6D_6, 202 MHz, 25°C): δ 41.4 (t, $^2J_{PP}$ = 18 Hz), 35.3 (t, $^2J_{PP}$ = 18 Hz). Elemental analysis calcd. (%) for $C_{69}H_{55}O_2P_4Ru$ (1140.39): C 73.26, H 4.96; found: C 73.14, H 5.12.

6.6.4. [Ru(DPEphos)($Ph_2PC_6H_4O$)H] (34)

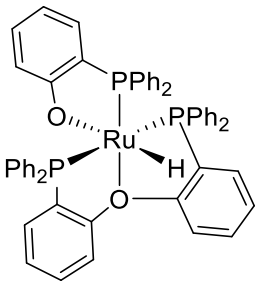

[$Ru(PPh_3)_4H_2$] (**32**, 0.3 g, 0.26 mmol) and DPEphos (0.31 g, 0.57 mmol) were dissolved in THF (3 mL) in an ampoule fitted with a J.Young's resealable tap and heated at 80°C overnight. The solution was subsequently filtered by cannula, reduced to dryness to give a yellow solid which was washed with pentane (3 x 10 mL) and dried in vacuo. Yield: 125 mg (51%). ^{1}H NMR (C_6D_6, 500 MHz, 25°C): δ 8.33-7.20 (m, 18H, Ar*H*), 7.09-6.33 (m, 24H, Ar*H*), -13.95 (q, $^2J_{HP}$ = 21.7 Hz, Ru*H*); ^{31}P{^{1}H} NMR (C_6D_6, 202 MHz, 25°C): δ 76.8 (t, $^2J_{PP}$ = 30.1 Hz, $Ph_2PC_6H_4O$), 49.9 (br s, DPEphos). ^{31}P{^{1}H} NMR ($C_6D_5CD_3$, 202 MHz, -15°C): δ 76.2 (t, $^2J_{PP}$ = 30.1 Hz, $Ph_2PC_6H_4O$), 49.6 (d, $^2J_{PP}$ = 30.1 Hz, DPEphos), 48.8 (d, $^2J_{PP}$ = 30.1 Hz, DPEphos).

6.6.5. [Ru(DPEphos)($Ph_2PC_6H_4O$)Cl] (35)

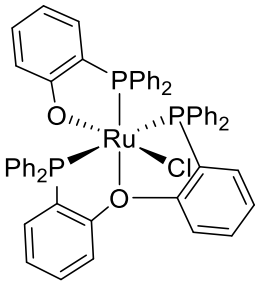

[Ru(DPEphos)($Ph_2PC_6H_4O$)H] (**34**, 60mg, 65.4 µL) was dissolved in CH_2Cl_2 in a J. Young's resealable NMR tube and refluxed overnight. **35** was obtained as an orange microcrystalline solid upon layering a concentrated solution with Et_2O. The solid was washed with Et_2O (3 x 0.5 mL) and dried in vacuo. Yield: 26 mg (42%).

$^{31}P\{^{1}H\}$ NMR (CH_2Cl_2, 202 MHz, 25°C): δ 64.5 (t, $^{2}J_{PP}$ = 29.5 Hz, $Ph_2P(C_6H_4)O$), 35.0 (br s, DPEphos), 30.7 (br s, DPEphos).

6.7. Experimental procedures and characterising data for Chapter 5

6.7.1. [Ru(PPh$_3$)$_3$HF] (37)

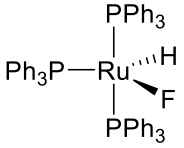

[$Ru(PPh_3)_4H_2$] (**32**, 0.3 g, 0.26 mmol) and $P(C_6F_5)_3$ (48 mg, 91.1 µmol) were dissolved in C_6H_6 (2 mL) and stirred at 25°C overnight. The solution was subsequently filtered by cannula and layered with pentane to afford **37** as dark red crystals. Yield: 203 mg (79%). ^{1}H NMR (THF-d_8, 500 MHz, 25°C): δ 7.27 (t, $^{3}J_{HP}$ = 7.8 Hz, 18H, *o*-PC_6H_5), 7.12 (t, $^{5}J_{HP}$ = 7.4 Hz, 9H, *p*-PC_6H_5), 6.94 (t, $^{4}J_{HP}$ = 7.6 Hz, 18H, *m*-PC_6H_5), -22.33 (q, $^{2}J_{HP}$ = 28.0 Hz, 1H, Ru*H*). $^{31}P\{^{1}H\}$ NMR (CD_2Cl_2, 162 MHz, -25°C): δ 88.9 (d, $^{2}J_{PF}$ = 79.3 Hz), 39.6 (s). ^{19}F NMR (CD_2Cl_2, 376 MHz, -25°C): δ -216.5 (d, $^{2}J_{FP}$ = 79.3 Hz). Elemental analysis calcd. (%) for $C_{54}FH_{46}P_3Ru$ (907.35): C 71.42, H 5.11; found: C 71.80, H 5.24.

6.7.2. [Ru(PPh$_3$)$_3$(SiEt$_3$)H$_3$] (38)

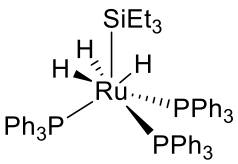

[$Ru(PPh_3)_3HF$] (**37**, 33.5 mg, 36.9 µmol) and Et_3SiH (11.7 µL, 73.8 µmol) were shaken vigorously in THF-d_8 in a J. Young's resealable NMR tube for 2 h to give a pale orange solution. Pale yellow crystals of **38** were obtained upon slow evaporation of solvent in the glovebox. These were washed with pentane (3 x 0.5 mL) and dried in

vacuo. Yield: 12.5 mg (42%). ^{1}H NMR (THF-d_8, 400 MHz, 25°C): δ 7.16 (t, $^{5}J_{HP}$ = 7.3 Hz, 9H, *p*-PC_6H_5), 7.11 (t, $^{3}J_{HP}$ = 8.0 Hz, 18H, *o*-PC_6H_5), 6.93 (t, $^{4}J_{HP}$ = 7.3 Hz, 18H, *m*-PC_6H_5), 0.61 (t, $^{3}J_{HH}$ = 7.6 Hz, 9H, $Si(CH_2CH_3)_3$), 0.43 (q, $^{3}J_{HH}$ = 7.6 Hz, 6H, $Si(CH_2CH_3)_3$), -10.58 (m, 3H, RuH_3). ^{31}P{^{1}H} NMR (THF-d_8, 162 MHz, 25°C): δ 41.8 (s). Elemental analysis calcd. (%) for $C_{60}H_{63}P_3RuSi$ (1005.46): C 71.61, H 6.31; found: C 71.32, H 6.66.

6.7.3. [Ru(PPh$_3$)$_3$(SiPh$_3$)H$_3$] (39)

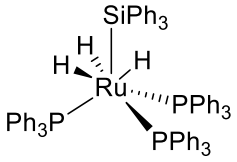

Ph_3SiH (34 mg, 0.13 mmol) was dissolved in C_6H_6 (2 mL) and slowly added to the C_6H_6 (5 mL) solution of [Ru(PPh$_3$)$_4$H$_2$] (**32**, 100 mg, 86.8 μmol). The reaction mixture was left undisturbed overnight, after which time the colour changed from pale yellow to colourless. The solution was subsequently layered with hexane and left at room temperature for a further few days to afford **39**, which was isolated as colourless crystals. Yield: 40 mg (80%). Selected ^{1}H NMR (C_6D_6, 500 MHz, 25°C): δ -9.37 (m, RuH_3). ^{31}P{^{1}H} NMR (C_6D_6, 202 MHz, 25°C): δ 37.5 (s). Elemental analysis calcd. (%) for $C_{72}H_{63}P_3RuSi$ (1150.37): C 75.17, H 5.52; found: C 75.16, H 5.82.

6.7.4. [Ru(PPh$_3$)$_3$(HBPin)H$_2$] (40)

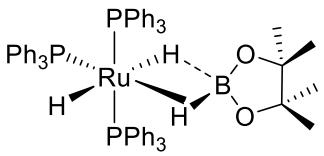

A C_6H_6 solution (0.5 ml) of [Ru(PPh$_3$)$_3$HF] (**37**, 15 mg, 16.5 μmol) and HBPin (24.0 μL, 0.16 mmol) was layered with pentane to afford a small amount of crystals of

40 over a period of ca. 2 weeks. ^{1}H NMR ($C_6D_5CD_3$, 400 MHz, -15°C): δ -8.04 (td, $^{2}J_{HP}$ = 27.2 Hz, $^{2}J_{HP}$ = 16.3 Hz, Ru*H*), -9.49 (dm, $J \approx 37$ Hz, Ru*H*), -10.46 (dt, $^{2}J_{HP}$ = 59.7, $^{2}J_{HP}$ = 17.5 Hz, Ru*H*). ^{31}P{^{1}H} NMR ($C_6D_5CD_3$, 162 MHz, -15°C): δ. 52.2 (d, $^{2}J_{PP}$ = 25.0 Hz), 50.4 (t, $^{2}J_{PP}$ = 25.0 Hz).

6.8. References for Chapter 6

(1) Sheldrick, G. M. *Acta Crystallogr. A* **1990**, *46*, 467.

(2) Kuhn, N.; Kratz, T. *Synthesis* **1993**, *1993*, 561.

(3) Schaub, T.; Backes, M.; Radius, U. *Organometallics* **2006**, *25*, 4196.

(4) Ansell, M. B.; Roberts, D. E.; Cloke, F. G. N.; Navarro, O.; Spencer, J. *Angew. Chem. Int. Ed.* **2015**, *54*, 5578.

(5) Hallman, P. S.; Stephenson, T. A.; Wilkinson, G. In *Inorganic Syntheses*; Parry, R. W., Ed.; John Wiley & Sons, Inc., 1970; pp 237–240.

(6) Samouei, H.; Miloserdov, F. M.; Escudero-Adán, E. C.; Grushin, V. V. *Organometallics* **2014**, *33*, 7279.

(7) van der Eide, E. F.; Liu, T.; Camaioni, D. M.; Walter, E. D.; Bullock, R. M. *Organometallics* **2012**, *31*, 1775.

(8) Würtemberger, M.; Ott, T.; Döring, C.; Schaub, T.; Radius, U. *Eur. J. Inorg. Chem.* **2011**, 405.

(9) Bramananthan, N.; Mas-Marzá, E.; Fernandéz, F. E.; Ellul, C. E.; Mahon, M. F.; Whittlesey, M. K. *Eur. J. Inorg. Chem.* **2012**, 2213.

(10) Wolf, R.; Plois, M.; Hepp, A. *Eur. J. Inorg. Chem.* **2010**, 918.

(11) Cybulski, M. K.; Riddlestone, I. M.; Mahon, M. F.; Woodman, T. J.; Whittlesey, M. K. *Dalton Trans.* **2015**.

(12) Davies, C. J. E.; Lowe, J. P.; Mahon, M. F.; Poulten, R. C.; Whittlesey, M. K. *Organometallics* **2013**, *32*, 4927.